OCEANIC COAL AUSTRALIA LIMITED

ACN 003 856 782

Managed by

xstrata coal

WEST WALLSEND COLLIERY CONTINUED OPERATIONS PROJECT

ENVIRONMENTAL ASSESSMENT

Umwelt Environmental Consultants

JULY 2010

VOLUME 2

Appendices 5A (Part 2)-8

appendix 5A
Part 2

Subsidence Assessment (Appendices)

APPENDIX A - Extracts from ACARP, 2003 and SDPS® User Manual

ACARP, 2003 EMPIRICAL SUBSIDENCE PREDICTION MODEL

A1 Introduction

This appendix provides a description of how subsidence develops above longwall panels and provides a summary of the empirical subsidence prediction models used in this study: **ACARP, 2003** and SDPS (Surface Deformation Prediction System).

The **ACARP, 2003** model was originally developed by Strata Engineering (Australia) Pty Ltd under ACARP funding with the goal of providing the industry with a robust and reliable technique to utilise the significant amount of geological and testing information already gathered by mining companies.

Over the past six years the **ACARP, 2003** model has been used successfully by the model's author, Steven Ditton, at several longwall mines in the Newcastle, Hunter Valley, Western and Southern Coalfields of NSW and the Bowen Basin, Queensland.

Subsidence prediction work for Stage 1 of the Moolarben Coal Project in 2006 resulted in further external scrutinization of the model and the robustness of the methodology by an Independent Hearing and Assessment Panel (IHAP), which was set up to assess Environmental Impact Assessments for new coal mining projects by NSW Department of Planning (DoP).

The outcomes of the IHAP for Moolarben resulted in several refinements to the model, as requested by the independent subsidence expert, Emeritus Professor J M Galvin, UNSW School of Mining and Director of Galvin and Associates Pty Ltd.

The refinements generally included several technical adjustments and clarification of the terminology used, to enable a better understanding of the model by the wider technical community.

Over the past two years, Ditton Geotechnical Services Pty Ltd (DgS) has modified the **ACARP, 2003** model to be able to use it to calibrate an influence function model (SDPS®) that was developed by the Polytechnical Institute for the US Coalfields. The SDPS® program allows a wider range of topographic and complex mining layouts (including longwall and pillar extraction panels) to be assessed.

This appendix summarises the **ACARP, 2003** model in its current format and explains the refinements made to the original model. Details of the **SDPS®** model itself are provided at the back of this appendix and discussed further in the main body of the report.

A2 Description of Subsidence Development Mechanisms Above Longwalls

After the extraction of a single longwall panel, the immediate mine roof usually collapses into the void left in the seam. The overlying strata or overburden then sags down onto the collapsed material, resulting in settlement of the surface.

The maximum subsidence occurs in the middle of the extracted panel and is dependent on the mining height, panel width, cover depth, overburden strata strength and stiffness and bulking characteristics of the collapsed strata. For the case of single seam mining, maximum panel subsidence has not exceeded 60% of the mining height (T) in over 95% of the published cases for the Newcastle, and Southern Coalfields (refer ACARP, 2003 and Holla and Barclay, 2000). For the 5% of cases, which did exceed 60%T, the maximum subsidence did not exceed 65%T (i.e. 2.7 m for a 4.2m mining height). The actual subsidence may also be lower than this value due to the spanning or bridging capability of the strata above the collapsed ground (or the goaf).

The combination of the above factors determines whether a single longwall panel will be sub-critical, critical, or supercritical in terms of maximum subsidence.

Sub-critical subsidence refers to panels that are narrow and deep enough for the overburden to bridge or 'arch' across the extracted panel regardless of geology. It is therefore termed 'geometrical' or 'deep beam arching'.

Beyond the sub-critical range, the overburden becomes Critical, and is unable to arch without the presence of massive, competent strata. Failure of the strata starts to develop and it sags down onto the collapsed or caved roof strata immediately above the extracted seam. Critical panels refer to panels with widths where maximum possible subsidence starts to develop.

If relatively thick and strong massive strata exist, then 'critical arching' or 'shallow Voussoir beam' behaviour can occur for panel W/H ratios up to1.8 (e.g. massive Wollar Sandstone strata > 33 m thick, has spanned across 250 m wide and 140 m deep longwall panels at Ulan Mine in the Western Coalfield. Panel sag subsidence was 1.2 m for a mining height of 3.2 m).

Supercritical panels refer to panels with widths that cause complete collapse of the overburden. In the case of super-critical panels, maximum panel subsidence does not usually continue to increase significantly with increasing panel width.

In the Australian coalfields, sub-critical or (geometrical arching) behaviour generally occurs when the panel width (W) is <0.6 times the cover depth (H) and supercritical when W/H > 1.4. Critical behaviour usually occurs between W/H ratios of 0.6 and 1.4 and represents the transition between 'geometrical arching' to 'shallow beam bending' to 'complete failure' of the overburden.

The maximum subsidence for sub-critical and critical panel widths is < 60% of the longwall extraction height and could range between 10% and 40% (of the extraction height).

The surface effect of extracting several adjacent longwall panels is dependent on the stiffness of the overburden and the chain pillars left between the panels. Invariably, 'extra' subsidence occurs above a previously extracted panel and is caused primarily by the compression of the chain pillars and adjacent strata between the extracted longwall panels.

A longwall chain pillar undergoes the majority of life-cycle compression when subject to double abutment loading (i.e. the formation of goaf on both sides of it, after two adjacent panels have been extracted). Surface survey data indicates that an extracted panel can affect the chain pillars between three or four previously extracted panels. The stiffness of the overburden and chain pillar system will determine the extent of load transfer to the preceding chain pillars. If the chain pillars go into yield, the load on the pillars will be mitigated to some extent by load transfer to adjacent fallen roof material or goaf.

The surface subsidence usually extends outside the limits of extraction for a certain distance (i.e. the angle of draw). The angle of draw distance is usually less than or equal to 0.5 to 0.7 times the depth of cover (or angles of draw to the vertical of 26.5^{o} to 35^{o}) in the NSW and QLD Coalfields.

The effect of extracting several adjacent longwall panels is dependent on the stiffness of the overburden and the chain pillars left between the panels. Invariably, 'extra' subsidence occurs above a previously extracted panel and is caused primarily by the compression of the chain pillars and adjacent strata between the extracted longwall panels.

A longwall chain pillar undergoes the majority of life-cycle compression when subject to double abutment loading (i.e. the formation of goaf on both sides of it, after two adjacent panels have been extracted). Surface survey data indicates that an extracted panel can affect the chain pillars between three or four previously extracted panels. The stiffness of the overburden and chain pillar system will determine the extent of load transfer to the preceding chain pillars. If the chain pillars go into yield, the load on the pillars will be mitigated to some extent by load transfer to adjacent fallen roof material or goaf.

The surface subsidence usually extends outside the limits of extraction for a certain distance (i.e. the angle of draw). The angle of draw distance is usually less than or equal to 0.5 to 0.7 times the depth of cover (or angles of draw to the vertical of 26.5^{o} to 35^{o}) in the NSW and QLD Coalfields.

A3 ACARP Project Overview

The original **ACARP, 2003** model was originally developed for the Newcastle Coalfield to deal with the issue of making reliable subsidence predictions over longwall panels by using both geometrical and geological information.

The project was initially focused on the behaviour of massive sandstone and conglomerate strata in the Newcastle Coalfield, but has now been successfully used in other coalfields since development over the past six years. This has occurred naturally due to the expansion of the

model's database with data from other coalfields and has resulted in generic refinements to the model to deal with the wider range of geometrical and geological conditions.

In regards to geometry, the subsidence above a series of longwalls is strongly influenced by the panel width, the cover depth, the extraction height and the stiffness of the interpanel pillars (i.e. the chain pillars) and immediate roof and floor strata.

In regards to geology, the presence of massive strata units, such as conglomerate and sandstone channels above longwall panels, has resulted in reduced subsidence compared to that measured over longwall panels with similar geometry and thinner strata units.

Geological structure, such as faults and dykes, can cause increases in subsidence due to their potential to adversely affect the spanning capability of the overburden.

During the original development of the model, a database of maximum single and multi longwall panel subsidence and associated massive strata units was compiled for the Newcastle Coalfield. The database draws on subsidence data from over fifty longwall panels and covers a panel width to cover depth (W/H) ratio from 0.2 to 2.0 (cover depth ranges between 70 m and 351 m), as shown in **Figure A1**.

The original project database includes single seam longwall mining data from eleven collieries within the Newcastle Coalfield, as presented in **Table A1**.

Table A1 - Empirical Database Sources from Newcastle Coalfield

Colliery	**Colliery**	**Colliery**
Cooranbong	Lambton	Wyee
New Wallsend No. 2 (Gretley)	Teralba	
Moonee	Burwood	
Stockton Borehole	West Wallsend	
Newstan	John Darling	

The wide range of single longwall panel W/H ratios in the database was considered unique compared to the other Australian coalfields and enabled the study to focus on overburden and chain pillar behaviour effects separately.

Pillar extraction or multiple seam data was not used to produce the subsidence prediction curves, as it invariably makes the assessment of geological influences more difficult. Other NSW and QLD longwall and high pillar extraction mine data that have been added to the model database over the past 6 years are shown in **Table A2**.

Table A2 - Empirical Longwall Database Sources from Other Coalfields

Coalfield	Colliery	Colliery
Newcastle	West Wallsend	Newstan
	Tasman	
Hunter Valley	United	Wollemi
	Austar	
Southern	Berrima	Appin
	Elouera	Dendrobium
Western	Springvale	Angus Place
	Ulan	
Queensland	Cook	Oaky Creek
	Moranbah North	

In summary, the key features of the **ACARP, 2003** model are that it:

- Is derived from a comprehensive database of measured subsidence, strain, tilt and curvature above longwalls in the Newcastle, Hunter Valley, Western and Southern Coalfields.

- Has been validated with measured subsidence profile data over the past 6 years.

- Adds to the **DMR, 1987** model for the Newcastle Coalfield, as it addresses multiple panels and contains significantly more longwall data.

- Includes the effects of massive sandstone/conglomerate lithology on subsidence, based on the linking of borehole and subsidence data.

- Allows reliable predictions of maximum single panel subsidence, chain pillar subsidence, tilt, curvature, strain and the angle of draw within a 90% Confidence Interval.

- Enables 'greenfield' sites (i.e. where there is no subsidence data) to be assessed rapidly and accurately.

- Provides maximum subsidence predictions based on Upper 95% Confidence Limits (or 5% Probability of Exceedence limits), which in practice have rarely been exceeded.

  The confidence limits have been derived by the application of central limit theory and the likely normal distribution of residuals about lines of best fit or regression lines determined for the model database.

- Utilises historical information directly - predictions are based on actual data.

- Enables prediction of secondary tilt, curvature and strain magnitudes. Effects such as 'skewing' due to rapid surface terrain variations, surface 'hump' or step development and cracking can result in tilt, curvature and strain magnitudes significantly greater than predicted 'smooth' profile values.

  This issue has been addressed empirically by linking measured impact parameters with key mining geometry variables. Strain concentration factors and database confidence limits have been developed to estimate the likely range of subsidence impact parameters.

- Is amenable to subsidence contouring and allows the impacts on surface features to be assessed, including post-mining topography levels for watercourse impact assessment.

- Predictions of subsidence at specific locations can be done to provide an indication of likely subsidence magnitude; however, depending on the sensitivity of the feature, it may be prudent to adopt maximum predicted subsidence for a given panel.

- Incorporates an empirical model of sub-surface fracturing and far-field displacements.

Recent far-field horizontal displacement model work in the Newcastle Coalfield suggests the empirical model is conservative.

The following key input parameters are required to make subsidence predictions using the model:

- Panel Width (W)

- Cover Depth (H)

- Seam Working Height (T)

- Overburden lithology details, specifically the thickness and location of massive strata units (t, y).

- Chain Pillar Height (h), Width (w_{cp}) and Length (l) [solid dimensions]

- Roadway width

- Number of panels to be extracted

The statistical inferences and estimates of the model uncertainty associated with the prediction methodology are presented in the following sections.

A4 Single Panel Subsidence Predictions

A4.1 Geometrical Factors

The major finding of the **ACARP, 2003** project in regards to mining geometry was that the historical relationship between subsidence and panel width to cover depth ratio (W/H) is not a constant for the range of cover depths (H) involved.

Figure A2 shows the range of maximum subsidence that can occur above longwall panels with similar mining geomtries and a range of cover depths. The apparent differences between the DMR's Southern NSW and Newcastle Coalfield curves and laminated overburden theory (**Heasley, 2000**) also support the above finding.

For an overburden consisting of sedimentary rock layers, **Heasley, 2000** applied laminated beam theory by **Salamon, 1989** to form the basis of the pseudo-numerical subsidence prediction program LAMODEL ("LAyered MODEL" of overburden) that has been found to have reasonable success in the US Coalfields.

According to Lamodel theory, the maximum seam roof convergence (C_{max}) above a longwall panel of mining height (T), width (W) and cover depth (H), with an idealised overburden of uniform lamintation thickness (t), Youngs Modulus (E), unit weight (γ) and Poisson's Ratio (v) is:

$C_{max} = \sqrt{(12(1-v^2)/t)}\ (\gamma H/E)\ (W^2/4)$ or T (whichever is the lower value)

In terms of traditional empirical models of estimating subsidence, the above equation indicates that the maximum single panel subsidence is a function of $(W^2/t^{0.5})$, $(\gamma H/E)$ and T.

The **ACARP, 2003** model surmised that single panel subsidence was a function of W/H, γH/E or H, T, W/t and y/H. The first three parameters are related to panel geometry (Width, Cover Depth and Mining Height, whilst the last two parameters (strata unit thickness, t , and distance ,y, to the unit above the workings) infer geological influences of massive strata units (*Note: that the W/t parameter was incorrectly inversed in **ACARP, 2003***).

Based on the above, surface subsidence increases with increasing cover depth (H) for the same W/H ratio, and is primarily a function of the increasing panel width (W). For constant single panel width (W), subsidence will therefore decrease with increasing cover depth (H).

The subsidence data was subsequently separated into three cover depth categories of H = 100, 200 and 300 m +/-50 m and is presented in **Figures A3** to **A5**.

The influence of overburden lithology was found to be readily apparent, once the database was filtered using the above cover depth ranges.

A4.2 Geological Factors

Once the first stage in the development of the subsidence prediction model had addressed the influence of cover depth the effect of "significant" overburden lithology above single longwall / miniwall panels could be addressed.

Figure A6 illustrates a physical model, showing the subsidence reducing effects of a massive strata unit.

Borehole data was used to derive the thickness and location of massive strata units considered to be critically important for surface subsidence prediction, for a given panel width and depth. The methodology takes into account the maximum massive strata unit thickness (t) at each location and the height to the base of the unit above the longwall panel (y).

The subsidence above a panel, given cover depth (H) and panel width (W) decreases significantly when a massive strata unit is thicker than a certain minimum limit value. The thickness is also reduced when the unit is closer to the surface. The strata unit is considered to have a 'high' subsidence reduction potential (SRP) when it exceeds a minimum thickness for a given y/H ratio, as shown in **Figures A7.1** to **A7.3** for each cover depth category.

For a thin strata unit located relatively close to a panel, the 'Subsidence Reduction Potential (SRP) will be 'low'. However, there is also an intermediate zone, where a single strata unit (or several thinner units) below the 'high' subsidence reduction thickness can result in a 'moderate' reduction in subsidence. A second limit line can therefore be drawn, which represents the threshold between 'moderate' and 'low' SRP.
It is considered that the 'high' SRP limit line represents the point between elastic and yielding behaviour of a spanning beam. The 'moderate' SRP limit line represents the point between yielding behaviour and collapse or failure of a spanning beam (which has been yielding).

The limit lines have been determined for the strata units located at various heights (y) above the workings in each depth category, as shown in **Figures A8** to **A10**.

A4.3 Summary of Model Concepts

The **ACARP, 2003** model introduces several new parameters, to improve the definition of various types of overburden behaviour and the associated mechanics.

As outlined in **Section A4.2**, the 'Subsidence Reduction Potential' (SRP) of massive or thickly bedded geological units above single longwall panels for the Newcastle Coalfield has been introduced to describe the influence that a geological unit may have on subsidence magnitudes. The massive geological units are defined in terms of 'high', 'moderate' or 'low' SRP.

Massive unit thickness, panel width, depth of cover and height of unit above the workings are considered to be key parameters for assessing overburden stiffness and spanning capability over a given panel width, controlling surface subsidence. A conceptual model for overburden behaviour is illustrated in **Figure A11**.

Variation in subsidence along the length of a panel may therefore be due to the geometry and / or SRP variation of geological units within the overburden.

The database also indicates the presence of a 'Geometrical Transition Zone', whereby subsidence increases significantly regardless of the SRP of the geological units, as shown in **Figure A12**. This behaviour occurs when panel width to cover height ratio (W/H) ranges from 0.6 to 0.8. This phenomenon can be simply explained as a point of significant shift in structural behaviour and the commencement of overburden breakdown.

The model allows the user to determine the range of expected subsidence magnitudes and the location of geology related SRP and/or 'geometrical transition zones' along a panel. Identification of the transition zones is an important factor in assessing potential damage risks of differential subsidence to important infrastructure, buildings and natural surface features, such as rivers, lakes and cliff lines etc.

For W/H ratios <0.7, the overburden spans across the extracted panel like a 'deep' beam or linear arch, whereby the mechanics of load transfer to the abutments is governed by axial compression along an approximately parabolic shaped line of thrust, see **Figure A13**.

For W/H ratios >0.7 the overburden geometry no longer allows axially compressive structural behaviour to dominate, as the natural line of thrust now lies outside of the overburden. Bending action due to subsequent block rotation occurs. Provided that the abutments are able to resist this rotation, flatter lines of thrust still develop within the overburden, but the structural action is now dominated by bending action. This type of overburden behaviour has been defined as 'shallow' beam behaviour, which in structural terms is fundamentally less stiff than 'deep' beam behaviour. This results in a significant increase in subsidence or sag across an extracted longwall panel (all other factors being equal), as shown **Figure A13**.

"Voussoir beam" or "fractured linear arch" theory can be used to explain both types of overburden behaviour, as deep seated or flatter arches develop in the strata in an attempt to balance the disturbing forces.

The 'strata unit location factor' (y/H) was developed to assist in assessing the behaviour of massive strata units above the workings. The y/H factor is a simple way to include the influence of the unit location above the workings in terms of the effective span of the unit and the stresses acting upon it.

The key elements of this factor and their influence on the behaviour of the strata unit are:

- y, the height of the beam above the workings, which determines the effective span of the beam, and
- H, cover depth over the workings, which exerts a strong influence on the stress environment and, hence, the propensity for buckling or compressive failure of the beam.

Essentially beam failure due to the action of increasing horizontal stress (i.e. crushing or buckling) appears more likely as y decreases and H increases. The ratio of y/H may therefore be used to differentiate between the SRP of a beam of similar thickness, but at varying heights above the workings. The model also demonstrates that as the depth of cover increases, a thicker beam is required to produce the same SRP above a given panel width.

A5 Multiple Longwall Panel Subsidence Prediction

A5.1 General

The effect of extracting several adjacent longwall panels is governed by the stiffness of the overburden and the chain pillars left between the panels. Invariably, 'extra' subsidence occurs above a previously extracted panel and is caused primarily by cracking of the overburden and the compression of the chain pillars and adjacent strata between the extracted longwall panels.

A conceptual model of subsidence mechanisms above adjacent longwall panels in a single seam is shown in **Figure A14**.

A5.2 Predicting Subsidence above Chain Pillars (ACARP, 2003 Model)

A chain pillar undergoes the majority of life-cycle compression when subject to double abutment loading (i.e. the formation of goaf on either side, after two adjacent panels have been extracted). Surface survey data indicates that an extracted panel can affect the chain pillars of up to three or four previously extracted panels. The stiffness of the overburden and chain pillar system will determine the extent of load transfer to preceding chain pillars.

Multiple-panel effects have therefore been included in the model by adding empirical estimates of surface subsidence over chain pillars to the maximum subsidence predictions for single panels.

The empirical model presented in **ACARP, 2003** for estimating the subsidence above a chain pillar, was based on the regression equation presented in **Figure A15**. The model compares the ratio of chain pillar subsidence (Sp) over the extraction height (T), to the width of the chain pillar divided by the cover depth multiplied by the total extracted width (1000w/W'H).

A regression analysis on the data indicates a strong exponential relationship for 1000wcp/W'H values up to 0.543. For values > 0.543, the relationship becomes constant.

$S_p/T = 7.4044e–10.329F$ ($R^2 = 0.92$) for $F < 0.543$, and

$S_p/T = 0.023$ for $F > 0.543$

where

$F = 1000w/W'H$

W' = The total extracted width which includes the width of the panels extracted on both sides of the subject chain pillar, and the width of the chain pillar itself (i.e. W' = Wi + w(i) + Wi+1).

Note that the final subsidence for a longwall panel with several subsequent extracted panels was then determined empirically by adding 50% of the predicted chain pillar subsidence (S_p) to the single panel S_{max} estimate.

This approach however, did not include an abutment angle to estimate pillar loads, which are likely to vary significantly between sub-critical and supercritical panel layouts.

*The chain pillar model has now been amended to include better predictions of chain pillar load that are consistent with ALTS methodology (refer **ACARP, 1998a**) and has resulted in the modified version presented in Section A5.2.*

A5.2 Predicting Subsidence above Chain Pillars (DgS, 2008 Model)

After the **ACARP, 2003** model was published; further studies on chain pillar subsidence measurements were undertaken at several mine sites in the Western (Springvale, Angus Place and Ulan) and Southern Coalfields (Appin and Elouera). The measured subsidence above the chain pillars was significantly greater than the Newcastle Coalfield pillars and considered to be linked to the stress acting on the pillars and the longwall mining height.

Maximum subsidence above the chain pillars invariably occurred after the pillars were subject to double abutment loading conditions (i.e. goaf on both sides).

The **ACARP, 2003** model for estimating chain pillar subsidence was subsequently superseded by the pillar stress v. strain type approach presented in **Figure A16**. The chain pillar stress was estimated by assuming a design abutment angle of 21^o for the pillar load, according to the methodology presented in **ACARP, 1998a**.

Prediction of subsidence above the chain pillars (S_p) was determined based on the following regression equation using the mining height, T and pillar stress, σ:

$$S_p/T = 0.238469/(1+e^{-[(\sigma-25.5107)/7.74168]}) \qquad (R^2 = 0.833)$$

The uncertainty of the predictions was estimated by calculating the variance of the residuals about the regression lines and calculating 90% Confidence Limits for the database as follows:

$$90\%\ CL\ S_p\ error = 0.048T$$

It was also considered necessary to test if the above stress v. strain type approach was adequate for reliable predictions, by comparing the subsidence outcomes with the pillar Factor of Safety; see **Figure A17**.

The strength of the chain pillars was estimated using the rectangular pillar strength formulae presented in **ACARP, 1998b**. The FoS was derived by dividing the pillar strength by the pillar load (i.e. stress).

Generally it has been found that significant surface subsidence above the chain pillar (i.e. 10 - 30% of pillar height) starts to occur when the pillar FoS is < 2. For FoS values greater than 2, subsidence above the pillars is virtually independent of FoS and the pillars generally perform elastically under load.

The database indicates that when the FoS is < 2, the stiffness of the pillar starts to decrease, due to the development of load induced fracturing within the pillar. FoS values of < 2 represent pillar stresses that exceed 50% of the pillar strength. Laboratory testing of coal and sandstone samples also show sample 'softening' as the ultimate load carrying capacity of the sample is approached.

For pillars with FoS values < 1, the subsidence above the chain pillars tend to a maximum limit of approximately 25 to 30% of the mining height. This type of behaviour is expected for chain pillars that have width to height ratios w/h > 5, which is the point where 'strain hardening' deformation starts to develop with increased confinement of the 'pillar core'.

A5.3 Calculation of First and Final Subsidence for Multiple Longwall Panels

Multiple panel predictions can be made by adding the predicted single panel subsidence to a proportion of the chain pillar subsidence (including the residual subsidence) to estimate first and final subsidence above a given longwall panel.

The definition of first and final S_{max} is as follows:

First S_{max} = the total subsidence after the extraction of a longwall panel, including the effects of previously extracted longwall panels adjacent to the subject panel.

Final S_{max} = the total subsidence over an extracted longwall panel, after at least three more panels have been extracted, or when mining is completed.

First and final S_{max} values for a panel are predicted by adding 50% and 100% of the predicted subsidence over the chain pillars (i.e. between the previous and current panel) less the goaf edge subsidence (see **Section A5**).

Residual subsidence above chain pillars and longwall blocks tends to occur after extraction due to (i) increased overburden loading on pillars and (ii) on-going goaf consolidation or creep effects. Based on the final chain pillar subsidence measurements presented in **Figure A16**, the residual movements can increase subsidence by a further 10 to 30%.

An example of measured multiple longwall subsidence behaviour is presented in **Figure A18**.

Final subsidence is normally estimated by assuming a further 20% of the chain pillar subsidence will occur. However, this may be increased or decreased, depending on local experience.

The prediction of first and final subsidence originally presented in **ACARP, 2003** involved the use of several empirical coefficients, which have proven to be difficult to apply in practice. The interested may refer to this methodology, however, the above method is considered easier to apply and likely to result in a similar outcome.

In summary, the mean values of the first S_{max} and final S_{max} are calculated as:

First S_{max} = Single S_{max} + 0.5($S_{p(i-1)}$ - S_{goe})

Final S_{max} = First S_{max} + 1.2(Final $S_{p(i)}$ - First S_{goe})

The U95% Confidence Limits or Credible Worst Case Values are then:

U95% First S_{max} = mean First S_{max} + 1.64 (U95% S_{max} error + U95% S_p error)$^{1/2}$.

U95% Final S_{max} = mean Final S_{max} + 1.64 (U95% S_{max} error + U95% S_p error)$^{1/2}$.

A6 Subsidence Profile and Impact Parameter Predictions

Part of the **ACARP, 2003** project included the development of several models to predict the maximum panel deformation parameters and surface profiles associated with subsidence. The following models were developed:

- panel goaf edge or rib subsidence,
- angle of draw,
- maximum transverse and longitudinal tilt, curvature and strain,
- the locations of the above parameters over the longwall panel for the purposes of subsidence profile development, and
- heights of continuous and discontinuous fracturing above the longwall, based on measured surface tensile strains and fracture limit horizons over extracted panels (see **Section A7** for details).

A conceptual model of surface deformation profiles that develop above longwall panels is given in **Figure A19**.

All of the above subsidence parameters have been statistically linked to key geometrical parameters such as the cover depth (H), panel width (W), working height (T) and chain pillar width (w_{cp}) and shown in **Figures A20 to A27**.

A summary of all the empirical model relationships between the key subsidence profile parameters that were developed in **ACARP, 2003** and DgS are presented in **Table A3**.

Table A3 - Summary of Subsidence Impact Parameter Prediction Models Developed from ACARP, 2003

Parameter	Regression Equation and +/- 90% Confidence Limits or Upper95%CL	Coefficient of Determination (R^2)	Figure No.
Subsidence Reduction Potential (SRP) of Strata Unit in Overburden with thickness t, panel width, W and location factor, y/H above workings for Cover Depth Category	**High** SRP t for a given panel W plots above line for given strata unit y/H. **Moderate** SRP t plots between High SRP line and next y/H line below it. **Low** SRP t plots below Moderate SRP limit line.	N/A - curve location determined by successful re-prediction of >90% of cases I databases	**Figure A8** for H<150m; **Figure A9** for H< 250m; **Figure A10** for H< 350m
Single Maximum Longwall Panel Subsidence (Single S_{max}) for Assessed Strata Unit SRP of Low, Moderate or High	Upper and Lower bound prediction lines for a given SRP are used to estimate range of S_{max}/T for a given Panel W/H. Average of limit lines value is mean Single S_{max} value +/- 0.03T for W/H < 0.6; +/- 0.1T for 0.6<W/H<0.9; +/-0.05T for W/H>0.9	N/A - curve location determined by successful re-prediction of >90% of cases I databases	**Figure A3** for H<150m; **Figure A4** for H< 250m; **Figure A5** for H< 350m
Chain Pillar Subsidence, S_p (m)	Mean $S_p/T = 0.238469/(1+e^{-[(\sigma DAL-25.5107)/7.74168]})$ +/- 0.048T	$R^2 = 0.833$	**Figure A16**
Goaf Edge Subsidence	Mean $S_{goe}/S_{max} = 0.0722(W/H)^{-2.557}$ U95%CL $S_{goe}/S_{max} = 0.0719(W/H)^{-1.9465}$	$R^2 = 0.82$	**Figure A20**
Angle of Draw	Mean AoD = $7.646Ln(S_{goe})+32.259$ U95%CL = Mean AoD + 8.7^o	$R^2 = 0.56$	**Figure A21**
Maximum Tilt T_{max} (mm/m)	$T_{max} = 1.1925(S_{max}/W')^{1.3955}$ +/- $0.4T_{max}$ (W' = lesser of W and 1.4H)	$R^2 = 0.94$	**Figure A22**
Maximum Convex Curvature C_{max} (km^{-1})	Mean $C_{max} = 15.60(S_{max}/W'^2)$ +/- 0.5Mean	$R^2 = 0.79$	**Figure A23**
Maximum Concave Curvature C_{min} (km^{-1})	Mean $C_{min} = 19.79(S_{max}/W'^2)$ +/- 0.5Mean	$R^2 = 0.79$	**Figure A24**
Maximum Tensile Strain E_{max} (mm/m)	Mean 'smooth' $E_{max} = 5.2C_{max}$ +/- 0.5 Mean Mean 'Cracked' $E_{max} = 14.4C_{max}$	$R^2 = 0.72$ $R^2 = 0.32$	**Figure A25**
Maximum Compressive E_{min} (mm/m)	Mean $E_{max} = 5.2(C_{min})$ +/- 0.5 Mean Mean 'Cracked' $E_{min} = 14.4C_{min}$	$R^2 = 0.72$ $R^2 = 0.32$	**Figure A25**
Critical Panel Width	W_{crit} = 1.4H where H = cover depth	N/A	**ACARP, 2003**

Table A3 (Continued) - Summary of Subsidence Impact Parameter Prediction Models Developed from ACARP, 2003

Subsidence at Inflexion Point or Maximum Tilt STmax	Mean S_{Tmax}/S_{max} = -0.0925(W/H)+0.7356 +/- 0.2	R^2 = 0.5	**ACARP, 2003**
Distance to Inflexion Point, d/H	d/H = 0.2425Ln(W/H) + 0.3097	R^2 = 0.73	**Figure A27**
Distance to Peak Tensile Strain (mm/m)	d_t/H = 0.1643Ln(W/H) + 0.2203 for W/H >0.6; d_t/H = 0.2425Ln(W/H) + 0.2387 for W/H <0.6;	R^2 = 0.28	**Figure A27**
Distance to Peak Compressive Strain (mm/m)	d_c/H = 0.3409Ln(W/H) + 0.3996 for W/H >0.6; d_c/H = 0.2425Ln(W/H) + 0.3767 for W/H <0.6	R^2 = 0.59	**Figure A27**

* - If H within 25 m of depth category boundary, then average result with overlying or underlying depth category value.

- Centreline profile parameters are not presented here (refer to **ACARP, 2003**).

A7 Subsidence Profile Predictions above Longwall Panels

Predicted 'smooth' subsidence profiles above single and multiple longwall panels have been determined based on cubic spline curve interpolation through seven key points along the subsidence trough (i.e. maximum in-panel subsidence, inflexion point, maximum tensile and compressive strain, goaf edge subsidence, subsidence over chain pillars and 20 mm subsidence or angle of draw limit).

The locations of these points have been determined empirically, based on regression relationships between the variables and the geometry of the panels (see **Table A3**). Both transverse and longitudinal profiles have been derived in this manner.

First and second derivatives of the fitted spline curves provide 'smooth' or continuous subsidence profiles and values for tilt and curvature. Horizontal displacement and strain profiles were derived by multiplying the tilt and curvature profiles by an empirically derived constant associated with the bending surface beam thickness (based on the linear regression relationship between the variables, as discussed in **ACARP, 2003**).

An allowance for the possible horizontal shift in the location of the inflexion point (within the 95% Confidence Limits of the database) has also been considered, for predictions of subsidence at features located over the goaf or extracted area.

A8 Subsidence Contour Predictions above Longwall Panels

Subsidence contours can be derived with geostatistical kriging techniques over a 10 m square grid using Surfer 8® software and the empirically derived subsidence profiles along cross lines, centre lines and corner lines around the ends of the longwall panels. Vertical 'slices' may taken through the contours to (i) determine subsidence profiles along creeks or infrastructure, and (ii) assess the likely impacts on the relevant surface features.

A8.1 Subsidence Contours

Subsidence contour predictions have been made in this study using SPDS®, which is an influence function based model that firstly calculates seam convergence and pillar displacements empirically around the workings. The influence of an extracted element of coal is transmitted to the surface via a 3-D influence function, which also takes varying topography into account.

The model is usually calibrated to measured maximum subsidence values by adjusting key parameters such as influence angles and inflexion point location from extracted panel sides.

A8.2 Tilt and Curvature Contours

The predicted principal tilt and curvature contours were derived using the calculus module of the Surfer8® program and the predicted subsidence contours from the SPDS® runs. The subsidence contours were based on a 10 m grid.

Principal tilts (i.e. surface gradient or slope) were calculated by taking the first derivative of the subsidence contours in x and y directions as follows:

$$T_p = [(\partial s/\partial x)^2 + (\partial s/\partial y)^2]^{0.5}$$

where ∂s = subsidence increment over distances ∂x and ∂y along x and y axes.

Principal curvatures (i.e. rate of change in slope or surface bending) were calculated by taking the second derivative of the subsidence contours in x and y directions as follows:

$$C_p = [(\partial^2 s/\partial x^2)(\partial s/\partial x)^2 + 2(\partial^2 s/\partial x \partial y)(\partial s/\partial x)(\partial s/\partial y) + (\partial^2 s/\partial y^2)(\partial s/\partial y)^2]/pq^{2/3}$$

where $p = (\partial s/\partial x)^2 + (\partial s/\partial y)^2$ and $q = 1+p$

A8.3 Strain

Before predictions of strain can be made, the relationship between the measured curvatures and strain must be understood. As discussed in **NERDDP, 1993b** and **ACARP, 2003**, structural and geometrical analysis theories indicate that strain is linearly proportional to the curvature of an elastic, isotropic bending 'beam'; see **Figure A28**. This proportionality

actually represents the depth to the neutral axis of the beam, or in other words, half the beam thickness. **NERDDP, 1993b** studies returned strain over curvature ratios ranging between 6 and 11 m for NSW and Queensland Coalfields. Near surface lithology strata unit thickness and jointing therefore dictate the magnitude of the proportionality constant between curvature and strain.

ACARP, 2003 continued with this approach and introduced the concept of secondary curvature and strain concentration factors due to cracking. The peak strain / curvature ratio for 'smooth' subsidence profiles in the Newcastle Coalfield was assessed to equal 5.2 m (mean) and 7.8 m (U95%CL) with the possibility that surface cracking could increasing the 'smooth-profile' strains to 10 or 15 times the curvature. The above values may also be affected by the thickness of near surface geology.

Reference to **DMR, 1987** also suggests a curvature to strain multiplier of 10 for high pillar extraction and longwall panels in the Newcastle Coalfield.

Attempts by others to reduce the variability in strain and curvature data by introducing additional parameters, such as the radius of influence, r, by **Karmis et al, 1987** and cover depth, H, by **Holla and Barclay, 2000**, appear to have achieved moderate success in the coalfields in which they were applied. However, when these models were applied to the Newcastle Coalfield data presented in **ACARP, 2003**, the results did not appear to improve things unfortunately; see **Figures A29.1** and **A29.2**.

It is therefore considered that the variability in behaviour is probably due to other parameters, which are very difficult to measure (such as the thickness and flexural, buckling and shear strengths of the near surface strata).

Provided that the likelihood of cracking can be ascertained from the strain predictions, then appropriate subsidence management plans can still be implemented.

A9 Prediction Of Subsidence Impact Parameters And Uncertainty Using Regression Analysis Techniques

A9.1 Regression Analysis

Key impact parameters have been predicted using normalised longwall subsidence data from the Newcastle Coalfield. This approach allows a reasonable assessment of the uncertainty involved using statistical regression techniques. A linear or non-linear regression line has been fitted to the database for each impact parameter, normalised to easily measured parameters, such as maximum subsidence, panel width and cover depth. The quality or significance of the regression line is influenced by the following parameters:

(i) the size of the database,

(ii) the presence of outliers, and

(iii) the physical relationship between the key parameters.

The regression curves were reviewed carefully, as such curves can be (i) affected by outliers, and (ii) misleading, in that by adopting a mathematical relationship which gives the best fit (i.e. R^2) the curves are controlled by the database and may not reflect the true underlying physical dependencies or mechanisms that the data represents.

These issues are inherent in all prediction modelling techniques because, for example, all models must be calibrated to field observations to validate their use for prediction or back analysis purposes.

The regression techniques presented in the **ACARP, 2003** was done by firstly assessing conceptual models of the mechanics and key parameter dependencies (based on established solid mechanics and structural analysis theories), before generating the regression equations.

Several outliers in the model databases were excluded in the final regression equations, but only when a reasonable explanation could be given for each anomaly (i.e. multiple seam subsidence, geological faults and surface cracking effects).

The regression equations in **ACARP, 2003** have R^2 (i.e. Coefficients of Determination) values generally greater than 50%; indicating that the relationships between the variables are significant. For cases where the R^2 values are < 50%, the regression lines are almost horizontal (i.e. the parameter doesn't change significantly over the range of the database), and the use of the regression line will be close to the mean of the database anyway.

A9.2 Prediction Model Uncertainty

The level of uncertainty in the model predictions has been assessed using statistical analysis of the residuals or differences between the measured data and regression lines (i.e. lines of best fit). The *Standard Error* of the prediction has been derived from the

residuals, which has then been multiplied by the appropriate 'z' or 't' statistic for the assumed normal probability distribution, to define Upper (and Lower) Confidence Limits.

The residual population errors for single panel subsidence are shown in **Figure A30**.

The empirical database therefore allows an assessment of variance and standard error such that the required subsidence parameter's mean and upper 95% Confidence Limit (Credible Worst Case) values can be determined for a given mining geometry and geology.

Provided there are (i) more than 10 data points in the data sets covering the range of the prediction cases, and (ii) the impact parameter and independent variables have an established physical relationship based on solid or structural mechanics theories, then it is considered unlikely that the regression lines will be significantly biased away from the underlying physical relationship between the variables by any limitations of the data set.

On-going review of each of the regression equations over the past six years by DgS has not required significant adjustment of the equations to include new measured data points. The regression equations derived are also amenable to spreadsheet calculation and program automation.

It is also important to make the distinction between the terms confidence *limit* and confidence *interval*. The Credible Worst Case terminology used in the model is **not** the upper limit of the 95% Confidence **Interval** - which would encompass 95% of the data. Since the lower 95% Confidence Limit is rarely used in practice, it was considered appropriate to adopt the 5% Probability of Exceedence values instead (this by definition represents the upper limit of the **90% Confidence Interval**).

Further, the term *Upper 95% Confidence Limit* used in the **ACARP, 2003** model is considered acceptable in the context of 'one-tailed' probability distribution limits (i.e. the Lower 95% Confidence Limit is generally of little practical interest).

A10 Subsidence Model Validation Studies

A10.1 Model Development

The **ACARP, 2003** model was developed such that the outcomes would re-predict > 90% of the database. Validation studies also included comparison of measured and predicted subsidence, tilt and strain profiles above several longwall panel crosslines and centrelines. Examples of predicted and measured profiles above multiple panels for the Newcastle Coalfield are shown in **Figures A31** to **A34** using the **ACARP, 2003** model. Subsequent predictions v. measured subsidence profiles are presented in **Figures A35** to **A38** using the updated version of the model discussed herein.

DgS is usually required to review predicted v. measured subsidence profiles after the completion of a longwall panel and report the results to DPI . Over the past six years, the model has generally over predicted measured subsidence, with the data falling somewhere between the mean and U95%CL values.

The predictions of curvature and strain, however, are generally problematic due to the common effects of discontinuous or cracking behaviour (i.e. lithological variation and cracking), resulting in measured strains that can be two to four times greater than predicted 'smooth' profile strains. This issue is discussed further in **Section A10.2**.

A10.2 Field Testing of Strain Predictions

Strain and curvature concentrations can increase 'smooth' profile strains by 2 to 4 times in the Newcastle Coalfield, when the panel width to cover depth ratio (W/H) exceeds 0.8 or radius of curvature is less than 2 km, see **ACARP, 2003**.

In the context of subsidence surveys, the definition of strain is the change in length (extension or compression) of a bay-length, divided by the original value of the bay length.

Where cracking occurs, measured strains will be highly dependent on the bay-length, and where rock exposures exist with widely spaced or adversely orientated jointing exist, much larger crack widths (than for the deep soil profile case) can occur.

For example, for a measured strain of 3 to 6 mm/m along a recently observed cross line above a longwall panel in the Newcastle area, several cracks developed in the soil surface, which ranged in width between 10 and 30 mm, whilst within 10 m of the area, a single 100 mm wide crack developed in a sandstone rock exposure of medium strength and with widely spaced jointing, see **Figure A39**.

At the moment, it is not possible to predict the magnitude of strains accurately, however, it is possible to make reasonable predictions that strains > 2 mm/m will cause cracking within the tensile strain zones and shearing, buckling within the compressive zones above a longwall with shallow surface rock. The strains and cracking can therefore be managed effectively by assuming cracks will occur and may need to be repaired after each longwall is completed.

A11 Sub-Surface Fracturing Model Development Outcomes

A11.1 Whittaker and Reddish Physical Model

It is considered that the published physical modelling work in **Whittaker and Reddish, 1989** provides valuable insight into the mechanics of sub-surface fracturing over longwall panels. The outcomes included specific guidelines (over and above such work as the Wardell Guidelines) for the prevention of inundation of mine workings beneath surface and sub-surface water bodies.

Their model was developed in response to the water ingress problems associated with early longwall extraction at the Wistow Mine in Selby, UK. The longwall panel was located at 350 m depth and experienced groundwater inflows of 121 to 136 litres/sec when sub-surface fracturing intersected a limestone aquifer 77 m above the seam.

The model identifies two distinct zones of fracturing above super-critical width extractions (continuous and discontinuous fracturing) and relates the height of each to "measured maximum tensile strain at the surface". As such, its use is also based upon being able to make credible subsidence predictions. The basis of the model is summarised in **Figure A40**.

The definition of the extent of 'continuous' fracturing refers to the height at which a direct connection of the fractures occurs within the overburden and the workings; it represents a 'direct' hydraulic connection for groundwater inflows.

The definition of the extent of 'discontinuous' fracturing refers to the height at which the horizontal permeability increases as a result of strata de-lamination and fracturing. Direct connection of fractures within the overburden and workings is still considered possible, but will depend on the geology (e.g. massive units and / or the presence of persistent vertical structure, such as faults and joints).

A review of the methodology applied to develop the model and its key features are summarised below:

- The model was based on laboratory experiments of longwall extraction physical models.

- The physical model was constructed from multiple layers of coloured sand and plaster fixtures, with sawdust bond breakers placed between each successive layer. The model was initially devoid of vertical joints.

- The scale and mechanical properties of the model satisfied dimensional analysis and similtude laws.

The model was used to simulate the overburden behaviour of a panel with a W/H ratio of 1.31 and a progressively increasing working height range that commenced at 1.2 m and finished at 10.8 m. The advancing longwall face was simulated by removing timber blocks at the base of the model in 1.2 m to 2.0 m lift stages.

The extent or heights of 'continuous' and 'discontinuous' fracturing above the longwall 'face' was measured and plotted with the associated peak tensile strain predictions at the surface.

The fracturing path progressed up at an angle from the solid rib and inwardly towards the centre of the panel; see **Figure A40**.

The fracturing in question occurred close to the rib-side only, as fracturing in the overburden above the middle portion of the panel tended to 'close' and did not appear to represent an area in which groundwater inflows into the workings would be generated.

Any inflow conditions were therefore considered to be "mainly associated with the longwall rib-side fracture zone [or tensile strain zone]".

A case study at Oaky Creek Colliery in the Bowen Basin was presented in Colwell, 1993; this attempted to calibrate the Whittaker and Reddish model with actual drilling and strain measurement data. Three fully cored boreholes were drilled over previously extracted longwall panels with a W/H ratio of 2.11 and strain measurement data was obtained from a nearby operating panel with a W/H of 1.37. The results of the study were very positive and have been subsequently collated with further case histories in **Section A8.2**.

A11.2 Preliminary Sub-Surface Fracturing Prediction Model For Australian Coalfields

The database of drilling data from previously published documents is summarised ACARP, 2003. Australian data was initially plotted with the UK Model results and a regression analysis was used to define a convenient relationship between the parameters and assessing whether other parameters of significance could be identified.

The results are presented in **Figure A41** and summarised below:

{A-Line} $A = a/H = 0.2077\ \mathrm{Ln}(E_{max}) + 0.150$, $R^2 = 0.44$

{B-Line} $B = b/H = 0.1582\ \mathrm{Ln}(E_{max}) + 0.651$, $R^2 = 0.49$

where

a, b = height above workings to A and B Horizons,
H = cover depth,
E_{max} = the maximum predicted tensile strain for a 'smooth' profile,

The Australian database appears to be similar to the Whittaker and Reddish model, however the predicted surface strains are much lower for a given height of 'continuous' and 'discontinuous' fracturing above the workings. It is also apparent that the model relies on the measured surface strain data, which has been noted previously for its high variability.

To overcome this issue it was decided to re-plot the database using the previously derived S_{max}/W^2, term to provide a readily measurable field parameter that would not be compromised by surface strain concentration effects. The revised regression results are shown in **Figure A42** and summarised below:

{A-Line} $A = a/H = 0.2295 \text{ Ln}(S_{max}/W'^2) + 1.132$, $R^2 = 0.44$;

{B-Line} $B = b/H = 0.1694 \text{ Ln}(S_{max}/W'^2) + 1.381$, $R^2 = 0.46$;

where

a, b = height above workings to A and B Horizons,
H = cover depth (m).
S_{max}/W'^2 = Overburden Curvature Index,
W' = lesser of W and 1.4H

Based on the alternative approach, the same apparent differences still remain between the Australian height of fracturing database and the UK physical modelling results. The apparent discrepancies between the model and measured values indicate that there are fundamental differences present (i.e. in particular the physical model had no preexisting subsurface fracturing present).

The A and B horizons in the sub-surface fracturing model presented in **Whittaker and Reddish, 1989** also appear to be the similar in regards to definition to the heights to the top of the 'Fractured Zone' and 'Constrained Zone' above an extracted longwall panel defined in **Forster, 1993**. There is also a departure in this model from assessing heights of fracturing based on the extraction height only, although the predicted tensile strain or S_{max} is directly related to the extraction height. It is considered that sub-surface fracture heights are a function of overburden bending and therefore primarily a function of the significant geometrical parameters Smax, W, H and T. The influence of massive lithology is included in the Smax prediction.

Overall, the **ACARP, 2003** sub-surface fracturing model was considered preliminary, more drilling data was required. The heights of fracturing derived, however, did appear to be conservative based on reference to several NSW and Queensland case studies.

It was also noted in **ACARP, 2003** that future calibration work on the model would be required to improve confidence in its use.

A11.3 Influence of Geology on Sub-Surface Fracture Heights

For the purposes of study completeness, an assessment was made on whether the geology had the potential to control or limit the height of fracturing above a longwall panel. Reference to the database presented in **ACARP, 2003**, indicates that two of the case studies were assessed to have High SRP and had A Horizons that coincided with the base of the massive strata units. The other data points had low SRP with no massive units present.

The massive strata unit affected data, however, did not appear to plot at lower than predicted levels compared to the low SRP cases, although this observation was based on a small sample of data. At this stage, the potential for a spanning strata unit to mitigate the height of continuous fracturing above the workings cannot be ignored.

Overall, the results suggest that the presence of massive sandstone or conglomerate lithology could control the height of direct hydraulic fracturing. Due to the complex nature of this problem, it is usually recommended that a mine undertake a sub-surface fracture-monitoring program, which includes a combination of borehole extensometer and piezometer measurements during extraction in non-sensitive areas of the mining lease. Mitigation strategies for longwall mining are generally limited to (i) reducing the extraction height and (ii) decreasing the panel width.

A12 Far-Field Displacements and Strain Predictions

A12.1 Background

The term far-field displacements (FFD) generally refer to the horizontal surface movements that occur outside the vertical subsidence limit or angle of draw to an extracted pillar panel or longwall block. It is currently understood that FFDs are a phenomenon caused by the reduction of horizontal stress when collapse of overburden rock (i.e. goafing) occurs above an extracted area. There also appears to be a strong correlation between the FFDs and the surface subsidence magnitude (which is also an indicator of horizontal stress relief). A conceptual model of the mechanics of FFDs is presented in **Figure A43**.

Horizontal stress in rock is normally greater than the vertical stress at a given depth of cover; it has been 'locked' into the strata by tectonic movements and over-consolidation pressures (i.e. stress). Over-consolidation stresses occur in sedimentary rock after uplift and erosion over millennia has gradually removed the overlying material since the time of formation. Tectonic induced stress usually results in strong directional bias between the major and minor principal stress magnitudes, with variation due to stiffness of the lithological units as well (refer to **Nemcik et al, 2005**, **Pells, 2004**, **McQueen, 2004, Enever, 1999** and **Walker, 2004**).

It is considered that both of the abovementioned horizontal stress development mechanisms are likely to be present in the near surface rocks in the western area of the Newcastle Coalfield.

FFD's have only recently become an issue in the Newcastle Coalfield because of adverse surface impact experiences in the Southern Coalfield (e.g. horizontal movements of around 25 mm have been measured over 1.5 km away from extracted longwall panels on a concrete dam wall. No cracking damage occurred to the dam wall because of these movements however).

The strains associated with FFDs are usually very low, however, there is one case in the Southern Coalfield where a bridge was subject to lateral shearing of approximately 50 mm along the river bed axis.

To-date, it is understood that there are no precedents in the Newcastle Coalfield where similar FFD effects (measured or inferred via damage) have occurred around longwalls or total extraction panels. Horizontal movements have been measured outside the angle of draw limits from mine workings however, albeit at smaller distances and magnitudes (eg. 20 mm of horizontal movement has been measured in undulating terrain at 250 m from one longwall block where the cover depth was 135 m).

The horizontal stress in the Newcastle Coal Measures has been measured at several locations along the F3 Freeway to the west of Wyong and Newcastle (**Lohe and Dean-Jones, 1995**). The magnitude of the measured horizontal stress indicates that it is relatively high, with magnitudes that are 1.5 to >5 times the vertical stress, in relatively flat or moderately undulated terrain.

The major principal horizontal stress is usually orientated N to NE in the Western Newcastle Coalfield, but it can be re-orientated parallel to the axis of a ridge due to natural weathering processes near the surface (which cause lateral unloading towards the gullies); refer to **Lohe and Dean Jones, 1995**.

A12.2 Insitu Stress Field

Reference to stress measurement data in **Lohe and Dean-Jones, 1995** indicates that the 'shallow' (ie < 100 m below the surface) regional stress field in the undulating terrain along the eastern and eastern sides of Lake Macquarie is likely to have it's major principal horizontal stress > 5 x vertical stress (and assuming horizontal stress is zero at the surface). Deeper strata at depths > 150 m is likely to have it's major principal horizontal stress <2 x vertical stress.

The stress data from the above reference was measured using over-coring / HI-Cell techniques and is presented in Table A4.

Table A4 - Horizontal Stress Field Measurements in Newcastle Coalfield Relevant to Tasman

Location	Depth (m)	In-situ Stress Measurements*			
		Major Sigma 1 (MPa)	Minor Sigma 2 (MPa)	Vertical Sigma 3 (MPa)	Sigma1+/ Sigma 3
Wakefield	24	10.4	0.42	0.6	17.3
Wallsend Borehole	100	13.3	9.7	2.5	5.3
West Wallsend No. 2	190	27.4	20.3	4.75	5.8
Kangy Angy	70	11.8	4.2	1.75	6.7
Moonee	90	11.7	8.3	2.25	5.2
West Wallsend	170	6.4	n/a	4.25	1.5
Ellalong	320	6.5	4.6	8.0	0.8

* - All measurements in medium strength sandstone.
+ - ratio assumes horizontal stress is zero at the surface (which is not always correct).

The shallow stress data is plotted in **Figure A44** and indicates that the major principal horizontal stress could be as high as 6 MPa at the surface (unless weathered rock and soil is present) with the Major and Minor Principal Horizontal stresses equal to approximately 4 times the vertical stress for depths up to 250 m.

This high Sigma 1 reading, however, may be associated with a sandstone / conglomerate ridgeline and not typical for the areas away from ridgelines (although a residual 'surface' horizontal stress range from 1.5 to 6.5 MPa has also been assessed for the Sydney Metropolitan area in **McQueen, 1999** and **Pells, 2002**).

Another commonly used assumption in the NSW Coalfields is that the major principal horizontal stress is approximately 2 x the vertical stress and the minor principal horizontal stress is 1.4 ~ 1.5 x the vertical stress (or the Major Principal Horizontal Stress is 1.33~1.4 x

the Minor Principal Horizontal Stress). It is also acknowledged that the horizontal stress in the Newcastle and Sydney areas can be 4 to 5 times the vertical stress, based on shallow rock mass data at depths < 50 m; refer to **Lohe and Dean Jones, 1995**. The sources of this stress field imbalance has been explained in **Enever, 1999**, **Pells, 2002** and **Fell *et al*, 1992** as being due to:

(i) the 'overconsolidation' ratio; where the vertical pressure due to ancient surface at the time of consolidation has since been eroded away, leaving a 'locked' in horizontal stress component in today's sedimentary rock mass. The OCR can be shown to decrease exponentially with depth and is equal in all directions at a given point.

(ii) Tectonic strain; where crustal plate movements apply a strain to the rock mass and the resultant stress is dependent on the stiffness of the individual beds and direction of movement.

(iii) Geological structure (faults/dykes); where discontinuities can change the magnitude and orientations of the regional stress field significantly.

(iv) Topographic relief (ridges/valleys/gorges); where the magnitude and direction of the regional stress field can vary due to geometric affects.

The influence of underground mining can also result in changes (both increases and decreases) in horizontal and vertical stress field magnitudes as the rock mass adjusts to a new equilibrium state.

Based on the measured stress conditions, the horizontal stress magnitudes may be estimated based on the equations presented in **Nemcik et al, 2005**:

$\sigma_H = K\sigma_v + E\varepsilon = \sigma_v [(\upsilon/1-\upsilon)OCR] + E\varepsilon$

$\sigma_h = f(\sigma_H)$ and $\sigma_v = 0.025H$ (MPa)

where,

σ_H = Major Horizontal Principal Stress;

σ_h = Minor Horizontal Principal Stress;

σ_v = Vertical Stress;

υ = Poisson's Ratio (normally ranges between 0.15 and 0.4 in coal measure rocks);

$(\upsilon/1-\upsilon)$ = Horizontal to vertical stress ratio factor (K_o) due to Poisson's Ratio effect on its own;

OCR = The over-consolidation ratio, which relates vertical pre-consolidation pressure (σ_{vo}) with current vertical pressure (σ_v) as follows, $OCR = \sigma_{vo}/\sigma_v = H_o/H$.

(*Note: This is an additional term that has been introduced by DgS, and has been mentioned (but not derived) in* **Pells, 2002** *and calculated in* **Fell et al, 1992**).

E = Young's Modulus for rock-mass unit;

ε = Tectonic Stress Factor (TSF) or Tectonic Strain.

Due to the wide range of horizontal stress values noted in the literature, it is recommended that the horizontal stress magnitudes be measured in-situ at several lithological horizons before high extraction mining commences.

Based on the apparent complexity and large variation between the interpretations of published stress field data, it was considered necessary to conduct a sensitivity analysis on the stress field profiles during the calibration of Map-3D® using the flat terrain data (see **Section A12.3** for details).

Total horizontal displacement measurements outside the ends and corners of several longwall panels in the Newcastle Coalfield (Newstan and West Wallsend Collieries), have been plotted against distance from the panel goaf edge / cover depth at the panel; refer to **Figure A45**.

Curves of best fit have been fitted to identify data trends from various locations from the ends and corners of the panels (note: the movements outside the corners of a longwall are typically smaller than the panel ends). The data has been obtained using GPS / EDM traverse techniques with quoted accuracy limits of +/- 7 to 10 mm.

The data in **Figure A45** has also been normalised to maximum measured subsidence (S_{max}) above a given panel and is presented in **Figure A46**. It is considered that presenting the data in this format allows all of the available data to be used appropriately to make subsequent FFD predictions.

The data presented in **Figures A47** was measured from the sides of several longwall panels using in-line, steel tape measurements. This method is considered more accurate than the EDM techniques, however, they do not capture all of the displacement. The measured values have subsequently been adjusted to absolute movements, based on the EDM measurements presented in **Figures A45** and **A46**.

A combined graph of normalised total displacement data from the ends and sides of the longwall panels is presented in **Figure A48** with worst-case design curves from ends, corners and sides of a longwall panel for flat terrain conditions.

The empirical models may be used for calibrating the numerical models input parameters when proposed mining layouts and topographical conditions are considered to be well outside the available database (see **DgS, 2007**).

A12.3 Numerical Far-Field Displacement Modeling

The numerical modelling program Map-3D® has been applied at several mines in the Newcastle Coalfield to-date for the purposes of estimating FFD movements. The model was chosen mainly due to its suitability for modelling large-scale rock masses.

The program is a 3-dimensional elastic, isotropic, boundary-element model, which essentially starts with an infinite solid space and calculates the effects of excavations, geological structure, varying material types, and free-surfaces on the regional stresses and strains. Further details about the software can be found at the Map-3D® web site.

The model is firstly calibrated to measured displacement data for a given mining geometry, regional horizontal stress field and surface topography. The Young's Modulus or stiffness of the overburden is then adjusted above an extracted panel (or panels) and assumed caving zone until a reasonable match is achieved.

Although the empirical models indicate that subsidence is a key parameter for predicting FFDs, numerical modelling of horizontal stress relief effects does not require the subsidence above the panels to be matched (by the model) because the extraction of coal and subsequent goafing behaviour can be calibrated to measured far-field displacements instead. Therefore, the modelling outcomes are not linked to the modelled subsidence directly.

Non-linearity can be introduced into the model to analyse the effects of fault planes and bedding using displacement-discontinuity elements with normal and shear stiffness and Mohr-Coulomb friction and cohesive strength properties.

Multiple mining stages and irregular topography can also be defined to enable mechanistic extrapolation of existing empirical databases with a reasonable degree of confidence.

An example of a predicted far-field displacement pattern around a high extraction pillar panel mine is presented in **Figure A49**.

A12.5 Empirical Strain Prediction Model

Strain measurements from the side of several longwall panels from West Wallsend and Newstan Collieries and were also normalised to maximum panel subsidence. The data are presented in **Figure A50**.

Several curves are shown with the data in the above figure, one is the best-fit or mean curve and two are upper limit confidence limit curves for the data (U95%CL and U99%CL). The confidence limit curves have been defined using weighted non-linear statistical techniques and the residual errors about the mean curve.

A13 References

ACARP, 1998a. **Chain Pillar Design (Calibration of ALPS)**. ACARP Project No. C6036, Colwell, M. Colwell Geotechnical Services.

ACARP, 1998b, **Project No. C5024, Establishing the Strength of Rectangular and Irregular Pillars**. J.M.Galvin, B.K. Hebblewhite, M.D.G. Salamon and B.B.Lin. School of Mining, UNSW.

ACARP, 2003. **Review of Industry Subsidence Data in Relation to the Impact of Significant Variations in Overburden Lithology and Initial Assessment of Sub-Surface Fracturing on Groundwater**. ACARP Project No. C10023. S. Ditton and R. Frith, Strata Engineering Report No. 00-181-ACR/1.

Colwell,1993. **Water Inflow Investigation for a Longwall Operation**. M. Colwell. Published in Queensland Coal Geology Groups Conference Proceedings, New Developments in Coal Geology, Brisbane.

DgS, 2007. **Prediction of Far-Field Displacements Due to Pillar Extraction or Longwall Mining in Mountainous Terrain**. S. Ditton. Proceedings of the 7th Triennial MSTS Conference on Mine Subsidence, University of Wollongong (November 26-27)

DMR, 1987. **Mining Subsidence in NSW: 2. Surface Subsidence Prediction in the Newcastle Coalfield**. L. Holla. Department of Minerals Resources (June).

Enever, 1999. **Near Surface In-situ Stress and its Counterpart at Depth in the Sydney Metropolitan Area**. Enever, J.R. Published in Australian Geomechanics Society (AGS) Conference Proceedings of the 8th Annual Conference on Geomechanics, Hobart.

Fell *et al*, 1992. **Geotechnical Engineering of Embankment Dams**. Fell, R., MacGregor, P. and Stapledon, D.A.A. Balkema.

Forster, 1995. **Impact of Underground Coal Mining on the Hydrogeological Regime, Central Coast, NSW**. I.R. Forster. Published in Australian Geomechanics Society (AGS) Conference Proceedings (February), Engineering Geology of Newcastle – Gosford Region, University of Newcastle.

Holla and Barclay, 2000. **Mine Subsidence in the Southern Coalfield**. L.Holla and E.Barclay. Department of Minerals Resources (June).

Karmis, et al, 1987. **Surface Deformation Characteristics Above Undermined Areas: Experiences from the Eastern United States Coalfields**. M. Karmis, A. Jarosz, P. Schilizzi & Z. Agioutantis. Published in Civil Engineering Transactions Journal, Institution of Engineers, Australia.

Lohe and Dean-Jones, 1995. **Structural Geology of the Newcastle-Gosford Region**. E.M. Lohe and G.L. Dean-Jones. Published in Australian Geomechanics Society (AGS)

Conference Proceedings (February), Engineering Geology of Newcastle – Gosford Region, University of Newcastle.

McQueen, 2004. **In-situ Rock Stress and Its Effect in Tunnels and Deep Excavations in Sydney**. McQueen. L.B. Article presented in Australian Geomechnics Journal Vol 39. No. 3 (September).

Nemcik et al, 2005. **Statistical Analysis of Underground Stress Measurements in Australian Coal Mines**. Nemcik, J., Gale, W. and Mills, K. Published in proceedings of the Bowen Basin Geology Symposium.

Pells, 2002. **Developments in the Design of Tunnels and Caverns in the Triassic Rocks of the Sydney Region**. International Journal of Rock Mechanics and Mining Sciences No. 39. Pells, P.J.N.

Pells, 2004. **Substance and Mass Properties for the Design of Engineering Structures in the Hawkesbury Sandstone**. Article presented in Australian Geomechnics Journal Vol 39. No. 3 (September).

Walker, 2004. **Stress Relief on Hillsides and Hillside Excavations**. Walker, B.F. Article presented in Australian Geomechnics Journal Vol 39. No. 3 (September).

Whittaker & Reddish, 1989. **Subsidence, Occurrence, Prediction and Control**. B. N. Whittaker and D.J. Reddish. Department of Mining Engineering, University of Nottingham, UK.

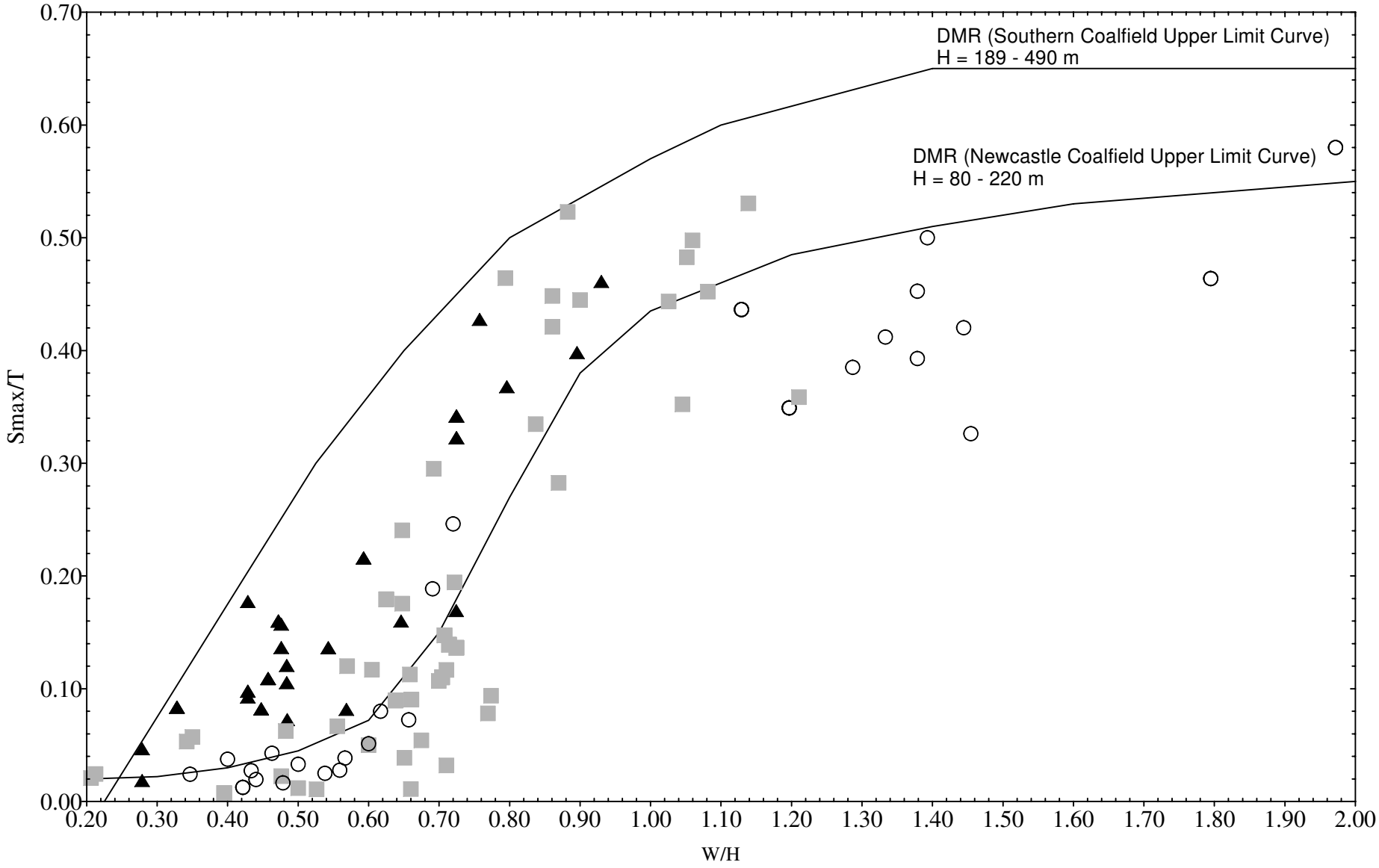

LEGEND
Cover Depth, H (m)
- ○ H = 70m to H = 151m
- ■ H = 151m to H = 251m
- ▲ H = 251m to H = 350m

DgS

Ditton Geotechnical Services Pty Ltd

Engineer:	S.Ditton
Drawn:	S.Ditton
Date:	08.06.08

Client:	Adapted from ACARP, 2003
Title:	Project Database and DMR Subsidence Prediction Curves for Single Longwall Panels in Newcastle Coalfield
Scale:	NTS
Figure No:	A1

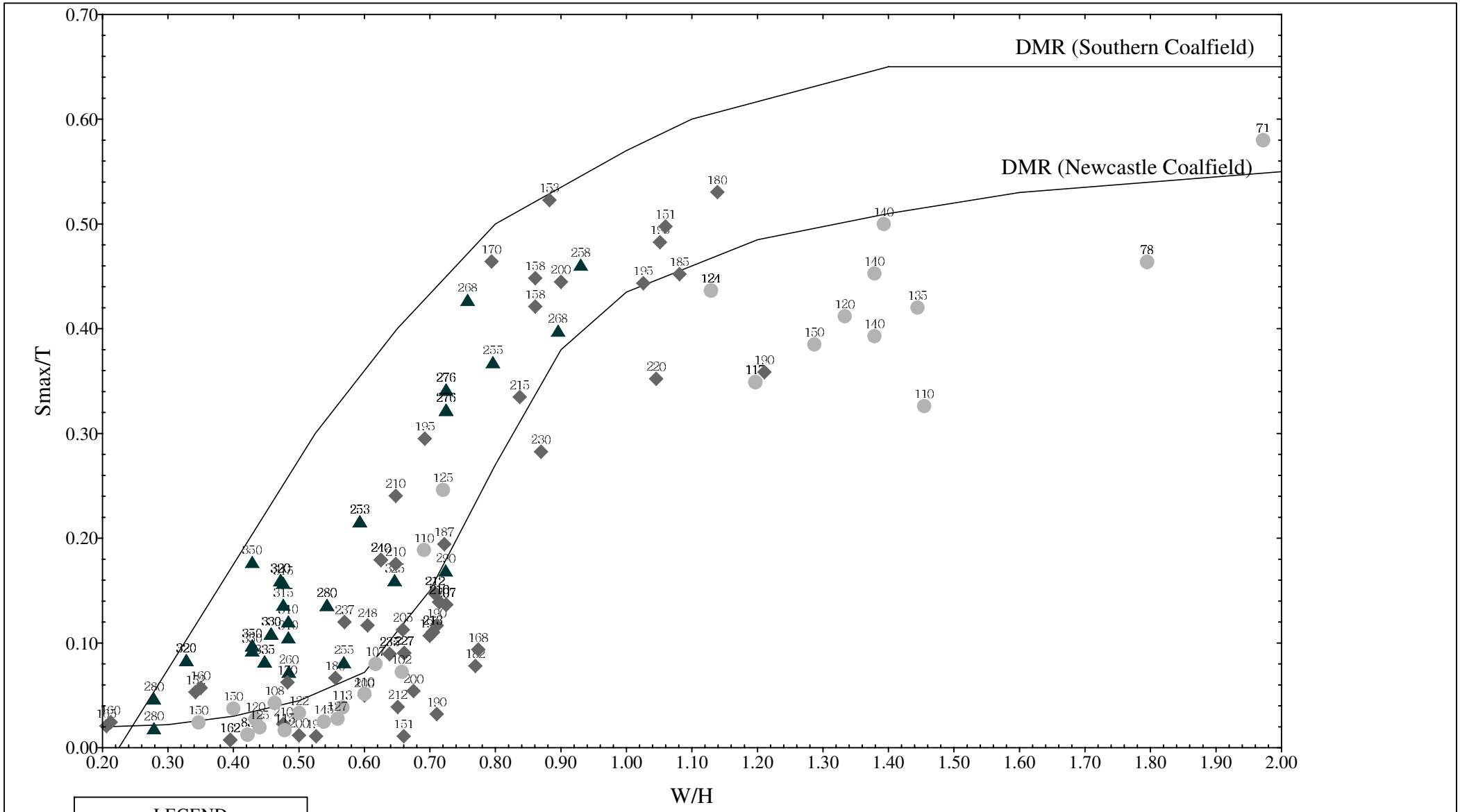

LEGEND
Data Point
Cover Depth, H (m)

- H = 70m to H = 151m
- H = 151m to H = 251m
- H = 251m to H = 350m

DgS

Ditton Geotechnical Services Pty Ltd

Engineer:	S.Ditton
Drawn:	S.Ditton
Date:	08.06.08

Client:	Adapted from ACARP, 2003
Title:	Project Database for Single Longwall Panels in Newcastle Coalfield showing Cover Depth for Each Point
Scale:	NTS
Figure No:	A2

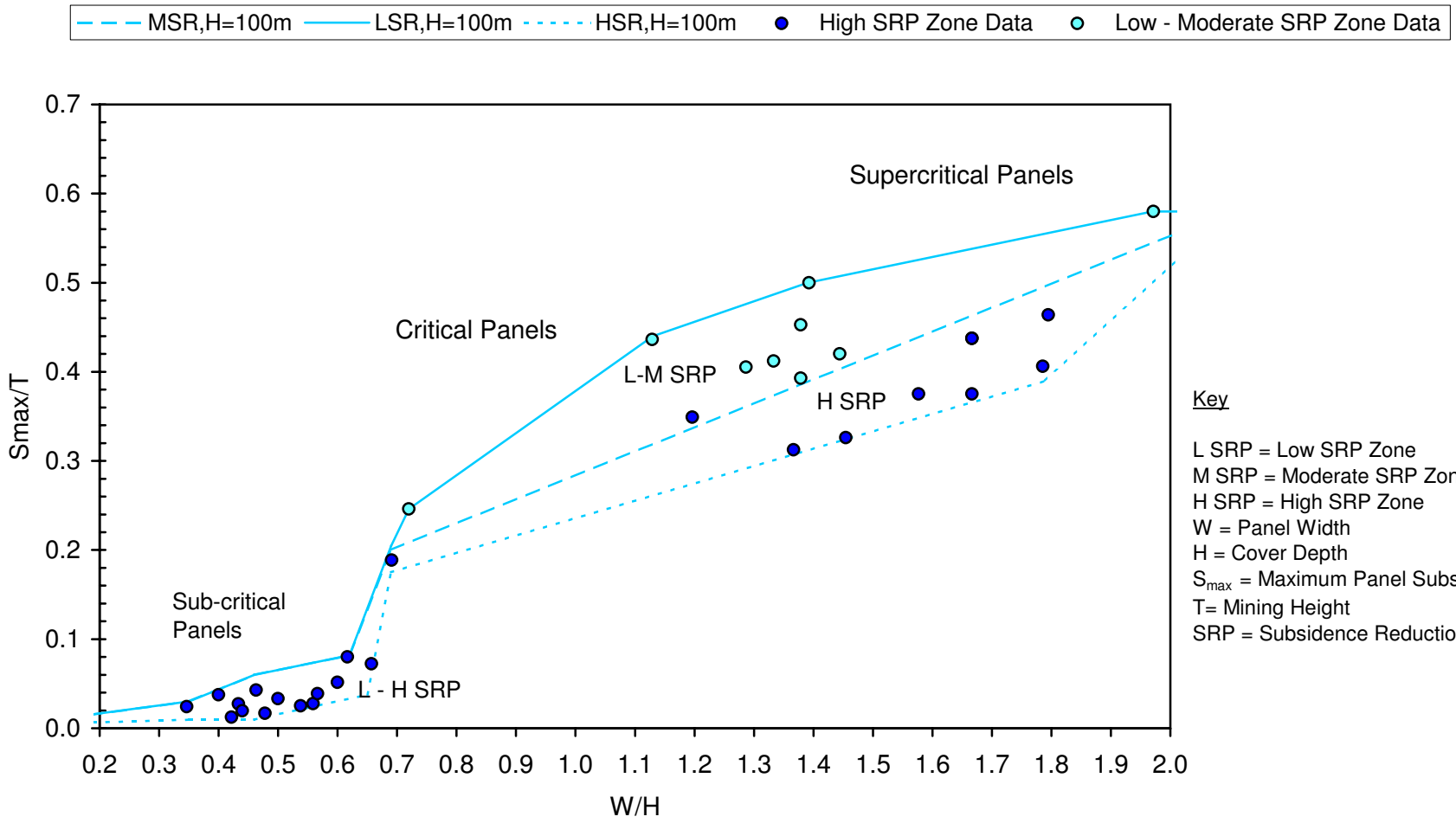

Note: No SRP distinguishment for panels with W/H<0.65

DgS	Engineer:	S.Ditton	Client:	Adapted from ACARP, 2003	
	Drawn:	S.Ditton			
	Date:	08.08.08	Title:	Empirical Model for Predicting Subsidence Above Panels with Cover Depths Between 50 and 150 m and Low to High SRP Zones	
	Ditton Geotechnical Services Pty Ltd		Scale:	NTS	Figure No: A3

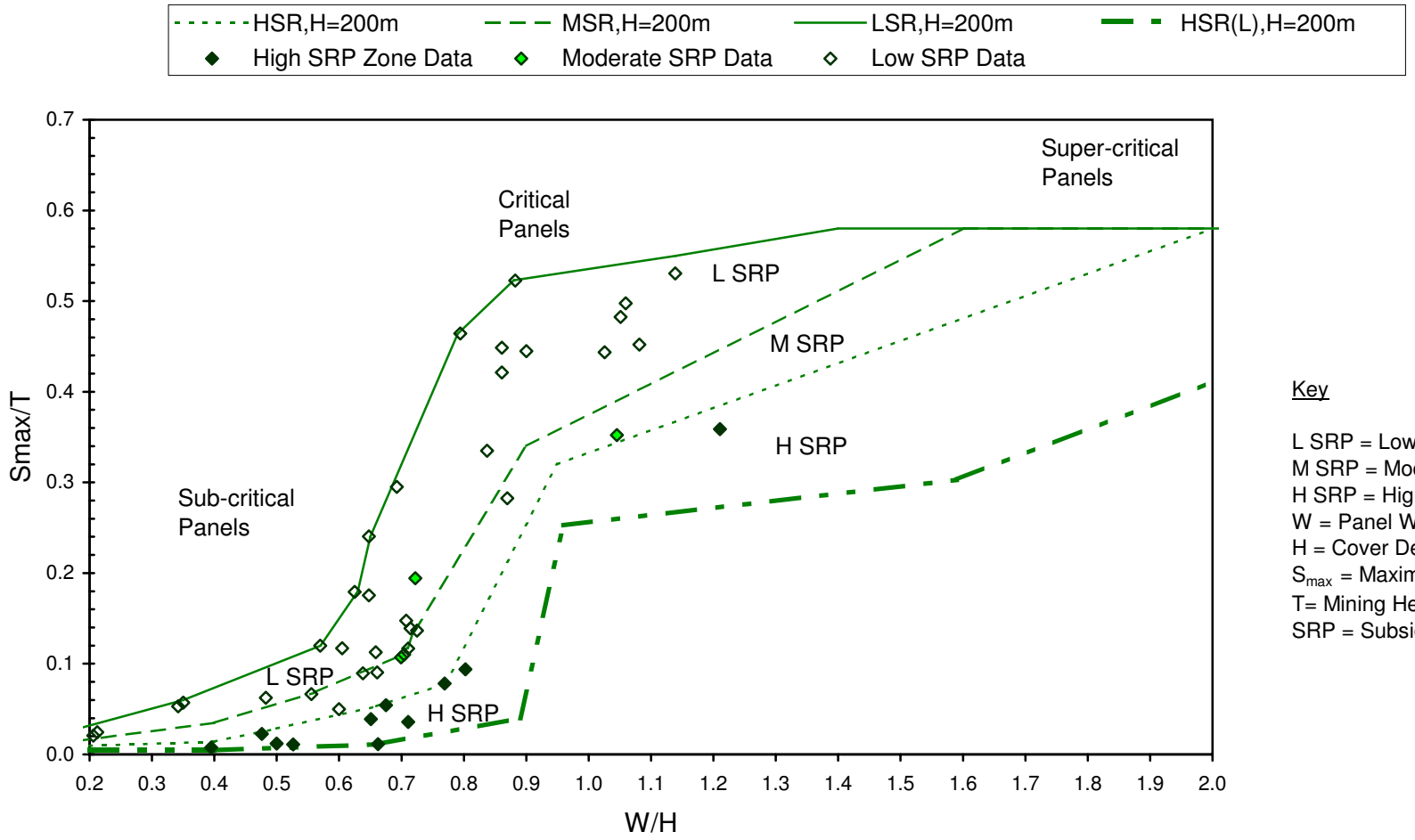

Key

L SRP = Low SRP Zone
M SRP = Moderate SRP Zone
H SRP = High SRP Zone
W = Panel Width
H = Cover Depth
S_{max} = Maximum Panel Subsidence
T= Mining Height
SRP = Subsidence Reduction Potential

DgS	Engineer:	S.Ditton	Client:	Adapted from ACARP, 2003	
	Drawn:	S.Ditton			
	Date:	08.08.08	Title:	Empirical Model for Predicting Subsidence Above Panels with Cover Depths Between 250 and 350 m and Low to High SRP Zones	
	Ditton Geotechnical Services Pty Ltd		Scale:	NTS	Figure No: A4

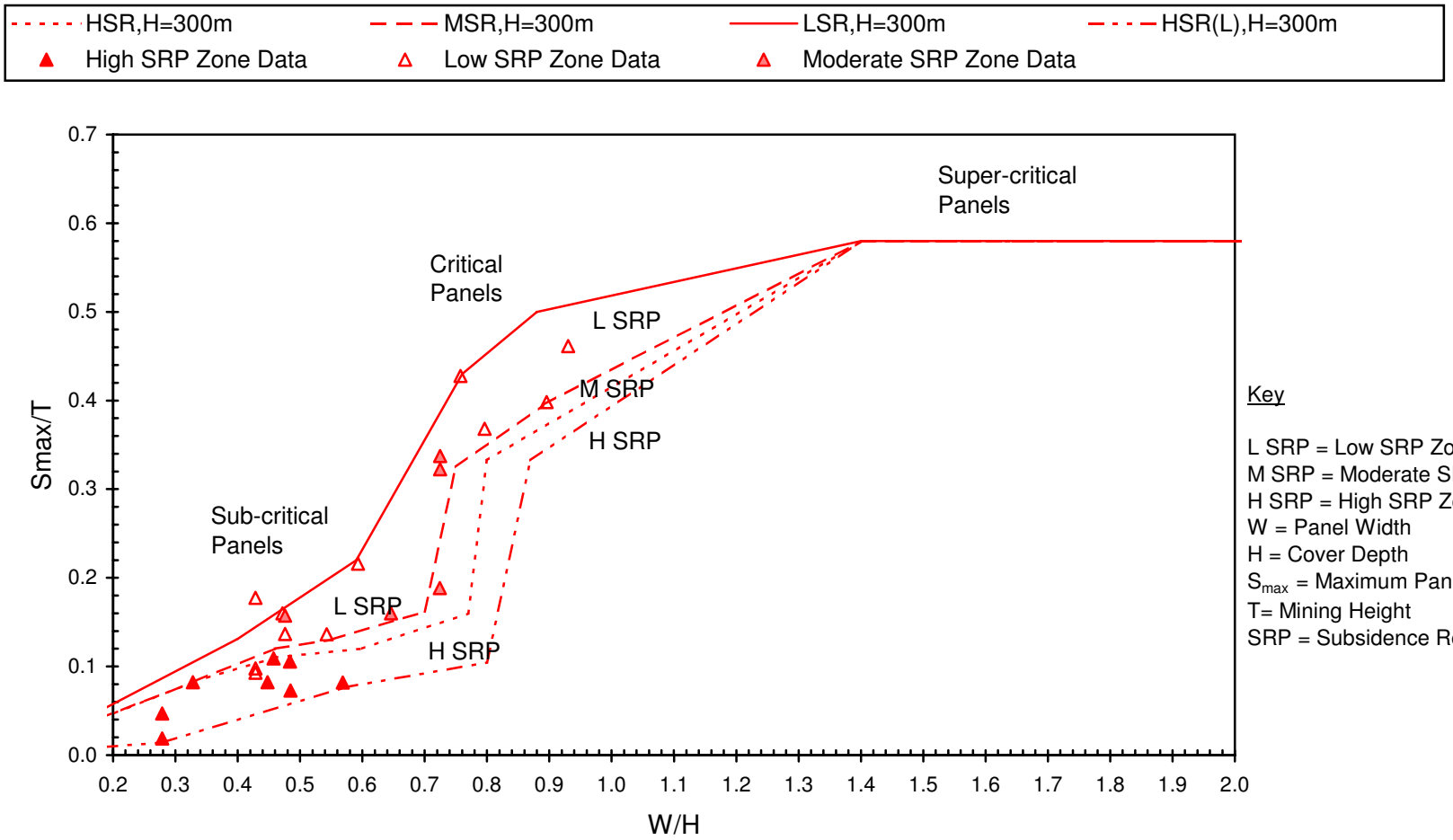

DgS	Engineer:	S.Ditton	Client:	Adapted from ACARP, 2003	
	Drawn:	S.Ditton			
	Date:	08.08.08	Title:	Empirical Model for Predicting Subsidence Above Panels with Cover Depths Between 250 and 350 m and Low to High SRP Zones	
	Ditton Geotechnical Services Pty Ltd		Scale:	NTS	Figure No: A5

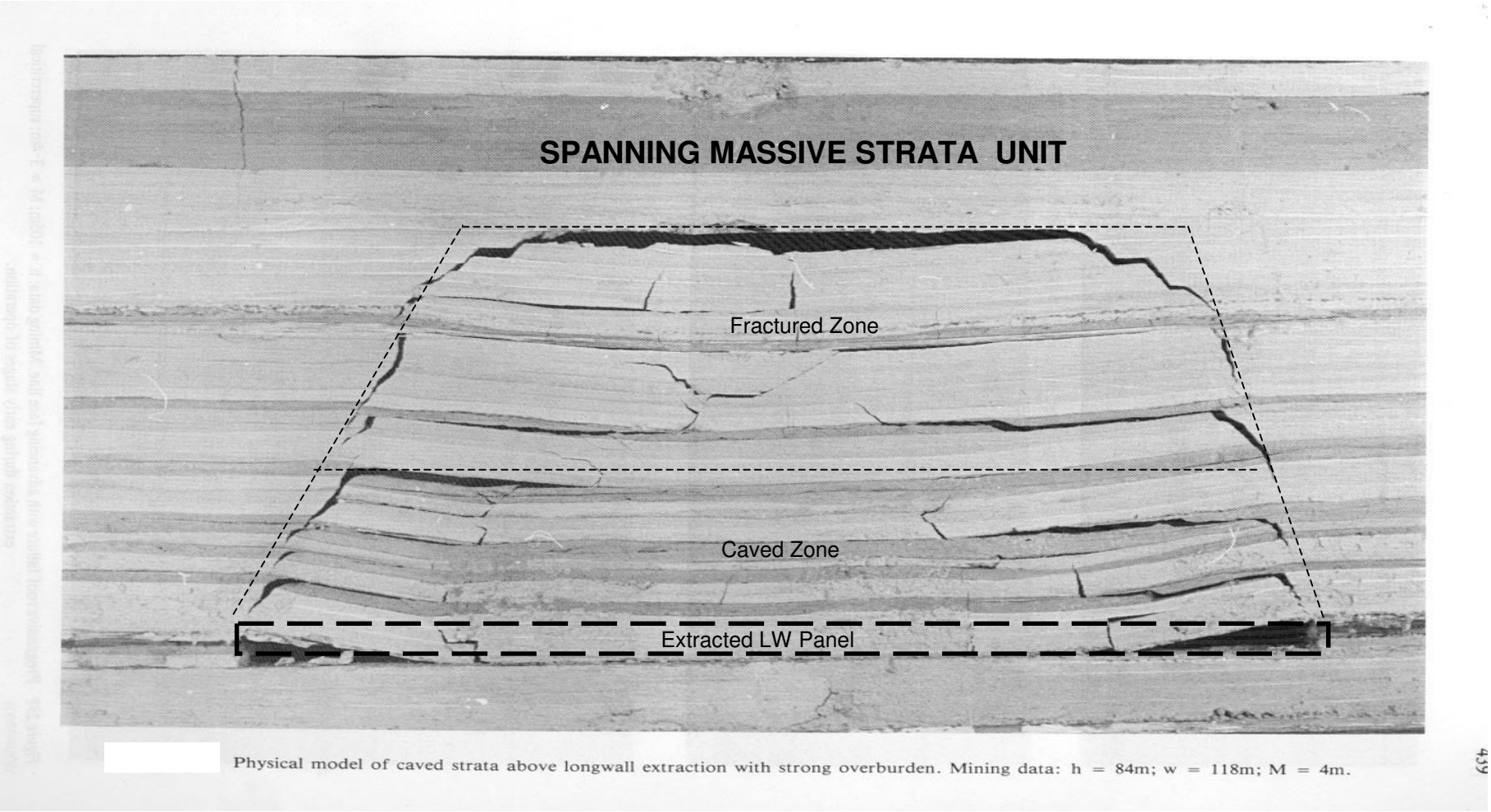

Physical model of caved strata above longwall extraction with strong overburden. Mining data: h = 84m; w = 118m; M = 4m.

439

DgS	Engineer:	S.Ditton	Client:	Adapted from ACARP, 2003	
	Drawn:	S.Ditton			
	Date:	08.08.08	Title:	Physical Overburden Model Showing the Subsidence Reducing Effect of a Massive Strata Unit At the Surface	
	Ditton Geotechnical Services Pty Ltd		Scale:	NTS	Figure No: A6

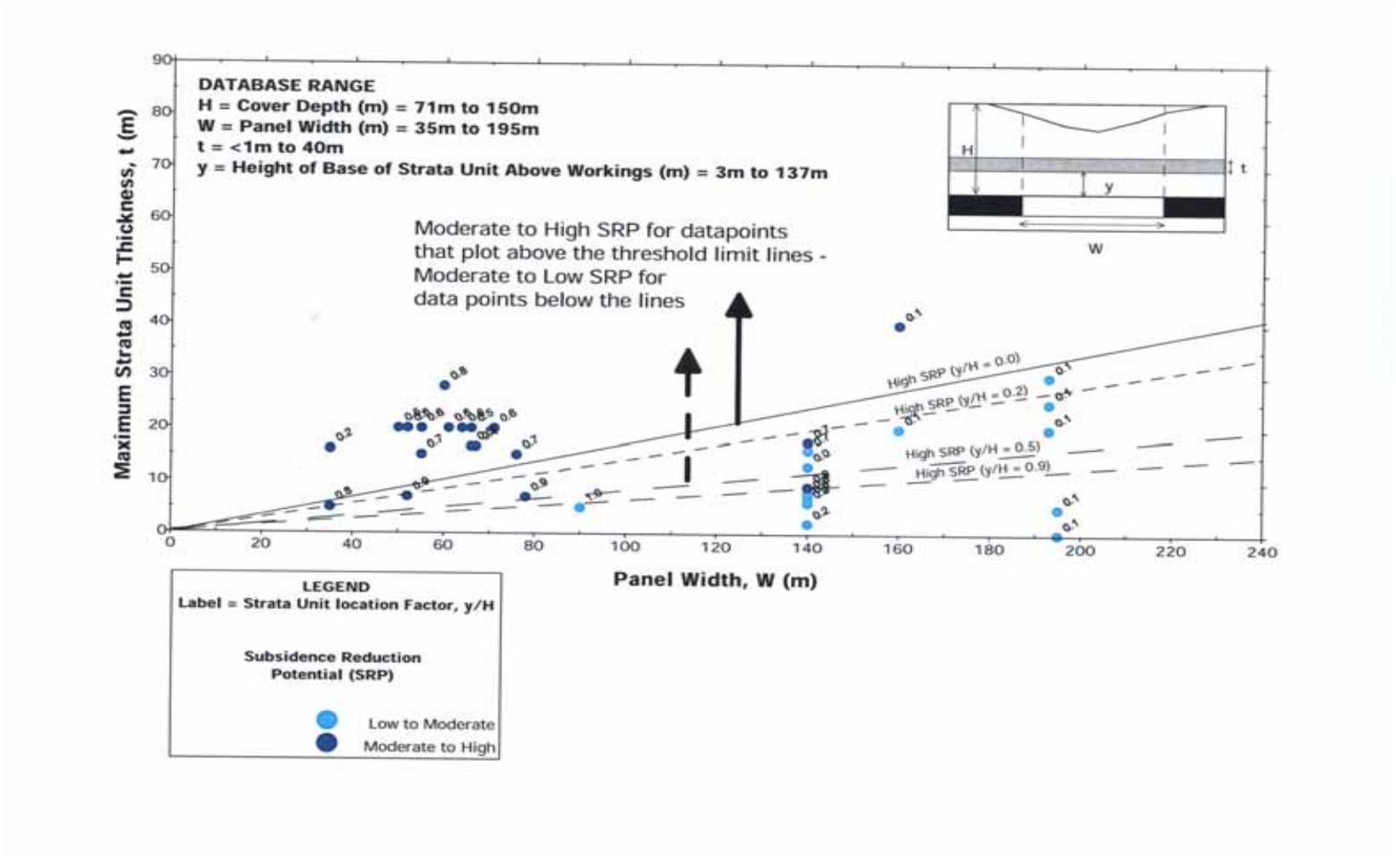

DgS	Engineer:	S.Ditton	Client:	Extract from ACARP, 2003	
	Drawn:	S.Ditton			
	Date:	08.08.08	Title:	Project Database of Maximum Strata Unit Thickness and SRP Threshold Limit Lines for H=50 m to 150 m	
	Ditton Geotechnical Services Pty Ltd		Scale:	NTS	Figure No: A7.1

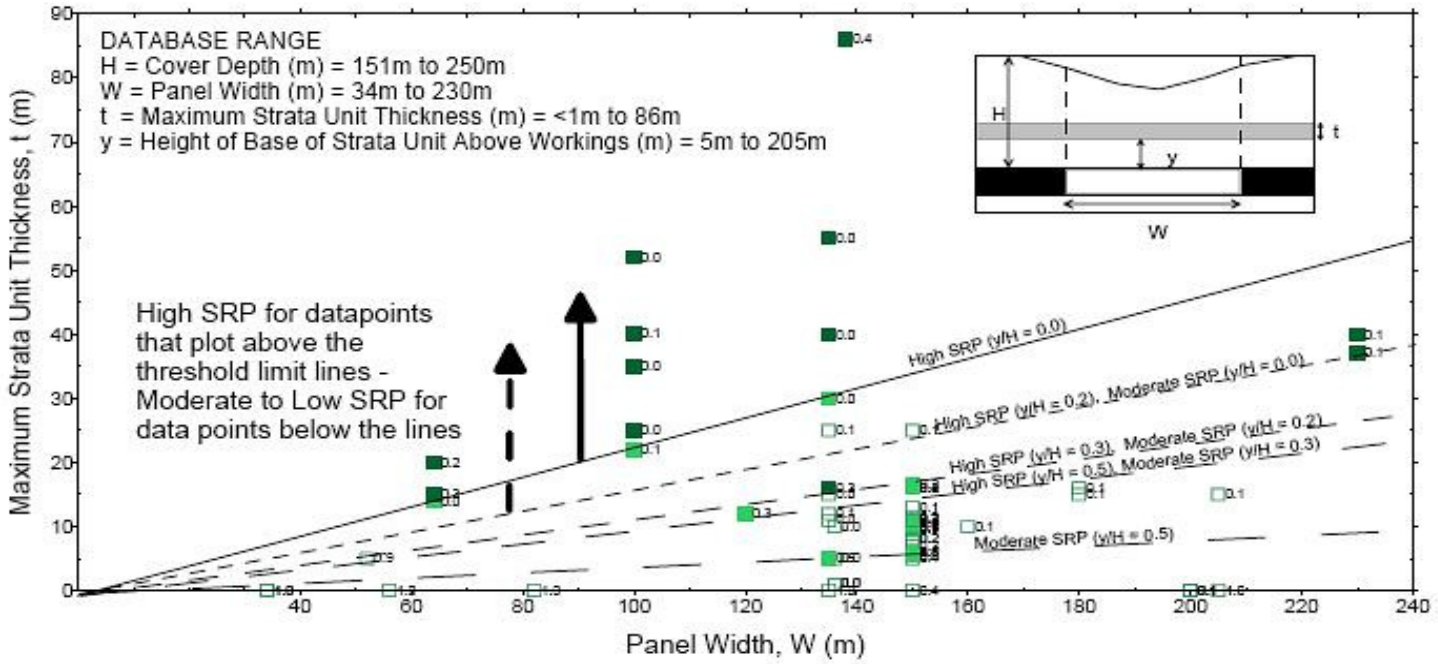

DgS	Engineer:	S.Ditton	Client:	Extract from ACARP, 2003	
	Drawn:	S.Ditton			
	Date:	08.08.08	Title:	Project Database of Maximum Strata Unit Thickness and SRP Threshold Limit Lines for H=150 m to 250 m	
	Ditton Geotechnical Services Pty Ltd		Scale:	NTS	Figure No: A7.2

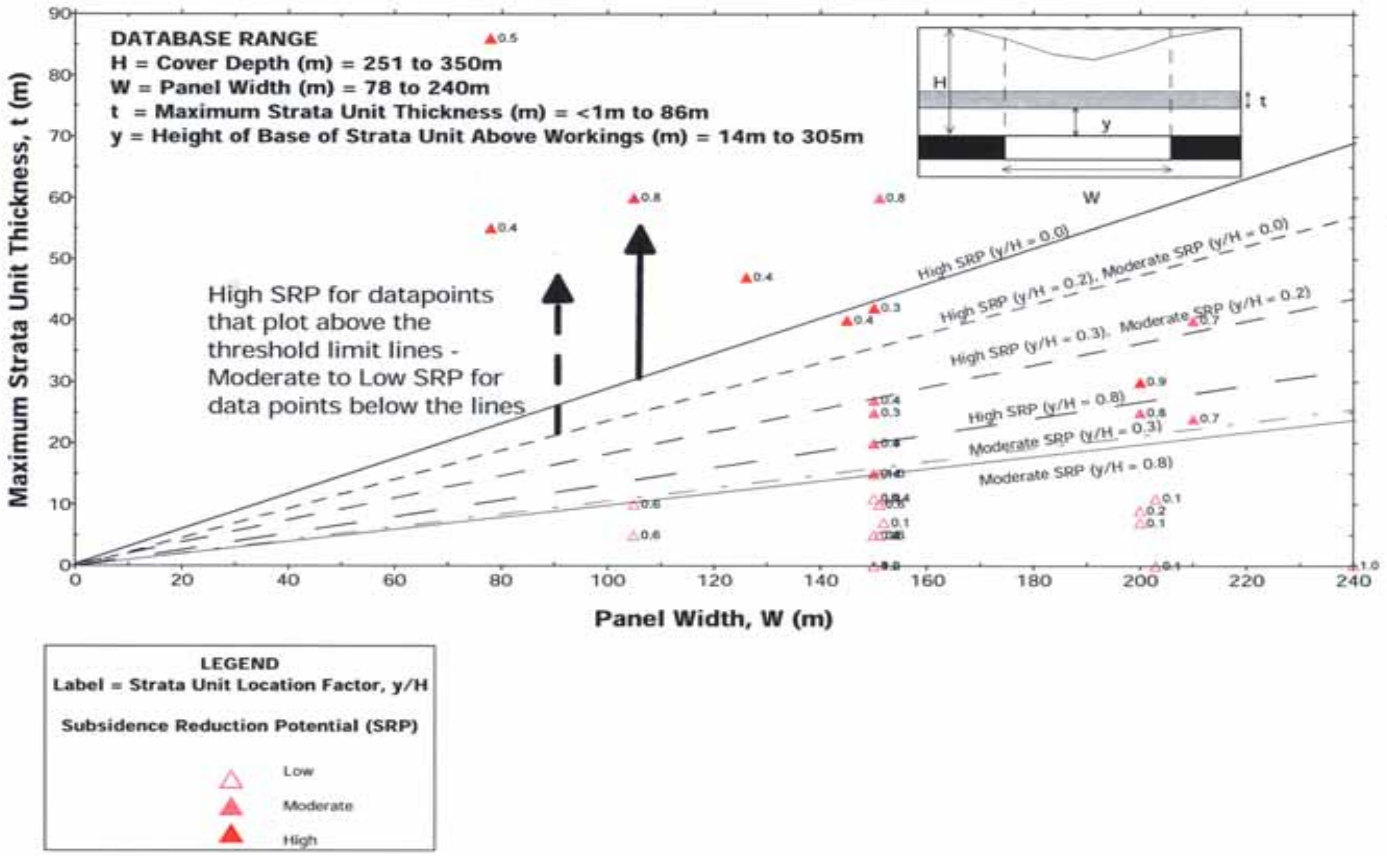

DgS	Engineer:	S.Ditton	Client:	Extract from ACARP, 2003	
	Drawn:	S.Ditton			
	Date:	08.08.08	Title:	Project Database of Maximum Strata Unit Thickness and SRP Threshold Limit Lines for H=250 m to 350 m	
	Ditton Geotechnical Services Pty Ltd		Scale:	NTS	Figure No: A7.3

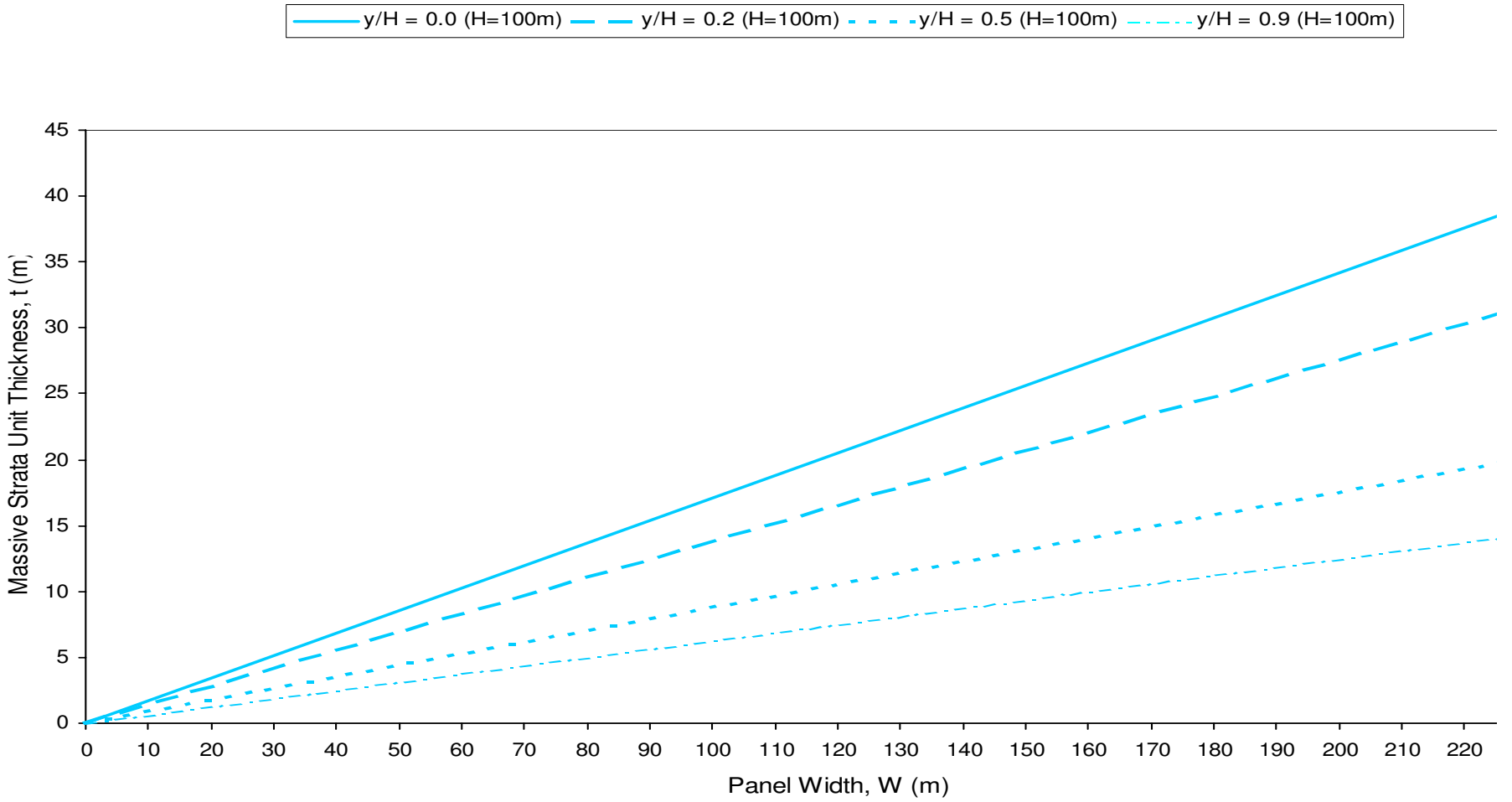

DgS	Engineer:	S.Ditton	Client:	Adapted from ACARP, 2003	
	Drawn:	S.Ditton			
	Date:	08.08.08	Title:	Empirical Model for Predicting Subsidence Reduction Potential Above Panels with Cover Depths Between 50 and 150 m	
	Ditton Geotechnical Services Pty Ltd		Scale:	NTS	Figure No: A8

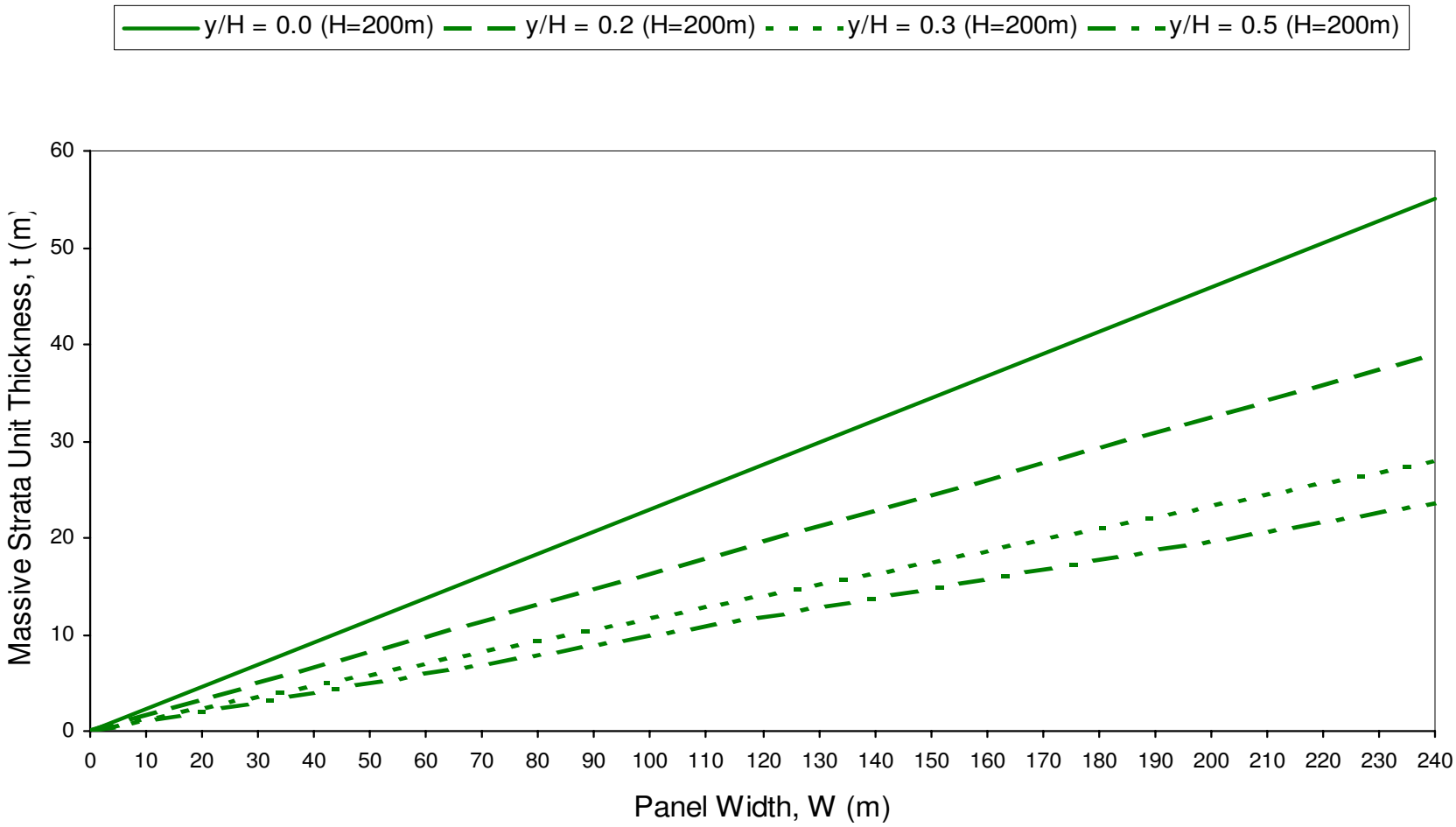

DgS	Engineer:	S.Ditton	Client:	Adapted from ACARP, 2003	
	Drawn:	S.Ditton			
	Date:	08.08.08	Title:	Empirical Model for Predicting Subsidence Reduction Potential Above Panels with Cover Depths Between 150 and 250 m	
	Ditton Geotechnical Services Pty Ltd		Scale:	NTS	Figure No: A9

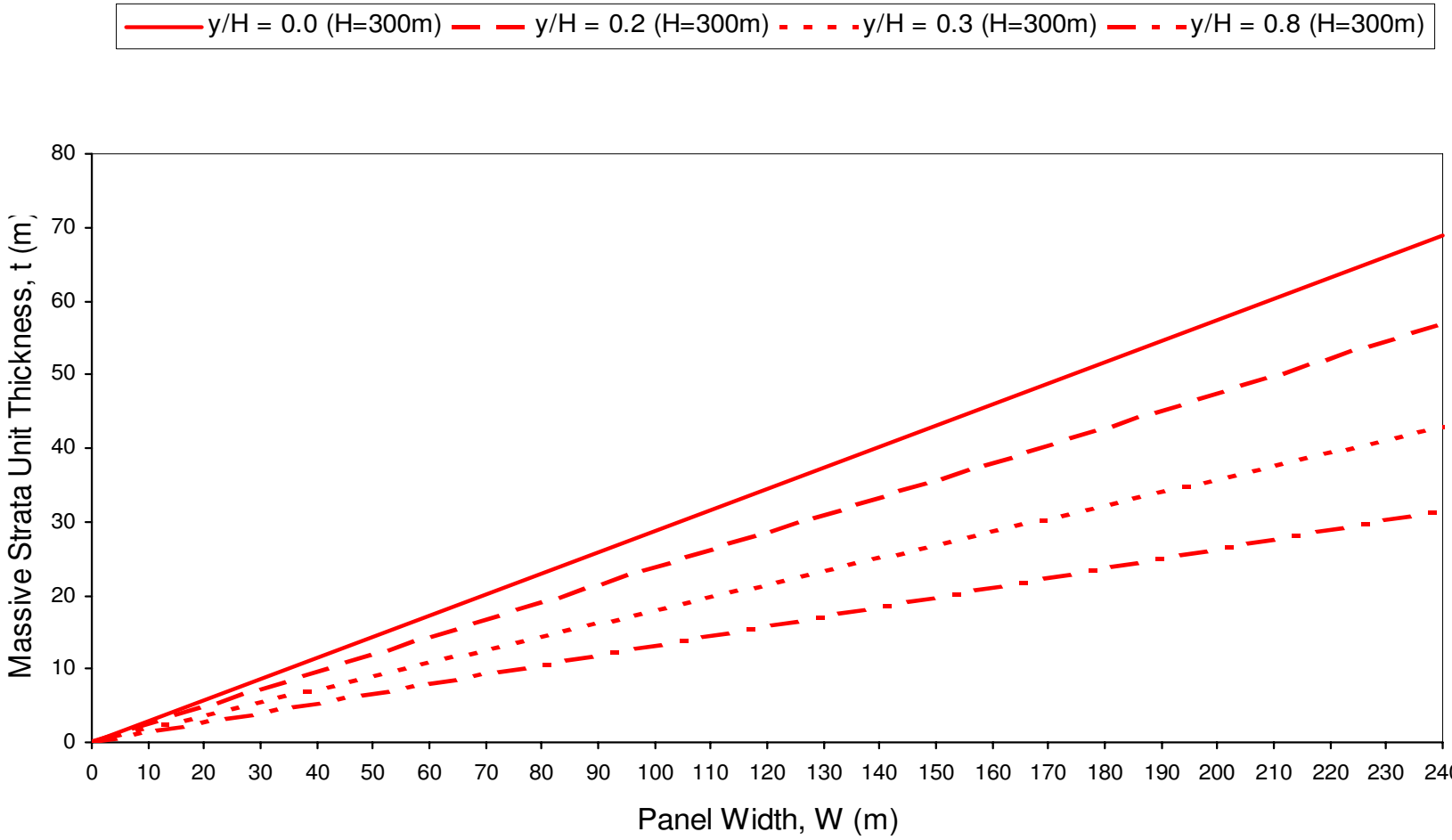

DgS	Engineer:	S.Ditton	Client:	Adapted from ACARP, 2003	
	Drawn:	S.Ditton			
	Date:	08.08.08	Title:	Empirical Model for Predicting Subsidence Reduction Potential Above Panels with Cover Depths Between 250 and 350 m	
	Ditton Geotechnical Services Pty Ltd		Scale:	NTS	Figure No: A10

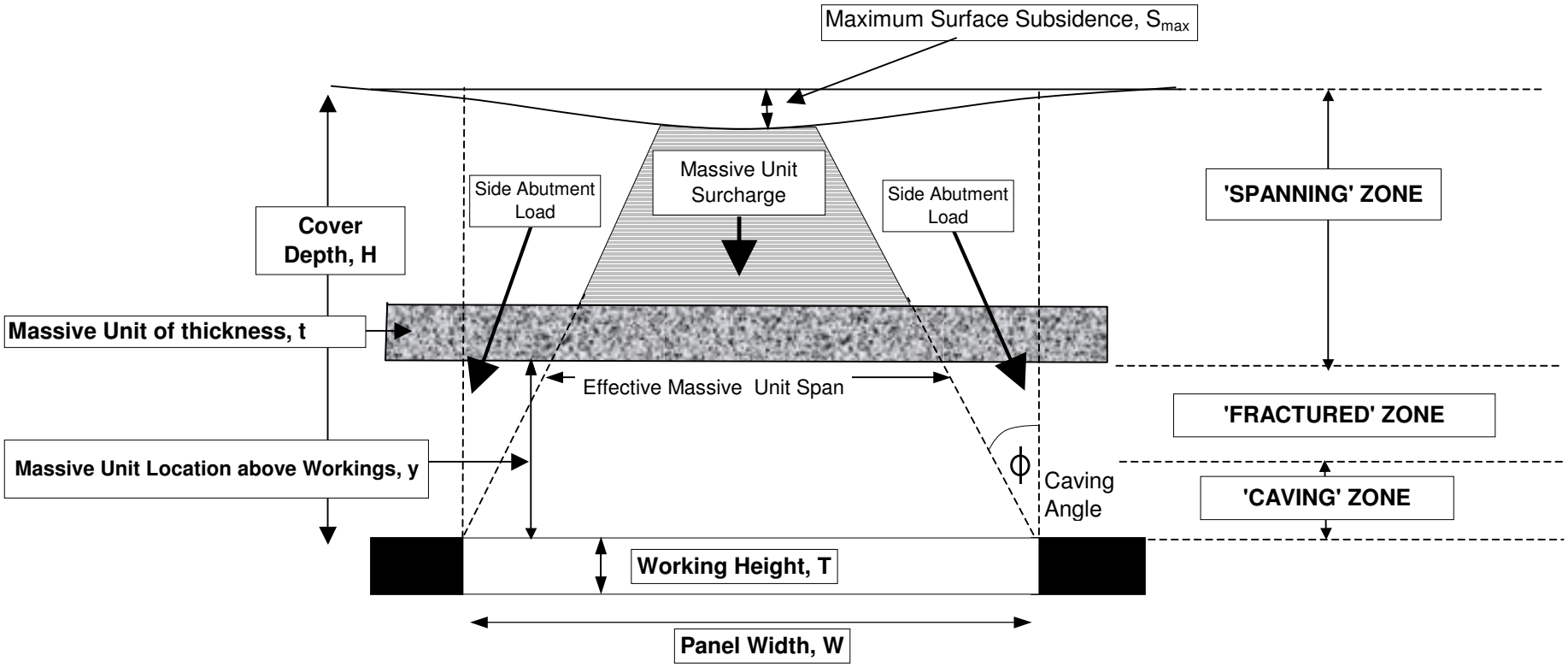

DgS	Engineer:	S.Ditton	Client:	Adapted from ACARP, 2003	
	Drawn:	S.Ditton			
	Date:	08.08.08	Title:	Overburden with Massive Strata Unit Behaviour Concept Model and Key Parameter Definitions	
	Ditton Geotechnical Services Pty Ltd		Scale:	NTS	Figure No: A11

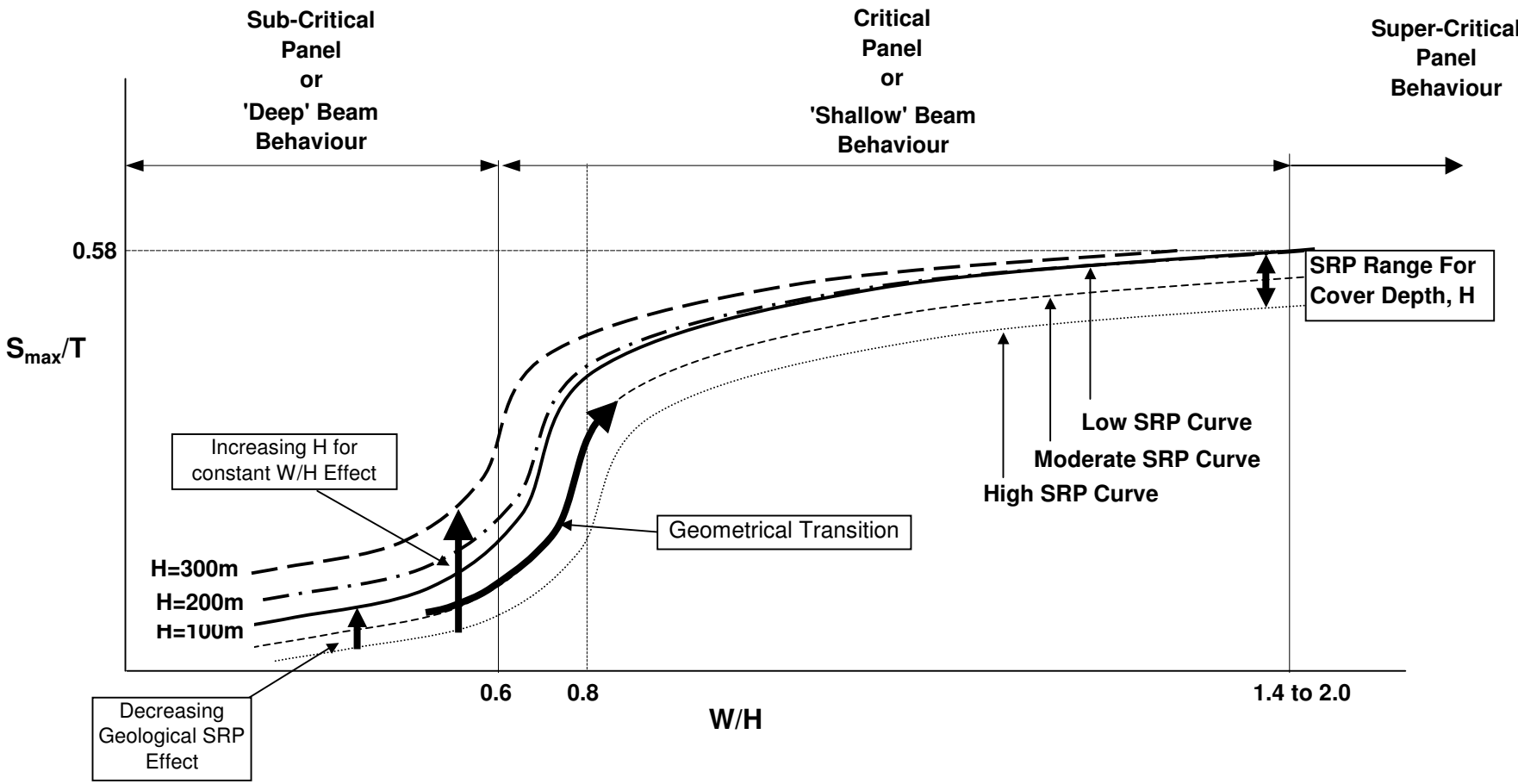

DgS	Engineer:	S.Ditton	Client:	Adapted from ACARP, 2003	
	Drawn:	S.Ditton			
	Date:	08.08.08	Title:	Geomechnical and Geological Effects of Overburden Behaviour on Maimum Subsidence for Single Panels	
	Ditton Geotechnical Services Pty Ltd		Scale:	NTS	Figure No: A12

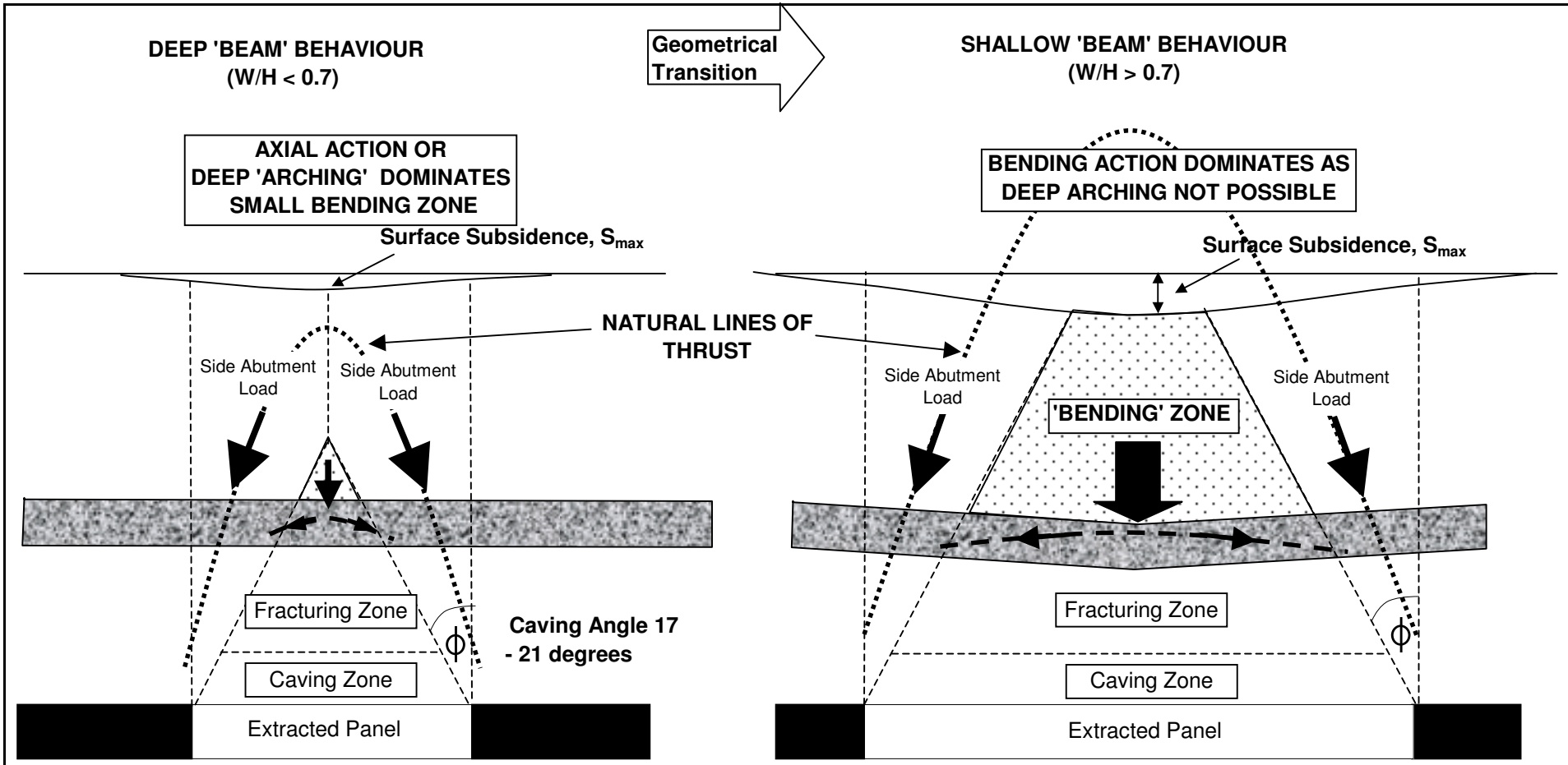

DgS	Engineer:	S.Ditton	Client:	Adapted from ACARP, 2003	
	Drawn:	S.Ditton			
	Date:	08.08.08	Title:	Overburden with Massive Strata Units Behaviour Concept Models of Beam Action Types for Subcritical and Supercritical Longwall Panels	
	Ditton Geotechnical Services Pty Ltd		Scale:	NTS	Figure No: A13

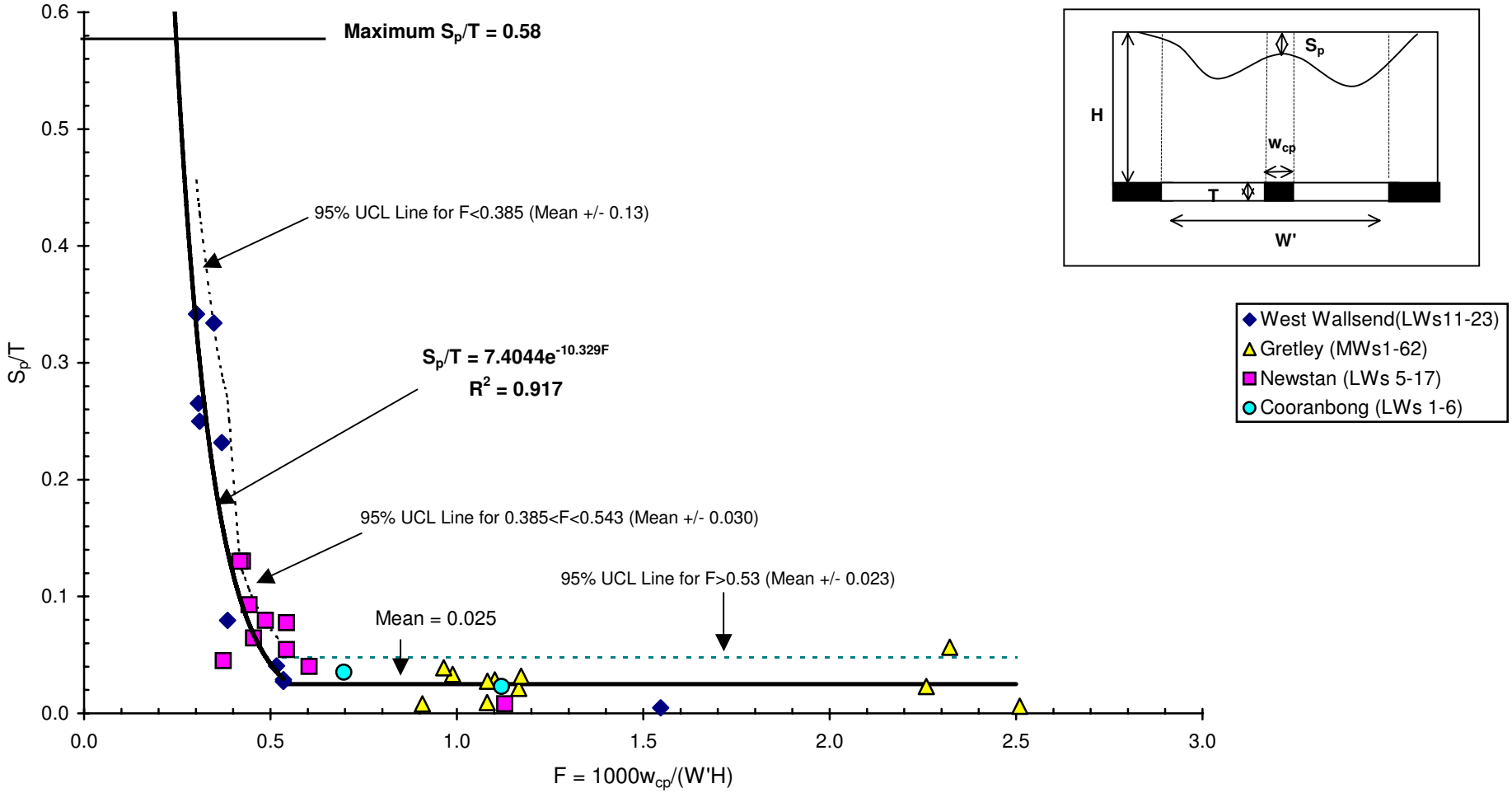

DgS	Engineer:	S.Ditton	Client:	Extract from ACARP, 2003	
	Drawn:	S.Ditton			
	Date:	08.08.08	Title:	2003 Empirical Model for Predicting Subsidence above Chain Pillars Subject to Double Abutment Loading	
	Ditton Geotechnical Services Pty Ltd		Scale:	NTS	Figure No: A14

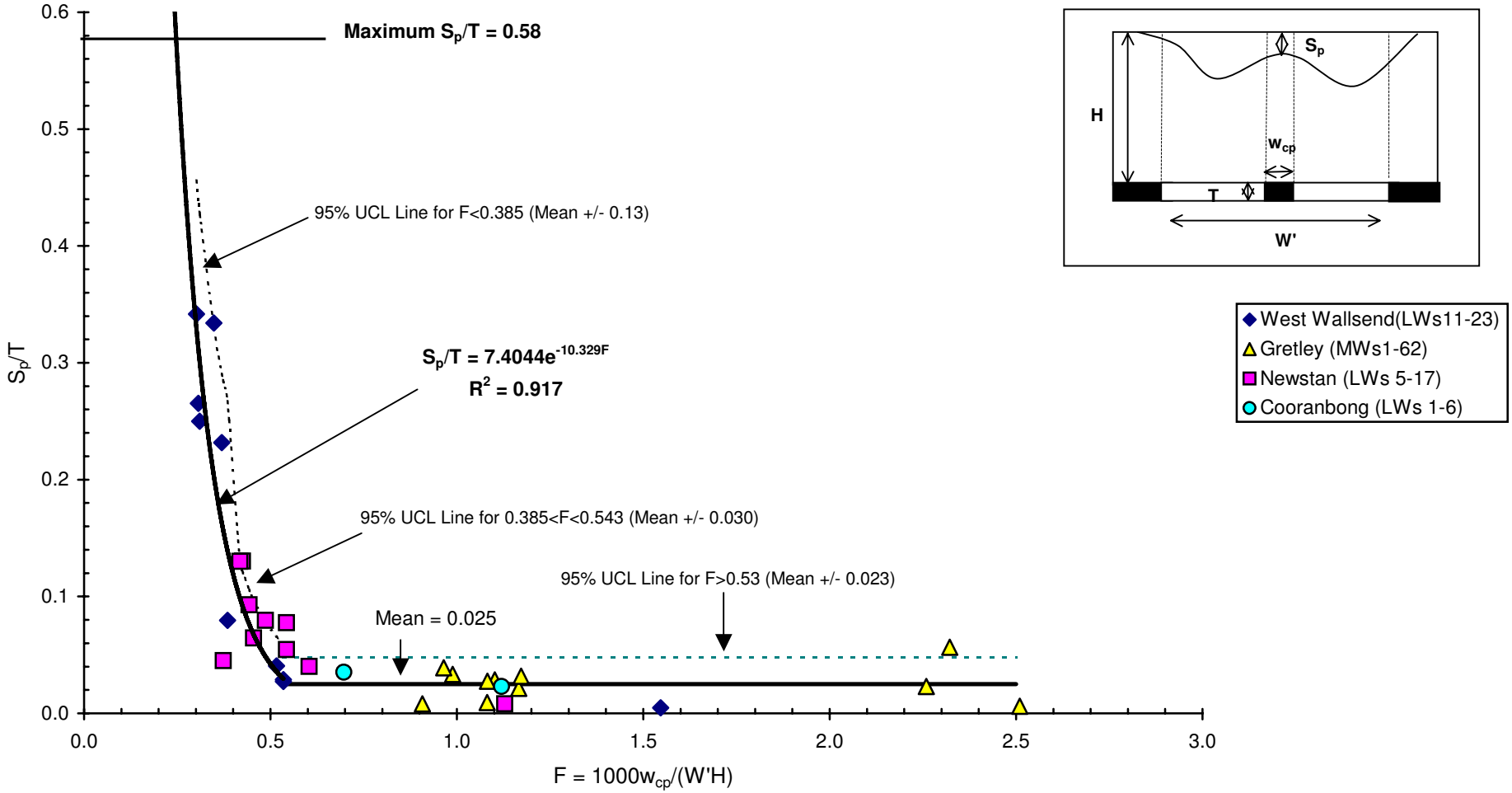

DgS	Engineer:	S.Ditton	Client:	Extract from ACARP, 2003	
	Drawn:	S.Ditton			
	Date:	08.08.08	Title:	2003 Empirical Model for Predicting Subsidence above Chain Pillars Subject to Double Abutment Loading	
	Ditton Geotechnical Services Pty Ltd		Scale:	NTS	Figure No: A15

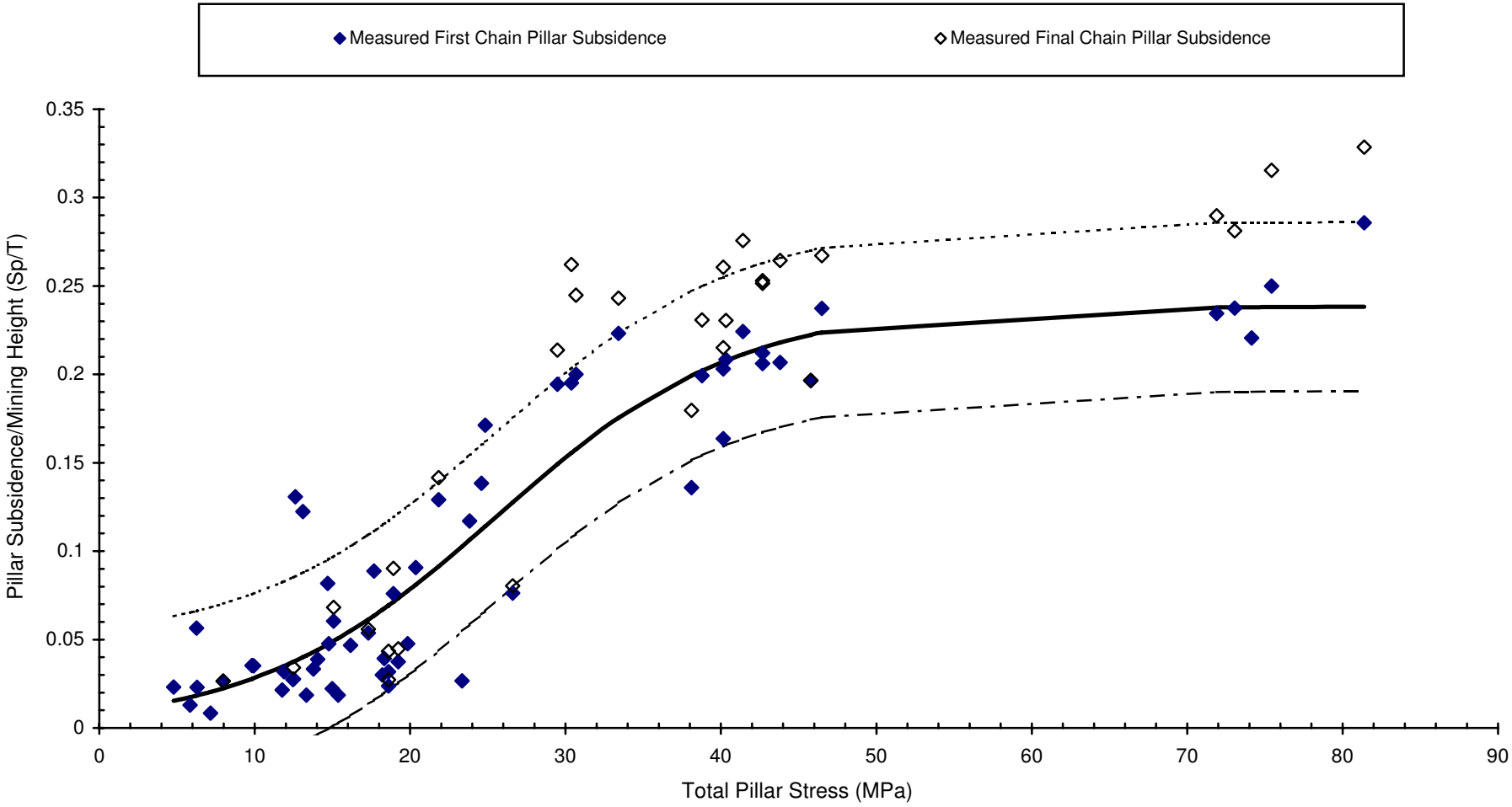

DgS	Engineer:	S.Ditton	Client:	Adapted from ACARP, 2003	
	Drawn:	S.Ditton			
	Date:	08.08.08	Title:	2008 Empirical Model (DgS) for Predicting Subsidence above Chain Pillars Subject to Double Abutment Loading	
	Ditton Geotechnical Services Pty Ltd		Scale:	NTS	Figure No: A16

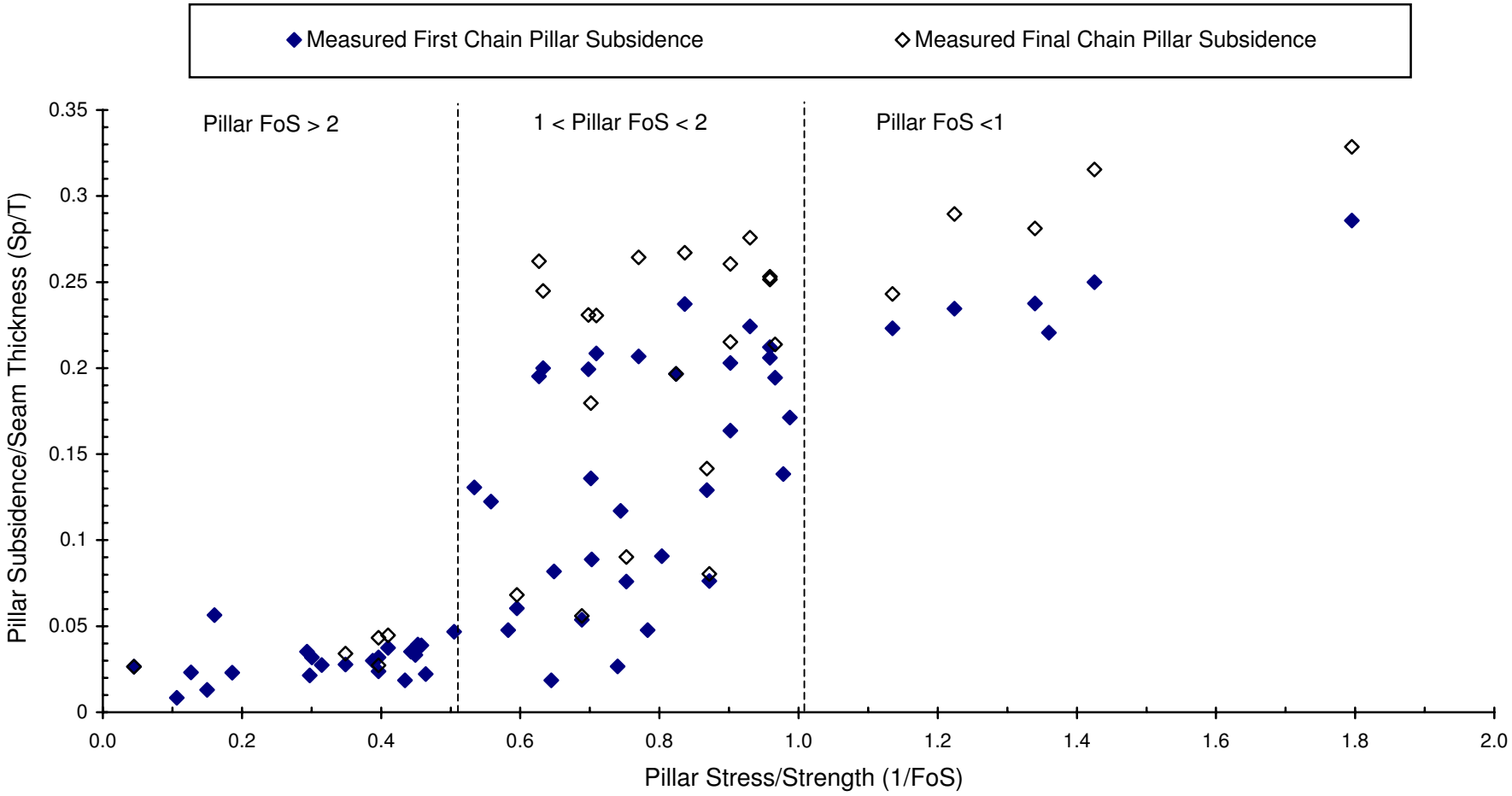

DgS	Engineer:	S.Ditton	Client:	Adapted from ACARP, 2003	
	Drawn:	S.Ditton			
	Date:	08.08.08	Title:	Empirical DgS, 2008 Model Data of 1/FoS v. Subsidence above Chain Pillars Subject to Double Abutment Loading	
	Ditton Geotechnical Services Pty Ltd		Scale:	NTS	Figure No: A17

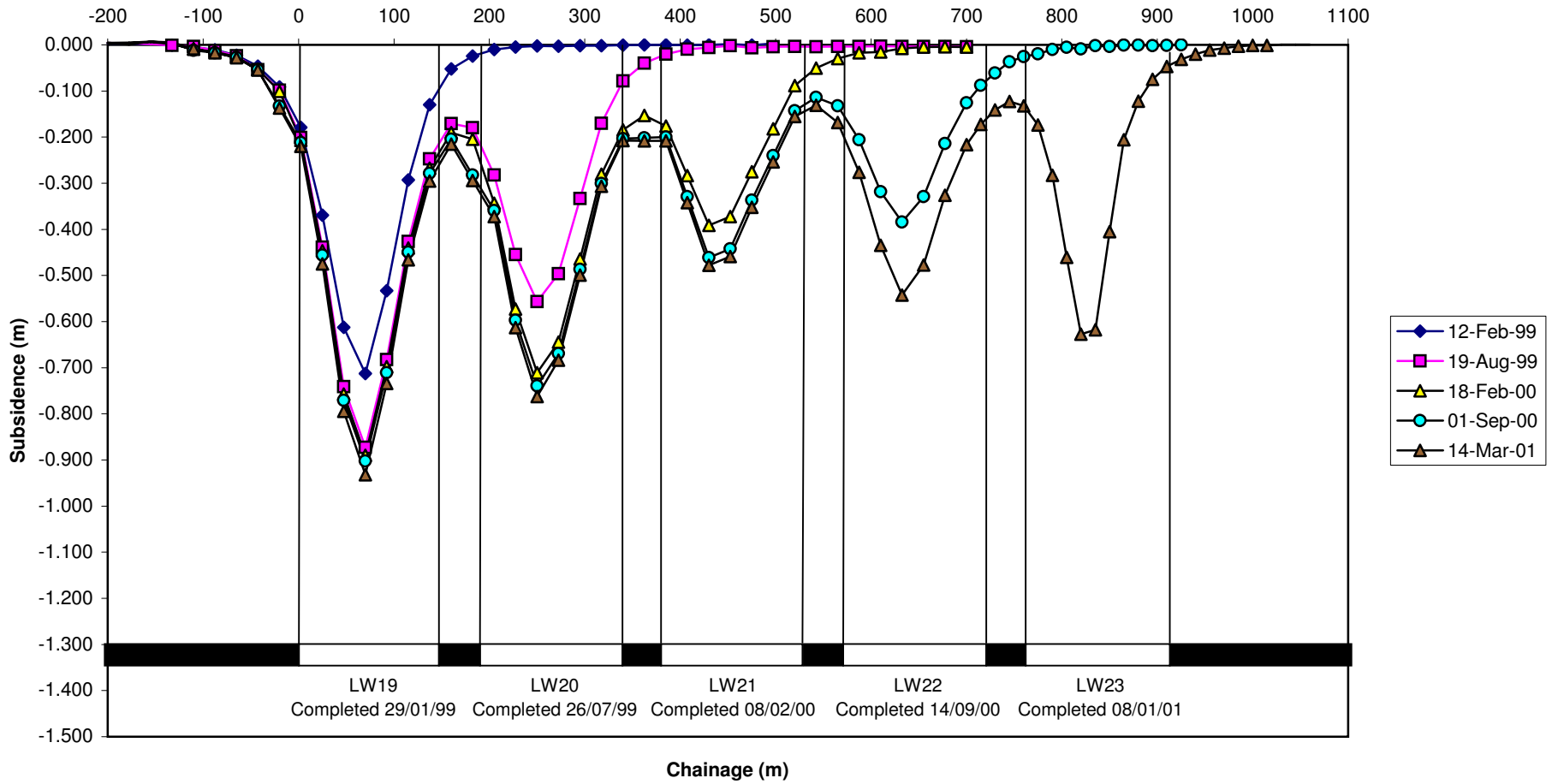

DgS	Engineer:	S.Ditton	Client:	Adapted from ACARP, 2003	
	Drawn:	S.Ditton			
	Date:	08.08.08	Title:	Measured Multiple Longwall Panel Subsidence in Newcastle Coalfield	
	Ditton Geotechnical Services Pty Ltd		Scale:	NTS	Figure No: A18

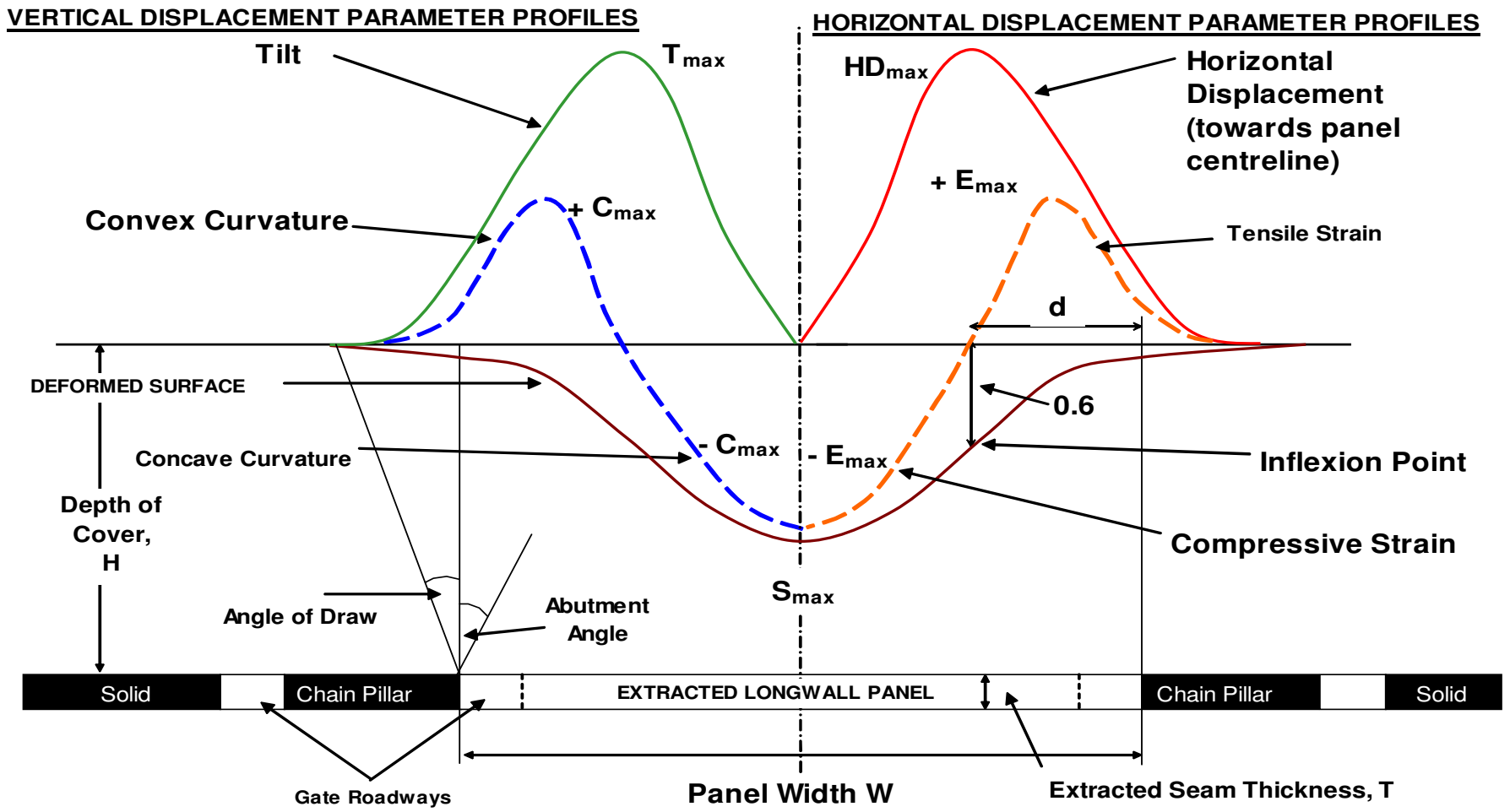

DgS	Engineer:	S.Ditton	Client:	Extract from ACARP, 2003	
	Drawn:	S.Ditton			
	Date:	08.08.08	Title:	Mine Subsidence Trough Deformation Parameters (adapted from Holla, 1987)	
	Ditton Geotechnical Services Pty Ltd		Scale:	NTS	Figure No: A19

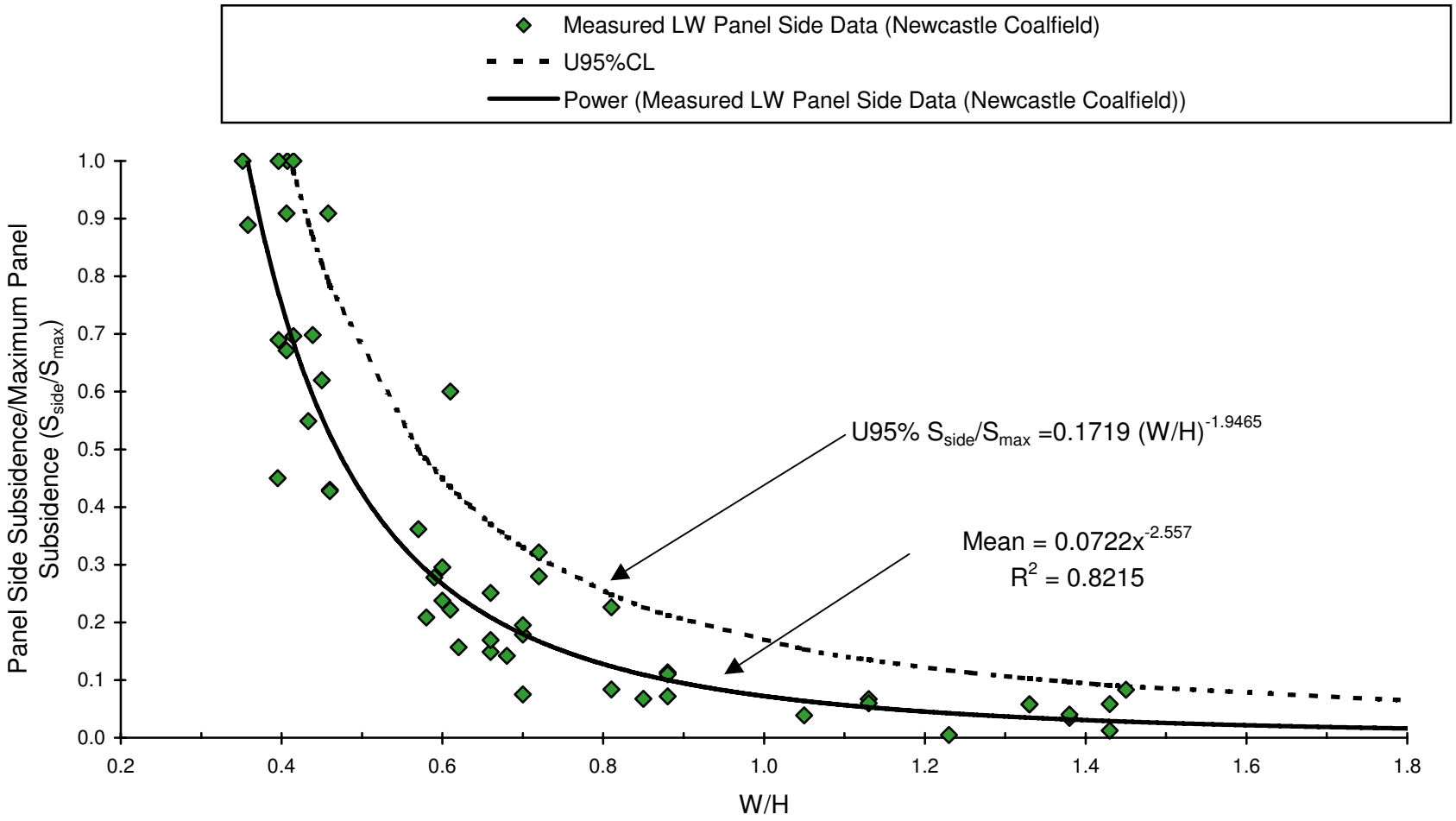

DgS	Engineer:	S.Ditton	Client:	Adapted from ACARP, 2003	
	Drawn:	S.Ditton			
	Date:	08.08.08	Title:	Empirical Model for Goaf Edge Subsidence Prediction Above Longwall Panels	
	Ditton Geotechnical Services Pty Ltd		Scale:	NTS	Figure No: A20

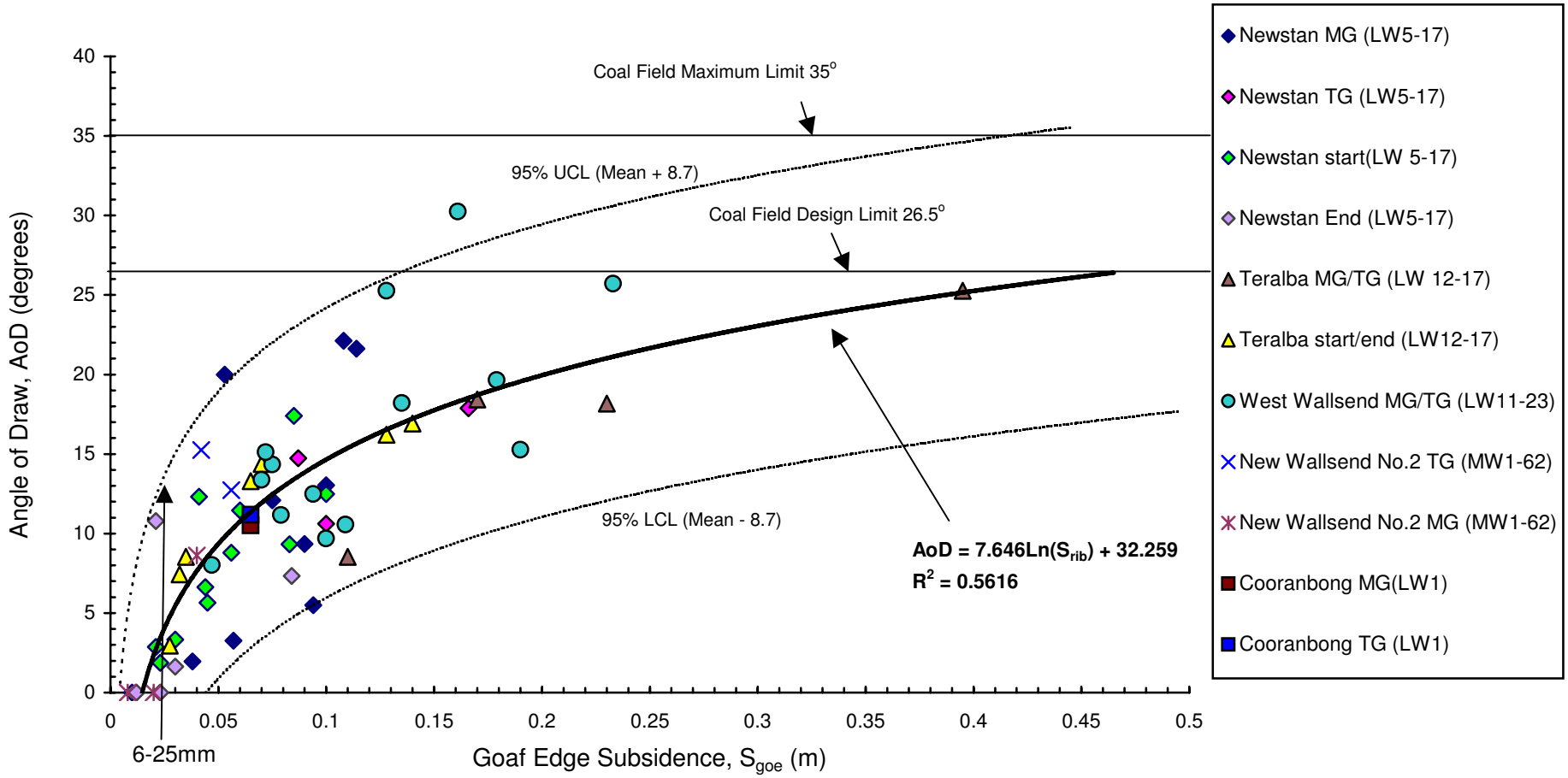

DgS	Engineer:	S.Ditton	Client:	Extracted from ACARP, 2003	
	Drawn:	S.Ditton			
	Date:	08.08.08	Title:	Empirical Prediction Model for Longwall Panel Angle of Draw	
	Ditton Geotechnical Services Pty Ltd		Scale:	NTS	Figure No: A21

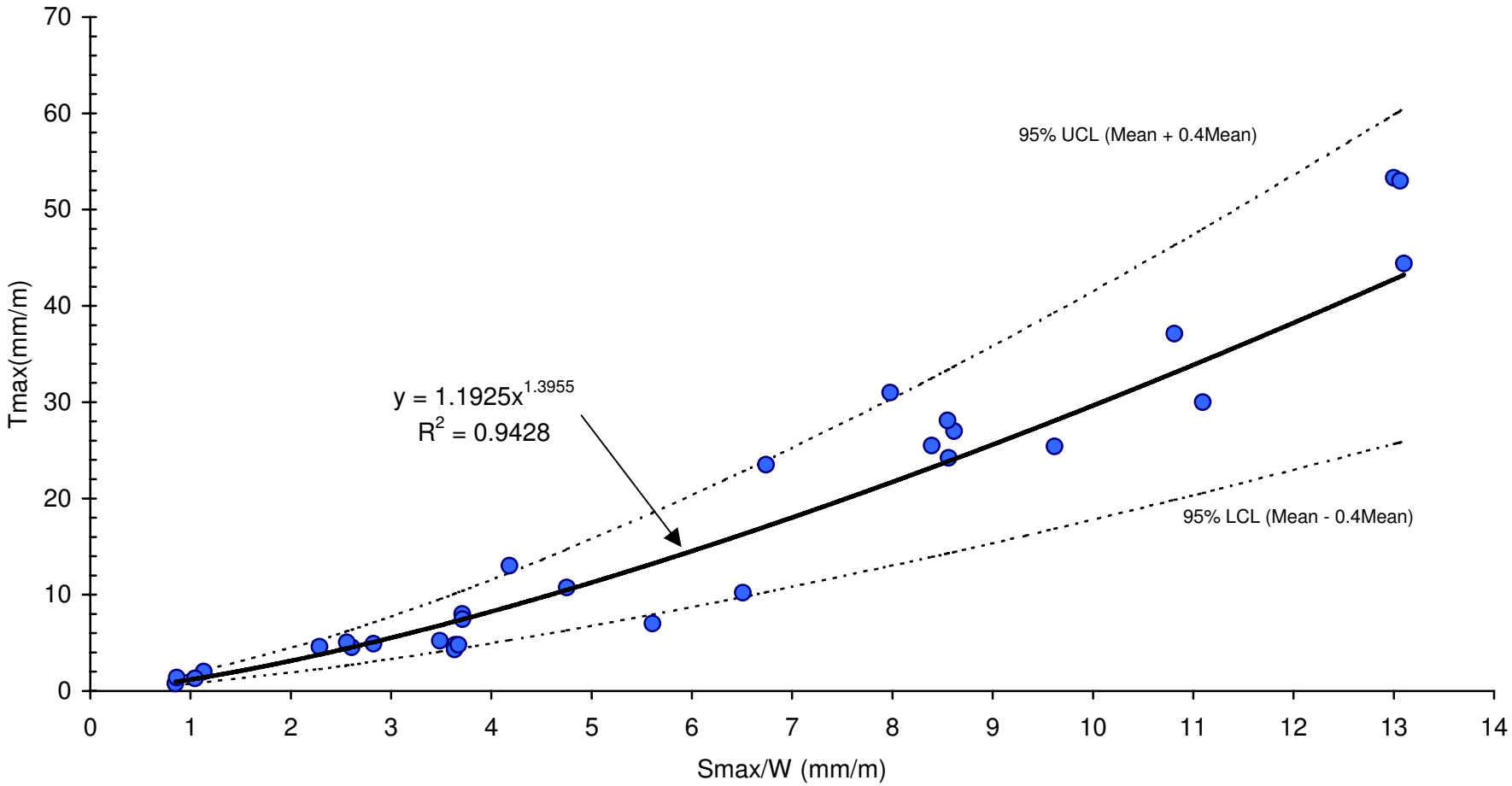

DgS	Engineer:	S.Ditton	Client:	Extract from ACARP, 2003	
	Drawn:	S.Ditton			
	Date:	08.08.08	Title:	Empirical Model for Maximum Panel Tilt Prediction Above Longwall Panels	
	Ditton Geotechnical Services Pty Ltd		Scale:	NTS	Figure No: A22

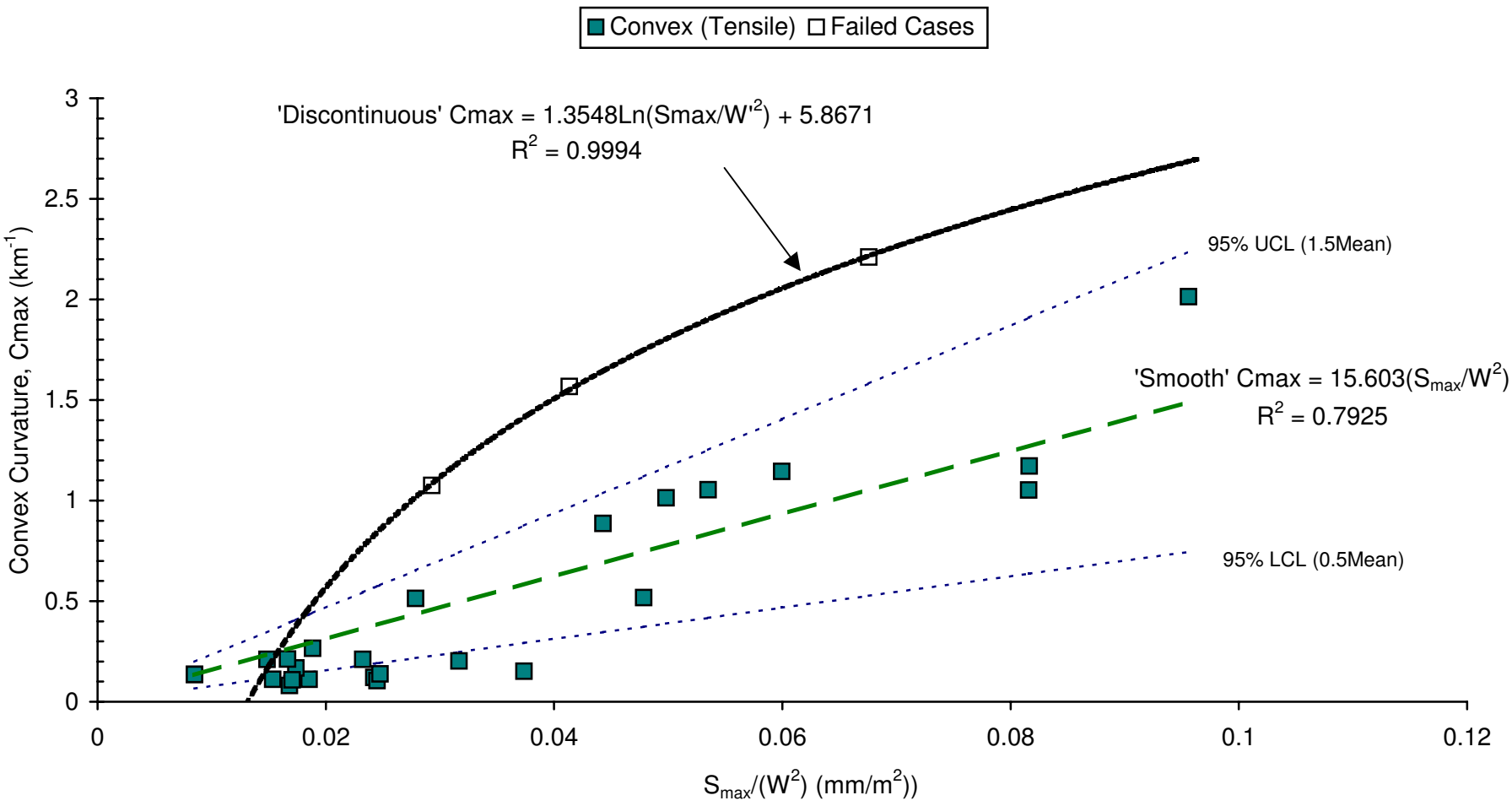

DgS	Engineer:	S.Ditton	Client:	Extract from ACARP, 2003	
	Drawn:	S.Ditton			
	Date:	08.08.08	Title:	Empirical Model for Maximum Panel Convex Curvature Prediction Above Longwall Panels for Smooth and Discontinuous Profiles	
	Ditton Geotechnical Services Pty Ltd		Scale:	NTS	Figure No: A23

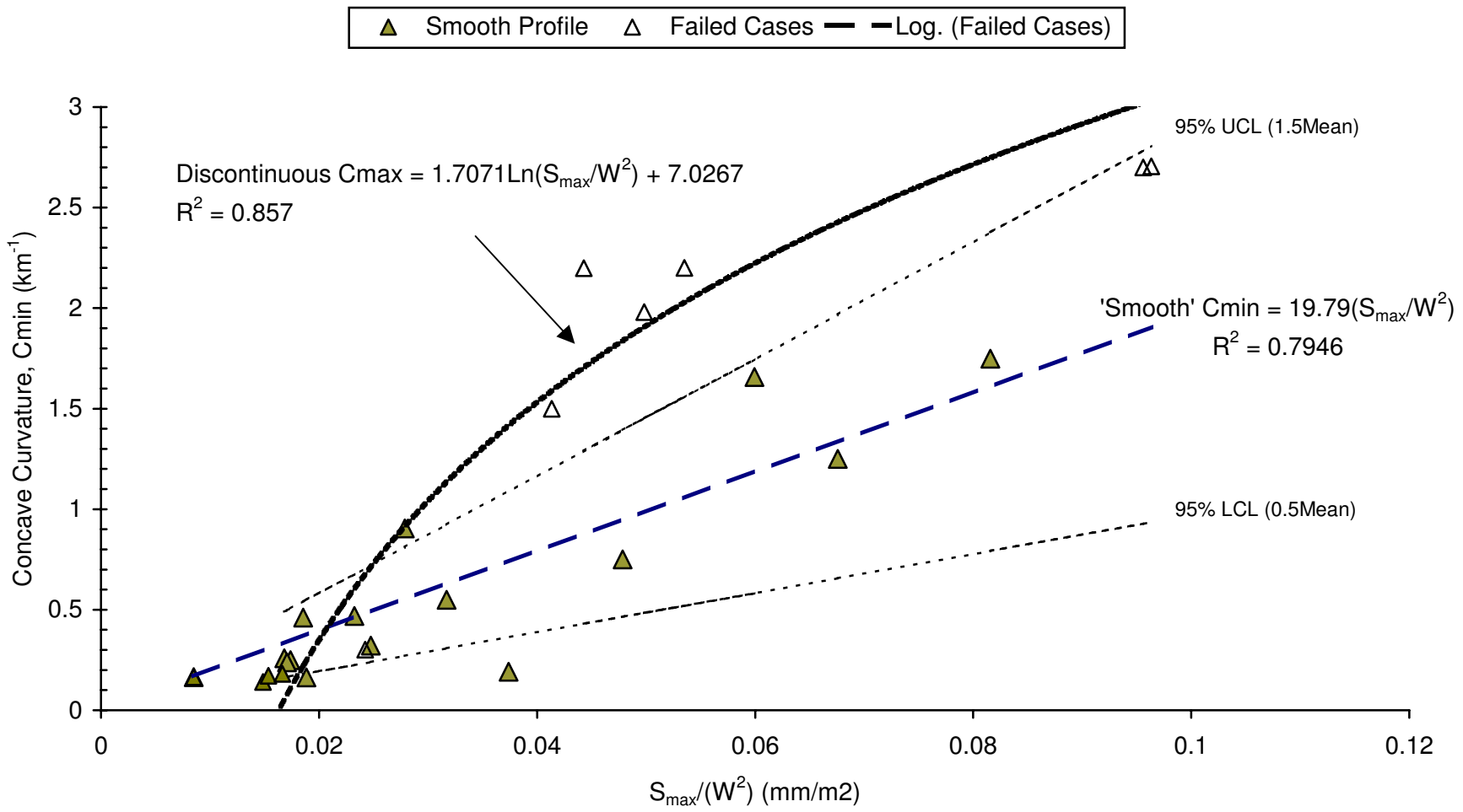

DgS	Engineer:	S.Ditton	Client:	Extract from ACARP, 2003	
	Drawn:	S.Ditton			
	Date:	08.08.08	Title:	Empirical Model for Maximum Panel Concave Curvature Prediction Above Longwall Panels for Smooth and Discontinuous Profiles	
	Ditton Geotechnical Services Pty Ltd		Scale:	NTS	Figure No: A24

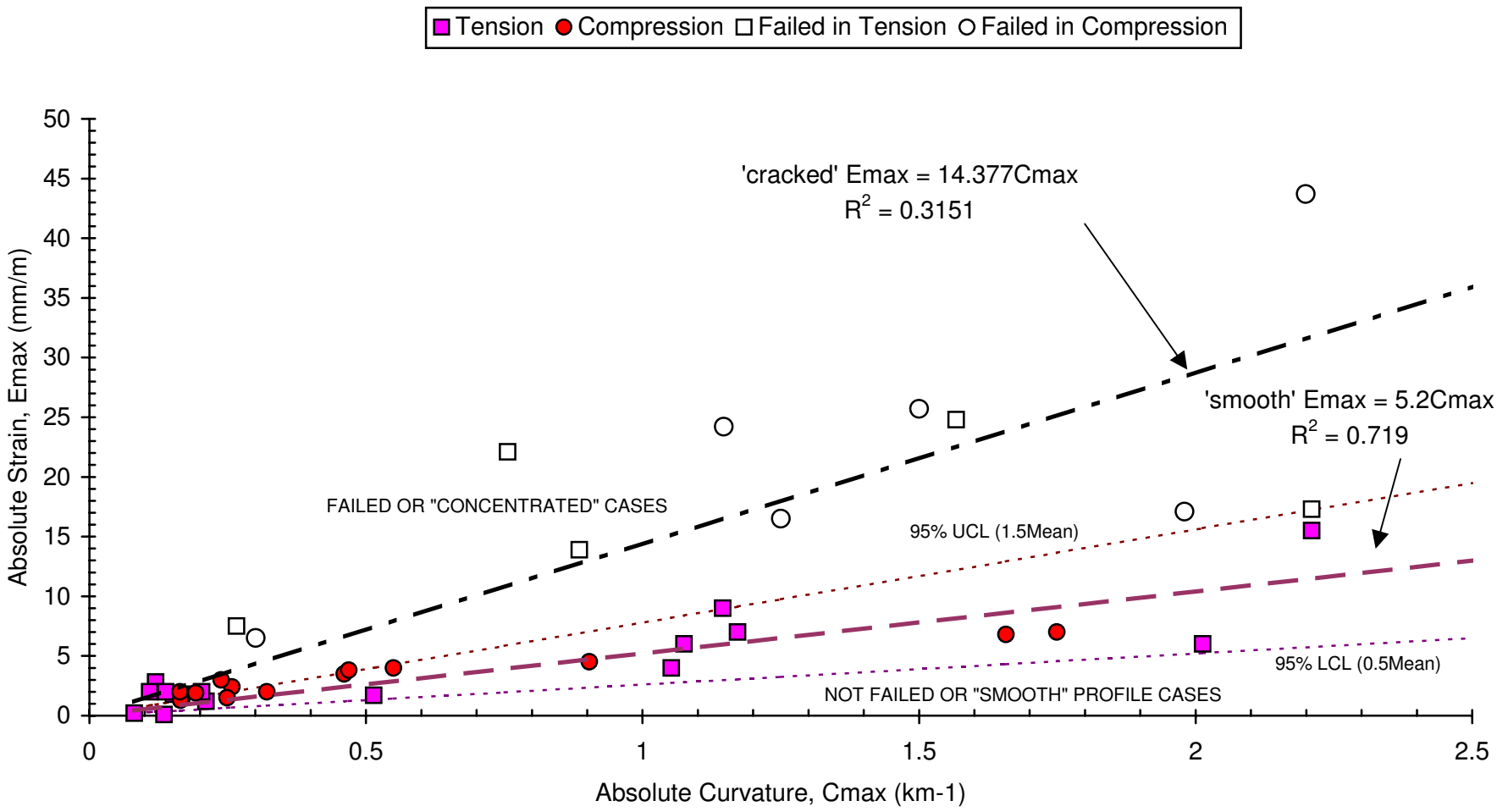

DgS	Engineer:	S.Ditton	Client:	Extract from ACARP, 2003	
	Drawn:	S.Ditton			
	Date:	08.08.08	Title:	Empirical Model for Maximum Panel Strain Prediction Above Longwall Panels for Smooth and Cracked Profiles	
	Ditton Geotechnical Services Pty Ltd		Scale:	NTS	Figure No: A25

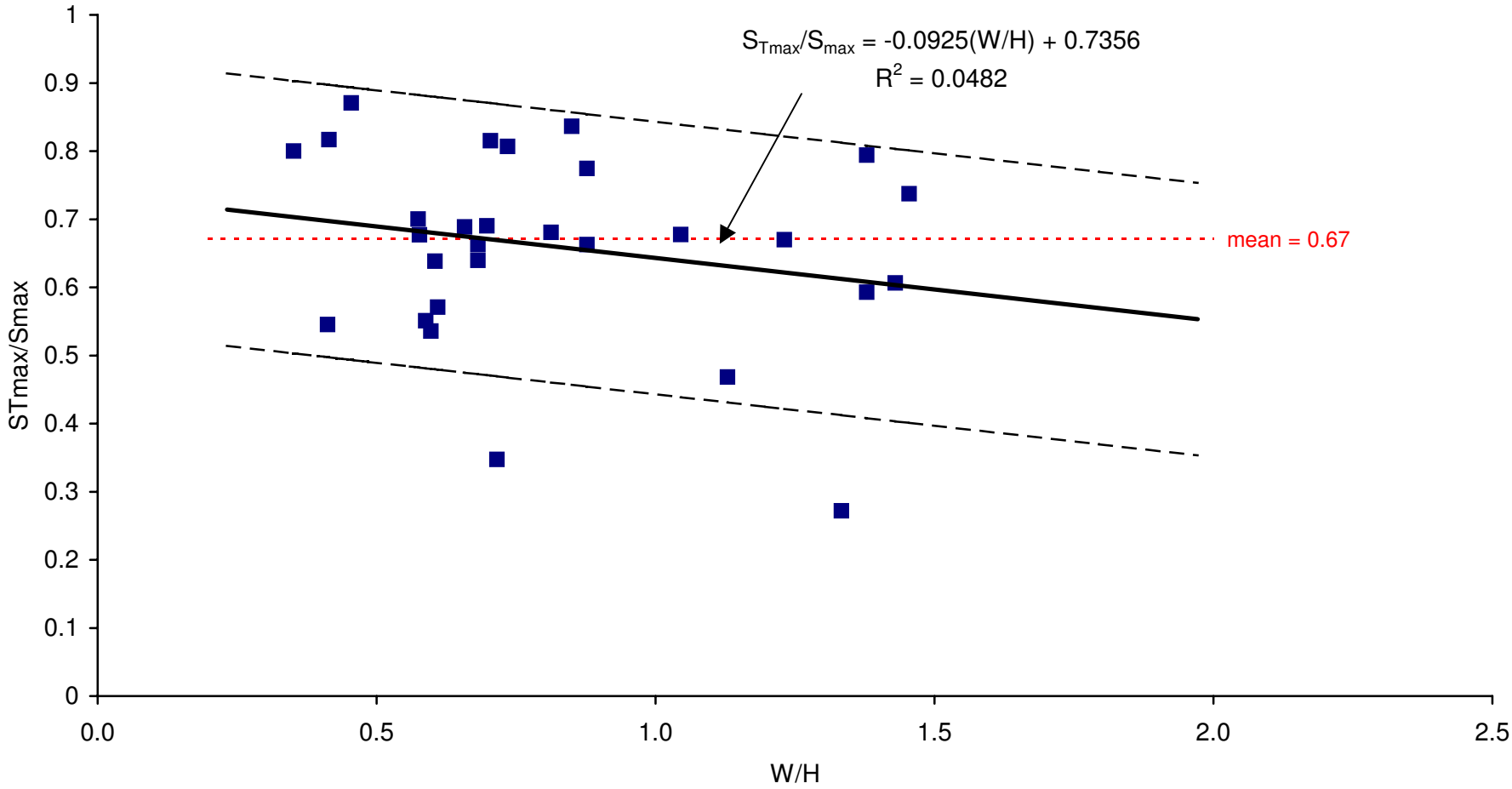

DgS	Engineer:	S.Ditton	Client:	Extract from ACARP, 2003	
	Drawn:	S.Ditton			
	Date:	08.08.08	Title:	Empirical Model for Subsidence at Maximum Tilt Above Longwall Panels	
	Ditton Geotechnical Services Pty Ltd		Scale:	NTS	Figure No: A26

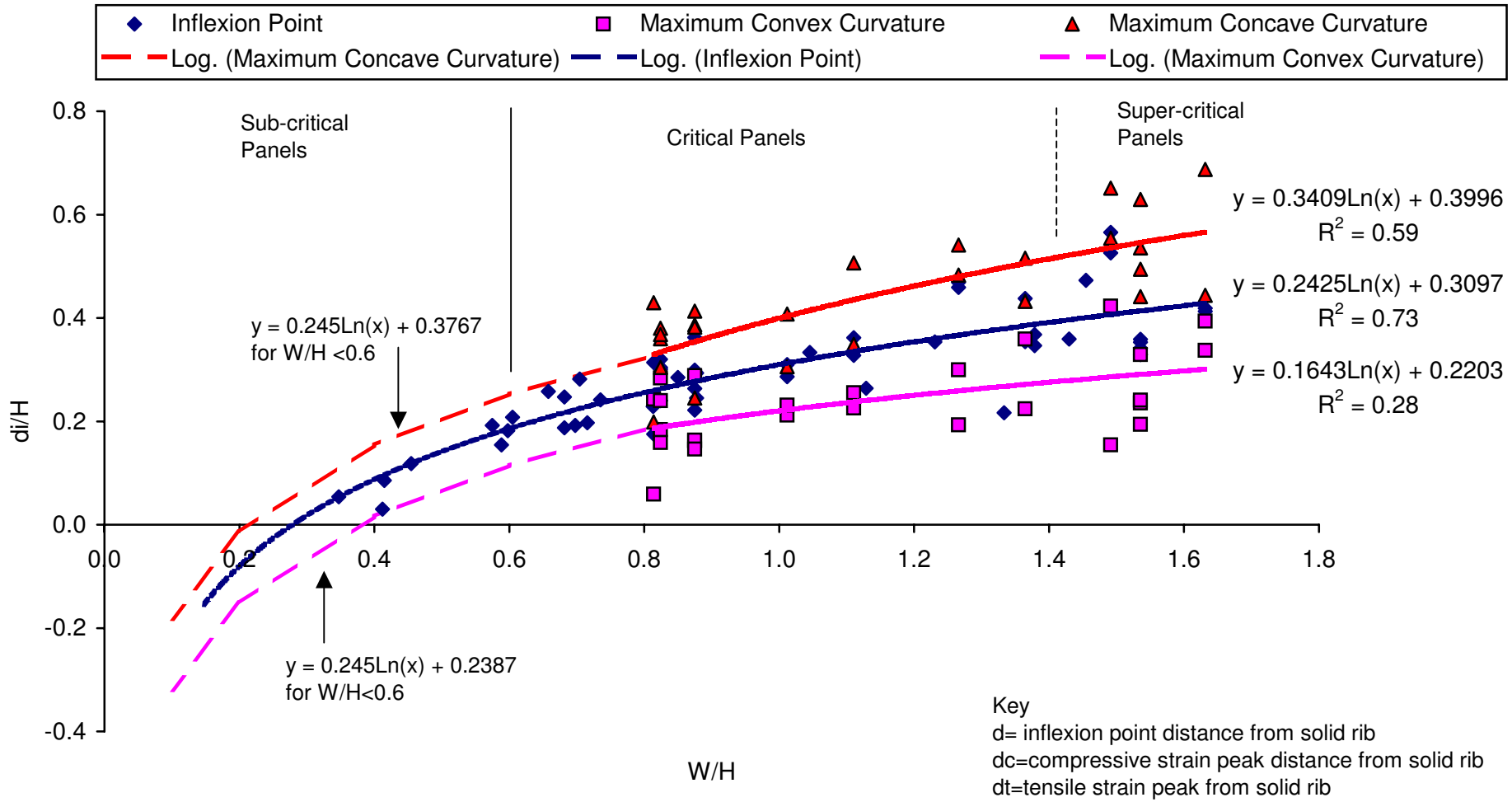

DgS	Engineer:	S.Ditton	Client:	Adapted from ACARP, 2003	
	Drawn:	S.Ditton			
	Date:	08.08.08	Title:	Empirical Model for Predicting the Location of Inflexion Point, Maximum Tensile and Compressive Strain Peaks due to Longwall Panel Subsidence in the Newcastle Coalfield	
	Ditton Geotechnical Services Pty Ltd		Scale:	NTS	Figure No: A27

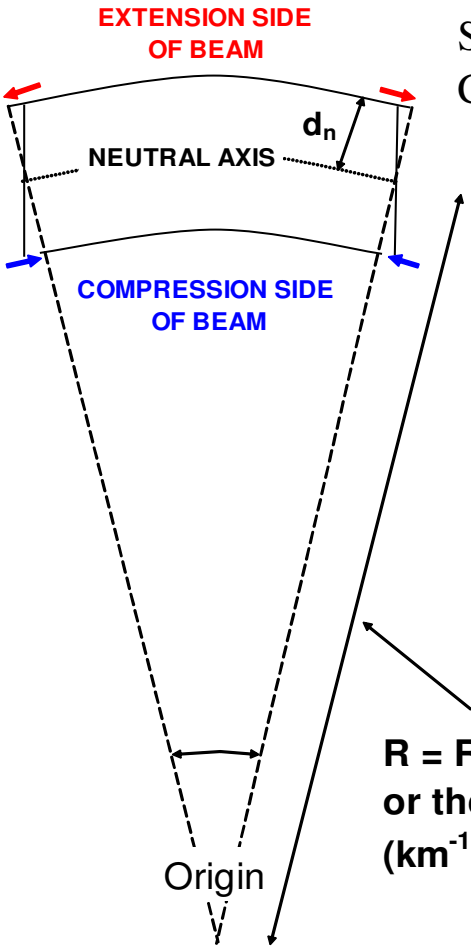

Strain E = (mm/m)
Curvature C = km-1

E = C x dn

Average
dn = 5.2 m
for database

R = Radius of curvature or the curvature, C = 1/R (km^{-1})

DgS	Engineer:	S.Ditton	Client:	Extract from ACARP, 2003	
	Drawn:	S.Ditton			
	Date:	08.08.08	Title:	Bending Beam Theory for Strain Prediction from Curvature Measurements	
	Ditton Geotechnical Services Pty Ltd		Scale:		Figure No: A28

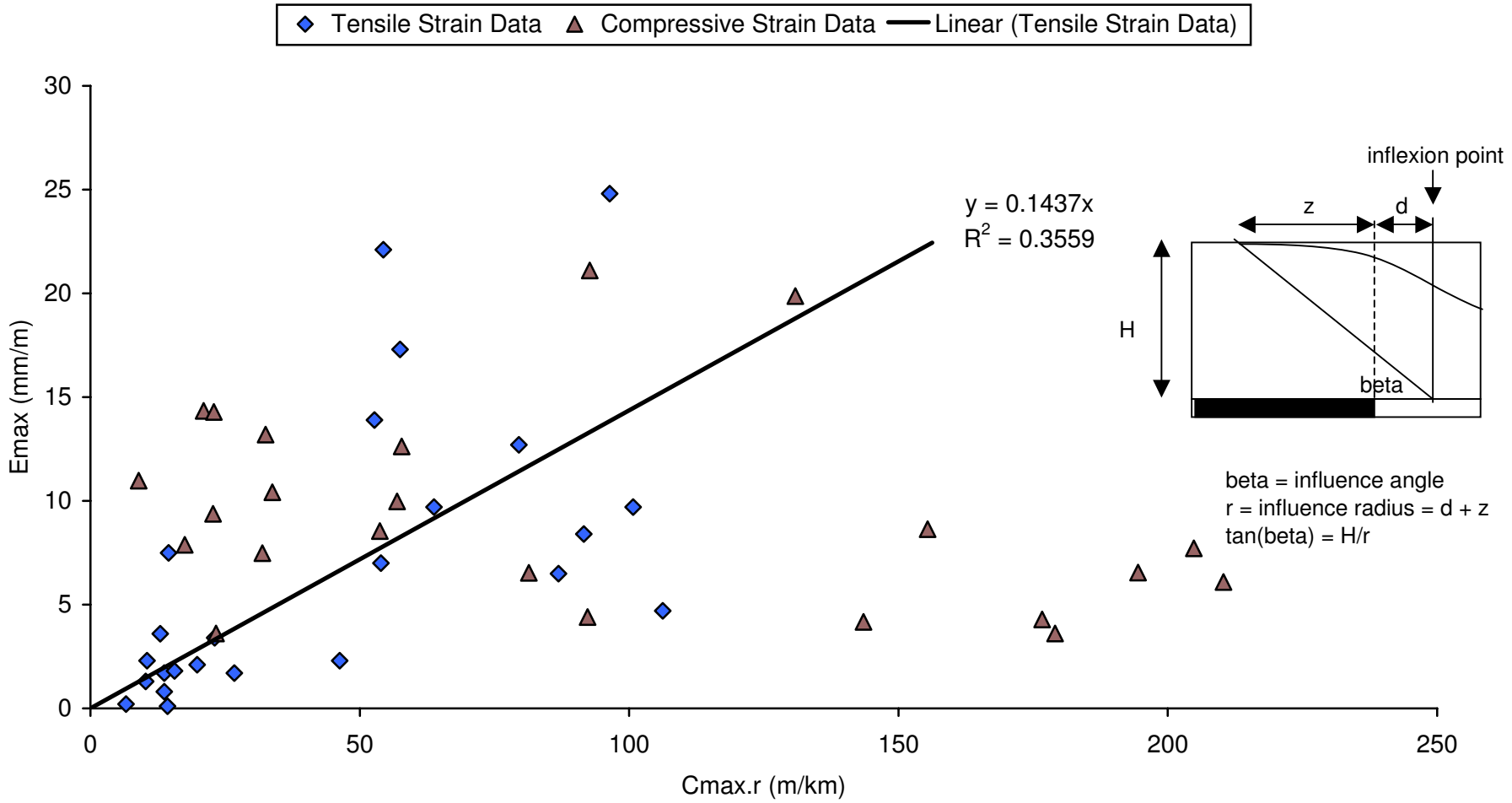

DgS	Engineer:	S.Ditton	Client:	Karmis, 1987 Adapted for ACARP, 2003	
	Drawn:	S.Ditton			
	Date:	08.08.08	Title:	Empirical Model Recommended by Karmis et al, 1987 for Predicting Strain from Curvature Above Longwall Panels in Newcastle Coalfield	
	Ditton Geotechnical Services Pty Ltd		Scale:	NTS	Figure No: A29.1

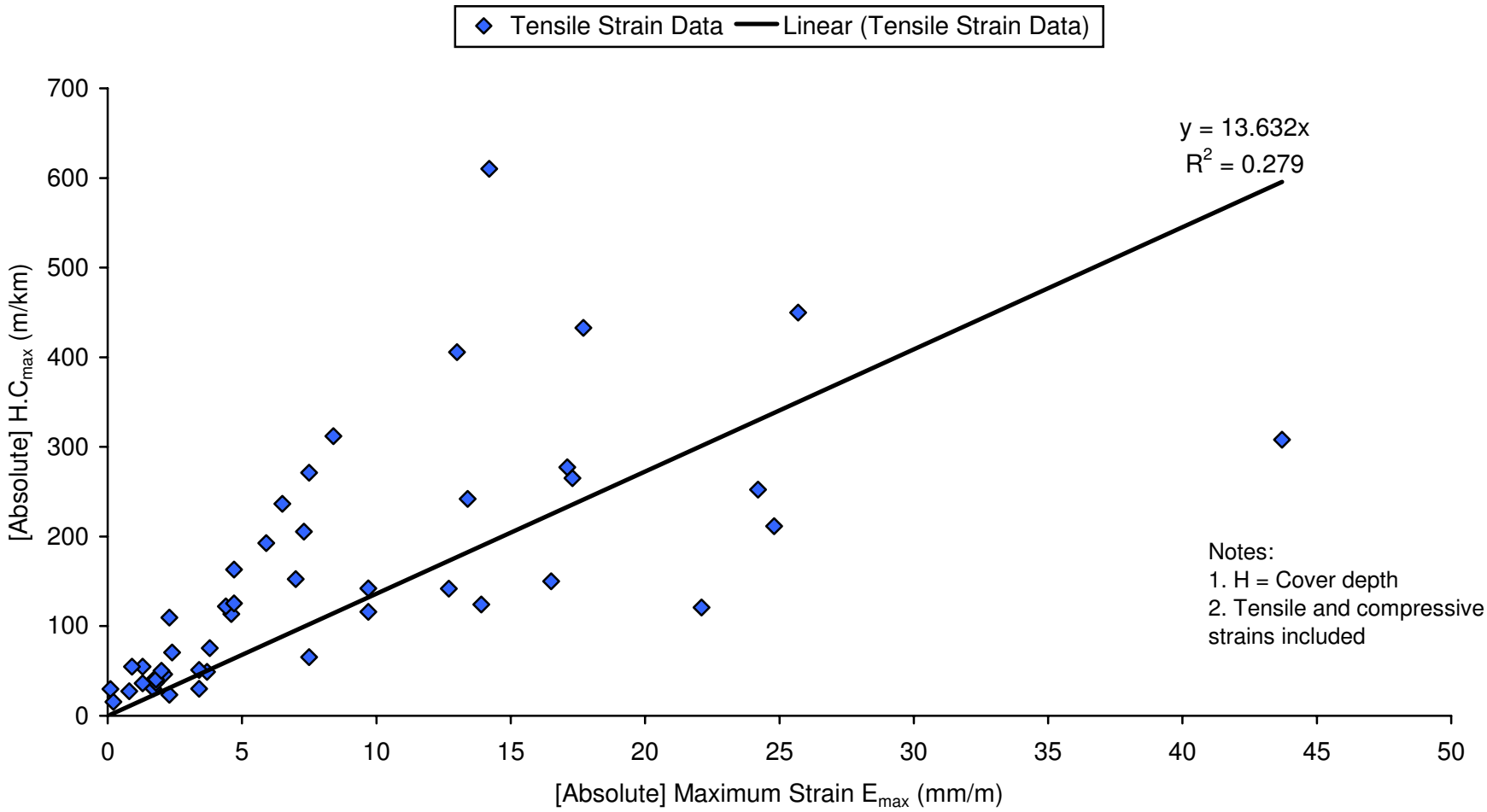

DgS	Engineer:	S.Ditton	Client:	Holla and Barclay, 2000 Adapted for ACARP, 2003	
	Drawn:	S.Ditton			
	Date:	08.08.08	Title:	Empirical Model Recommended by Holla and Barclay, 2000 for Predicting Curvature from Maximum Strain Above Longwall Panels in the Newcastle Coalfield	
	Ditton Geotechnical Services Pty Ltd		Scale:	NTS	Figure No: A29.2

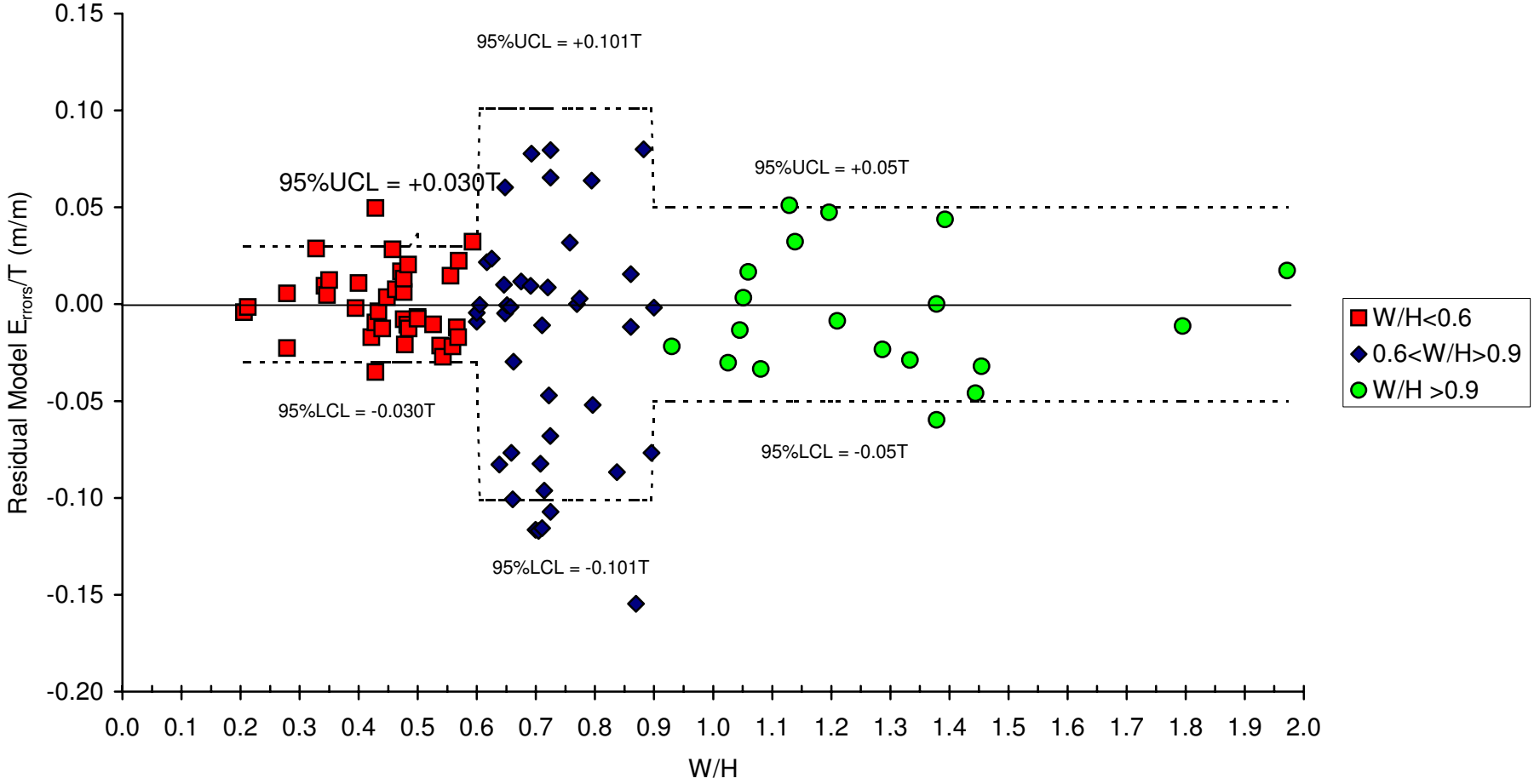

DgS	Engineer:	S.Ditton	Client:	Extract from ACARP, 2003	
	Drawn:	S.Ditton			
	Date:	08.08.08	Title:	Residual Errors of Database for Single Panel Prediction Model above Longwalls in the Newcastle Coalfield	
	Ditton Geotechnical Services Pty Ltd		Scale:	NTS	Figure No: A30

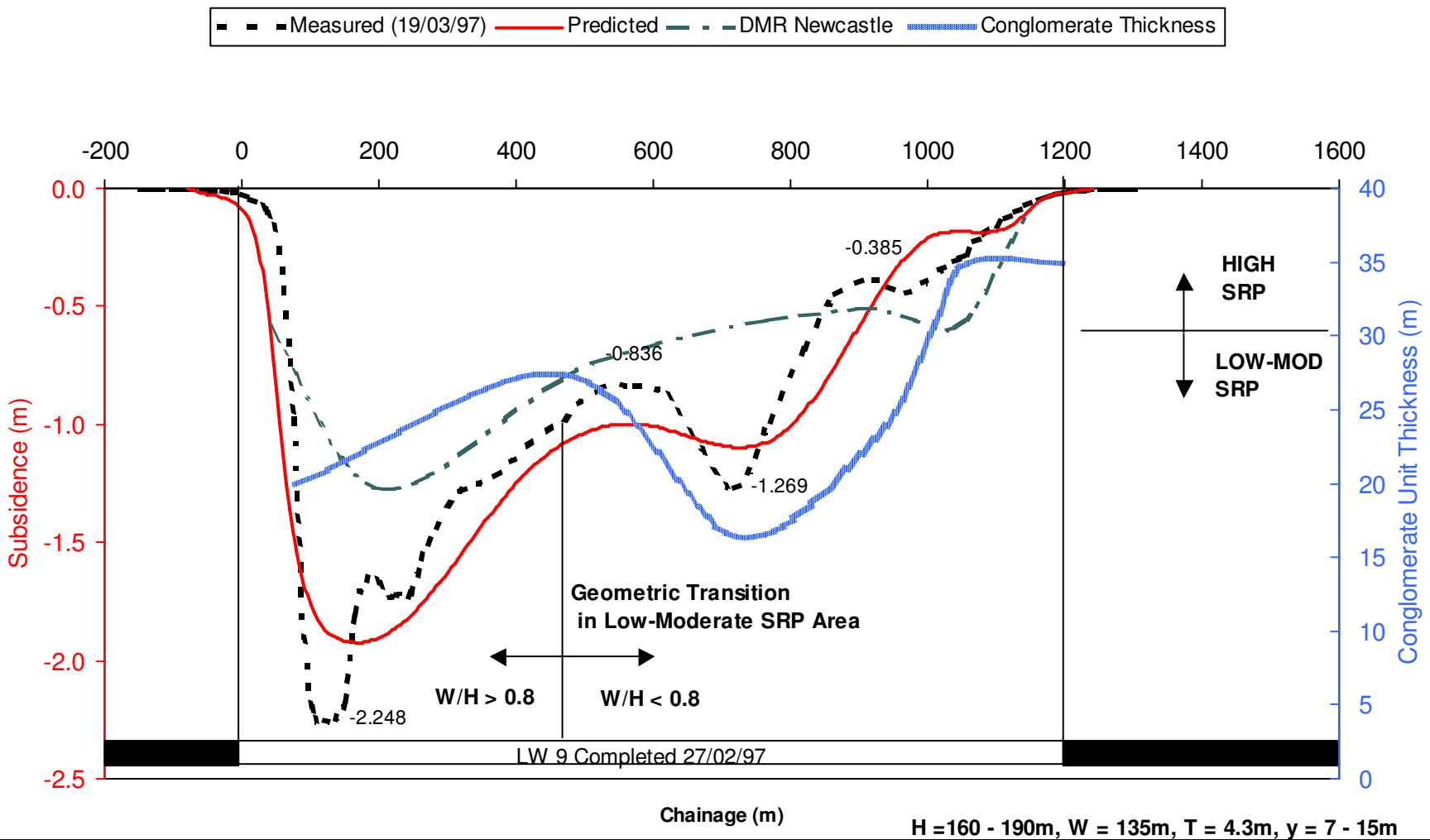

H =160 - 190m, W = 135m, T = 4.3m, y = 7 - 15m

DgS	Engineer:	S.Ditton	Client:	Extract from ACARP, 2003	
	Drawn:	S.Ditton			
	Date:	08.08.08	Title:	Predicted v. Measured Centreline Subsidence Profiles for a Newcastle Coalfield Longwall with Massive Conglomerate Strata and Sub-Critical to Supercritical Transition	
	Ditton Geotechnical Services Pty Ltd		Scale:	NTS	Figure No: A31

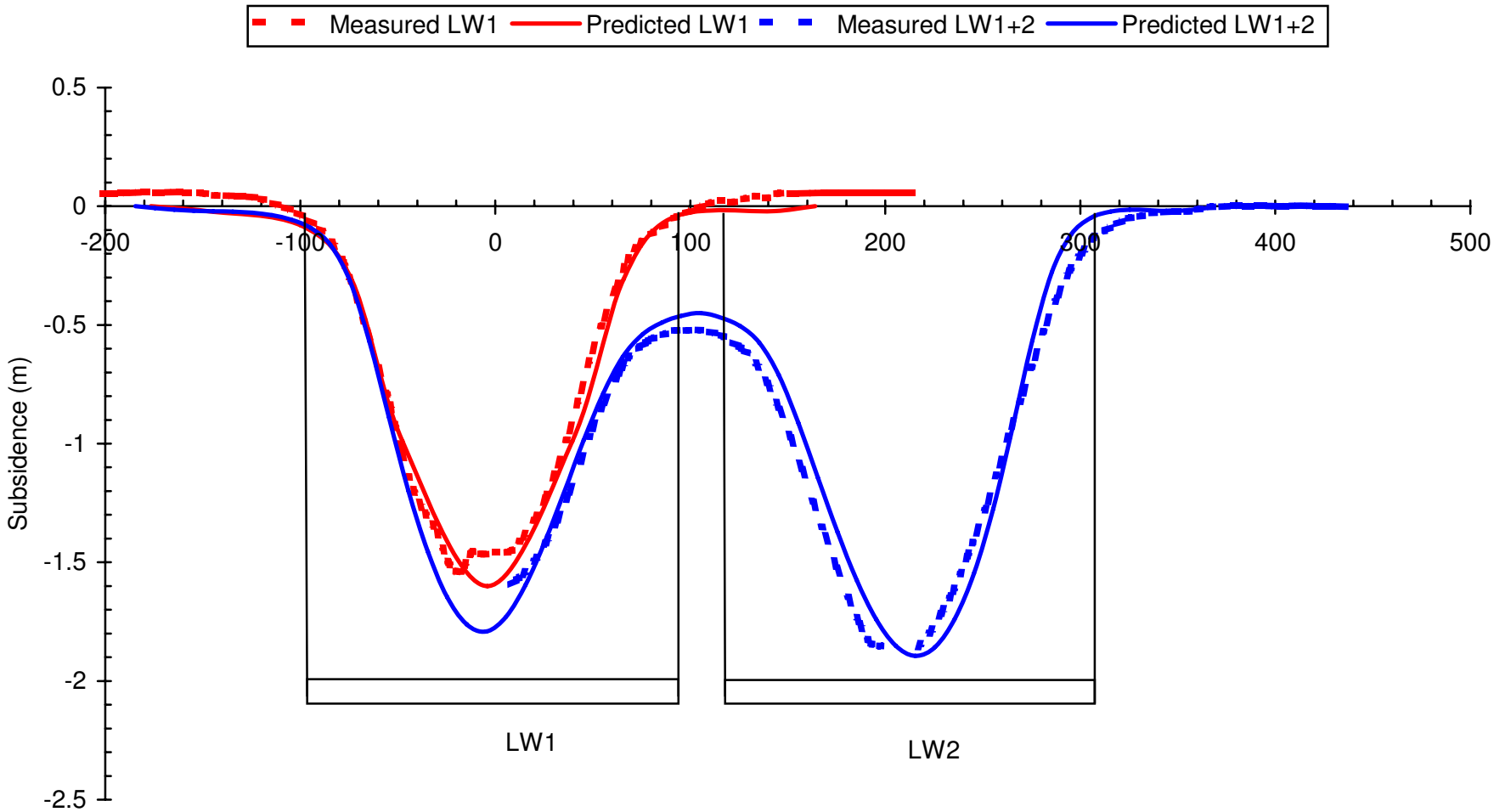

DgS	Engineer:	S.Ditton	Client:	Extract from ACARP, 2003	
	Drawn:	S.Ditton			
	Date:	08.08.08	Title:	Predicted v. Measured Crossline Subsidence Profiles for a Newcastle Coalfield Longwall Mine	
	Ditton Geotechnical Services Pty Ltd		Scale:	NTS	Figure No: A32

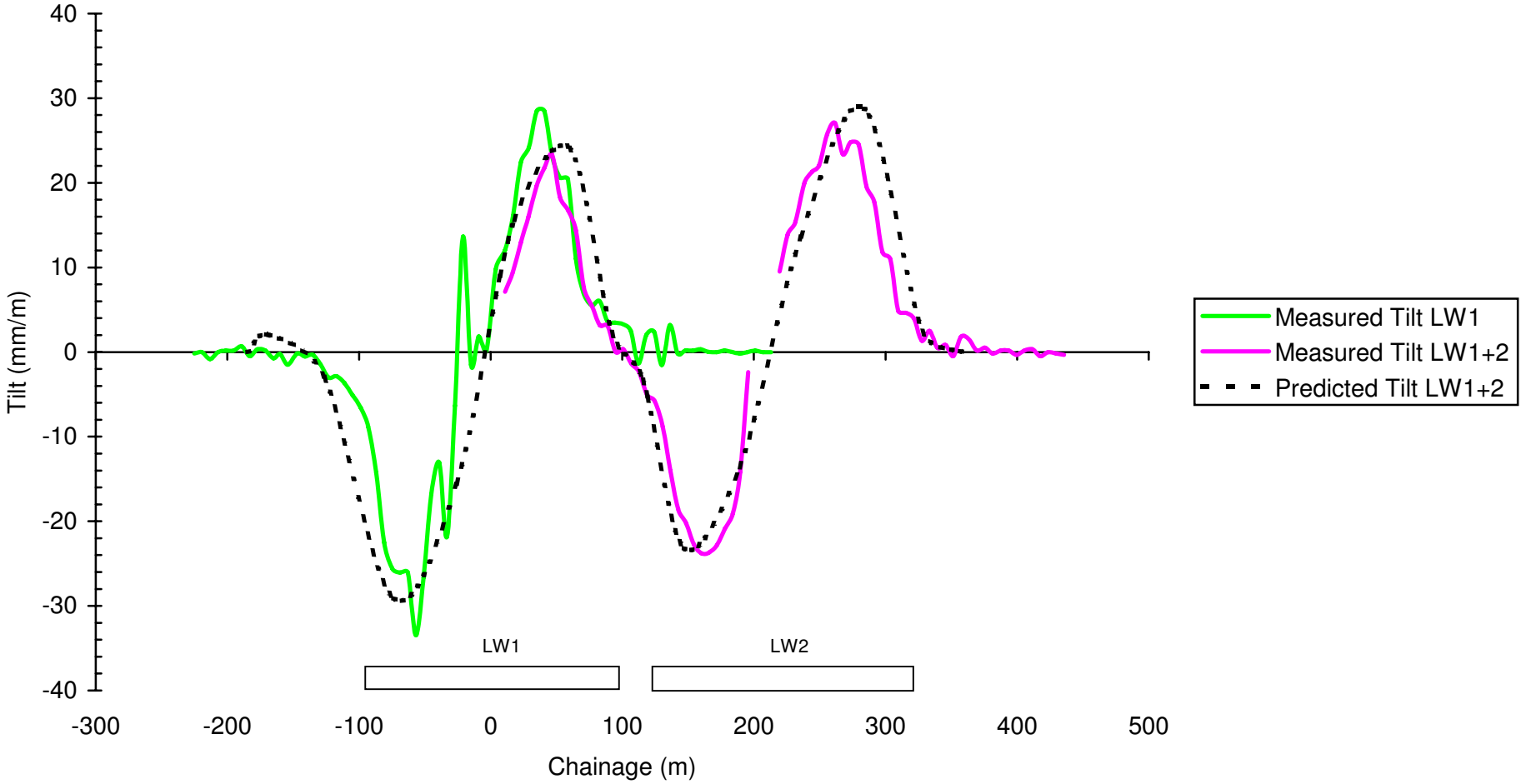

DgS	Engineer:	S.Ditton	Client:	Extract from ACARP, 2003	
	Drawn:	S.Ditton			
	Date:	08.08.08	Title:	Predicted v. Measured Crossline Tilt Profiles for a Newcastle Coalfield Longwall Mine	
	Ditton Geotechnical Services Pty Ltd		Scale:	NTS	Figure No: A33

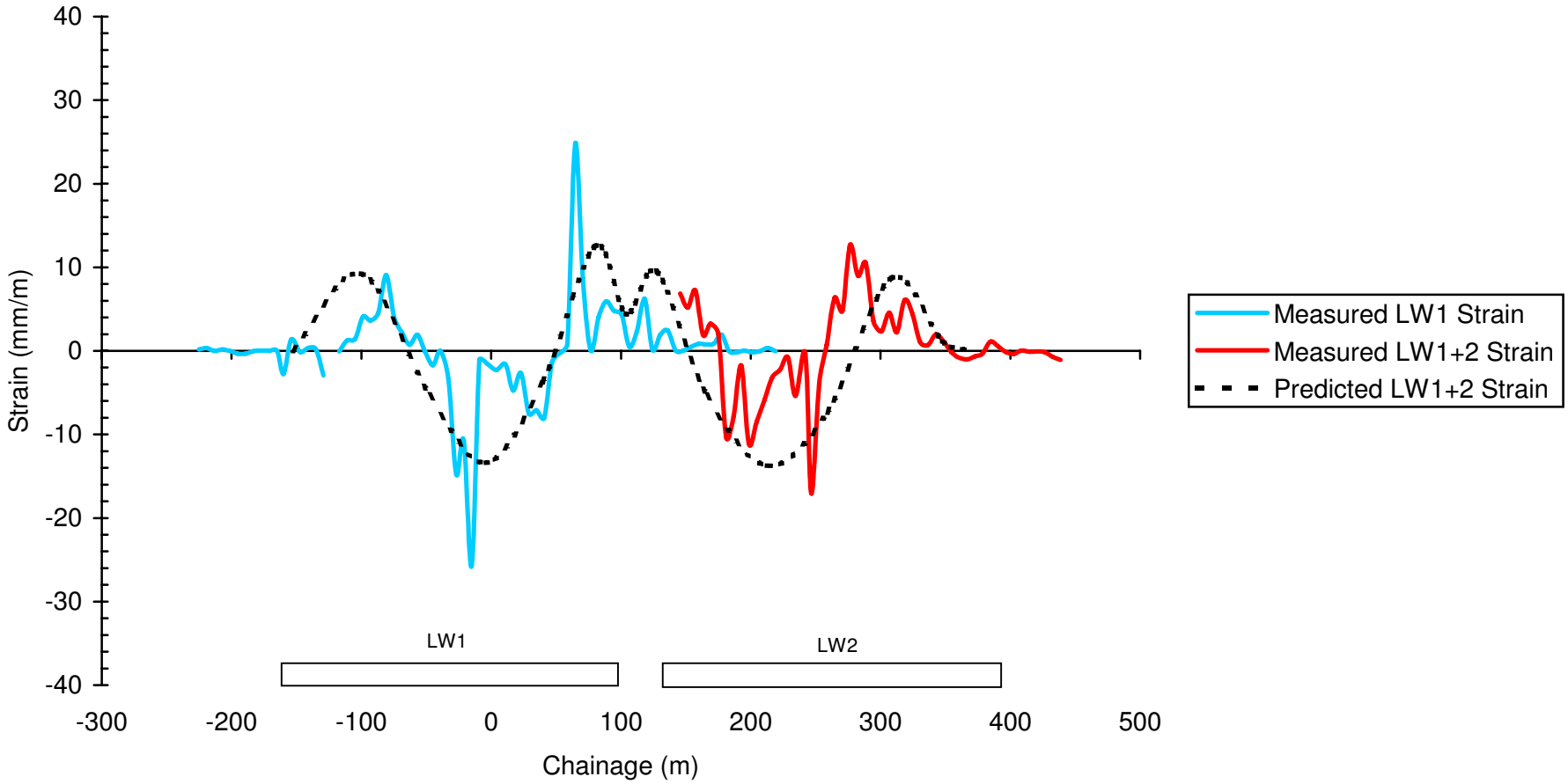

DgS	Engineer:	S.Ditton	Client:	Extract from ACARP, 2003	
	Drawn:	S.Ditton			
	Date:	08.08.08	Title:	Predicted v. Measured Crossline Strain Profiles for a Newcastle Coalfield Longwall Mine	
	Ditton Geotechnical Services Pty Ltd		Scale:	NTS	Figure No: A34

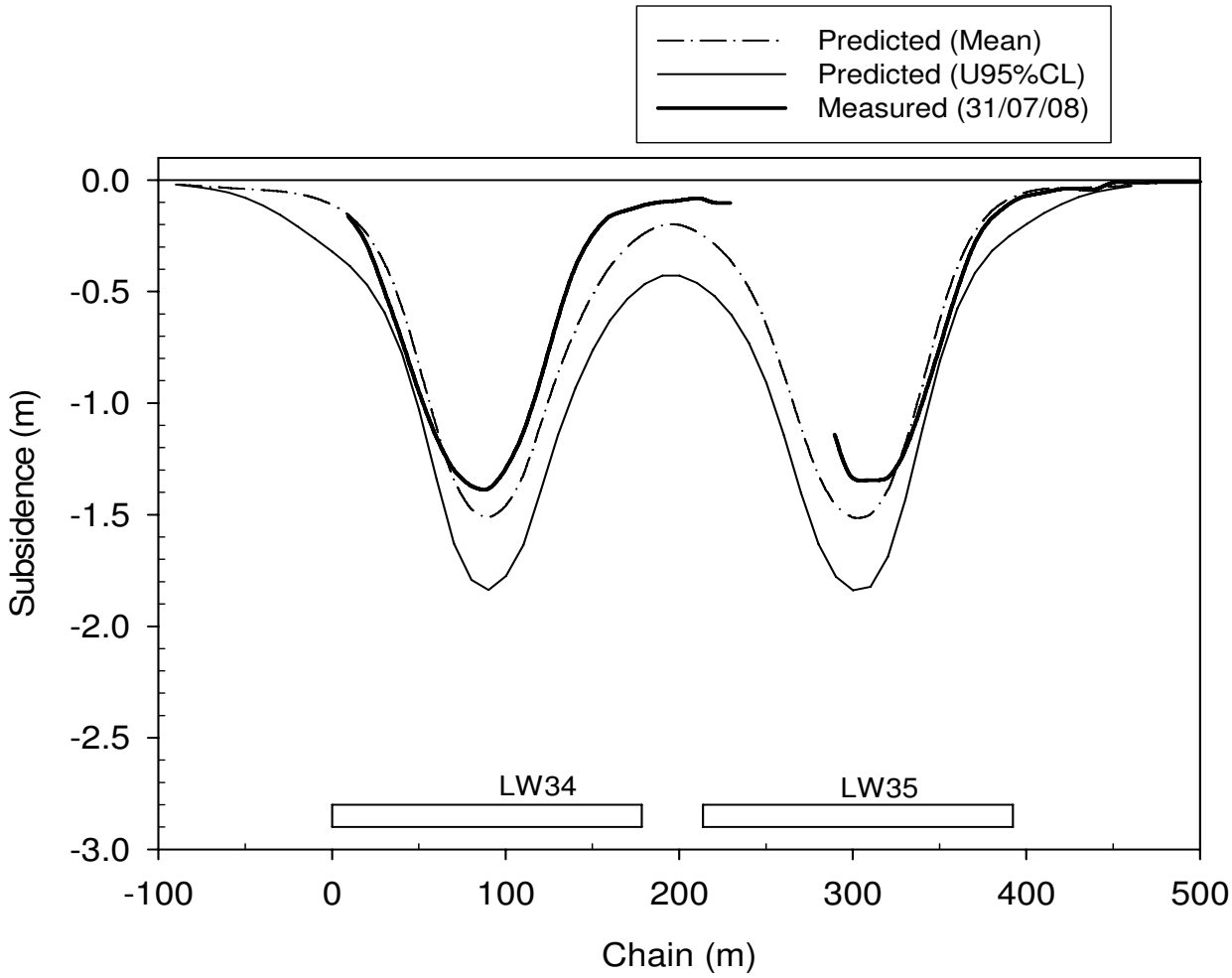

DgS	Engineer:	S.Ditton	Client:	DgS, 2008 Modified ACARP, 2003 Model Outcomes	
	Drawn:	S.Ditton			
	Date:	07.09.08	Title:	Predicted v. Measured Crossline Subsidence Profiles for a Newcastle Coalfield Longwall Longwall Panel	
	Ditton Geotechnical Services Pty Ltd		Scale:	NTS	Figure No: A35

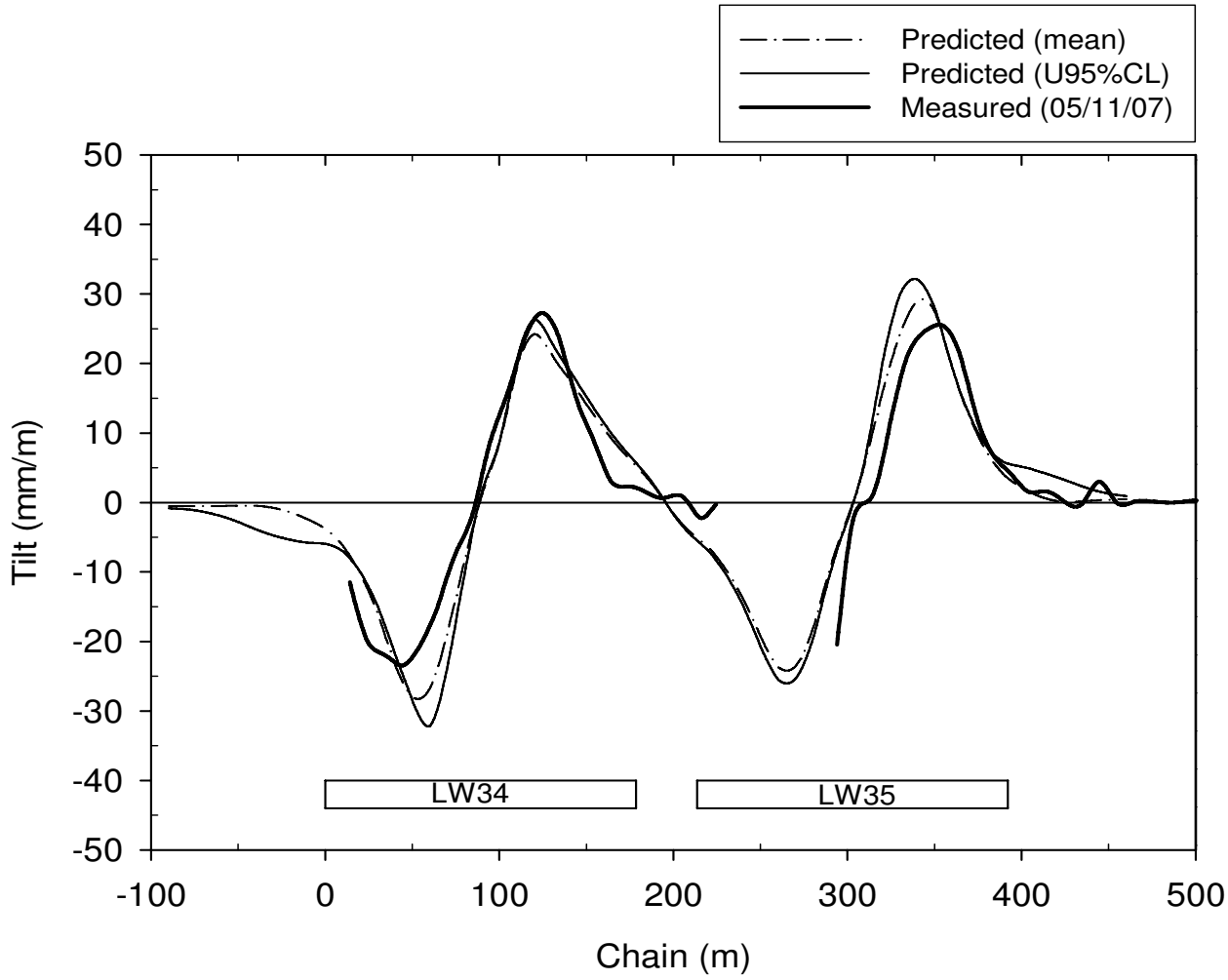

DgS	Engineer:	S.Ditton	Client:	DgS, 2008 Modified ACARP, 2003 Model Outcomes	
	Drawn:	S.Ditton			
	Date:	07.09.08	Title:	Predicted v. Measured Crossline Tilt Profiles for a Newcastle Coalfield Longwall Mine	
Ditton Geotechnical Services Pty Ltd			Scale:	NTS	Figure No: A36

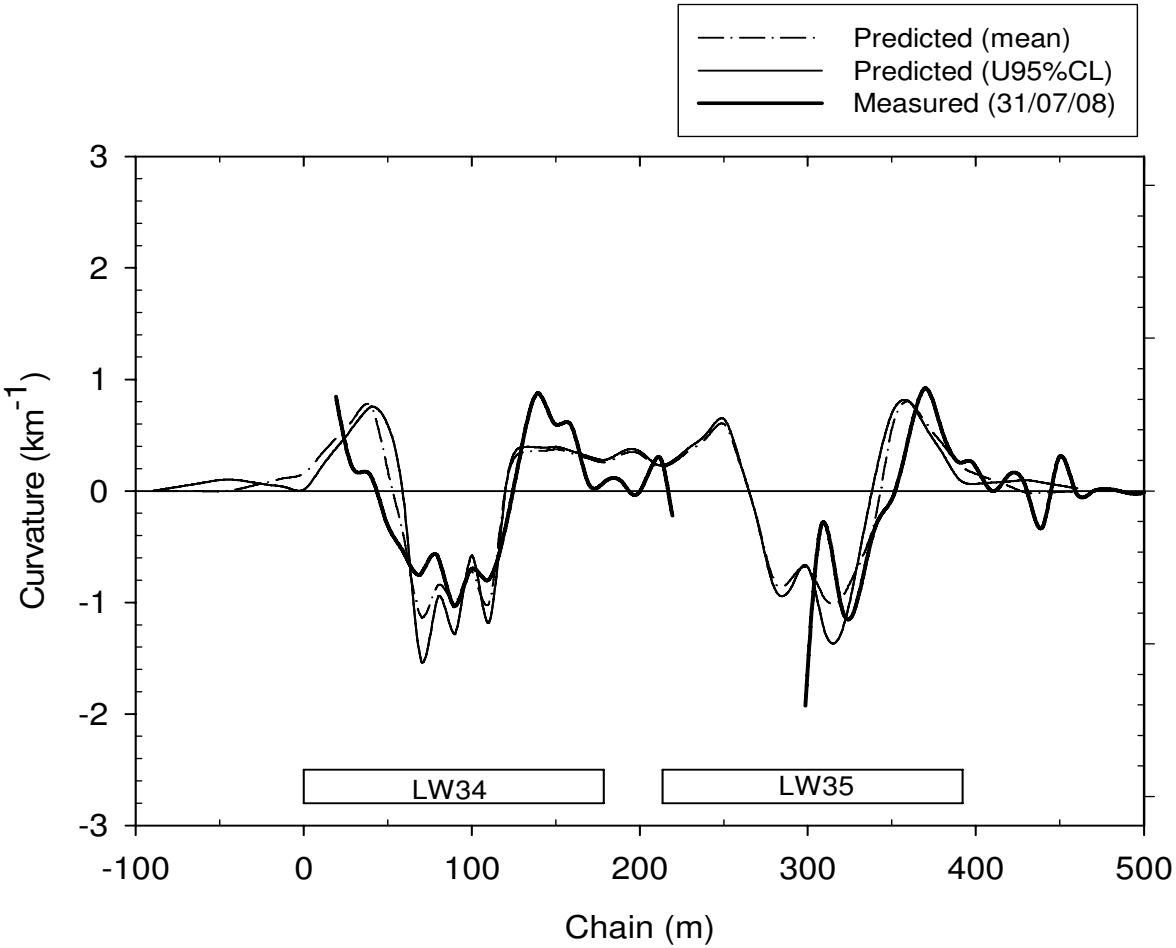

DgS	Engineer:	S.Ditton	Client:	DgS, 2008 Modified ACARP, 2003 Model Outcomes	
	Drawn:	S.Ditton			
	Date:	07.09.08	Title:	Predicted v. Measured Crossline Curvature Profiles for a Newcastle Coalfield Longwall Mine	
	Ditton Geotechnical Services Pty Ltd		Scale:	NTS	Figure No: A37

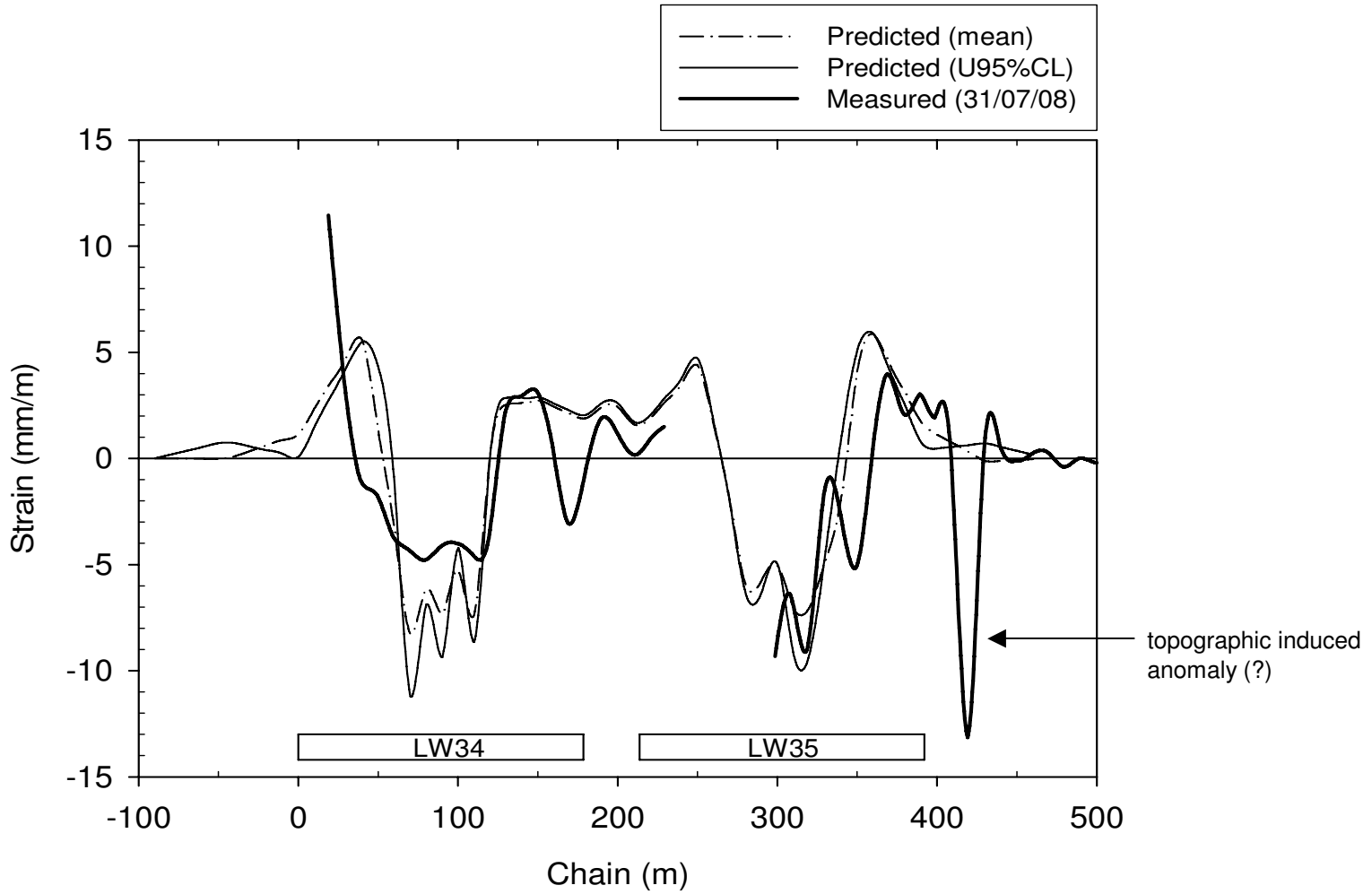

DgS	Engineer:	S.Ditton	Client:	DgS, 2008 Modified ACARP, 2003 Model Outcomes	
	Drawn:	S.Ditton			
	Date:	08.09.08	Title:	Predicted v. Measured Crossline Strain Profiles for a Newcastle Coalfield Longwall Mine	
	Ditton Geotechnical Services Pty Ltd		Scale:	NTS	Figure No: A38

Strain Concentration Factor Calculation for 10 m Baylength^

- Measured crack width = 100 mm.
- Measured crack depth >5 m
- Location = 27 m from solid rib.
  Smax = 1.4 m.
- Cover depth, H = 180 m.
- LW panel width, W= 175 m.
  (W/H = 0.97)
- Measured curvature,
  C = 1.15 km-1
  (radius of 867 m)
- Measured strain over 10 m,
  E = 5.8 mm/m*
- Concentrated strain = crack width/bay-length = 100/10 = 10 mm/m.

Therefore, concentrated strain = 10/5.8 = 1.7 x uniform strain.

*- peak strains measured 10 m to south of crack at same distance from rib.
^ - It is likely that strain concentration includes strain from adjacent 'bays'.

DgS	Engineer:	S.Ditton	Client:	Adapted from ACARP, 2003	
	Drawn:	S.Ditton			
	Date:	08.08.08	Title:	Example of Strain Concentration Effect Above Longwall with Shallow Surface Rock	
	Ditton Geotechnical Services Pty Ltd		Scale:	NTS	Figure No: A39

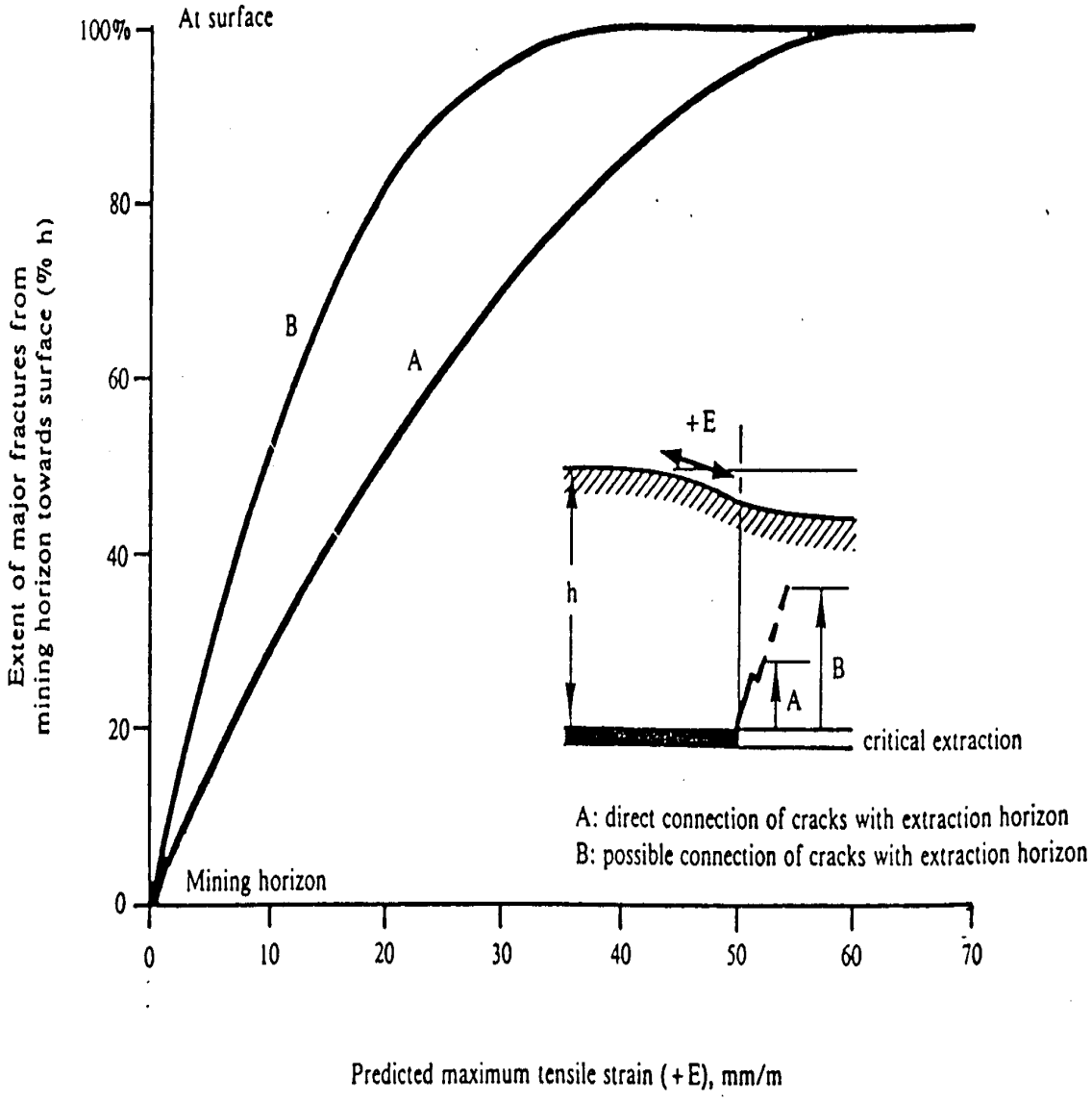

DgS	Engineer:	S.Ditton	Client:	Extract from ACARP, 2003		
	Drawn:	S.Ditton				
	Date:	30.04.07	Title:	Enpirically Based Sub-Surface Fracturing Model Presented in Whittaker & Reddish, 1989		
	Ditton Geotechnical Services Pty Ltd		Scale:	NTS	Figure No:	A40

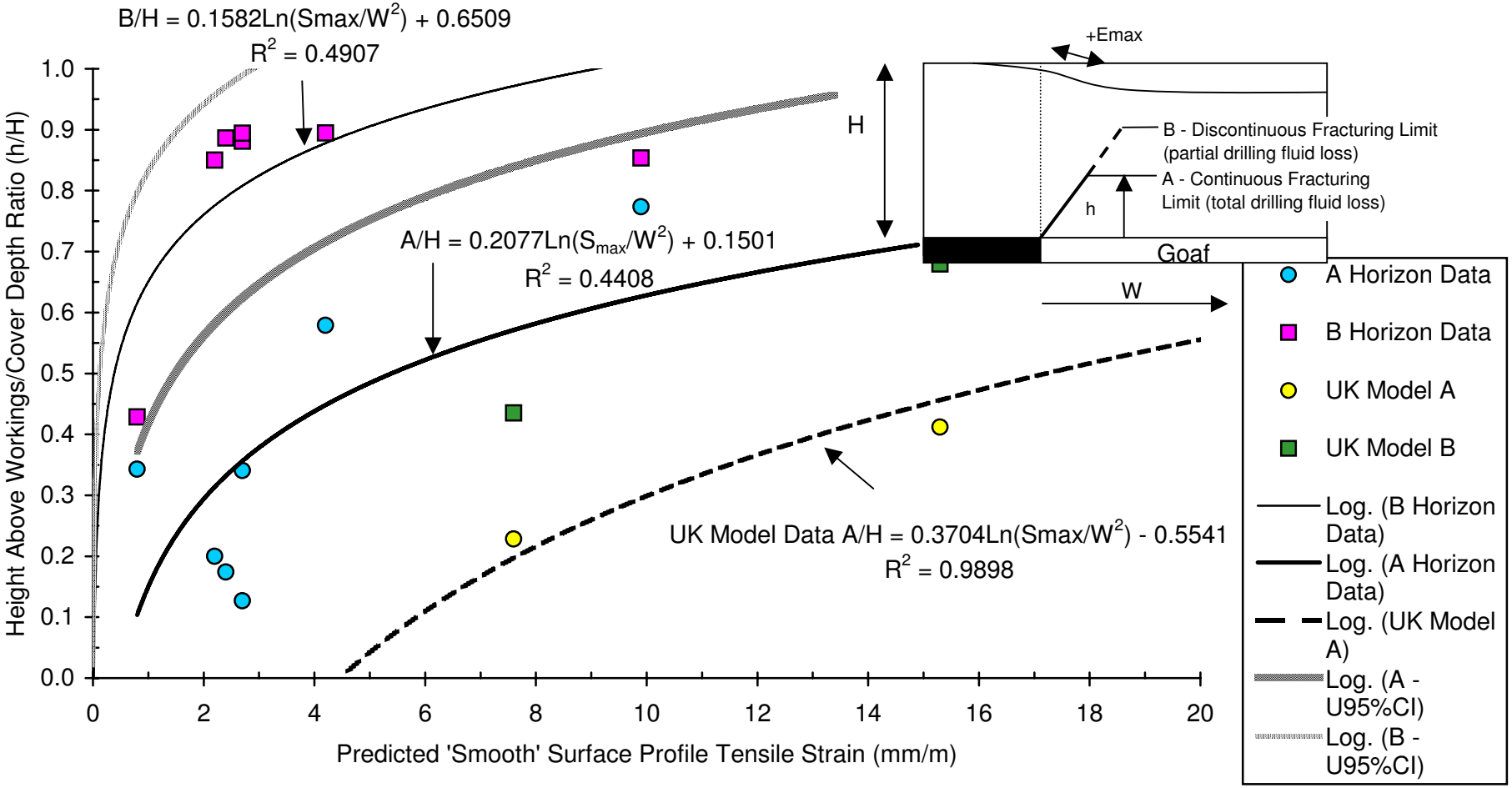

DgS	Engineer:	S.Ditton	Client:	Extract from ACARP, 2003	
	Drawn:	S.Ditton			
	Date:	12.08.08	Title:	Continuous and Discontinuous Sub-Surface Fracture Height Model above Longwalls using Surface Tensile Strains	
	Ditton Geotechnical Services Pty Ltd		Scale:	NTS	Figure No: A41

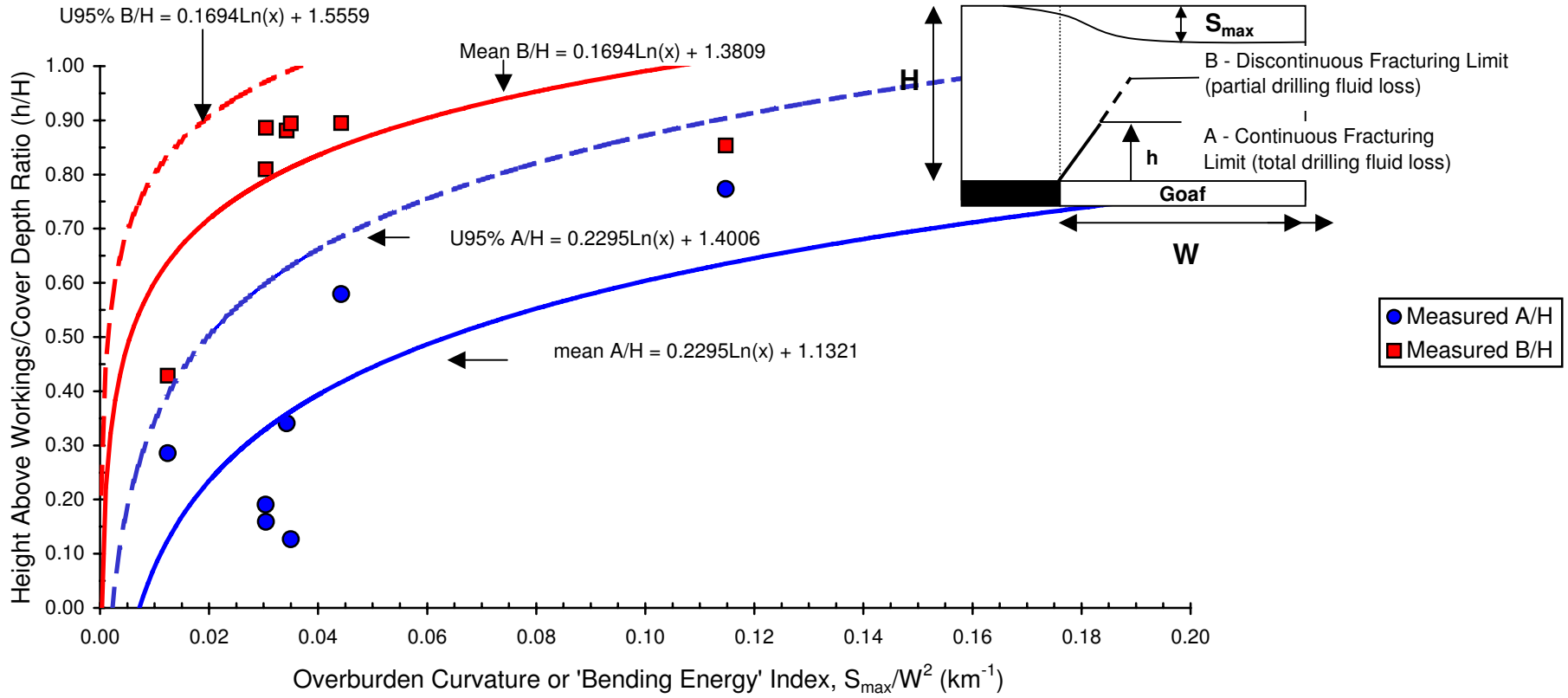

DgS	Engineer:	S.Ditton	Client:	Extract from ACARP, 2003	
	Drawn:	S.Ditton			
	Date:	12.08.08	Title:	Continuous and Discontinuous Sub-Surface Fracture Heights above Longwalls (based on ACARP, 2003)	
	Ditton Geotechnical Services Pty Ltd		Scale:	NTS	Figure No: A42

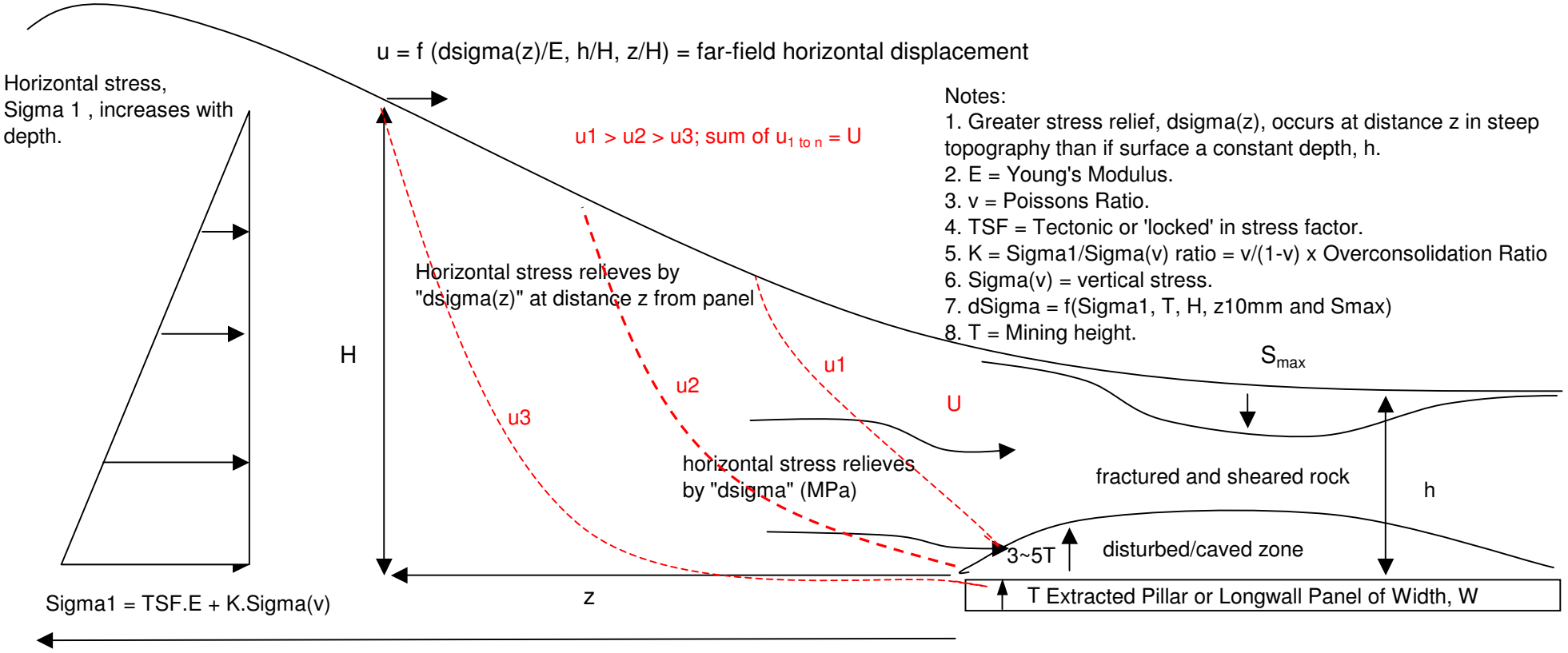

Simple Analytical Model for Predicting Total FFD : U = 0.5(Sigma1 x 12.3/2)z10mm/[E(H+h)/2] + 'tail' of 10mm + Smax component (refer to text)

DgS	Engineer:	S.Ditton	Client:	DgS, 2007	
	Drawn:	S.Ditton			
	Date:	22.05.07	Title:	Conceptual Model of Far-Field Displacement Outside Angle of Draw Limits from Pillar Extraction or Longwall Panels	
	Ditton Geotechnical Services Pty Ltd		Scale:	NTS	Figure No: A43

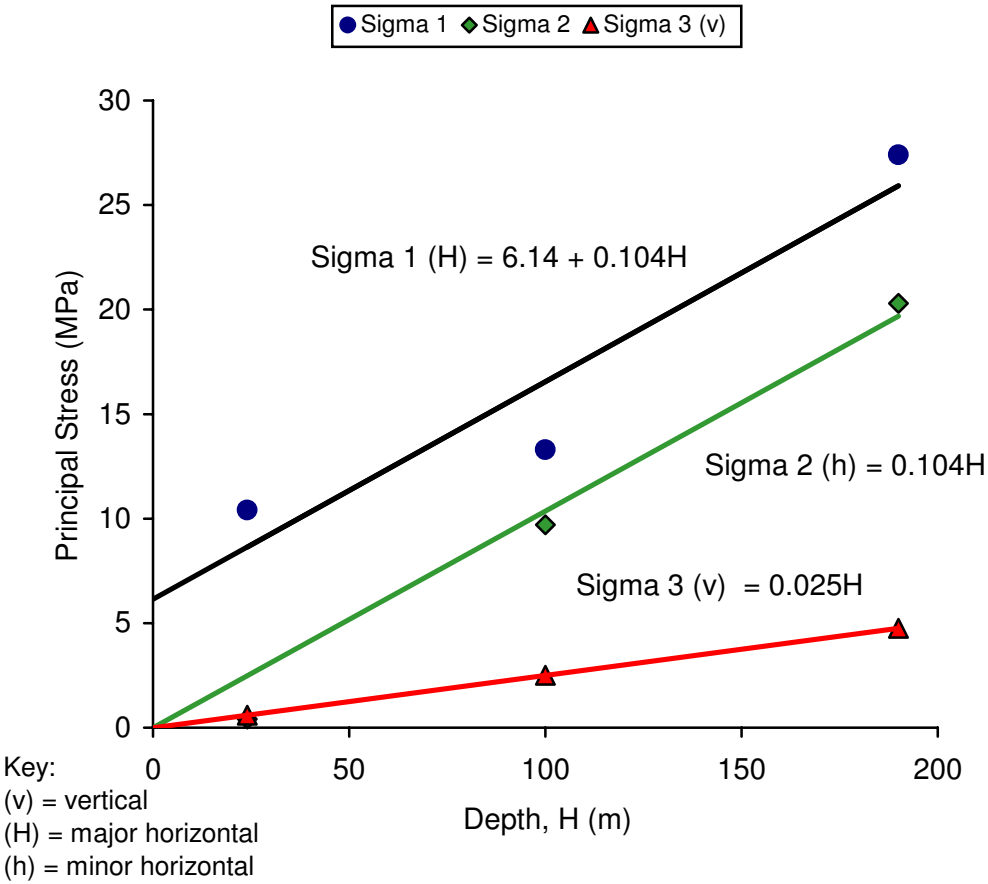

Measured Stress Field for F3 Freeway, West of Newcastle (Lohe & Dean Jones, 1995)

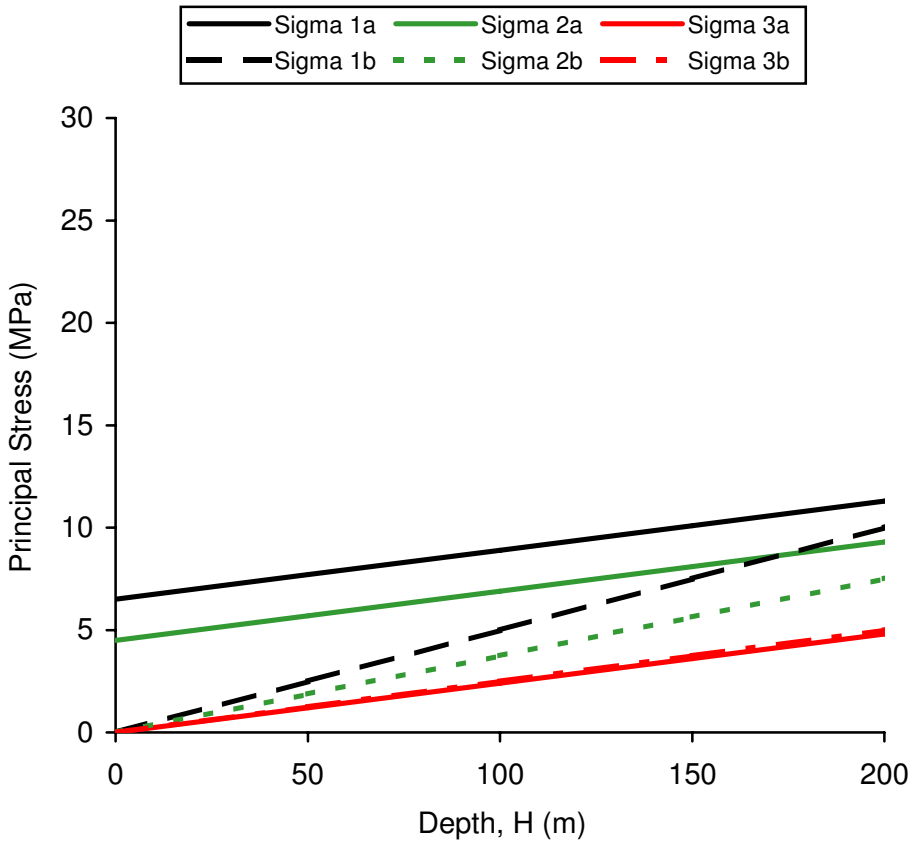

Typical Stress Field Models for Sydney Basin Overburden a) McQueen, 2004; b) Lohe & Dean Jones, 1995; c) Pells, 2002 not shown for clarity (refer to text).

DgS	Engineer:	S.Ditton	Client:	DgS, 2007	
	Drawn:	S.Ditton			
	Date:	12.07.07	Title:	Published Principal Stress Field Models for Sydney Basin and Western Area of Newcastle Coalfield	
	Ditton Geotechnical Services Pty Ltd		Scale:	NTS	Figure No: A44

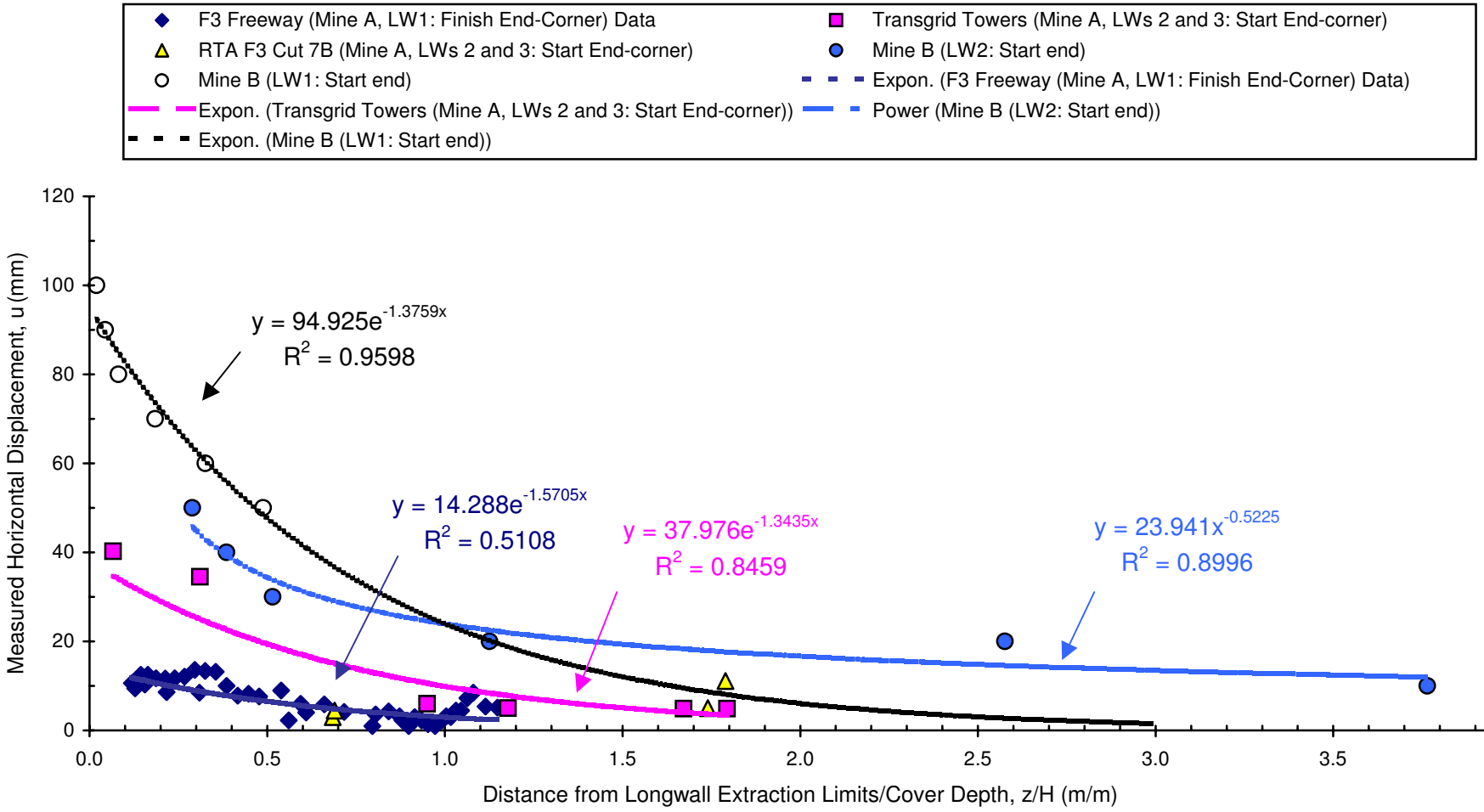

DgS	Engineer:	S.Ditton	Client:	DgS, 2007	
	Drawn:	S.Ditton			
	Date:	22.05.07	Title:	Empirical far-field displacement prediction model using total station electronic distance measurements from longwall panel ends	
	Ditton Geotechnical Services Pty Ltd		Scale:	NTS	Figure No: A45

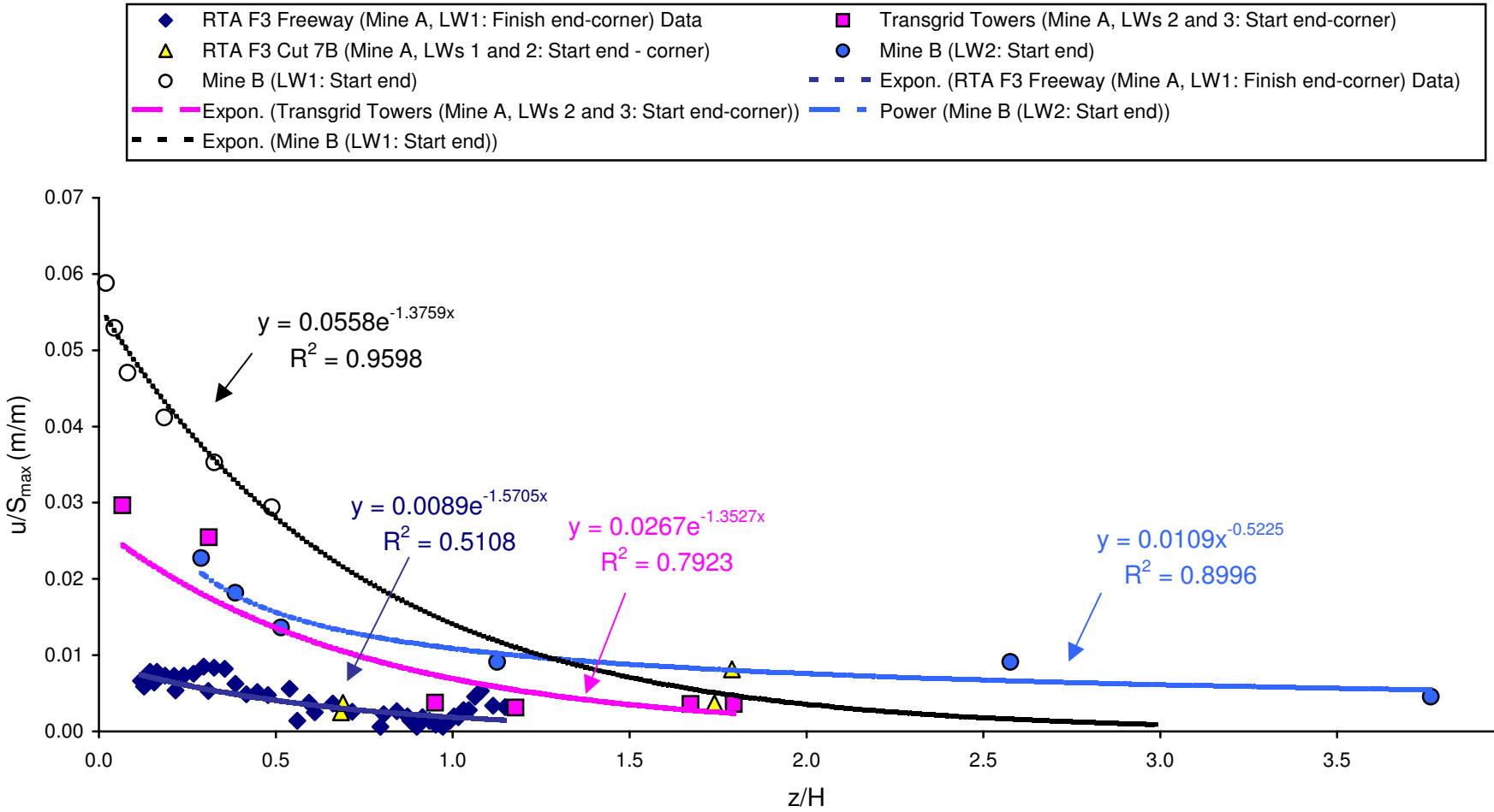

DgS	Engineer:	S.Ditton	Client:	DgS, 2007	
	Drawn:	S.Ditton			
	Date:	22.05.07	Title:	Empirical far-field displacement prediction model using total station electronic distance measurements from longwall panel ends and normalised to maximum panel subsidence	
	Ditton Geotechnical Services Pty Ltd		Scale:	NTS	Figure No: A46

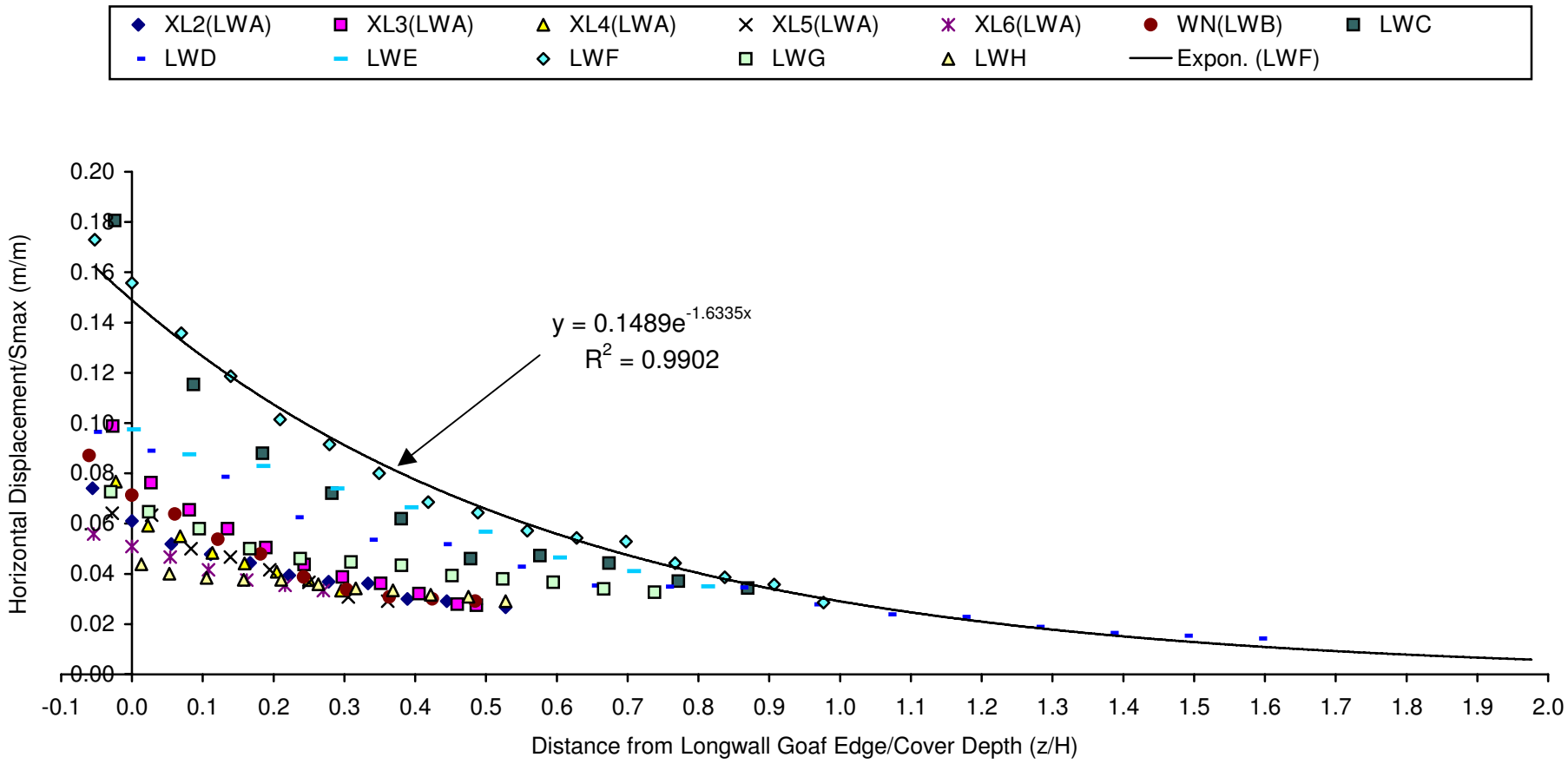

DgS	Engineer:	S.Ditton	Client:	DgS, 2007	
	Drawn:	S.Ditton			
	Date:	22.05.07	Title:	Empirical far-field displacement prediction model using cummulative steel tape measurements from longwall sides and normalised to maximum panel subsidence	
	Ditton Geotechnical Services Pty Ltd		Scale:	NTS	Figure No: A47

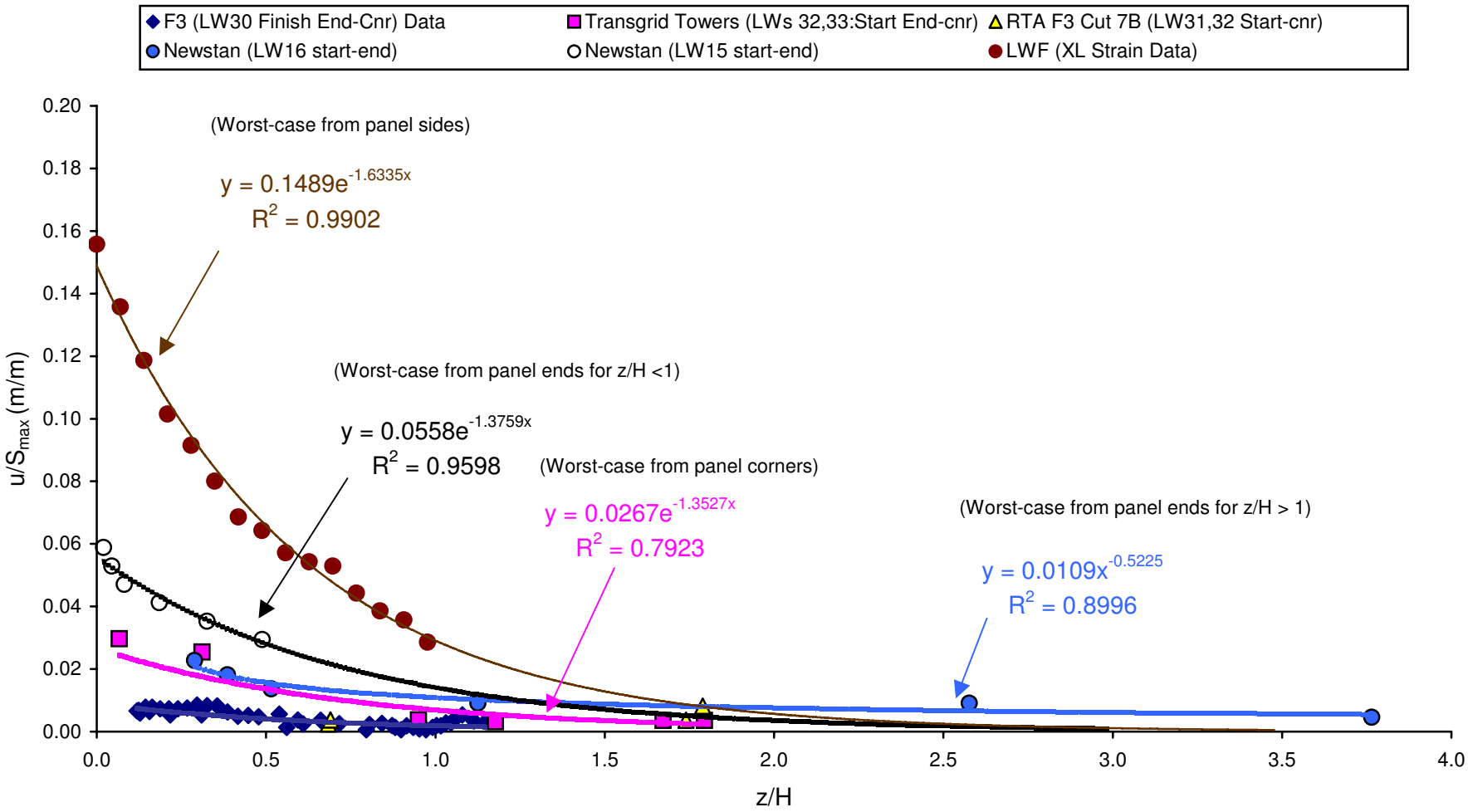

DgS	Engineer:	S.Ditton	Client:	DgS, 2007	
	Drawn:	S.Ditton			
	Date:	22.05.07	Title:	Combined empirical far-field displacement prediction models for longwall panel sides, ends and corners.	
	Ditton Geotechnical Services Pty Ltd		Scale:	NTS	Figure No: A48

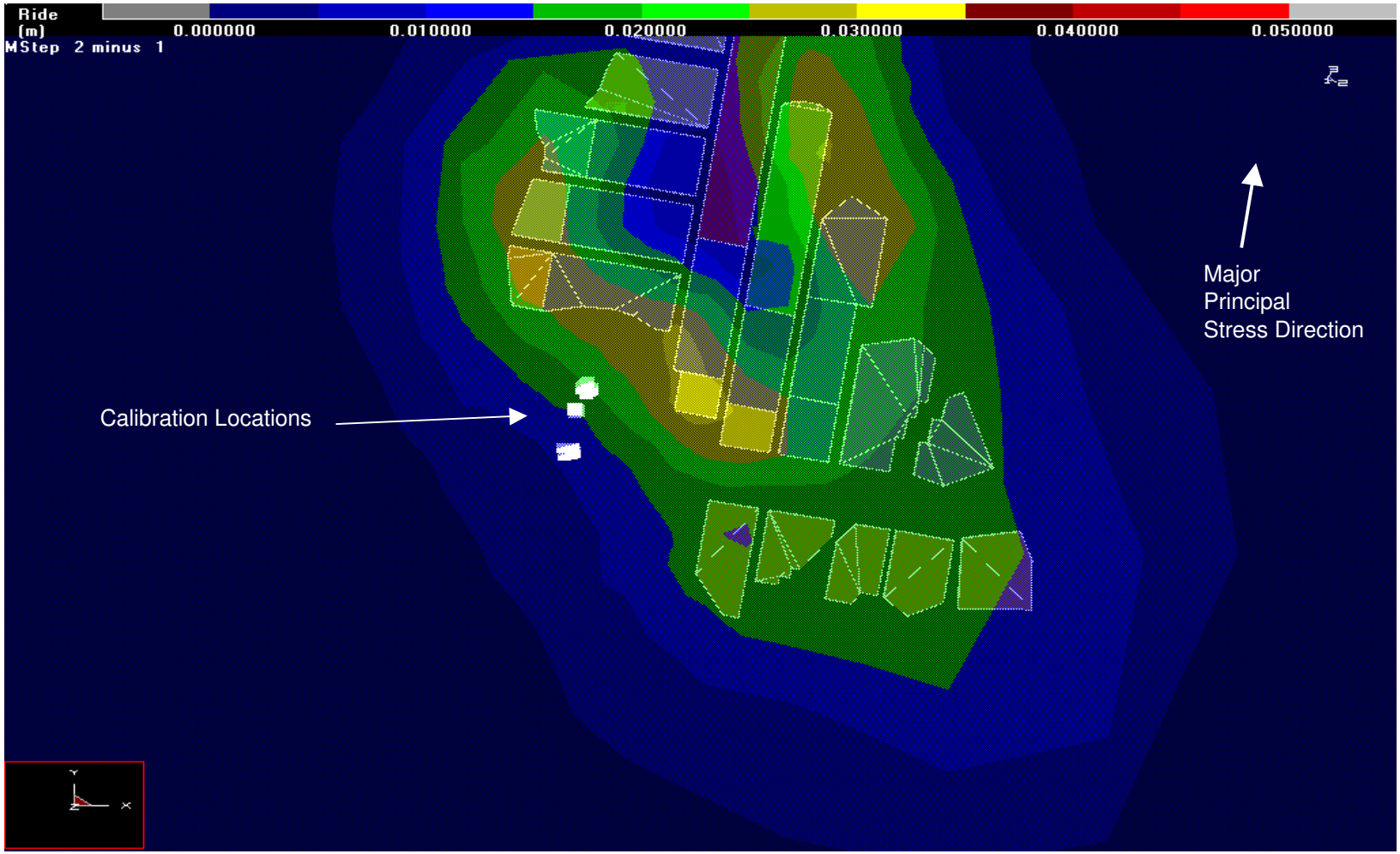

DgS	Engineer:	S.Ditton	Client:	DgS, 2007	
	Drawn:	S.Ditton			
	Date:	22.05.07	Title:	Example of Map-3D Elastic Boundary Element Model Far-Field Displacement Contours Around a Complex Pillar Extraction Mining Layout	
	Ditton Geotechnical Services Pty Ltd		Scale:	NTS	Figure No: A48

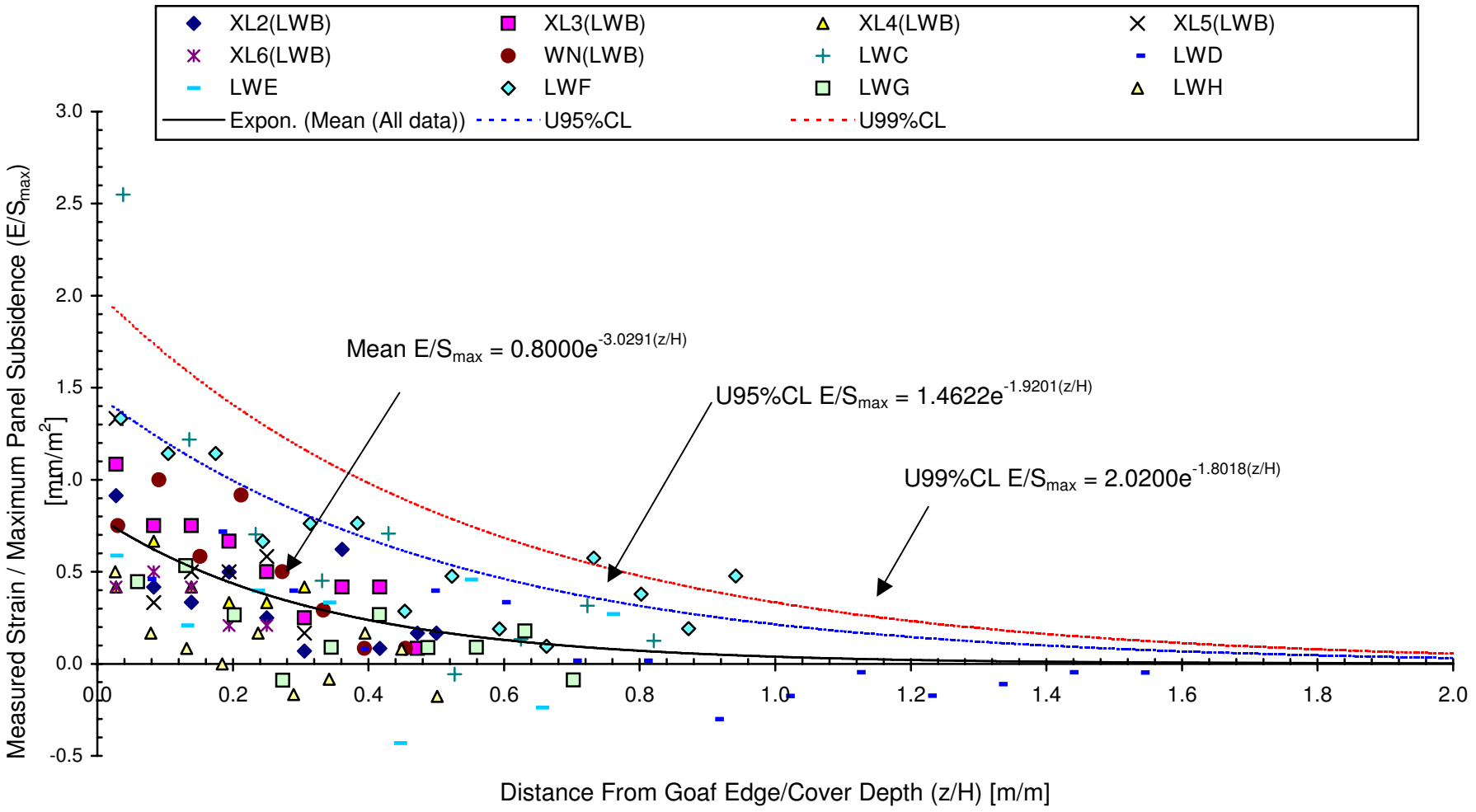

DgS	Engineer:	S.Ditton	Client:	DgS, 2007	
	Drawn:	S.Ditton			
	Date:	22.05.07	Title:	Empirical far-field strain prediction model using cummulative steel tape measurements from longwall sides and normalised to maximum panel subsidence	
	Ditton Geotechnical Services Pty Ltd		Scale:	NTS	Figure No: A50

S D P S

Surface Deformation Prediction System
for Windows
version 5.2

Quick Reference Guide and Working Examples

by

Dr. Zacharias Agioutantis and Dr. Michael Karmis
Department of Mining and Minerals Engineering
Virginia Polytechnic Institute and State University
Blacksburg, Virginia 24061-0239

February 2002

List of Symbols

w	the panel width; the minimum dimension of a panel
h	panel depth; the vertical distance between the mining horizon and the surface; also known as the overburden thickness
m	the seam thickness; the extraction thickness (note that the extraction thickness may be different than the seam thickness)
R	the extraction ratio
R*	the adjusted extraction ratio
d	the distance of the inflection point from the rib (a positive value indicates that the position of the inflectionpoint is inby); also referred to as the “edge effect”
β	the influence angle
r	the influence radius
Smax	the maximum subsidence
a	the maximum subsidence factor
Bs	the strain coefficient
%HR	the percent hardrock in the overburden
Wp	the pillar width
Hp	the pillar height
Wo	the opening width

1.7 Overview of Subsidence Parameters

Maximum Subsidence Factor
The values of maximum subsidence factor, as function of the width-to-depth ratio and the percent hardrock in the overburden, are shown in the supercritical subsidence factor tables for longwall panels and for room-and-pillar panels respectively. When using the profile function method, the subsidence factor is calculated for the actual width-to-depth ratio of the panel. For example, for a panel with W/h = 0.8 (subcritical) and %HR = 50% the subsidence factor is equal to 0.38.

When using the influence function method, the technique requires knowledge of the supercritical subsidence factor, which will subsequently be adjusted through the superposition concept by the program itself. For example, for a panel with W/h = 0.8 (subcritical) and %HR = 50% the subsidence factor is found for W/h = 1.5 (supercritical) and equal to 0.40.

Notes:
A panel is considered supercritical for W/h greater than 1.2. Due to numerical approximations there may be slight variations to the supercritical subsidence factors presented in the supercritical subsidence factor tables.

Inflection Point
The location of the inflection point from the rib, with respect to overburden depth (d/h), can be estimated based on two empirical curves (see the Inflection Point Diagram). Both curves were statistically generated from the available field data. The first is an average curve based on a least squares estimator, while the second is considered an envelope or conservative curve in the sense that it tends to overpredict the surface impact of a given excavation area. In essence, this means that for average data the predicted subsidence profile could be either inside or outside of the measured subsidence line, whereas for conservative (envelope) data, an attempt is made to keep the prediction lines outside the measured ones, i.e. overestimate the influence of the mined area to the surface.

From experience and constant validation of the programs, the authors recommend that, for Appalachian predictions, improved accuracy is obtained by using the following rule:
determine the d/h ratio using the conservative curve for subcritical panels (W/h < 1.2)
determine the d/h ratio using the average curve for supercritical panels (W/h >= 1.2).

Notes:
Always use the actual width-to-depth ratio.

Angle of Influence
The angle of principal influence (β, beta) is one of the basic parameters used in the influence function method since it has a major impact on the distribution of the deformations on the surface. It is measured in degrees from the horizontal and the

average value determined for the Appalachian coalfields is beta=67 deg. The parameter required for these calculations is the tangent of this angle (i.e. tanβ = 2.31). The angle of influence is related to the radius of influence as shown in the equation:

$$\tan\beta = \frac{h}{r}$$

where
h = the overburden depth
r = the radius of influence

This value should be determined for each site by fitting a calculated subsidence profile to a measured subsidence profile. If this is not possible, the influence angle can be approximately set as the complementary angle to the angle of draw.

Supercritical Subsidence Factor Tables
The supercritical subsidence factors used in the calculations are presented in Tables 1.7.1 and 1.7.2.

Table 1.7.1: Calculation of maximum subsidence factors (Smax/m) for longwall panels

	Percent Hardrock in the Overburden							
W/h	10%	20%	30%	40%	50%	60%	70%	80%
0.6	0.64	0.59	0.51	0.42	0.34	0.26	0.21	0.16
0.7	0.69	0.63	0.55	0.46	0.36	0.28	0.22	0.18
0.8	0.71	0.65	0.57	0.47	0.38	0.29	0.23	0.18
0.9	0.72	0.66	0.58	0.48	0.38	0.30	0.23	0.19
1.0	0.73	0.67	0.58	0.49	0.39	0.30	0.24	0.19
1.1	0.74	0.68	0.59	0.49	0.39	0.31	0.24	0.19
1.2	0.74	0.68	0.59	0.49	0.39	0.31	0.24	0.19
1.3	0.74	0.68	0.60	0.49	0.40	0.31	0.24	0.19
1.4	0.75	0.69	0.60	0.50	0.40	0.31	0.24	0.19
1.5	0.75	0.69	0.60	0.50	0.40	0.31	0.24	0.19
1.6	0.75	0.69	0.60	0.50	0.40	0.31	0.24	0.19
1.7	0.75	0.69	0.60	0.50	0.40	0.31	0.24	0.19
1.8	0.75	0.69	0.60	0.50	0.40	0.31	0.24	0.19
1.9	0.76	0.69	0.60	0.50	0.40	0.31	0.24	0.19
2.0	0.76	0.69	0.60	0.50	0.40	0.31	0.24	0.19

Table 1.7.2: Calculation of maximum subsidence factors (Smax/(m R*)) for high extraction room-and-pillar panels

	Percent Hardrock in the Overburden							
W/h	10%	20%	30%	40%	50%	60%	70%	80%
0.6	0.52	0.48	0.42	0.35	0.28	0.22	0.17	0.13
0.7	0.57	0.53	0.46	0.38	0.30	0.24	0.19	0.15
0.8	0.60	0.55	0.48	0.40	0.32	0.25	0.19	0.15
0.9	0.61	0.56	0.49	0.41	0.32	0.25	0.20	0.16
1.0	0.62	0.57	0.49	0.41	0.33	0.26	0.20	0.16
1.1	0.62	0.57	0.50	0.41	0.33	0.26	0.20	0.16
1.2	0.63	0.58	0.50	0.42	0.33	0.26	0.20	0.16
1.3	0.63	0.58	0.51	0.42	0.34	0.26	0.20	0.16
1.4	0.64	0.58	0.51	0.42	0.34	0.26	0.21	0.16
1.5	0.64	0.59	0.51	0.42	0.34	0.26	0.21	0.16
1.6	0.64	0.59	0.51	0.42	0.34	0.26	0.21	0.16
1.7	0.64	0.59	0.51	0.43	0.34	0.27	0.21	0.16
1.8	0.64	0.59	0.51	0.43	0.34	0.27	0.21	0.17
1.9	0.64	0.59	0.51	0.43	0.34	0.27	0.21	0.17
2.0	0.64	0.59	0.52	0.43	0.34	0.27	0.21	0.17

Horizontal Strain Factor

The value of this factor is directly related to the magnitude of the calculated strains and curvatures over an undermined area. It can be empirically estimated by the average ratio of measured strain and curvature over a set of surface points.

The average value determined for the Appalachian coalfields is:

$$Bs = (0.35 \pm 0.05)\ \frac{h}{\tan\beta}$$

where h is the excavation depth and tanβ is the influence angle. The horizontal strain factor is expressed in units of length. The horizontal strain coefficient is unitless and its default value is 0.35.

Note: The higher the value for this coefficient, the larger the predicted strains and displacements.

Chapter 3: The Influence Function Method

3.1 Overview of the Influence Function Method

Influence function methods for subsidence prediction have the ability to consider any mining geometry, to negotiate superposition of the influence from a number of excavated areas having different mining characteristics and, also, to calculate horizontal strains as well as other related deformation indices. The function utilized in SDPS is the bell-shaped Gaussian function. This method assumes that the influence function for the two-dimensional case is given by:

$$g(x,s) = \frac{S_o(x)}{r}\exp\left[-\pi\frac{(x-s)^2}{r^2}\right]$$

where:

r	=	the radius of principal influence = h / tan(beta);
h	=	the overburden depth;
beta	=	the angle of principal influence;
s	=	coordinate of the point P, where subsidence is considered;
x	=	coordinate of the infinitesimal excavated element; and
So(x)	=	convergence of the roof of the infinitesimal excavated element.

Subsidence at any point P(s), therefore, can be expressed by the following equation:

$$S(x,s) = \frac{1}{r}\int_{-\infty}^{+\infty} s_o(x)\exp\left[-\pi\frac{(x-r)^2}{r^2}\right]$$

where:

So(x)	=	m(x) a(x);
m(s)	=	extraction thickness; and
a(x)	=	roof convergence (subsidence) factor.

The influence function formulation can thus be applied to calculate surface deformations (subsidence, strain, slope, curvature, displacements) above longwall and room-and-pillar panels, given the geometry of the excavation, information on the overburden geology, as well as the location of the prediction points on the surface. More specifically, the required data include:

- the geometry of the mine plan and the associated properties (extraction thickness, subsidence factor for supercritical conditions)

- the location (coordinates) of the points on the surface for which prediction of the deformation indices (subsidence, strain, slope, curvature, horizontal displacement) is to be performed
- the empirical parameters that numerically represent the behavior of the overburden

The typical steps required to calculate surface deformations using the influence function method, are shown below. The corresponding flowchart is also shown in Figure 3.1.1. Figure 3.1.2 presents a schematic diagram for creating the input data. Figure 3.1.3 presents typical distributions for the deformation indices that can be calculated by the influence function method. Table 3.1.1 shows all the indices that can be calculated by the influence function method.

✓ Load the Influence Function Program
✓ Input Data
✓ Mine Plan Data
  - Prediction Point Data
  - Empirical Parameters
✓ Select calculation options
  - Subsidence
  - Horizontal Strain
  - Horizontal Displacement
  - Slope
  - Curvature
✓ Save Project File
✓ Calculate Surface Deformations
✓ Load Graphing Program
✓ View Calculated Deformations

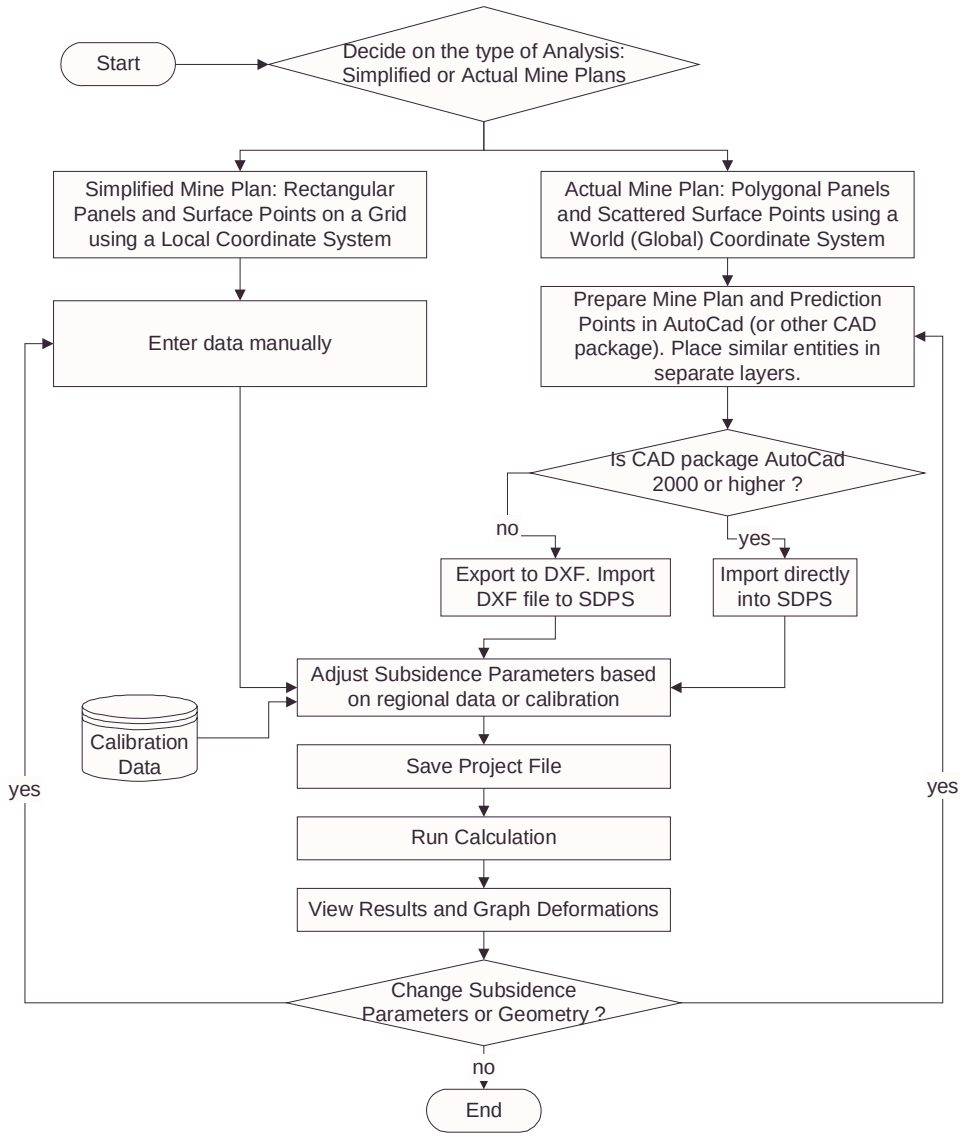

Figure 3.1.1: Flowchart diagram for using the influence function module

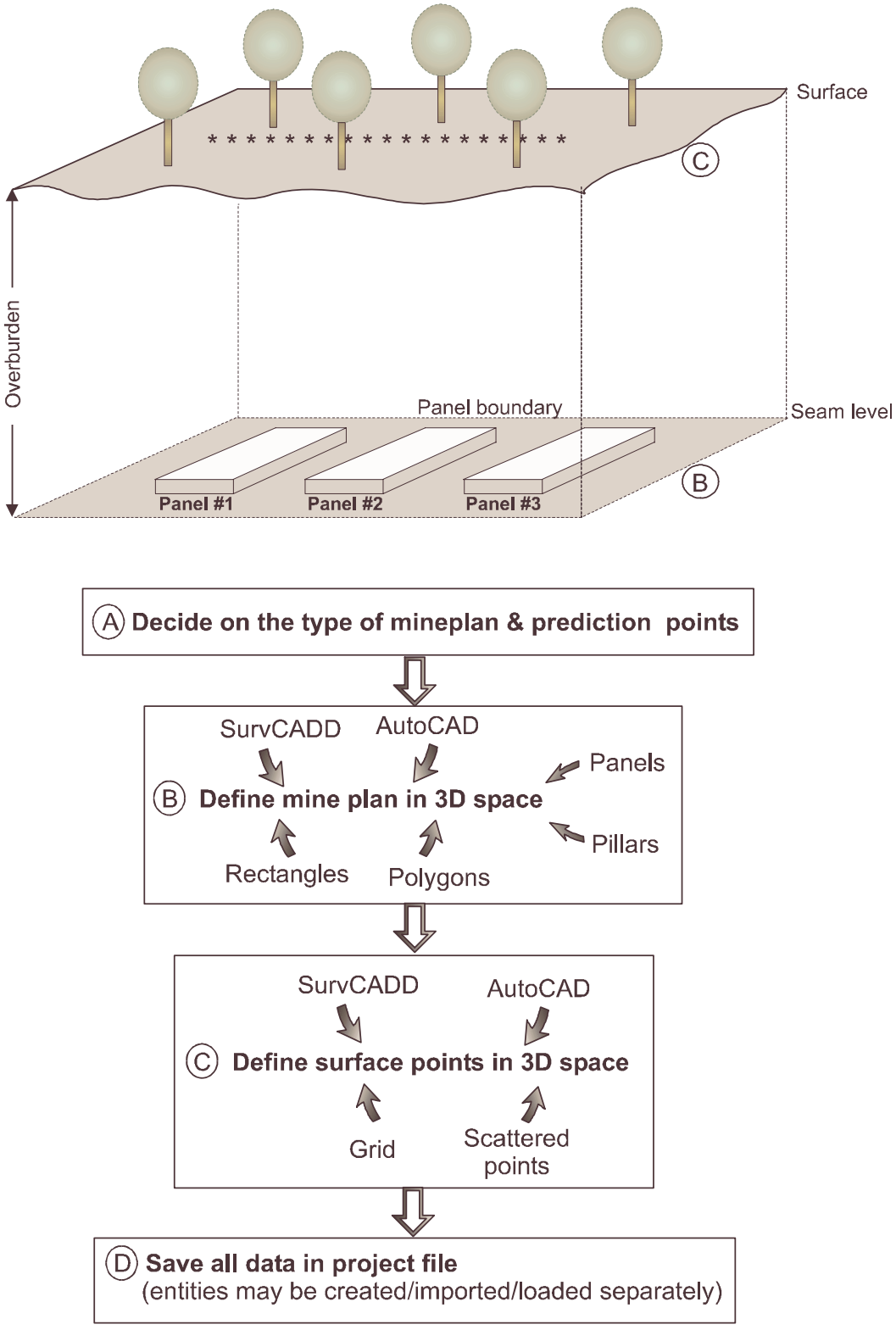

Figure 3.1.2: Steps in defining a project file

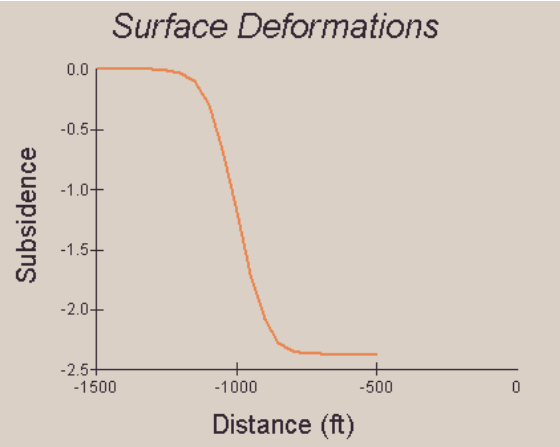

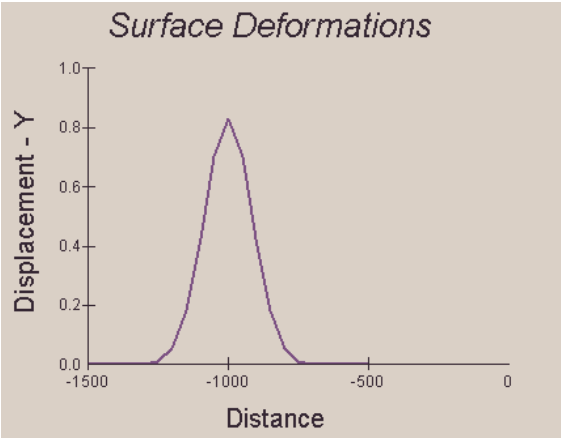

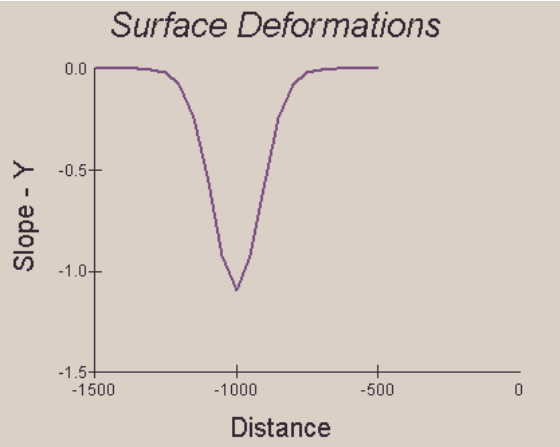

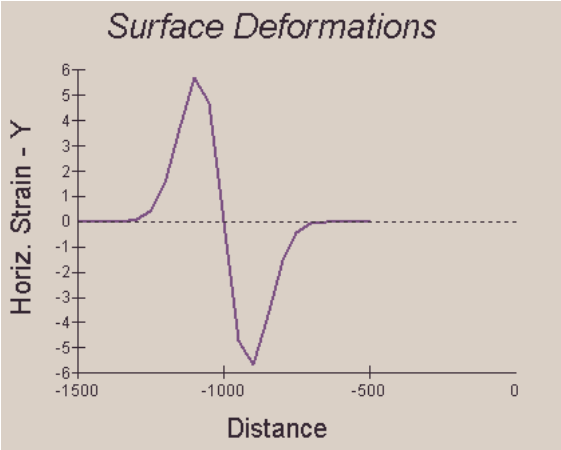

Figure 3.1.3: Typical deformation distributions

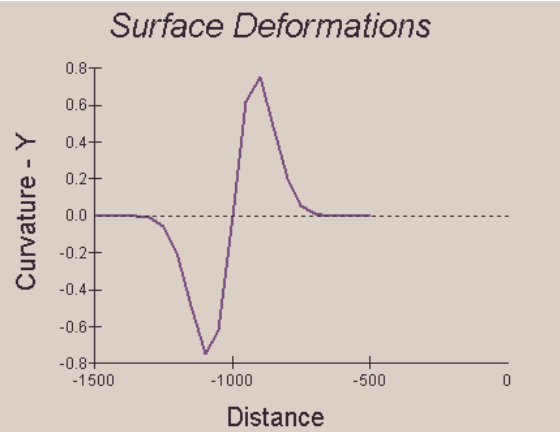

Table 3.1.1: Identification codes for deformation indices

Number	Deformation Index Name	Code	Units
1	Subsidence	SU	ft or m
2	Slope in the X-direction	TX	%
3	Slope in the Y-direction	TY	%
4	Directional Slope	TA	%
5	Maximum (Total) Slope	TM	%
6	Angle[1] of Maximum Slope	TE	deg
7	Horizontal Displacement in the X-direction	VX	ft or m
8	Horizontal Displacement in the Y-direction	VY	ft or m
9	Directional Horizontal Displacement	VA	ft or m
10	Maximum (Total) Horizontal Displacement	VM	ft or m
11	Angle[1] of Maximum Horizontal Displacement	VE	deg
12	Curvature in the X-direction	KX	1/ft or 1/m [2]
13	Curvature in the Y-direction	KY	1/ft or 1/m [2]
14	Directional Curvature	KA	1/ft or 1/m [2]
15	Maximum Principal Curvature	K1	1/ft or 1/m [2]
16	Minimum Principal Curvature	K2	1/ft or 1/m [2]
17	Maximum Curvature	KM	1/ft or 1/m [2]
18	Angle[1] of Maximum Principal Curvature	KE	deg
19	Horizontal Strain in the X-direction	EX	- [3]
20	Horizontal Strain in the Y-direction	EY	- [3]
21	Directional Horizontal Strain	EA	- [3]
22	Maximum Strain	EM	- [3]
23	Maximum Principal Strain	E1	- [3]
24	Minimum Principal Strain	E2	- [3]
25	Angle[1] of Maximum Principal Strain	EE	deg

[1] This angle is calculated in degrees from the positive x-axis in a counter-clockwise direction. It gives the direction of the maximum value of the corresponding index on the x-y plane.

[2] expressed in tenths of ppm (divide by 10.000 to obtain result)

[3] expressed in millistrains (divide by 1000 to obtain result)

3.2 Definition of the Mine Plan in the Influence Function Program

Mine plan data describe the extraction area under consideration using various conventions. An extraction area is always defined in three-dimensional space by specifying the X,Y,Z coordinates of the points defining that area. Mine panels and pillars are referred to as excavation parcels. A parcel can be either active or not active. A parcel, which is not active, is not deleted from the file, but it does not participate in the calculations.

Geometry and Boundary Adjustment:

The geometry of a mine plan is determined by the geometry of the excavation panels adjusted by the edge effect. This parameter represents the distance between the actual rib of the excavation and the position of the inflection point, as determined by panel geometry and site characteristics. The location of the inflection point, which defines the transition between horizontal tensile and compressive strain zones, is very important for the application of the influence function method. The distance of the inflection point from the rib using either an average and a conservative estimate as a function of the width-to-depth ratio of a panel can be estimated using this graph.

Thus, the magnitude of the edge effect can be determined as follows:

- ✓ from the graph estimating the location of the inflection point for the conservative or average estimate (Figure 3.1.1),
- ✓ by clicking on the *Subs.Parm* button in the rectangular mine plan form of the influence function program,
- ✓ by analyzing subsidence curves measured at a specific site or region.

Panel Representation:

- ✓ Simple mine layouts can usually be approximated using sets of rectangular extraction areas. In this case, the input required for every parcel includes the parcel number; the coordinates of the west, east, south, and north borders; the seam elevation; the extraction thickness (mining height); and the average supercritical subsidence factor (in percent) associated with it. These coordinates can be specified in a local or a global coordinate system with axes parallel to the parcel sides. In the Influence function module, this option is implemented as **Rectangular Mine Plans.**

- ✓ Complex mine layouts can usually be approximated by a closed polygon (i.e. a piece-wise linear shape). In this case, the input required for every point within a parcel includes the point reference number; the northing (Y), easting (X), and elevation (Z); the extraction thickness (mining height); and the supercritical subsidence factor (in percent) associated with it. The mine plan editor can

provide access to all points in a parcel, add new points, and add new parcels provided that the current parcel is defined by three or more points. The points should be entered in a counter-clockwise fashion. The location of each point should be adjusted to reflect the edge effect, or the relative position of the inflection point. The maximum number of parcels and points per parcel can be adjusted within the limits of the available memory. In the Influence function module, this option is implemented as Polygonal Mine Plans.

Warning:

Pillars can not exist outside extracted areas. If a pillar is defined outside an extracted area the results are unpredictable. Currently, the parcel definition module of the program can not check for such inconsistencies. Examples of erroneous panel definitions are given in Appendix 3.

Notes:

- ✓ If no adjustments are made to the geometry of the mine plan, the program assumes that the inflection point is over the rib of the excavation.
- ✓ The user must specify whether each parcel represents an extracted panel or a pillar within an extracted panel. A pillar is mathematically represented as a parcel with a negative subsidence factor. Setting the pillar option on a parcel will reset the subsidence factor associated with this parcel. In that sense, an extraction area can be either positive (i.e. longwall panel) or negative (i.e. pillar in the middle of a panel). Thus, a mine plan that consists only of pillars (without an extraction boundary) will produce a mathematically positive! subsidence.
- ✓ It should be emphasized that the subsidence factor used here is the subsidence factor for supercritical conditions.
- ✓ The reason for supporting more than one format for input data is for the user's convenience. For example, certain panels or pillars can be easily represented as rectangles and can be entered as single entities, compared to four or more entries required if these panels are digitized point by point. Additionally, calculations for rectangular parcels are much faster compared to calculations for parcels defined by individual points.

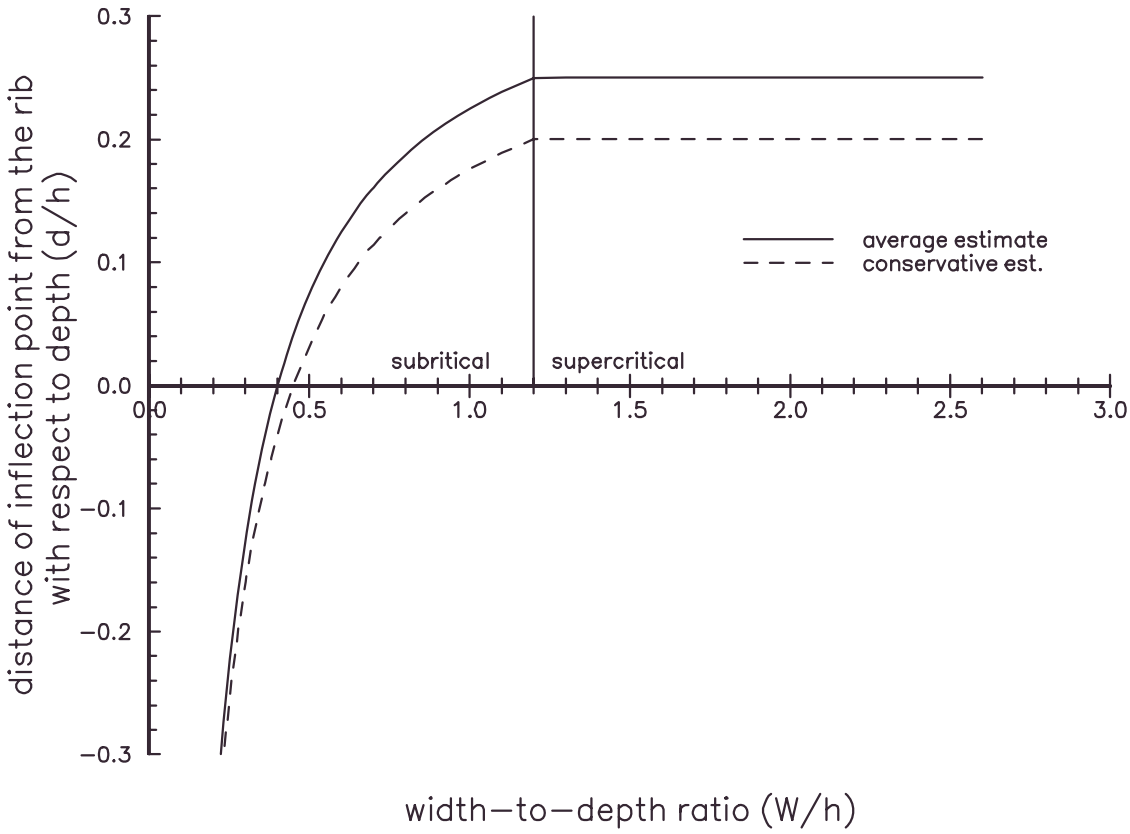

Figure 3.2.1: Determination of the offset of the inflection point.

3.3 Definition of the Prediction Points in the Influence Function Program

Prediction point data describe the surface points where the deformation indices will be calculated. Prediction points are always defined in three-dimensional space, by specifying the X,Y,Z coordinates of these points. A point can be either active or not active. A point which is not active is not deleted from the file but will not be included in the calculations.

Scattered Points

A scattered point set may consist of any number of points that are randomly located on the surface. If such points can be specified as part of a grid, then the Grid Points option should be used. Required parameters for each point include:

- ✓ the point reference code which can be any alphanumeric string,
- ✓ the easting, northing and elevation of each point,
- ✓ the point status, i.e. active or not active (an inactive point will not be displayed in the View option and will not participate in any of the calculations)

Grid Points

A grid point set may consist of any number of points in a window. This window is defined by minima and maxima in the X- and Y- directions as well as the cell size in each direction.

The grid can only be oriented parallel to the current coordinate system. If the grid needs to be oriented at an angle to the current coordinate system, the grid points should be generated by a different tool and imported as scattered points into the Influence Function module.

The user has two options regarding grid elevations.

- ✓ to consider a flat surface and specify a uniform elevation for all points, and
- ✓ to consider each point on an individual basis and specify individual point elevations.

Surface Deformation Characteristics Above Undermined Areas: Experiences from the Eastern United States Coalfields

M. KARMIS, A. JAROSZ, P. SCHILIZZI & Z. AGIOUTANTIS*

SUMMARY Damage resulting from surface movements due to underground mining may range from simple land settlement to severe structural damage. Since subsidence prevention is not feasible, it is important that accurate ground movement prediction techniques are developed, so that damage due to underground mining as well as the amount of coal lost due to the protection of surface structures can be minimized.

To facilitate the mitigation of the deleterious effects of subsidence in the Eastern U.S. region, empirical subsidence prediction techniques for longwall mining were developed from 45 case studies collected within the coalfield. From these subsidence prediction techniques a strain prediction model was also formulated. These subsidence and strain prediction methods can be used to predict ground movements as part of the mining plan and to evaluate the impacts of underground mining on the surface.

1 INTRODUCTION

Surface subsidence is rapidly gaining emphasis as an important environmental consequence of underground coal mining in the United States. Its impact has been witnessed in both rural and urban areas, and can be associated with active as well as abandoned mining operations. The damage associated with this phenomenon may include land settlement and fracturing, structural damage to surface buildings or facilities and disruption or contamination of ground water supplies.

As the need for energy increases, coal production will undoubtedly be accelerated, and since over 99 percent of all subsidence recorded in the United States arises from underground mining, it is evident that the incidence of subsidence will increase. With this increase in production and as underground mining moves into more populous areas, the prediction of surface subsidence, horizontal displacements, strains, and associated damages will surely become a requisite.

To exemplify the significance of this problem, a recent U.S. Bureau of Mines report indicated that over 32,000 km^2 have been undermined in the United States in extracting coal, metals and nonmetallic ores. Over one-fourth of this area, or approximately 8100 km^2, has been disturbed by subsidence, with underground mining of bituminous coal accounting for 7700 km^2 and metal and nonmetallic ores accounting for 68 km^2 of disturbed land. Thus, over 99 percent of all subsidence incidents are attributed to underground coal mining. Moreover, the Bureau of Mines estimates that an additional 10,000 km^2 will be undermined in the United States by the year 2000 (Chen et al., 1982), thus increasing considerably the number of areas in the country affected by subsidence.

Even though, under present technological and economic conditions, subsidence prevention is not feasible, it has been demonstrated in many coalfields that surface subsidence can be predicted and controlled, thus minimizing the deleterious effects of ground movement. Therefore, it is imperative that reliable methods of surface movement prediction and control be established for the United States. With such techniques available, ground movements can be predicted as part of the mining plan, and if environmentally, economically or legally unacceptable situations are foreseen, remedial measures can be implemented.

2 TYPES OF MINING SUBSIDENCE EXPERIENCED IN THE UNITED STATES

Underground excavations disturb the natural equilibrium of the rock mass, causing redistribution of loads in the medium and thus producing horizontal and vertical displacements. Subsidence occurs when these displacements propagate from the mine opening, through the overlying strata, to the surface and can manifest two principle modes of ground settlement: sinkhole and trough subsidence (Figure 1).

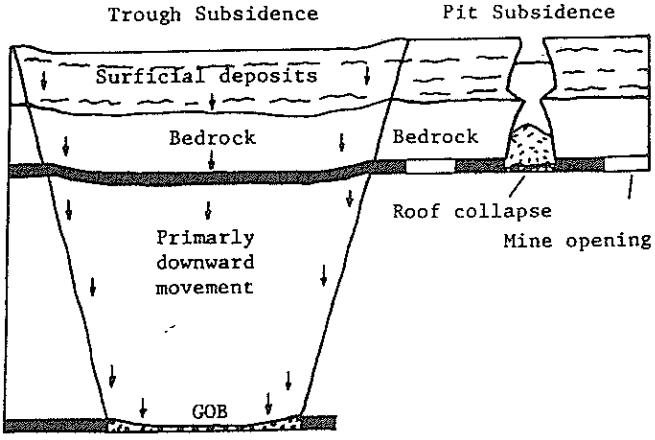

Figure 1 Trough and pit subsidence (after Wildanger et al., 1980).

2.1 Sinkholes, or Pit Subsidence

Sinkholes, or pit subsidence, are characterized by a sudden and sometimes violent collapse of the surface and usually occur above shallow, abandoned room and pillar mines with incompetent overburden; in rare instances, however, this type of subsidence

can also occur over active mines, given the proper mining and geological conditions. Pit subsidence is expressed by an abrupt drop in the surface and has vertical to bell-shaped walls. The washing of bedrock and surficial deposits into the mine void may cause the depth of sinkhole to exceed the mining height.

Obviously, the effects of pit subsidence can be serious. The damage caused is the result of a loss of support over all or part of the structure. Also, due to the uncertainty of mine and geologic parameters, the time, location and extend of such a subsidence event is very difficult to predict. Since the goal of subsidence and strain prediction is to minimize the cost of extracting coal in active mines that are below structures, the characteristics of trough subsidence have been studied more extensively than those of sinkholes.

2.2 Trough Subsidence

Trough subsidence is expressed by a gradual and general movement over an observed area with a subsidence basin being formed. Trough theory considers the phenomenon of subsidence to be represented by a complicated combination of material movement and interaction, as depicted in Figure 2. Caving occurs above the mine opening (zone a). The strata above the caving zone moves toward the excavation, experiencing fracturing (zone b) and beam bending phenomena (zone c). This representation of ground movement around a mining excavation is considerably complex to analyze and model; therefore, this concept is simplified by treating only the effects of underground excavation on the surface, or other strata levels within the bending zone.

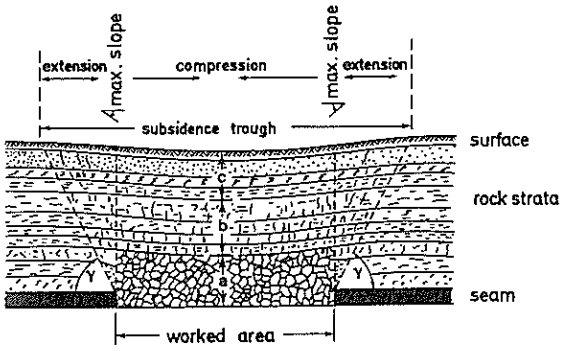

Figure 2 Strata movements above an extracted area (after Kratzsch, 1983)

Trough theory considers a zone of influence in which movement occurs and which spreads from the excavation to the surface, forming a subsidence trough. When an excavation is made at depth, the movement of the strata extends to the surface and manifests itself as vertical displacement (subsidence) and horizontal displacement within a zone of influence. The zone of influence is bounded by a plane that extends from the edge of extraction to the line on the surface where movement ceases. A vertical cross-section of the subsidence trough along with its associated parameters is shown in Figure 3. The angle defined by the vertical from the rib and the line of influence is the angle of draw (or limit angle).

3 DEVELOPMENT OF SUBSIDENCE PREDICTION METHODS

A number of different methods have been proposed for or applied to prediction of surface ground movements due to underground mining. These

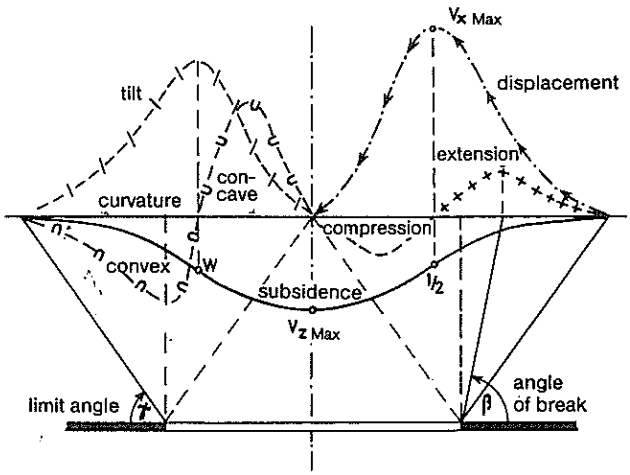

Figure 3 Components of ground movement (after Kratzsch, 1983)

approaches can be broadly divided into three groups. The first two are:

- Theoretical models based on the elastic, plastic, viscoelastic or other phenomenological models which are widely used in other engineering fields (Voight and Pariseau, 1970).

- Numerical methods, mostly used as solutions to complex situations involving the phenomenological methods.

Both these approaches assume that the strata in the overburden behaves in a specific and predictable manner. In using these models, considerable information describing the behavior of the overburden is required, which has often limited the applicability of these methods. Furthermore, in order to adapt their results to field data, a large number of adjusting coefficients may have to be determined.

The third approach can be defined as:

- Empirical or semi-empirical methods such as profile functions, influence functions, the zone area method (Brauner, 1973; Karmis et al., 1981b and 1983).

In this research, the latter approach was pursued since empirical methods are realistic, flexible, and easy to use. Their application, however, requires that a significant number of field measurements be made in order to determine the essential input parameters of the equations.

3.1 Data Collection and Analysis

During the initial stages of this research effort, a large number of subsidence case studies were collected from literature, the coal industry and government agencies. In total, data from 45 longwall panels and 70 room and pillar panels were collected. The limitations of the collected case studies data, i.e. accuracy of surveys, frequency of monitoring, lack of horizontal movement measurements, etc, led Virginia Polytechnic Institute and State University to the initiation of a detailed subsidence and strain monitoring program

above a number of active mines, located in three major coal producing counties of Virginia. The aim of this program was to enhance the data base with accurate and complete measurements of surface movements and to subsequently allow the refinement of the prediction techniques.

In this major monitoring effort, a total of sixteen room and pillar sections and seven longwall panels, in nine mines, were instrumented. Above each panel or section a number monument lines were installed. The lines were extended on either side of the panel well beyond the maximum expected area of influence. The final effort included approximately 1,200 stations over 35,000 feet of monitoring lines (Schilizzi et al., 1986).

This data bank was used to determine some basic ground movement relationships between the basic mining and subsidence parameters, in order to allow the evaluation of the various prediction methods for the Appalachian coal region.

Analysis of the subsidence information has revealed some interesting subsidence characteristics for Appalachian longwall panels. The observed angles of draw varied considerably; however, the angle of draw appears to approach a constant value of approximately 30 degrees at width-to-depth (W/h) ratios in excess of 1.2 (Figure 4). The range of maximum subsidence factors for the collected case studies is shown in Figure 5. It shows two lines constructed from the data. Line (1) represents the average values S_{max}/m, whereas line (2) is an envelope line, covering all data points. The figure also shows that this parameter asymptotes to a constant value at a width-to-depth ratios greater than 1.2. These results suggest that critical conditions are reached for W/h ratios of about 1.2,

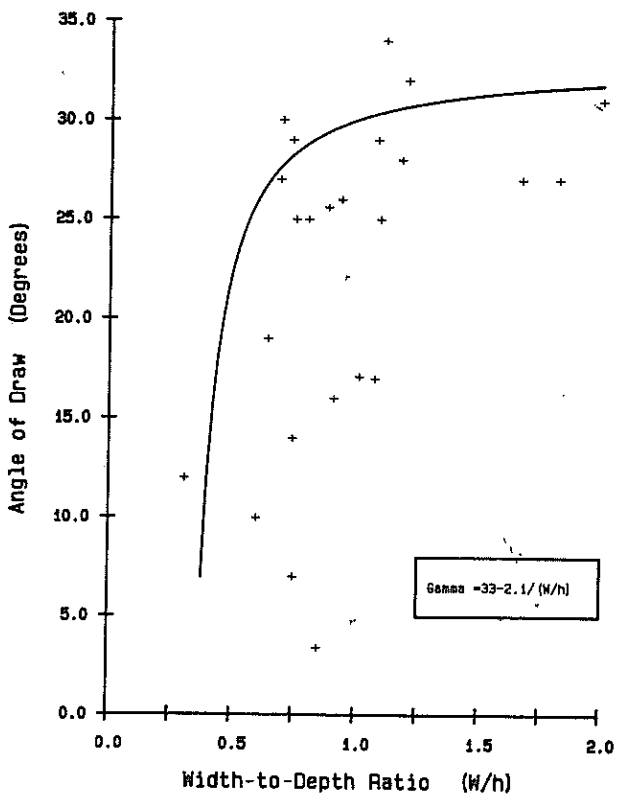

Figure 4 Observed angles of draw for various case studies

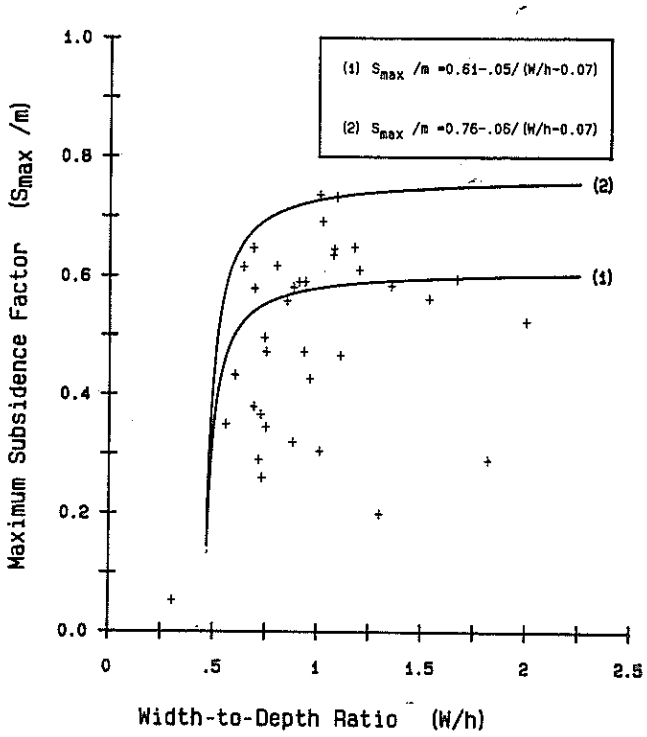

Figure 5 Influence of W/h ratio on maximum subsidence factor

as confirmed by the relationship between the position of the inflection point and the width-to-depth ratio of the panel shown on Figure 6.

According to the collected data and their dispersion, it was hypothesized that two factors influenced the subsidence: geology of the overburden and geometry of the panel. In order to establish the relationship between geology (lithology) and subsidence, the subsidence factor was plotted against the percent of hardrock (percent of limestone and sandstone) in the overburden for critical and supercritical panels only (Figure 7). Since the effect of panel geometry was thus eliminated, a relationship between subsidence and geological conditions was established. Once this correlation was possible, a complete relationship between subsidence and panel geometry was developed for varying lithologies (Figure 8).

To determine characteristic subsidence profiles, different empirical or semi-empirical methods were tested and adopted. Data collected during the monitoring program were primarily used, because of their completeness and accuracy.

3.2 Profile Function Methods

A profile function method defines the distribution of subsidence or strain values on the surface along a profile, orthogonal to the boundary of (theoretically) an infinitely long underground excavation. In general, a function which is tangent or asymptotic to two horizontal lines is required. The parameters to be used for this equation must be determined from field data.

The advantage of such a method is that it can be implemented easily through the use of a computer, or of pre-calculated tables. The main disadvantage is that it cannot negotiate excavations of complex shape or significant variations in mining

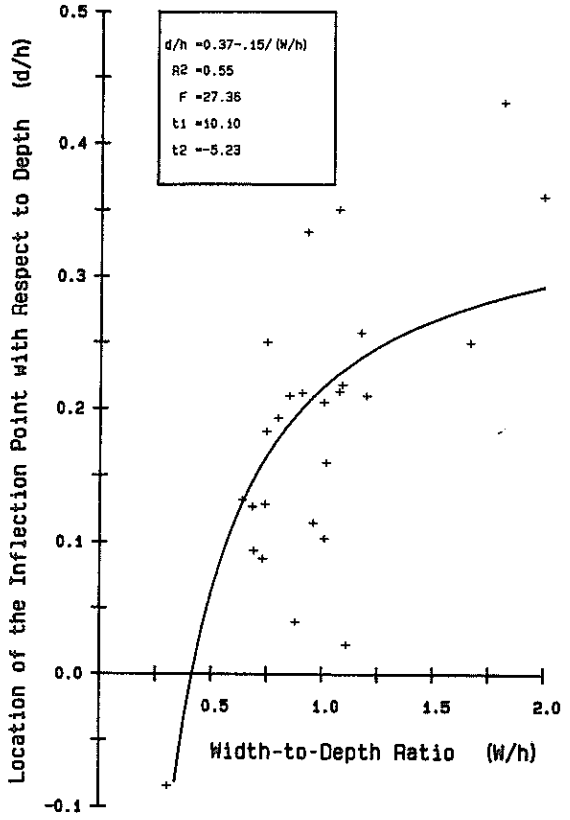

Figure 6 Effect of W/h ratio on inflection point location

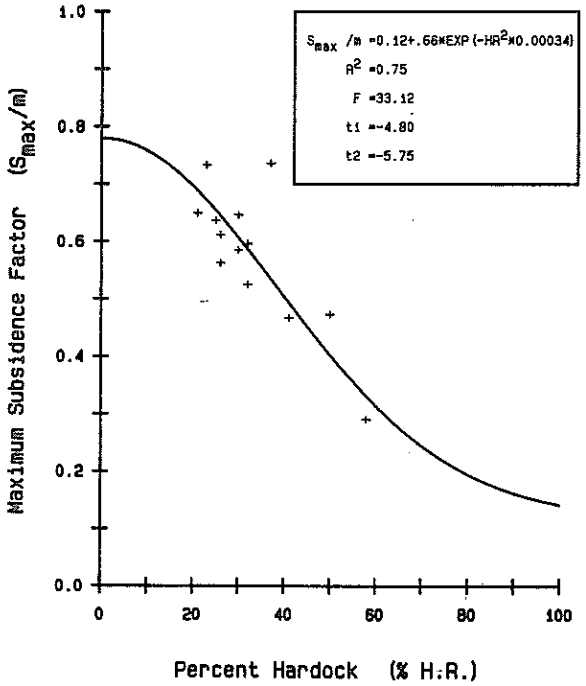

Figure 7 Effect of lithology on maximum subsidence factor

Parameters such as mining height, percent of extraction, and depth of the excavation (Brauner, 1973; Karmis et al., 1981a).

In this approach, a number of accepted profile functions were fitted to the subsidence profiles

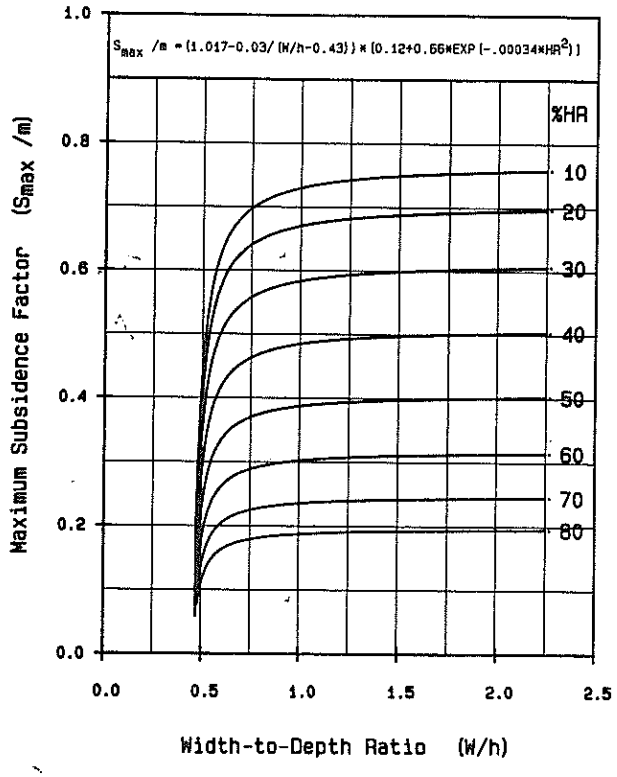

Figure 8 Nomograms for maximum subsidence prediction

developed from collected case studies. This analysis demonstrated that the hyperbolic tangent function given by the following equation, provided the best fit curve (Karmis et al., 1981b and 1984):

$$S(x) = 0.5\ S_{max}[1-\tanh(cx)/B] \qquad (1)$$

where,

S(x) = subsidence at a given point on the surface;
S_{max} = maximum subsidence (obtained from a table [Table 1] or nomogram [Figure 8]);
c = constant, calculated as 1.8 for critical or supercritical panels and 1.4 for subcritical panels;
x = distance from the inflection point to the point in question; and,
B = distance from the inflection point to S_{max} (which can be assessed from tables or nomograms [Figure 6] as a function of panel geometry and width-to-depth ratio).

The latter equation can be used in conjunction with predictions of S_{max} (Figure 8) and position of the inflection point (Figure 6) to allow for complete subsidence pre-calculation.

3.3 Influence Function Methods

This approach to subsidence prediction was initially developed by Dutch and German engineers (Bals, 1932) and has been extensively used in the Central and Eastern European coalfields. An influence function describes the distribution of vertical ground movement, i.e. subsidence, on the surface or other levels of the overburden, caused by an infinitesimal underground excavation. Considering the two dimensional situation:

$$dS(x_1,z) = f(x_1-x_2,z)dV \qquad (2)$$

where,

$dS(x_1,z)$ = subsidence at point $P(x_1,z)$;
dV = infinitesimal underground excavation (void);
$f(x_1-x_2,z)$ = influence function;
x_1 = coordinate of surface point;
x_2 = coordinate of infinitesimal excavation; and,
z = vertical distance from excavation to prediction point $P(x_1,z)$.

The Budryk-Knothe influence function method (Knothe, 1957), developed in Poland, was selected for this research as the most appropriate function for use in the Eastern U.S. coalfields. Initially, a two-dimensional situation was considered for the analysis of data obtained from panels of an almost orthogonal shape and with uniform mining conditions i.e. mining height, percent extraction, depth. The equation used is as follows:

$$f(x,z) = -\frac{1}{r}\exp(-\pi\frac{x^2}{r^2}) \qquad (3)$$

where,

r = the radius of influence (r=z/tan(b));
b = angle of influence; and,
x,z = coordinates of surface point on a system where the origin is located at the infinitesimal excavation.

For the three-dimensional approach:

$$f(x,y,z) = \frac{1}{r^2}\exp[-\pi\frac{(x^2+y^2)}{r^2}] \qquad (4)$$

where,

r = the radius of influence; and,
x,y,z = coordinates of a surface point on a system where the origin is located at the infinitesimal excavation.

Subsidence at any point will be:

$$S(x,y,z) = \frac{S_{max}}{r^2}\iint_A \exp[-\frac{\pi}{r^2}(x^2+y^2)]dxdy \qquad (5)$$

where,

$S(x,y,z)$ = subsidence at a point having coordinates x,y,z;
S_{max} = maximum subsidence for supercritical excavation;
r = the radius of influence; and,
A = the area of excavation.

The above integral was transformed and solved in polar coordinates, for polygonal excavations.

For this method, as with most mathematical models, the inflection point of the subsidence profile is located above the rib of the excavation. In practice, however, the inflection point is displaced at a distance, d, from the rib. In order to accommodate this, the outer boundaries of the excavation have been adjusted accordingly.

3.4 Zone Area Method

This method was initially developed in Britain for irregular longwall or room and pillar panels (Marr, 1975). It assumes that movement at a specific point on the surface is affected by the excavation of a circular underground area which is further sub-divided into a series of angular rings. To determine the amount of movement caused by each ring, the extracted area of the ring is calculated and multiplied by the zone factor of the respective ring. Appropriate zone factors for Appalachia have been calculated from the field data (Goodman, 1980; Karmis et al., 1981b and 1984). The same procedure is followed for all rings, and the superimposed results will yield total movement.

4 DEVELOPMENT OF STRAIN PREDICTION METHODS

One of the most damaging manifestations of surface subsidence is the development of horizontal strains. As noted previously, subsidence measured in Appalachia is smaller than that found in certain other coalfields, such as the U.K. However, the strains experienced in the U.S. often appear to be greater than those predicted for British conditions. Thus, an effort was directed toward the identification of the cause of these higher strains and toward the subsequent formulation of an acceptable strain prediction model for Appalachia.

As a first step, the relationship between strain and curvature had to be determined. Factor B was used to calculate horizontal strain as a function of curvature, i.e.:

$$\text{Horizontal Strain} = -B * \text{Curvature} \qquad (6)$$

In the original stages of this research a direct relationship between strain and curvature was sought which could describe B independent of any other mining parameters (Karmis et al., 1983). As more case studies were made available through this project, it became apparent that such a relationship will be difficult to establish (Figure 9). As a result, a different approach was adopted, based on the work of Awershin (1947), Budryk (1953) and Akimov and Zemicev (1970), which suggested that the magnitude of the horizontal strain factor (B) is a function of the excavation depth or the radius of principal influence (r).

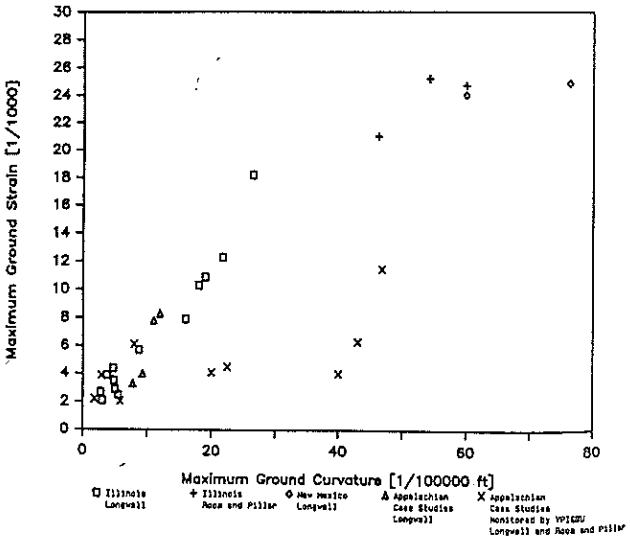

Figure 9 Maximum ground strain and curvature data

For each of the collected case studies, factor B was determined by comparing the measured strains and the fitted curvature profiles.

Using the established values of parameter B and the corresponding values of excavation depth (h), radius of influence (r), and angle of principal influence (b), a statistical relationship was found (Figure 10) as expressed by the equation:

$$B = (0.35 \pm 0.05)\ r \qquad (7)$$

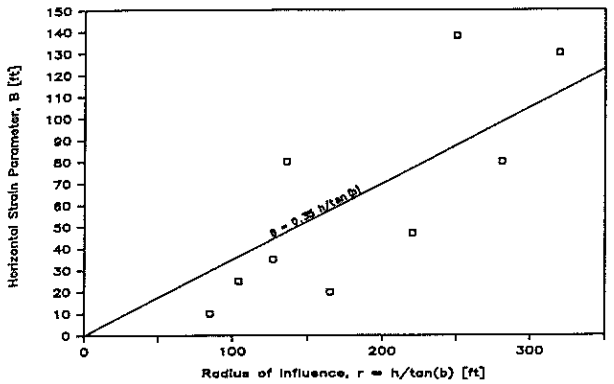

Figure 10 Effect of radius of influence on the horizontal strain parameter

or

$$B = (0.35 \pm 0.05)\ h/\tan(b) \qquad (8)$$

where,

r = radius of the principal influence;
h = depth of the excavation; and,
b = angle of the principal influence.

5 DEVELOPMENT OF COMPUTER SOFTWARE

The development of a comprehensive software package was necessary in order to facilitate the analysis of the field measurements. All field data were stored in an 880-line memory incorporated in the surveying instrument, and then transferred to magnetic diskettes for further processing on an HP micro-computer system. Stored field data included coordinates, sometimes on a localized system, elevations and the values of subsidence and strain for individual stations on the monitoring lines for each date.

Computer software for the application of the prediction methods under consideration was developed for two widely used personal computer systems.

For the profile function, the program is rather simple and involves the calculation of subsidence values along a line orthogonal to the rib of the excavation. The parameters used for this calculation depend on the given geologic conditions, width-to-depth ratio and mining height, and must be obtained from tables or nomograms and entered manually. The origin of the coordinates can be adjusted manually if necessary.

For the application of the influence function method, a number of programs were developed, each of them for specific conditions. For general cases involving complex mining conditions, where the mining section under consideration must be divided into polygons of uniform conditions, the influence function equation was converted to polar coordinates and was used in the program in this form. The computer program calculates subsidence at any point along a polygonal line or on a grid. For mine sections of irregular shape or where areas of different mining height, extraction ratio or seam elevation exist, the section is separated into homogeneous polygonal sub-sections. Subsidence and other related indices of deformation, in any given direction, caused by each of these sub-sections is calculated and their total value is determined by superposition. This procedure, however, requires considerable computational time for each point.

For simple conditions, however, where areas of different mining height, extraction ratio or seam elevation can be described by rectangular homogeneous sub-sections, different programs have been written for considerably faster execution on a microcomputer, yielding comparable results. Furthermore, a program using the two dimensional approach has been written for single panels of uniform overall parameters.

The program for the zone area method was initially developed for mainframe computers (Karmis et al., 1982); however, it is currently being adapted for use with personal computers.

It should be noted that these programs also produce data compatible with commercially available plotting and contouring software packages. Mine plan coordinates and the corresponding parameters can be entered manually or by a digitizer or by a plotter with digitizing capabilities.

6 APPLICATION OF PREDICTION METHODS

In this paper, data obtained from three case studies are presented to demonstrate and compare the prediction methods. The first two are from room and pillar mining operations, whereas the last one is from a longwall case study.

In the first example, the two dimensional approach was used. Predicted and fitted subsidence curves, using the profile and influence function methods, are presented in Figure 11.

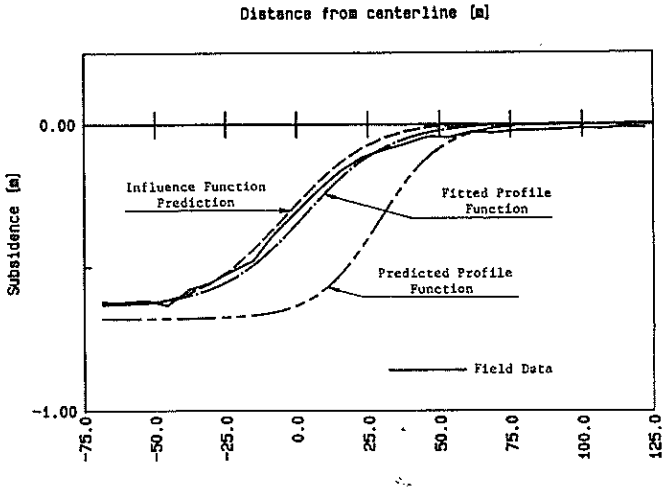

Figure 11 Example #1: Field data and prediction curves

In the second example (Figure 12), a three dimensional influence function approach was used to take into account a number of pillars left in place for roof control purposes. This case demonstrates the accuracy which can be obtained through adjustment of the influence function parameters, especially for subsidence predictions.

In the last example (Figure 13), a three dimensional influence function method was used for a longwall operation with considerable variation in overburden depth. Subsidence and horizontal strain values, calculated using this technique, show excellent correlation with the corresponding measured values.

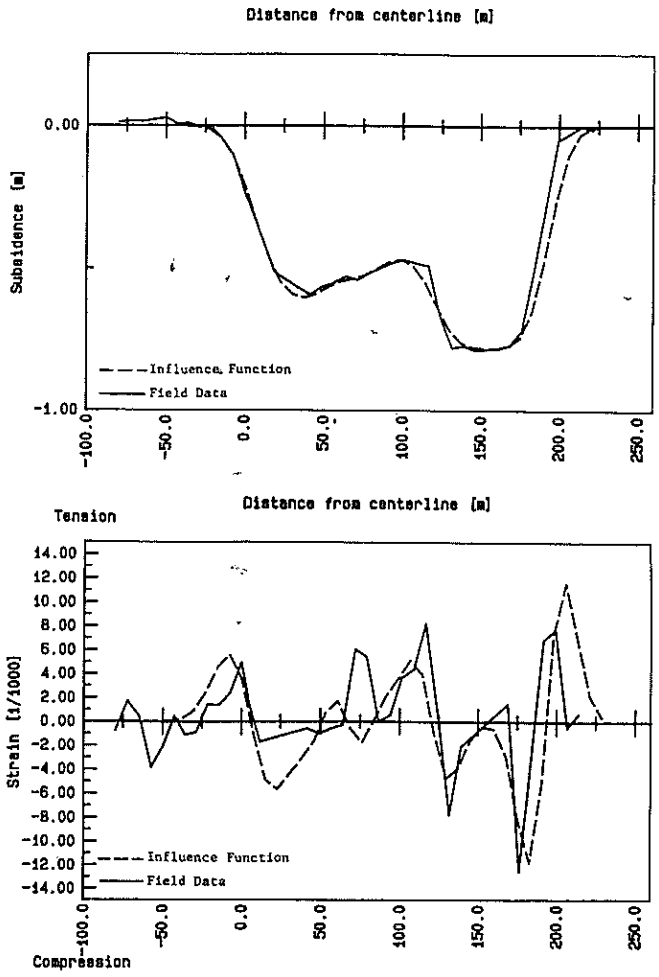

Figure 12 Example #2: Field data and prediction curves for subsidence and horizontal strain

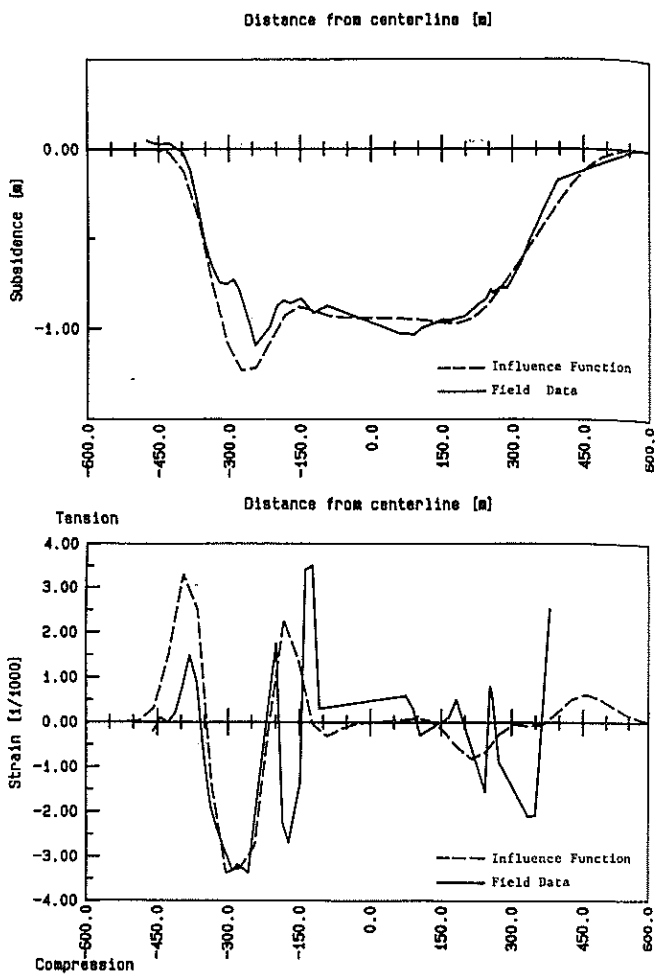

Figure 13 Example #3: Field data and prediction curves for subsidence and horizontal strain

7 CONCLUSIONS

The expansion of underground mining into more populous areas, and the resultant increase in the potential for surface and structural damage, have rendered the formulation of accurate surface deformation models an important requisite. To meet this demand, accurate subsidence and strain prediction techniques have been formulated for the Eastern U.S. coalfield. The semi-empirical subsidence prediction techniques discussed in this paper were developed from a substantial number of case studies collected within the Appalachian coalfield. Using the subsidence model as a base, the strain model was formulated using empirically and mathematically derived relationships. These models can greatly facilitate mine planning and allow the amount of coal lost due to the protection of surface structures to be minimized.

8 ACKNOWLEDGEMENTS

This research is based upon work sponsored by the Office of Surface Mining, Reclamation and Enforcement, the U.S. Department of the Interior and the Powell River Project. Any opinions, findings, conclusions or recommendations expressed in this paper are those of the authors and do not necessarily reflect the views of the sponsors. Finally, the cooperation, encouragement, and discussions offered by the technical personnel of numerous coal companies involved in this project are gratefully acknowledged.

9 REFERENCES

1. Akimov, A. and B. Zemicev, 1970, Subsidence of the Rock Strata Caused by the Underground Excavation of Coal and Lead Ores, Nedra Publishing, Moscow, (in Russian).

2. Awershin, S. G., 1947, Subsidence of the Rock Strata Caused by Underground Excavation, Ugletekhizdat Press, Moscow, (in Russian), 245 p.

3. Bals, R., 1932, "A Contribution to the Problem of Precalculating Mining Subsidence," Milteilungen aus dem Markscheidewesen, Vol. 42/43, pp. 98-111 (in German).

4. Brauner, G., 1973, "Subsidence Due to Underground Mining (in two parts)," U.S.B.M. Info. Circ. 8571, 8572.

5. Budryk, W., 1953, "Determination of the Magnitude of Horizontal Strains," Archives of Mining and Metallurgy, Vol. I, Part 1, (in Polish).

6. Chen, C. Y., D. E. Jones and D. K. Hunt, 1982, "Government Regulation of Surface Subsidence due to Underground Mining," Proceedings, International Symposium on the State of the Art of Ground Control in Longwall Mining and Mining Subsidence, Honolulu, Hawaii, pp. 245-252.

7. Goodman, G., 1980, "Computer Modeling of Mining Subsidence Using the Zone Area Method," M.S. Thesis, VPI&SU.

8. Karmis, M., C. Haycocks, I. Eitani and B. Webb, 1981a, "A Study of Longwall Subsidence in the Appalachian Coal Region Using Field Measurements and Computer Modeling Techniques," Proceedings, 1st Conference for Ground Control in Mining, West Virginia University, July 27-29, pp. 220-229.

9. Karmis, M., C. Haycocks, B. Webb and T. Triplett, 1981b, "The Potential of the Zone Area Method for Mining Subsidence Prediction in the Appalachian Coalfield," Proceedings, Workshop on Surface Subsidence Due to Underground Mining, Morgantown, West Virginia, November 30-December 2, pp. 48-62.

10. Karmis, M., G. Goodman, C. Haycocks and T. Triplett, 1982, "The Development and Testing of a Regional Subsidence Prediction Model," Proceedings, 17th Inter. Symposium on Computer Applications to the Mineral Industry, APCOM, Denver, Colorado, pp. 240-252.

11. Karmis, M., T. Triplett, C. Haycocks and G. Goodman, 1983, "Mining Subsidence and Its Prediction in the Appalachian Coalfield," Proceedings, 24th U.S. Symp. on Rock Mech., College Station, Texas, June, pp. 665-675.

12. Karmis, M., G. Goodman and G. Hasenfus, 1984, "Subsidence Prediction Techniques for Longwall and Room and Pillar Panels in Appalachia," Proceedings, Second International Conference on Stability in Underground Mining, Lexington, Kentucky, August 6-8, pp. 541-553.

13. Knothe, S., 1957, "Observations of Surface Movements Under Influence of Mining and the Theoretical Interpretation," Proceedings, European Congress on Ground Movement, The University of Leeds, April 9-12.

14. Kratzsch, H., 1983, "Mining Subsidence Engineering," Springer-Verlag, Berlin, Heidelberg, New York.

15. Marr, J. E., 1975, "The Application of the Zone Area System to the Prediction of Mining Subsidence," Min. Eng., Vol. 135, No. 176, pp. 53-62.

16. Schilizzi, P., M. Karmis and A. Jarosz, 1986, "Development of Subsidence Prediction Technology from an Extensive Monitoring Program," Proceedings, 2nd Workshop on Surface Subsidence Due to Underground Mining, Morgantown, West Virginia, June 9-11, in press.

17. Voight, B. and W. Pariseau, 1970, "State of Predictive Art in Subsidence Engineering," Journal of the Soil Mechanics and Foundations Div., Proc., ASCE, Vol. 96, No. SM2.

18. Wildanger, E. G., J. Mahar and A. Nieto, 1980, "Sinkhole-type Subsidence Over Abandoned Coal Mines in St. David, Illinois," Illinois Abandoned Mined Lands Reclamation Council, 88 p.

* (Paper C1570 originally presented at the Fourth Australia - New Zealand Conference on Geomechanics, Perth, May 1984)

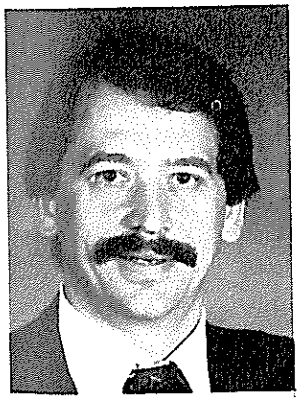

M KARMIS

Michael Karmis is Professor of Mining Engineering at Virginia Polytechnic Institute and State University, where he has been a member of the faculty since 1978. Previously he was with the faculty of the National Technical University of Athens, Greece. Dr Karmis is a graduate of the University of Strathclyde, Glasgow, Scotland, where he received the B.Sc. (Honors) and Ph.D. degrees in Mining Engineering.

Dr Karmis' research interest is in the area of rock mechanics and ground control and he is particularly interested in the application of such principles to the design and optimization of mining systems. He has authored or co-authored numerous technical papers and reports on this subject.

Dr Karmis is a Fellow of the Institution of Mining and Metallurgy, a Member of many professional societies, a Chartered and Professional Engineer, and serves as an independent consultant to the mining industry.

A P JAROSZ

Andrzej P Jarosz has been a Research Associate at the Department of Mining and Minerals Engineering, Virginia Polytechnic Institute and State University, since 1984. Previously he worked for the Mining and Metallurgy Academy in Cracow, Poland, as a faculty member and for the Central Mining Institute in Katowice, Poland, as head of the Mine Pillar Control Laboratory.

Dr Jarosz is a graduate of the Mining and Metallurgy Academy, Cracow, Poland, where he received his M.S. (Honors) and Ph.D. degrees in Mining Surveying.

Dr Jarosz's research interest is in the areas of subsidence monitoring and prediction as well as the practical applications of ground control principles in mining. He has authored or co-authored many technical papers on this subject.

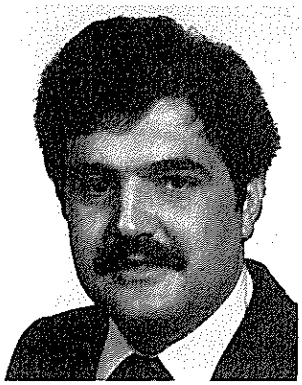

P P G SCHILIZZI

Paul P G Schilizzi received his education at the National Technical University, Athens, Greece, and graduated in July, 1980, with a Diploma in Mining and Metallurgical Engineering. Mr Schilizzi attended graduate school in the Department of Mining and Minerals Engineering, Virginia Polytechnic Institute and State University, where he completed his M.S. degree in July, 1982. He received an assistantship to continue his education leading to a Ph.D. degree in the same department and completed his work for this degree in January, 1987.

Z AGIOUTANTIS

Zacharias Agioutantis graduated from the National Technical University, Athens, Greece, in November, 1982, with a Diploma in Mining and Metallurgical Engineering. He was then admitted to the graduate program at Virginia Polytechnic Institute and State University, Blacksburg, Virginia, under an assistantship, and received his M.S. degree in Mining Engineering. Since September, 1984, he has been pursuing a Ph.D. degree at the same school while working on different research projects. His research work is reflected in several publications in the fields of Rock Mechanics and Ventilation.

APPENDIX B – Massive Unit Definition Details and Voussoir Beam Stability Calculations

B1 Voussoir Beam Analysis Details

To further understand the outcomes of the empirically based subsidence reduction potential (SRP) analysis, it is important to understand the physical relationships between the variables used.

Empirical models are usually expressed by a 'best fit' or regression equation (linear or non-linear) between the observed set of dependant and independent variables.

Some of the problems encountered with empirical models is (i) the lack of data or observations to cover the likely range of input cases, and (ii) whether the physical relationships between the variables are adequately defined by the fitted curves of the empirical model.

Analytical and numerical models, however, also require assumptions with regard to material strengths and their constitutive properties under load, initial regional stress field and service life loading history etc. Engineering judgment is therefore necessary to assess the likely variability of the 'unknowns' in both approaches.

The empirical SRP limit lines presented in the report were based on analytical linear arch or Voussoir Beam theory in order to justify their form physically. A simple in-house developed Voussoir Beam model, adapted from the model presented in **Diedrichs and Kaiser, 1999** with *in-situ* horizontal stress effects included, was then used to re-evaluate the minimum rock beam thicknesses required to span or bridge over the extracted panels.

Voussoir Beam theory allows a quantitative assessment of a jointed rock beam's spanning capability by arching action over an extracted longwall panel. The model assesses the Factor of Safety (FoS) against instability of the rock beam due to (i) abutment crushing, (ii) shear failure and (iii) buckling.

The determination of minimum beam thicknesses required to span the panel required assumptions regarding the following:

(i) the effective span width for each strata unit above the workings,

(ii) the horizontal stress acting on each unit prior to mining,

(iii) the resultant vertical load acting on each unit, and

(iv) the rock mass strength and yielding criteria.

The model is essentially indeterminate in that the number of unknown variables is greater than the number of equilibrium equations and boundary or beam end-support conditions. A solution therefore requires assumptions regarding internal stress distribution and thrust line location. The Voussoir Beam model used in this study was originally validated by comparison with results from the discrete block numerical model, UDEC.

The Voussoir Beam model described above was used to provide an indication of the beam deflections expected above the proposed longwall panels.

The following input constraints were assumed:

- A caving angle of 15^o up to the base of the massive basalt unit to estimate the effective span of the unit.
- An abutment angle of 21^o to estimate the effective loading height acting on the unit.
- Rock mass density = 2.5 t/m^3.
- Cover depth, H = 70 m to 360 m.
- Panel width, W = 178.6 m.
- Average Elastic Modulus = 200 x UCS
- Horizontal Stress/Vertical Stress Ratio = 2.
- A yielding rock mass beam factor of safety (FOS) of 1.5 with collapse at an FoS of 1.0.

The Voussoir Beam analysis calculations are presented graphically and in the attached spreadsheets.

As previously discussed, the assumptions that are required to be made mean that it is highly unlikely that the analytical model will produce results that have a higher order of accuracy than an empirical based model that has been linked to a credible mechanistic conceptual model of overburden behaviour.

The Voussoir Beam analysis also demonstrates that the overall depth of cover and relative location of a massive unit within the overburden are important factors (including the beam thickness, effective span, beam surcharge and material strength etc) when assessing its SRP across a given panel width.

Regardless of the actual mechanisms that may be involved, the empirical database enables realistic long-term subsidence predictions to be made, as it takes a lot of the guesswork out of assigning the multitude of input parameters required for analytical or numerical modelling techniques.

Overburden Stability Analysis Spreadsheet (1&2 Way Action)										
Input Parameters		Name:	West Wallsend		Case :	1				Name:
Geometry					Date:	02.12.08				
H	160	Overburden Depth								Overburden Depth
W	178.6	Panel Width								Panel Width
W/H	1.12	W/D								W/D
D	**30**	Base of Beam Depth(m)								Base of Beam Depth(m)
y	130	Base of Beam Height Above Seam (m)								Base of Beam Height Above Seam (m)
y/H	0.81	Beam Location Ratio								Beam Location Ratio
Hcritical	160.00	Maximum Caving Height (m)								Maximum Caving Height (m)
De	30.00	Effective Beam Loading Height (m)								Effective Beam Loading Height (m)
t	30	Beam Thickness (m)								Beam Thickness (m)
alpha	69	Caving Angle (degrees)								Caving Angle (degrees)
beta	75	Effective Span Angle (degrees)								Effective Span Angle (degrees)
L	109	Effective Span (m)								Effective Span (m)
Ltop	86	Effective Span Top Load Length (m)								Effective Span Top Load Length (m)
Seam	3.5	Working Height (m)								Working Height (m)
Panel	1	Structural Action (1-way = 1, 2-way = 2)								Structural Action (1-way = 1, 2-way = 2)
Rock Properties										
ρ	2.5	Density (tonnes/m3)								Density (tonnes/m3)
UCS	50	Unconfined Compressive Strength (MPa)								Unconfined Compressive Strength (MPa)
UTS	0	Ultimate Tensile Strength (MPa)								Ultimate Tensile Strength (MPa)
E	**11.25**	Youngs Modulus (GPa) (225 x UCS)								Youngs Modulus (GPa) (225 x UCS)
K	1.6	Vertical/Horizontal Stress Ratio								Vertical/Horizontal Stress Ratio
c	0.5	Rock Joint Cohesion (MPa)								Rock Joint Cohesion (MPa)
phi	35	Joint Angle of Friction (Degrees)								Joint Angle of Friction (Degrees)
theta.j	90	Joint Angle to Horizontal Plane (0 to 90)								Joint Angle to Horizontal Plane (0 to 90)
Load										
w	657.30	Uniformly Distributed Beam Load (KN/m)								Uniformly Distributed Beam Load (KN/m)
sigma v	0.74	virgin vertical stress (MPa)								virgin vertical stress (MPa)
sigma h	1.18	virgin horizontal stress (Mpa)								virgin horizontal stress (Mpa)
Stability Analysis										
Linear Elastic Beam										
M	9.75E+05	Fixed End Moment (KNm)								Fixed End Moment (KNm)
V	3.58E+04	Abutment Shear (KN)								Abutment Shear (KN)
a) Tensile Cracking										
re.sigi	0.00	Re-distributed insitu stress(MPa)								Re-distributed insitu stress(MPa)
sigt	-3.16	Maximum Tensile Stress (MPa)								Maximum Tensile Stress (MPa)
FOS	0.00	Cracking Factor of Safety (UTS/sigt)								Cracking Factor of Safety (UTS/sigt)
Verdict	**cracked**									
b) Crushing at Abutments										
sigb	7.68	Maximum Compressive Stress (MPa)								Maximum Compressive Stress (MPa)
FOS	6.51	Crushing Factor of Safety (UCS/n(x)bottom)								Crushing Factor of Safety (UCS/n(x)bottom)
Verdict	**stable**									
c) Shear Failure at Abutments										
v	1.79	Shear Stress (MPa)								Shear Stress (MPa)
s	3.66	Shear Strength (MPa)								Shear Strength (MPa)
FOS	2.05	Shear Factor of Safety (s/v)								Shear Factor of Safety (s/v)
Verdict	**stable**									
d) Buckling (Euler Fixed Ends)										
B	2807.07	Euler Elastic Buckling Stress (MPa)								Euler Elastic Buckling Stress (MPa)
sig.av	2.26	Average Horizontal Stress (MPa)								Average Horizontal Stress (MPa)
sr	12.58	Slenderness Ratio (L/r)								Slenderness Ratio (L/r)
FOS	1242.45	Buckling Factor of Safety (B/sig.av)								Buckling Factor of Safety (B/sig.av)
Verdict	**stable**									

Overburden Stability Analysis Spreadsheet (1&2 Way Action)									
Input Parameters	Name:	West Wallsend	Case :	1					Name:
Overburden Stability Analysis Spreadsheet (1&2 Way Action)									
Input Parameters	Name:	West Wallsend	Case :	1		0			Name:
Geometry			Date:	02.12.08					
D	160.00	Overburden Depth							Overburden Depth
De	30.00	Effective Caving Height (m)							Effective Caving Height (m)
t	30.00	Beam Thickness (m)							Beam Thickness (m)
alpha	69.00	Caving Angle (degrees)							Caving Angle (degrees)
W	108.93	Span (m)							Span (m)
W/D	1.12	Panel Width/Overburden Depth Ratio							Panel Width/Overburden Depth Ratio
Seam	3.50	Working Height (m)							Working Height (m)
Panel	1.00	Structural Action (1-way = 1, 2-way = 2)							Structural Action (1-way = 1, 2-way = 2)
Rock Properties									
p	2.5	Density (tonnes/m3)							Density (tonnes/m3)
UCS	50	Unconfined Compressive Strength (MPa)							Unconfined Compressive Strength (MPa)
E	11.25	Youngs Modulus (GPa)							Youngs Modulus (GPa)
K	1.6	Vertical/Horizontal Stress Ratio							Vertical/Horizontal Stress Ratio
phi	35	Internal Angle of Friction (Degrees)							Internal Angle of Friction (Degrees)
theta	90	Joint Angle to Horizontal Plane (0 to 90)							Joint Angle to Horizontal Plane (0 to 90)
Load									
w	657.30	Uniformly Distributed Beam Load (KN/m)							Uniformly Distributed Beam Load (KN/m)
sigma v	0.74	virgin vertical stress (MPa)							virgin vertical stress (MPa)
sigma h	1.18	virgin horizontal stress (Mpa)							virgin horizontal stress (Mpa)
Stability Analysis									
Voussoir Arch									
M	9.75E+05	Simply Supported Moment (KNm)							Simply Supported Moment (KNm)
V	3.58E+04	Abutment Shear (KN)							Abutment Shear (KN)
re.sigi	0.00	Re-distributed insitu stress at Seam Level Only(MPa)							Re-distributed insitu stress at Seam Level Only(MPa)
sigt	-6.50	Top Re-distributed Stress (MPa)							Top Re-distributed Stress (MPa)
sigb	7.68	Bottom Initial Stress (MPa)							Bottom Initial Stress (MPa)
n	0.54	Voussoir Stress Block/Beam Thickness Ratio							Voussoir Stress Block/Beam Thickness Ratio
Mt	-9.31E+05	Out of Balance Moment (KNm)							Out of Balance Moment (KNm)
Mv	1.91E+06	Balanced Moment (KNm)							Balanced Moment (KNm)
Hv	9.94E+04	Balanced Thrust (KN)							Balanced Thrust (KN)
a) Abutment Crushing									
sig.bot	12.24	Horizontal Stress (MPa) - Assumes yield zone stress re-distribution							Horizontal Stress (MPa) - Assumes yield zone stress re
sig.confine	1.20	Confining Stress for Strength Calculation (MPa)							Confining Stress for Strength Calculation (MPa)
Strength	54.43	Triaxial Strength (MPa)- Hoek Brown Criterion							Triaxial Strength (MPa)- Hoek Brown Criterion
FOS	4.45	Crushing Factor of Safety(UCS/sig.bot)							Crushing Factor of Safety(UCS/sig.bot)
Verdict	**stable**								
b) Abutment Shear									
Hv	9.94E+04	Horizontal Abutment Thrust (KN)							Horizontal Abutment Thrust (KN)
sig1.angle	19.80	Principle Plane Angle to Horizontal(Degrees)							Principle Plane Angle to Horizontal(Degrees)
sig1	13.83	Principle Stress (MPa)							Principle Stress (MPa)
vmax	6.92	Max Shear Stress (MPa)							Max Shear Stress (MPa)
vmax.angle	64.80	Max Shear Stress Plane Angle to Horizontal(Degrees)							Max Shear Stress Plane Angle to Horizontal(Degrees)
v	4.41	Joint Shear Stress (MPa)							Joint Shear Stress (MPa)
sig.j	19.16	Joint Normal Stress (MPa)							Joint Normal Stress (MPa)
s	13.92	Joint Shear Strength (MPa)							Joint Shear Strength (MPa)
FOS	3.16	Joint Shear Factor of Safety (s/v)							Joint Shear Factor of Safety (s/v)
Verdict	**stable**								
c) Buckling (Euler Pinned Ends)									
B	205.76	Buckling Strength (MPa)							Buckling Strength (MPa)
sig.av	6.12	Average Horizontal Normal Stress (MPa)							Average Horizontal Normal Stress (MPa)
FOS	33.61	Buckling Factor of Safety (B/sig.av)							Buckling Factor of Safety (B/sig.av)
Verdict	**stable**								
Sag Calculation									
Modulus	11.25	Effective Modulus							Effective Modulus
ubot	17.68	maximum horizontal displacement at abutment (mm)							maximum horizontal displacement at abutment (mm)
rotation	0.001	abutment rotation (radians)		0.1	(degrees)				abutment rotation (radians)
v	**0.06**	mid-span sag (m)	Rigid Beam Rotation (I.e. cracked beam solution)						mid-span sag (m)
S.S.	**0.04**	mid-span sag (m)	Simply Supported Elastic Beam (I.e. uncracked solution)						mid-span sag (m)
									Factor of Safety
Abutment Compression Calculation (see Pillar FoS Calculator)									Subsidence/Mining Height

	Overburden Stability Analysis Spreadsheet (1&2 Way Action)																		
Name:	**Input Parameters**	West Wallsend																	
	Geometry																		
Overburden Depth	H	80	100	120	140	160	180	200	220	240	260	280	300		80	100	120	140	160	180	200
Panel Width	W	178.6	178.6	178.6	178.6	178.6	178.6	178.6	178.6	178.6	178.6	178.6	178.6		178.6	178.6	178.6	178.6	178.6	178.6	178.6
W/D	W/H	2.23	1.79	1.49	1.28	1.12	0.99	0.89	0.81	0.74	0.69	0.64	0.60		2.23	1.79	1.49	1.28	1.12	0.99	0.89
Base of Beam Depth(m)	D	**40**	**50**	**60**	**70**	**80**	**90**	**100**	**110**	**120**	**130**	**140**	**150**		**60**	**75**	**90**	**105**	**120**	**135**	**150**
Base of Beam Height Above Seam (m)	y	40	50	60	70	80	90	100	110	120	130	140	150		20	25	30	35	40	45	50
Beam Location Ratio	y/H	0.50	0.50	0.50	0.50	0.50	0.50	0.50	0.50	0.50	0.50	0.50	0.50		0.25	0.25	0.25	0.25	0.25	0.25	0.25
Maximum Caving Height (m)	Hcritical	80.00	100.00	120.00	140.00	160.00	180.00	200.00	220.00	232.63	232.63	232.63	232.63		80.00	100.00	120.00	140.00	160.00	180.00	200.00
Effective Beam Loading Height (m)	De	40.00	50.00	60.00	70.00	80.00	90.00	100.00	110.00	112.63	102.63	92.63	82.63		60.00	75.00	90.00	105.00	120.00	135.00	150.00
Beam Thickness (m)	t	16	20	24	28	32	36	40	44	48	52	56	60		16	20	24	28	32	36	40
Caving Angle (degrees)	alpha	69	69	69	69	69	69	69	69	69	69	69	69		69	69	69	69	69	69	69
Effective Span Angle (degrees)	beta	75	75	75	75	75	75	75	75	75	75	75	75		75	75	75	75	75	75	75
Effective Span (m)	Lbot	157	152	146	141	136	130	125	120	114	109	104	98		168	165	163	160	157	154	152
Effective Span Top Load Length (m)	Ltop	126	113	100	87	74	61	48	35	28	30	32	35		122	108	93	79	65	51	37
Working Height (m)	Seam	3.5	3.5	3.5	3.5	3.5	3.5	3.5	3.5	3.5	3.5	3.5	3.5		3.5	3.5	3.5	3.5	3.5	3.5	3.5
Structural Action (1-way = 1, 2-way = 2)	Panel	1	1	1	1	1	1	1	1	1	1	1	1		1	1	1	1	1	1	1
	Rock Properties																				
Density (tonnes/m3)	*p*	2.5	2.5	2.5	2.5	2.5	2.5	2.5	2.5	2.5	2.5	2.5	2.5		2.5	2.5	2.5	2.5	2.5	2.5	2.5
Unconfined Compressive Strength (MPa)	UCS	50	50	50	50	50	50	50	50	50	50	50	50		50	50	50	50	50	50	50
Ultimate Tensile Strength (MPa)	UTS	0	0	0	0	0	0	0	0	0	0	0	0		0	0	0	0	0	0	0
Youngs Modulus (GPa) (225 x UCS)	E	**7.5**	**7.5**	**7.5**	**7.5**	**7.5**	**7.5**	**7.5**	**7.5**	**7.5**	**7.5**	**7.5**	**7.5**		**7.5**	**7.5**	**7.5**	**7.5**	**7.5**	**7.5**	**7.5**
Vertical/Horizontal Stress Ratio	K	1	1	1	1	1	1	1	1	1	1	1	1		1	1	1	1	1	1	1
Rock Joint Cohesion (MPa)	c	0.5	0.5	0.5	0.5	0.5	0.5	0.5	0.5	0.5	0.5	0.5	0.5		0.5	0.5	0.5	0.5	0.5	0.5	0.5
Joint Angle of Friction (Degrees)	phi	35	35	35	35	35	35	35	35	35	35	35	35		35	35	35	35	35	35	35
Joint Angle to Horizontal Plane (0 to 90)	theta.j	90	90	90	90	90	90	90	90	90	90	90	90		90	90	90	90	90	90	90
	Load																				
Uniformly Distributed Beam Load (KN/m)	w	884.26	1070.12	1238.81	1388.37	1516.54	1620.68	1697.69	1743.93	1715.62	1605.11	1490.37	1370.68		1268.33	1517.28	1736.28	1923.83	2078.31	2198.00	2281.07
virgin vertical stress (MPa)	sigma v	0.78	0.98	1.18	1.37	1.57	1.76	1.96	2.16	2.17	1.88	1.58	1.29		1.27	1.59	1.91	2.23	2.55	2.87	3.19
virgin horizontal stress (Mpa)	sigma h	0.78	0.98	1.18	1.37	1.57	1.76	1.96	2.16	2.17	1.88	1.58	1.29		1.27	1.59	1.91	2.23	2.55	2.87	3.19
	Stability Analysis																				
	Linear Elastic Beam																				
Fixed End Moment (KNm)	M	2.73E+06	3.08E+06	3.32E+06	3.45E+06	3.49E+06	3.44E+06	3.32E+06	3.12E+06	2.80E+06	2.38E+06	2.00E+06	1.65E+06		4.47E+06	5.18E+06	5.73E+06	6.14E+06	6.42E+06	6.56E+06	6.57E+06
Abutment Shear (KN)	V	6.95E+04	8.12E+04	9.07E+04	9.79E+04	1.03E+05	1.06E+05	1.06E+05	1.04E+05	9.80E+04	8.74E+04	7.72E+04	6.73E+04		1.06E+05	1.25E+05	1.41E+05	1.54E+05	1.63E+05	1.70E+05	1.73E+05
	a) Tensile Cracking																				
Re-distributed insitu stress(MPa)	re.sigi	0.00	0.00	0.00	0.00	0.00	0.00	0.00	0.00	0.00	0.00	0.00	0.00		0.00	0.00	0.00	0.00	0.00	0.00	0.00
Maximum Tensile Stress (MPa)	sigt	-41.68	-29.60	-21.59	-15.91	-11.68	-8.42	-5.84	-3.75	-1.92	-0.34	0.88	1.84		-68.35	-49.92	-37.61	-28.78	-22.13	-16.93	-12.75
Cracking Factor of Safety (UTS/sigt)	FOS	0.00	0.00	0.00	0.00	0.00	0.00	0.00	0.00	0.00	0.00	1.00	1.00		0.00	0.00	0.00	0.00	0.00	0.00	0.00
	Verdict	**cracked**	**cracked**	**cracked**	**cracked**	**cracked**	**cracked**	**cracked**	**cracked**	**cracked**	**cracked**	**un-cracked**	**un-cracked**		**cracked**	**cracked**	**cracked**	**cracked**	**cracked**	**cracked**	**cracked**
	b) Crushing at Abutments																				
Maximum Compressive Stress (MPa)	sigb	64.77	47.22	35.77	27.81	22.03	17.70	14.40	11.83	9.47	7.16	5.41	4.04		106.00	79.24	61.63	49.25	40.15	33.22	27.83
Crushing Factor of Safety (UCS/n(x)bottom)	FOS	0.77	1.06	1.40	1.80	2.27	2.82	3.47	4.23	5.28	6.98	9.25	12.36		0.47	0.63	0.81	1.02	1.25	1.50	1.80
	Verdict	**failed**	**stable**	**stable**	**stable**	**stable**	**stable**	**stable**	**stable**	**stable**	**stable**	**stable**	**stable**		**failed**	**failed**	**failed**	**stable**	**stable**	**stable**	**stable**
	c) Shear Failure at Abutments																				
Shear Stress (MPa)	v	6.51	6.09	5.67	5.25	4.82	4.40	3.98	3.56	3.06	2.52	2.07	1.68		9.98	9.40	8.82	8.24	7.66	7.07	6.49
Shear Strength (MPa)	s	16.67	12.84	10.43	8.83	7.75	7.00	6.49	6.15	5.78	5.28	4.90	4.62		26.87	21.02	17.32	14.84	13.12	11.91	11.05
Shear Factor of Safety (s/v)	FOS	2.56	2.11	1.84	1.68	1.61	1.59	1.63	1.73	1.89	2.09	2.37	2.74		2.69	2.24	1.96	1.80	1.71	1.68	1.70
	Verdict	**stable**	**stable**	**stable**	**stable**	**stable**	**stable**	**stable**	**stable**	**stable**	**stable**	**stable**	**stable**		**stable**	**stable**	**stable**	**stable**	**stable**	**stable**	**stable**
	d) Buckling (Euler Fixed Ends)																				
Euler Elastic Buckling Stress (MPa)	B	255.73	428.28	662.68	971.81	1371.51	1881.46	2526.21	3336.65	4352.00	5622.45	7212.94	9208.41		224.12	361.63	538.06	757.12	1022.90	1339.91	1713.12
Average Horizontal Stress (MPa)	sig.av	11.55	8.81	7.09	5.95	5.17	4.64	4.28	4.04	3.77	3.41	3.14	2.94		18.83	14.66	12.01	10.24	9.01	8.15	7.54
Slenderness Ratio (L/r)	sr	34.03	26.29	21.14	17.46	14.69	12.54	10.83	9.42	8.25	7.26	6.41	5.67		36.35	28.61	23.46	19.78	17.01	14.87	13.15
Buckling Factor of Safety (B/sig.av)	FOS	22.15	48.62	93.49	163.33	265.06	405.38	590.55	826.41	1153.88	1647.96	2294.15	3130.66		11.90	24.68	44.80	73.95	113.52	164.48	227.30
	Verdict	**stable**	**stable**	**stable**	**stable**	**stable**	**stable**	**stable**	**stable**	**stable**	**stable**	**stable**	**stable**		**stable**	**stable**	**stable**	**stable**	**stable**	**stable**	**stable**

	Overburden Stability Analysis Spreadsheet (1&2 Way Action)																		
Name:	**Input Parameters**	West Wallsend																	
	Overburden Stability Analysis Spreadsheet (1&2 Way Action)																		
Name:	**Input Parameters**																		
	Geometry																		
Overburden Depth	D	80.00	100.00	120.00	140.00	160.00	180.00	200.00	220.00	240.00	260.00	280.00	300.00		80.00	100.00	120.00	140.00	160.00	180.00	200.00
Effective Caving Height (m)	De	40.00	50.00	60.00	70.00	80.00	90.00	100.00	110.00	112.63	102.63	92.63	82.63		60.00	75.00	90.00	105.00	120.00	135.00	150.00
Beam Thickness (m)	t	16.00	20.00	24.00	28.00	32.00	36.00	40.00	44.00	48.00	52.00	56.00	60.00		16.00	20.00	24.00	28.00	32.00	36.00	40.00
Caving Angle (degrees)	alpha	69.00	69.00	69.00	69.00	69.00	69.00	69.00	69.00	69.00	69.00	69.00	69.00		69.00	69.00	69.00	69.00	69.00	69.00	69.00
Span (m)	W	157.16	151.81	146.45	141.09	135.73	130.37	125.01	119.65	114.29	108.93	103.57	98.22		167.88	165.20	162.52	159.84	157.16	154.48	151.81
Panel Width/Overburden Depth Ratio	W/H	2.23	1.79	1.49	1.28	1.12	0.99	0.89	0.81	0.74	0.69	0.64	0.60		2.23	1.79	1.49	1.28	1.12	0.99	0.89
Working Height (m)	Seam	3.50	3.50	3.50	3.50	3.50	3.50	3.50	3.50	3.50	3.50	3.50	3.50		3.50	3.50	3.50	3.50	3.50	3.50	3.50
Structural Action (1-way = 1, 2-way = 2)	Panel	1.00	1.00	1.00	1.00	1.00	1.00	1.00	1.00	1.00	1.00	1.00	1.00		1.00	1.00	1.00	1.00	1.00	1.00	1.00
	Rock Properties																				
Density (tonnes/m3)	p	2.5	2.5	2.5	2.5	2.5	2.5	2.5	2.5	2.5	2.5	2.5	2.5		2.5	2.5	2.5	2.5	2.5	2.5	2.5
Unconfined Compressive Strength (MPa)	UCS	50	50	50	50	50	50	50	50	50	50	50	50		50	50	50	50	50	50	50
Youngs Modulus (GPa)	E	7.5	7.5	7.5	7.5	7.5	7.5	7.5	7.5	7.5	7.5	7.5	7.5		7.5	7.5	7.5	7.5	7.5	7.5	7.5
Vertical/Horizontal Stress Ratio	K	1	1	1	1	1	1	1	1	1	1	1	1		1	1	1	1	1	1	1
Internal Angle of Friction (Degrees)	phi	35	35	35	35	35	35	35	35	35	35	35	35		35	35	35	35	35	35	35
Joint Angle to Horizontal Plane (0 to 90)	theta	90	90	90	90	90	90	90	90	90	90	90	90		90	90	90	90	90	90	90
	Load																				
Uniformly Distributed Beam Load (KN/m)	w	884.26	1070.12	1238.81	1388.37	1516.54	1620.68	1697.69	1743.93	1715.62	1605.11	1490.37	1370.68		1268.33	1517.28	1736.28	1923.83	2078.31	2198.00	2281.07
virgin vertical stress (MPa)	sigma v	0.78	0.98	1.18	1.37	1.57	1.76	1.96	2.16	2.17	1.88	1.58	1.29		1.27	1.59	1.91	2.23	2.55	2.87	3.19
virgin horizontal stress (Mpa)	sigma h	0.78	0.98	1.18	1.37	1.57	1.76	1.96	2.16	2.17	1.88	1.58	1.29		1.27	1.59	1.91	2.23	2.55	2.87	3.19
	Stability Analysis																				
	Voussoir Arch																				
Simply Supported Moment (KNm)	M	2.73E+06	3.08E+06	3.32E+06	3.45E+06	3.49E+06	3.44E+06	3.32E+06	3.12E+06	2.80E+06	2.38E+06	2.00E+06	1.65E+06		4.47E+06	5.18E+06	5.73E+06	6.14E+06	6.42E+06	6.56E+06	6.57E+06
Abutment Shear (KN)	V	6.95E+04	8.12E+04	9.07E+04	9.79E+04	1.03E+05	1.06E+05	1.06E+05	1.04E+05	9.80E+04	8.74E+04	7.72E+04	6.73E+04		1.06E+05	1.25E+05	1.41E+05	1.54E+05	1.63E+05	1.70E+05	1.73E+05
Re-distributed insitu stress at Seam Level Only(MPa)	re.sigi	0.00	0.00	0.00	0.00	0.00	0.00	0.00	0.00	0.00	0.00	0.00	0.00		0.00	0.00	0.00	0.00	0.00	0.00	0.00
Top Re-distributed Stress (MPa)	sigt	-63.01	-45.50	-33.71	-25.41	-19.29	-14.62	-10.97	-8.06	-5.53	-3.37	-1.77	-0.55		-103.26	-76.30	-58.10	-45.14	-35.44	-27.93	-21.95
Bottom Initial Stress (MPa)	sigc	64.58	46.97	35.48	27.47	21.64	17.26	13.91	11.29	9.06	7.19	5.88	4.96		105.81	78.99	61.33	48.91	39.76	32.78	27.34
Voussoir Stress Block/Beam Thickness Ratio	n	0.51	0.51	0.51	0.52	0.53	0.54	0.56	0.58	0.62	0.68	0.77	0.90		0.51	0.51	0.51	0.52	0.53	0.54	0.55
Out of Balance Moment (KNm)	Mt	-2.65E+06	-2.98E+06	-3.15E+06	-3.19E+06	-3.10E+06	-2.89E+06	-2.58E+06	-2.16E+06	-1.61E+06	-9.69E+05	-4.26E+05	-6.57E+04		-4.35E+06	-4.99E+06	-5.42E+06	-5.66E+06	-5.70E+06	-5.55E+06	-5.21E+06
Balanced Moment (KNm)	Mv	5.38E+06	6.06E+06	6.47E+06	6.64E+06	6.59E+06	6.34E+06	5.89E+06	5.28E+06	4.41E+06	3.35E+06	2.42E+06	1.72E+06		8.82E+06	1.02E+07	1.12E+07	1.18E+07	1.21E+07	1.21E+07	1.18E+07
Balanced Thrust (KN)	Hv	5.08E+05	4.59E+05	4.10E+05	3.63E+05	3.18E+05	2.75E+05	2.35E+05	1.97E+05	1.57E+05	1.18E+05	8.89E+04	7.17E+04		8.32E+05	7.70E+05	7.07E+05	6.45E+05	5.85E+05	5.25E+05	4.67E+05
	a) Abutment Crushing																				
Horizontal Stress (MPa) - Assumes yield zone stress re	sig.bot	125.43	90.29	66.60	49.91	37.61	28.26	21.01	15.31	10.52	6.67	4.13	2.65		205.44	151.29	114.70	88.62	69.13	54.06	42.13
Confining Stress for Strength Calculation (MPa)	sig.confine	1.00	1.25	1.50	1.75	2.00	2.25	2.50	2.75	3.00	3.25	3.50	3.75		1.50	1.88	2.25	2.63	3.00	3.38	3.75
Triaxial Strength (MPa)- Hoek Brown Criterion	Strength	53.69	54.61	55.54	56.46	57.38	58.30	59.23	60.15	61.07	61.99	62.92	63.84		55.54	56.92	58.30	59.69	61.07	62.45	63.84
Crushing Factor of Safety(UCS/sig.bot)	FOS	0.43	0.60	0.83	1.13	1.53	2.06	2.82	3.93	5.80	9.30	15.24	24.05		0.27	0.38	0.51	0.67	0.88	1.16	1.52
	Verdict	**collapsed**	**collapsed**	**collapsed**	**yielding**	**stable**	**stable**	**stable**	**stable**	**stable**	**stable**	**stable**	**stable**		**collapsed**	**collapsed**	**collapsed**	**collapsed**	**collapsed**	**yielding**	**stable**
	b) Abutment Shear																				
Horizontal Abutment Thrust (KN)	Hv	5.08E+05	4.59E+05	4.10E+05	3.63E+05	3.18E+05	2.75E+05	2.35E+05	1.97E+05	1.57E+05	1.18E+05	8.89E+04	7.17E+04		8.32E+05	7.70E+05	7.07E+05	6.45E+05	5.85E+05	5.25E+05	4.67E+05
Principle Plane Angle to Horizontal(Degrees)	sig1.angle	7.79	10.04	12.48	15.10	17.92	20.98	24.31	27.95	32.01	36.53	40.97	43.20		7.29	9.25	11.29	13.40	15.61	17.91	20.33
Principle Stress (MPa)	sig1	127.78	93.12	69.87	53.55	41.55	32.42	25.29	19.63	14.64	10.33	7.24	4.99		208.81	155.30	119.27	93.65	74.52	59.70	47.91
Max Shear Stress (MPa)	vmax	63.89	46.56	34.93	26.77	20.77	16.21	12.65	9.81	7.32	5.16	3.62	2.50		104.40	77.65	59.64	46.83	37.26	29.85	23.95
Max Shear Stress Plane Angle to Horizontal(Degrees)	vmax.angle	52.79	55.04	57.48	60.10	62.92	65.98	69.31	72.95	77.01	81.53	85.97	88.20		52.29	54.25	56.29	58.40	60.61	62.91	65.33
Joint Shear Stress (MPa)	v	17.16	15.99	14.74	13.47	12.17	10.84	9.49	8.13	6.58	4.94	3.58	2.49		26.30	24.64	22.90	21.12	19.31	17.47	15.61
Joint Normal Stress (MPa)	sig.j	189.32	136.85	101.54	76.69	58.39	44.47	33.66	25.13	17.84	11.83	7.75	5.15		309.84	228.94	174.34	135.45	106.39	83.91	66.08
Joint Shear Strength (MPa)	s	133.07	96.33	71.60	54.20	41.38	31.64	24.07	18.09	12.99	8.78	5.92	4.11		217.46	160.80	122.57	95.34	74.99	59.26	46.77
Joint Shear Factor of Safety (s/v)	FOS	7.75	6.02	4.86	4.02	3.40	2.92	2.54	2.23	1.97	1.78	1.65	1.65		8.27	6.53	5.35	4.51	3.88	3.39	3.00
	Verdict	**stable**	**stable**	**stable**	**stable**	**stable**	**stable**	**stable**	**stable**	**stable**	**stable**	**stable**	**stable**		**stable**	**stable**	**stable**	**stable**	**stable**	**stable**	**stable**
	c) Buckling (Euler Pinned Ends)																				
Buckling Strength (MPa)	B	16.38	27.63	43.56	65.56	95.86	137.92	197.42	284.10	419.45	651.61	1066.68	1865.72		14.35	23.39	35.47	51.19	71.47	97.66	131.77
Average Horizontal Normal Stress (MPa)	sig.av	62.72	45.15	33.30	24.96	18.81	14.13	10.50	7.66	5.26	3.33	2.06	1.33		102.72	75.64	57.35	44.31	34.56	27.03	21.06
Buckling Factor of Safety (B/sig.av)	FOS	0.26	0.61	1.31	2.63	5.10	9.76	18.79	37.11	79.71	195.48	516.84	1405.81		0.14	0.31	0.62	1.16	2.07	3.61	6.26
	Verdict	**buckling**	**buckling**	**stable**	**stable**	**stable**	**stable**	**stable**	**stable**	**stable**	**stable**	**stable**	**stable**		**buckling**	**buckling**	**buckling**	**stable**	**stable**	**stable**	**stable**
	Sag Calculation (assuming beam is in elastic range)																				
Effective Modulus	Modulus	1.13	1.13	1.13	2.80	7.50	7.50	7.50	7.50	7.50	7.50	7.50	7.50		1.13	1.13	1.13	1.13	1.13	3.11	7.50
maximum horizontal displacement at abutment (mm)	u	902.93	815.35	728.55	259.58	84.85	73.46	62.64	52.43	41.82	31.47	23.70	19.12		1478.72	1368.12	1256.64	1147.08	1039.52	338.42	124.63
abutment rotation (radians)	rotation	0.111	0.080	0.059	0.018	0.005	0.004	0.003	0.002	0.001	0.001	0.001	0.000		0.183	0.134	0.102	0.079	0.061	0.017	0.006
mid-span sag (m)	Smax	**2.03**	**2.03**	**2.03**	**1.26**	**0.34**	**0.25**	**0.18**	**0.12**	**0.08**	**0.05**	**0.03**	**0.02**		**2.03**	**2.03**	**2.03**	**2.03**	**2.03**	**1.34**	**0.43**
mid-span sag (m)	S.S.	**2.03**	**2.03**	**2.03**	**1.17**	**0.27**	**0.17**	**0.11**	**0.07**	**0.05**	**0.03**	**0.02**	**0.01**		**2.03**	**2.03**	**2.03**	**2.03**	**2.03**	**1.13**	**0.33**
Factor of Safety	FoS	0.26	0.60	0.83	1.13	1.53	2.06	2.54	2.23	1.97	1.78	1.65	1.65		0.14	0.31	0.51	0.67	0.88	1.16	1.52
Subsidence/Mining Height	**Smax/T**	**0.58**	**0.58**	**0.58**	**0.36**	**0.10**	**0.07**	**0.05**	**0.03**	**0.02**	**0.01**	**0.01**	**0.00**		**0.58**	**0.58**	**0.58**	**0.58**	**0.58**	**0.38**	**0.12**

Name:																					
Overburden Depth	220	240	260	280	300		80	100	120	140	160	180	200	220	240	260	280	300		80	100
Panel Width	178.6	178.6	178.6	178.6	178.6		178.6	178.6	178.6	178.6	178.6	178.6	178.6	178.6	178.6	178.6	178.6	178.6		178.6	178.6
W/D	0.81	0.74	0.69	0.64	0.60		2.23	1.79	1.49	1.28	1.12	0.99	0.89	0.81	0.74	0.69	0.64	0.60		2.23	1.79
Base of Beam Depth(m)	**165**	**180**	**195**	**210**	**225**		**72**	**90**	**108**	**126**	**144**	**162**	**180**	**198**	**216**	**234**	**252**	**270**		**20**	**25**
Base of Beam Height Above Seam (m)	55	60	65	70	75		8	10	12	14	16	18	20	22	24	26	28	30		60	75
Beam Location Ratio	0.25	0.25	0.25	0.25	0.25		0.10	0.10	0.10	0.10	0.10	0.10	0.10	0.10	0.10	0.10	0.10	0.10		0.75	0.75
Maximum Caving Height (m)	220.00	232.63	232.63	232.63	232.63		80.00	100.00	120.00	140.00	160.00	180.00	200.00	220.00	232.63	232.63	232.63	232.63		80.00	100.00
Effective Beam Loading Height (m)	165.00	172.63	167.63	162.63	157.63		72.00	90.00	108.00	126.00	144.00	162.00	180.00	198.00	208.63	206.63	204.63	202.63		20.00	25.00
Beam Thickness (m)	44	48	52	56	60		16	20	24	28	32	36	40	44	48	52	56	60		8	10
Caving Angle (degrees)	69	69	69	69	69		69	69	69	69	69	69	69	69	69	69	69	69		69	69
Effective Span Angle (degrees)	75	75	75	75	75		75	75	75	75	75	75	75	75	75	75	75	75		75	75
Effective Span (m)	149	146	144	141	138		174	173	172	171	170	169	168	167	166	165	164	163		146	138
Effective Span Top Load Length (m)	22	14	15	16	17		119	104	89	74	59	45	30	15	6	6	6	7		131	119
Working Height (m)	3.5	3.5	3.5	3.5	3.5		3.5	3.5	3.5	3.5	3.5	3.5	3.5	3.5	3.5	3.5	3.5	3.5		3.5	3.5
Structural Action (1-way = 1, 2-way = 2)	1	1	1	1	1		1	1	1	1	1	1	1	1	1	1	1	1		1	1
Density (tonnes/m3)	2.5	2.5	2.5	2.5	2.5		2.5	2.5	2.5	2.5	2.5	2.5	2.5	2.5	2.5	2.5	2.5	2.5		2.5	2.5
Unconfined Compressive Strength (MPa)	50	50	50	50	50		50	50	50	50	50	50	50	50	50	50	50	50		50	50
Ultimate Tensile Strength (MPa)	0	0	0	0	0		0	0	0	0	0	0	0	0	0	0	0	0		0	0
Youngs Modulus (GPa) (225 x UCS)	**7.5**	**7.5**	**7.5**	**7.5**	**7.5**		**7.5**	**7.5**	**7.5**	**7.5**	**7.5**	**7.5**	**7.5**	**7.5**	**7.5**	**7.5**	**7.5**	**7.5**		**7.5**	**7.5**
Vertical/Horizontal Stress Ratio	1	1	1	1	1		1	1	1	1	1	1	1	1	1	1	1	1		1	1
Rock Joint Cohesion (MPa)	0.5	0.5	0.5	0.5	0.5		0.5	0.5	0.5	0.5	0.5	0.5	0.5	0.5	0.5	0.5	0.5	0.5		0.5	0.5
Joint Angle of Friction (Degrees)	35	35	35	35	35		35	35	35	35	35	35	35	35	35	35	35	35		35	35
Joint Angle to Horizontal Plane (0 to 90)	90	90	90	90	90		90	90	90	90	90	90	90	90	90	90	90	90		90	90
Uniformly Distributed Beam Load (KN/m)	2325.54	2315.64	2268.76	2221.43	2173.60		1484.31	1765.28	2008.86	2214.35	2381.02	2508.15	2594.97	2640.70	2641.57	2623.93	2606.24	2588.50		464.31	570.03
virgin vertical stress (MPa)	3.50	3.64	3.47	3.30	3.13		1.57	1.96	2.35	2.74	3.14	3.53	3.92	4.31	4.52	4.43	4.33	4.23		0.39	0.49
virgin horizontal stress (Mpa)	3.50	3.64	3.47	3.30	3.13		1.57	1.96	2.35	2.74	3.14	3.53	3.92	4.31	4.52	4.43	4.33	4.23		0.39	0.49
Fixed End Moment (KNm)	6.46E+06	6.21E+06	5.86E+06	5.53E+06	5.20E+06		5.64E+06	6.62E+06	7.44E+06	8.10E+06	8.60E+06	8.95E+06	9.14E+06	9.18E+06	9.07E+06	8.89E+06	8.72E+06	8.55E+06		1.24E+06	1.36E+06
Abutment Shear (KN)	1.73E+05	1.70E+05	1.63E+05	1.57E+05	1.50E+05		1.29E+05	1.53E+05	1.73E+05	1.89E+05	2.02E+05	2.12E+05	2.18E+05	2.20E+05	2.19E+05	2.16E+05	2.13E+05	2.10E+05		3.40E+04	3.94E+04
Re-distributed insitu stress(MPa)	0.00	0.00	0.00	0.00	0.00		0.00	0.00	0.00	0.00	0.00	0.00	0.00	0.00	0.00	0.00	0.00	0.00		0.00	0.00
Maximum Tensile Stress (MPa)	-9.31	-6.37	-3.89	-1.91	-0.27		-42.67	-31.40	-23.79	-18.27	-14.06	-10.72	-8.00	-5.72	-3.76	-2.12	-0.76	0.40		-38.60	-26.93
Cracking Factor of Safety (UTS/sigt)	0.00	0.00	0.00	0.00	0.00		0.00	0.00	0.00	0.00	0.00	0.00	0.00	0.00	0.00	0.00	0.00	1.00		0.00	0.00
	cracked	**cracked**	**cracked**	**cracked**	**cracked**		**cracked**	**cracked**	**cracked**	**cracked**	**cracked**	**cracked**	**cracked**	**cracked**	**cracked**	**cracked**	**cracked**	**un-cracked**		**cracked**	**cracked**
Maximum Compressive Stress (MPa)	23.54	19.81	16.48	13.87	11.80		133.70	101.30	79.89	64.76	53.55	44.96	38.20	32.78	28.14	24.16	21.01	18.47		117.09	82.39
Crushing Factor of Safety (UCS/n(x)bottom)	2.12	2.52	3.03	3.60	4.24		0.37	0.49	0.63	0.77	0.93	1.11	1.31	1.53	1.78	2.07	2.38	2.71		0.43	0.61
	stable	**stable**	**stable**	**stable**	**stable**		**failed**	**failed**	**failed**	**failed**	**failed**	**stable**	**stable**	**stable**	**stable**	**stable**	**stable**	**stable**		**failed**	**failed**
Shear Stress (MPa)	5.91	5.30	4.70	4.20	3.76		12.13	11.47	10.81	10.15	9.49	8.83	8.17	7.51	6.84	6.23	5.71	5.26		6.37	5.92
Shear Strength (MPa)	10.46	9.91	9.31	8.88	8.57		64.24	49.44	39.78	33.05	28.15	24.47	21.65	19.45	17.58	15.93	14.68	13.71		55.45	39.33
Shear Factor of Safety (s/v)	1.77	1.87	1.98	2.12	2.28		5.30	4.31	3.68	3.26	2.97	2.77	2.65	2.59	2.57	2.56	2.57	2.61		8.70	6.65
	stable	**stable**	**stable**	**stable**	**stable**		**stable**	**stable**	**stable**	**stable**	**stable**	**stable**	**stable**	**stable**	**stable**	**stable**	**stable**	**stable**		**stable**	**stable**
Euler Elastic Buckling Stress (MPa)	2148.03	2650.74	3227.98	3887.24	4636.84		207.88	328.85	479.46	660.80	874.00	1120.23	1400.72	1716.72	2069.55	2460.57	2891.19	3362.89		73.63	128.80
Average Horizontal Stress (MPa)	7.11	6.72	6.29	5.98	5.77		45.51	34.95	28.05	23.24	19.74	17.12	15.10	13.53	12.19	11.02	10.13	9.44		39.24	27.73
Slenderness Ratio (L/r)	11.74	10.57	9.58	8.73	7.99		37.74	30.01	24.85	21.17	18.41	16.26	14.54	13.13	11.96	10.97	10.12	9.38		63.41	47.95
Buckling Factor of Safety (B/sig.av)	302.02	394.45	513.07	649.57	804.23		4.57	9.41	17.09	28.43	44.26	65.44	92.75	126.87	169.73	223.28	285.54	356.41		1.88	4.65
	stable	**stable**	**stable**	**stable**	**stable**		**stable**	**stable**	**stable**	**stable**	**stable**	**stable**	**stable**	**stable**	**stable**	**stable**	**stable**	**stable**		**stable**	**stable**

Name:																				
Name:																				
Overburden Depth	220.00	240.00	260.00	280.00	300.00		80.00	100.00	120.00	140.00	160.00	180.00	200.00	220.00	240.00	260.00	280.00	300.00	80.00	100.00
Effective Caving Height (m)	165.00	172.63	167.63	162.63	157.63		72.00	90.00	108.00	126.00	144.00	162.00	180.00	198.00	208.63	206.63	204.63	202.63	20.00	25.00
Beam Thickness (m)	44.00	48.00	52.00	56.00	60.00		16.00	20.00	24.00	28.00	32.00	36.00	40.00	44.00	48.00	52.00	56.00	60.00	8.00	10.00
Caving Angle (degrees)	69.00	69.00	69.00	69.00	69.00		69.00	69.00	69.00	69.00	69.00	69.00	69.00	69.00	69.00	69.00	69.00	69.00	69.00	69.00
Span (m)	149.13	146.45	143.77	141.09	138.41		174.31	173.24	172.17	171.10	170.03	168.95	167.88	166.81	165.74	164.67	163.59	162.52	146.45	138.41
Panel Width/Overburden Depth Ratio	0.81	0.74	0.69	0.64	0.60		2.23	1.79	1.49	1.28	1.12	0.99	0.89	0.81	0.74	0.69	0.64	0.60	2.23	1.79
Working Height (m)	3.50	3.50	3.50	3.50	3.50		3.50	3.50	3.50	3.50	3.50	3.50	3.50	3.50	3.50	3.50	3.50	3.50	3.50	3.50
Structural Action (1-way = 1, 2-way = 2)	1.00	1.00	1.00	1.00	1.00		1.00	1.00	1.00	1.00	1.00	1.00	1.00	1.00	1.00	1.00	1.00	1.00	1.00	1.00
Density (tonnes/m3)	2.5	2.5	2.5	2.5	2.5		2.5	2.5	2.5	2.5	2.5	2.5	2.5	2.5	2.5	2.5	2.5	2.5	2.5	2.5
Unconfined Compressive Strength (MPa)	50	50	50	50	50		50	50	50	50	50	50	50	50	50	50	50	50	50	50
Youngs Modulus (GPa)	7.5	7.5	7.5	7.5	7.5		7.5	7.5	7.5	7.5	7.5	7.5	7.5	7.5	7.5	7.5	7.5	7.5	7.5	7.5
Vertical/Horizontal Stress Ratio	1	1	1	1	1		1	1	1	1	1	1	1	1	1	1	1	1	1	1
Internal Angle of Friction (Degrees)	35	35	35	35	35		35	35	35	35	35	35	35	35	35	35	35	35	35	35
Joint Angle to Horizontal Plane (0 to 90)	90	90	90	90	90		90	90	90	90	90	90	90	90	90	90	90	90	90	90
Uniformly Distributed Beam Load (KN/m)	2325.54	2315.64	2268.76	2221.43	2173.60		1484.31	1765.28	2008.86	2214.35	2381.02	2508.15	2594.97	2640.70	2641.57	2623.93	2606.24	2588.50	464.31	570.03
virgin vertical stress (MPa)	3.50	3.64	3.47	3.30	3.13		1.57	1.96	2.35	2.74	3.14	3.53	3.92	4.31	4.52	4.43	4.33	4.23	0.39	0.49
virgin horizontal stress (Mpa)	3.50	3.64	3.47	3.30	3.13		1.57	1.96	2.35	2.74	3.14	3.53	3.92	4.31	4.52	4.43	4.33	4.23	0.39	0.49
Simply Supported Moment (KNm)	6.46E+06	6.21E+06	5.86E+06	5.53E+06	5.20E+06		5.64E+06	6.62E+06	7.44E+06	8.10E+06	8.60E+06	8.95E+06	9.14E+06	9.18E+06	9.07E+06	8.89E+06	8.72E+06	8.55E+06	1.24E+06	1.36E+06
Abutment Shear (KN)	1.73E+05	1.70E+05	1.63E+05	1.57E+05	1.50E+05		1.29E+05	1.53E+05	1.73E+05	1.89E+05	2.02E+05	2.12E+05	2.18E+05	2.20E+05	2.19E+05	2.16E+05	2.13E+05	2.10E+05	3.40E+04	3.94E+04
Re-distributed insitu stress at Seam Level Only(MPa)	0.00	0.00	0.00	0.00	0.00		0.00	0.00	0.00	0.00	0.00	0.00	0.00	0.00	0.00	0.00	0.00	0.00	0.00	0.00
Top Re-distributed Stress (MPa)	-17.07	-12.93	-9.50	-6.80	-4.63		-130.37	-97.62	-75.48	-59.61	-47.67	-38.35	-30.85	-24.69	-19.50	-15.28	-11.88	-9.10	-116.20	-81.53
Bottom Initial Stress (MPa)	23.00	19.40	16.51	14.35	12.72		133.50	101.05	79.59	64.41	53.16	44.52	37.71	32.24	27.74	24.19	21.48	19.39	116.99	82.27
Voussoir Stress Block/Beam Thickness Ratio	0.57	0.60	0.63	0.68	0.73		0.51	0.51	0.51	0.52	0.53	0.54	0.55	0.57	0.59	0.61	0.64	0.68	0.50	0.50
Out of Balance Moment (KNm)	-4.69E+06	-3.97E+06	-3.13E+06	-2.28E+06	-1.48E+06		-5.49E+06	-6.39E+06	-7.05E+06	-7.48E+06	-7.69E+06	-7.66E+06	-7.40E+06	-6.90E+06	-6.18E+06	-5.32E+06	-4.42E+06	-3.48E+06	-1.23E+06	-1.35E+06
Balanced Moment (KNm)	1.12E+07	1.02E+07	8.99E+06	7.81E+06	6.69E+06		1.11E+07	1.30E+07	1.45E+07	1.56E+07	1.63E+07	1.66E+07	1.65E+07	1.61E+07	1.52E+07	1.42E+07	1.31E+07	1.20E+07	2.48E+06	2.72E+06
Balanced Thrust (KN)	4.11E+05	3.53E+05	3.00E+05	2.55E+05	2.18E+05		1.05E+06	9.85E+05	9.18E+05	8.52E+05	7.85E+05	7.19E+05	6.53E+05	5.88E+05	5.22E+05	4.62E+05	4.11E+05	3.67E+05	4.66E+05	4.08E+05
Horizontal Stress (MPa) - Assumes yield zone stress re	32.53	24.55	18.16	13.41	9.92		259.36	193.59	149.05	117.11	93.08	74.34	59.37	47.17	37.06	29.02	22.81	17.98	232.06	162.66
Confining Stress for Strength Calculation (MPa)	4.13	4.50	4.88	5.25	5.63		1.80	2.25	2.70	3.15	3.60	4.05	4.50	4.95	5.40	5.85	6.30	6.75	0.50	0.63
Triaxial Strength (MPa)- Hoek Brown Criterion	65.22	66.61	67.99	69.37	70.76		56.64	58.30	59.96	61.62	63.28	64.95	66.61	68.27	69.93	71.59	73.25	74.91	51.85	52.31
Crushing Factor of Safety(UCS/sig.bot)	2.01	2.71	3.74	5.17	7.13		0.22	0.30	0.40	0.53	0.68	0.87	1.12	1.45	1.89	2.47	3.21	4.17	0.22	0.32
	stable	**stable**	**stable**	**stable**	**stable**		**collapsed**	**collapsed**	**collapsed**	**collapsed**	**collapsed**	**collapsed**	**yielding**	**yielding**	**stable**	**stable**	**stable**	**stable**	**collapsed**	**collapsed**
Horizontal Abutment Thrust (KN)	4.11E+05	3.53E+05	3.00E+05	2.55E+05	2.18E+05		1.05E+06	9.85E+05	9.18E+05	8.52E+05	7.85E+05	7.19E+05	6.53E+05	5.88E+05	5.22E+05	4.62E+05	4.11E+05	3.67E+05	4.66E+05	4.08E+05
Principle Plane Angle to Horizontal(Degrees)	22.89	25.63	28.55	31.59	34.60		7.03	8.83	10.67	12.54	14.46	16.42	18.45	20.55	22.74	25.04	27.41	29.81	4.18	5.52
Principle Stress (MPa)	38.32	30.19	23.54	18.49	14.64		263.30	198.26	154.34	122.91	99.26	80.80	65.97	53.79	43.57	35.35	28.94	23.89	233.30	164.18
Max Shear Stress (MPa)	19.16	15.10	11.77	9.24	7.32		131.65	99.13	77.17	61.45	49.63	40.40	32.99	26.90	21.78	17.68	14.47	11.94	116.65	82.09
Max Shear Stress Plane Angle to Horizontal(Degrees)	67.89	70.63	73.55	76.59	79.60		52.03	53.83	55.67	57.54	59.46	61.42	63.45	65.55	67.74	70.04	72.41	74.81	49.18	50.52
Joint Shear Stress (MPa)	13.73	11.77	9.88	8.25	6.84		31.96	30.06	28.08	26.05	24.00	21.91	19.80	17.68	15.54	13.56	11.82	10.30	16.94	15.71
Joint Normal Stress (MPa)	51.69	39.64	29.93	22.66	17.24		391.01	292.72	226.22	178.56	142.71	114.75	92.35	74.06	58.84	46.69	37.27	29.93	348.71	244.75
Joint Shear Strength (MPa)	36.69	28.26	21.46	16.36	12.57		274.29	205.46	158.90	125.53	100.42	80.85	65.17	52.36	41.70	33.20	26.60	21.46	244.67	171.88
Joint Shear Factor of Safety (s/v)	2.67	2.40	2.17	1.98	1.84		8.58	6.83	5.66	4.82	4.19	3.69	3.29	2.96	2.68	2.45	2.25	2.08	14.44	10.94
	stable	**stable**	**stable**	**stable**	**stable**		**stable**	**stable**	**stable**	**stable**	**stable**	**stable**	**stable**	**stable**	**stable**	**stable**	**stable**	**stable**	**stable**	**stable**
Buckling Strength (MPa)	176.92	238.59	325.08	447.24	622.84		13.30	21.27	31.58	44.56	60.73	80.84	105.94	137.62	178.35	231.13	299.71	389.44	4.63	8.12
Average Horizontal Normal Stress (MPa)	16.26	12.27	9.08	6.71	4.96		129.68	96.79	74.52	58.56	46.54	37.17	29.68	23.58	18.53	14.51	11.40	8.99	116.03	81.33
Buckling Factor of Safety (B/sig.av)	10.88	19.44	35.80	66.69	125.61		0.10	0.22	0.42	0.76	1.31	2.17	3.57	5.84	9.63	15.93	26.28	43.31	0.04	0.10
	stable	**stable**	**stable**	**stable**	**stable**		**buckling**	**buckling**	**buckling**	**buckling**	**stable**	**stable**	**stable**	**stable**	**stable**	**stable**	**stable**	**stable**	**buckling**	**buckling**
Effective Modulus	7.50	7.50	7.50	7.50	7.50		1.13	1.13	1.13	1.13	1.13	1.13	2.68	6.83	7.50	7.50	7.50	7.50	1.13	1.13
maximum horizontal displacement at abutment (mm)	109.52	94.26	79.92	67.94	58.16		1866.28	1750.49	1632.06	1513.80	1395.79	1278.14	487.44	172.11	139.24	123.33	109.65	97.92	827.88	726.19
abutment rotation (radians)	0.004	0.003	0.002	0.002	0.001		0.231	0.172	0.132	0.104	0.083	0.066	0.022	0.007	0.005	0.004	0.003	0.002	0.206	0.145
mid-span sag (m)	**0.32**	**0.24**	**0.17**	**0.13**	**0.09**		**2.03**	**2.03**	**2.03**	**2.03**	**2.03**	**2.03**	**1.86**	**0.58**	**0.41**	**0.32**	**0.25**	**0.19**	**2.03**	**2.03**
mid-span sag (m)	**0.23**	**0.17**	**0.12**	**0.09**	**0.06**		**2.03**	**2.03**	**2.03**	**2.03**	**2.03**	**2.03**	**1.57**	**0.46**	**0.31**	**0.24**	**0.18**	**0.15**	**2.03**	**2.03**
Factor of Safety	2.01	2.40	2.17	1.98	1.84		0.10	0.22	0.40	0.53	0.68	0.87	1.12	1.45	1.89	2.45	2.25	2.08	0.04	0.10
Subsidence/Mining Height	**0.09**	**0.07**	**0.05**	**0.04**	**0.03**		**0.58**	**0.58**	**0.58**	**0.58**	**0.58**	**0.58**	**0.53**	**0.16**	**0.12**	**0.09**	**0.07**	**0.06**	**0.58**	**0.58**

Name:										
Overburden Depth	120	140	160	180	200	220	240	260	280	300
Panel Width	178.6	178.6	178.6	178.6	178.6	178.6	178.6	178.6	178.6	178.6
W/D	1.49	1.28	1.12	0.99	0.89	0.81	0.74	0.69	0.64	0.60
Base of Beam Depth(m)	30	35	40	45	50	55	60	65	70	75
Base of Beam Height Above Seam (m)	90	105	120	135	150	165	180	195	210	225
Beam Location Ratio	0.75	0.75	0.75	0.75	0.75	0.75	0.75	0.75	0.75	0.75
Maximum Caving Height (m)	120.00	140.00	160.00	180.00	200.00	220.00	232.63	232.63	232.63	232.63
Effective Beam Loading Height (m)	30.00	35.00	40.00	45.00	50.00	55.00	52.63	37.63	22.63	7.63
Beam Thickness (m)	12	14	16	18	20	22	24	26	28	30
Caving Angle (degrees)	69	69	69	69	69	69	69	69	69	69
Effective Span Angle (degrees)	75	75	75	75	75	75	75	75	75	75
Effective Span (m)	130	122	114	106	98	90	89	89	89	89
Effective Span Top Load Length (m)	107	95	84	72	60	48	49	60	72	83
Working Height (m)	3.5	3.5	3.5	3.5	3.5	3.5	3.5	3.5	3.5	3.5
Structural Action (1-way = 1, 2-way = 2)	1	1	1	1	1	1	1	1	1	1
Density (tonnes/m3)	2.5	2.5	2.5	2.5	2.5	2.5	2.5	2.5	2.5	2.5
Unconfined Compressive Strength (MPa)	50	50	50	50	50	50	50	50	50	50
Ultimate Tensile Strength (MPa)	0	0	0	0	0	0	0	0	0	0
Youngs Modulus (GPa) (225 x UCS)	7.5	7.5	7.5	7.5	7.5	7.5	7.5	7.5	7.5	7.5
Vertical/Horizontal Stress Ratio	1	1	1	1	1	1	1	1	1	1
Rock Joint Cohesion (MPa)	0.5	0.5	0.5	0.5	0.5	0.5	0.5	0.5	0.5	0.5
Joint Angle of Friction (Degrees)	35	35	35	35	35	35	35	35	35	35
Joint Angle to Horizontal Plane (0 to 90)	90	90	90	90	90	90	90	90	90	90
Uniformly Distributed Beam Load (KN/m)	670.08	763.32	848.34	923.26	985.61	1032.02	997.78	772.88	500.59	180.91
virgin vertical stress (MPa)	0.59	0.69	0.78	0.88	0.98	1.08	1.00	0.60	0.21	-0.18
virgin horizontal stress (Mpa)	0.59	0.69	0.78	0.88	0.98	1.08	1.00	0.60	0.21	-0.18
Fixed End Moment (KNm)	1.42E+06	1.43E+06	1.39E+06	1.30E+06	1.19E+06	1.05E+06	9.95E+05	7.70E+05	4.99E+05	1.80E+05
Abutment Shear (KN)	4.37E+04	4.67E+04	4.85E+04	4.91E+04	4.84E+04	4.65E+04	4.46E+04	3.45E+04	2.24E+04	8.08E+03
Re-distributed insitu stress(MPa)	0.00	0.00	0.00	0.00	0.00	0.00	0.00	0.00	0.00	0.00
Maximum Tensile Stress (MPa)	-19.33	-14.06	-10.23	-7.38	-5.21	-3.53	-2.57	-1.32	-0.24	0.70
Cracking Factor of Safety (UTS/sigt)	0.00	0.00	0.00	0.00	0.00	0.00	0.00	0.00	0.00	1.00
	cracked	**cracked**	**cracked**	**cracked**	**cracked**	**cracked**	**cracked**	**cracked**	**cracked**	**un-cracked**
Maximum Compressive Stress (MPa)	59.90	44.40	33.25	25.01	18.81	14.08	11.36	7.44	4.03	1.02
Crushing Factor of Safety (UCS/n(x)bottom)	0.83	1.13	1.50	2.00	2.66	3.55	4.40	6.72	12.41	48.94
	failed	**stable**	**stable**	**stable**	**stable**	**stable**	**stable**	**stable**	**stable**	**stable**
Shear Stress (MPa)	5.46	5.00	4.54	4.09	3.63	3.17	2.78	1.99	1.20	0.40
Shear Strength (MPa)	28.91	21.74	16.62	12.84	10.02	7.89	6.65	4.78	3.15	1.71
Shear Factor of Safety (s/v)	5.29	4.35	3.66	3.14	2.76	2.49	2.39	2.40	2.63	4.23
	stable	**stable**	**stable**	**stable**	**stable**	**stable**	**stable**	**stable**	**stable**	**stable**
Euler Elastic Buckling Stress (MPa)	209.05	323.17	483.56	708.10	1023.16	1468.57	1782.21	2091.62	2425.79	2784.71
Average Horizontal Stress (MPa)	20.29	15.17	11.51	8.81	6.80	5.28	4.39	3.06	1.89	0.86
Slenderness Ratio (L/r)	37.63	30.27	24.74	20.45	17.01	14.20	12.89	11.90	11.05	10.31
Buckling Factor of Safety (B/sig.av)	10.30	21.30	42.02	80.33	150.47	278.24	405.76	683.79	1281.31	3231.44
	stable	**stable**	**stable**	**stable**	**stable**	**stable**	**stable**	**stable**	**stable**	**stable**

Name:										
Name:										
Overburden Depth	120.00	140.00	160.00	180.00	200.00	220.00	240.00	260.00	280.00	300.00
Effective Caving Height (m)	30.00	35.00	40.00	45.00	50.00	55.00	52.63	37.63	22.63	7.63
Beam Thickness (m)	12.00	14.00	16.00	18.00	20.00	22.00	24.00	26.00	28.00	30.00
Caving Angle (degrees)	69.00	69.00	69.00	69.00	69.00	69.00	69.00	69.00	69.00	69.00
Span (m)	130.37	122.33	114.29	106.25	98.22	90.18	89.30	89.30	89.30	89.30
Panel Width/Overburden Depth Ratio	1.49	1.28	1.12	0.99	0.89	0.81	0.74	0.69	0.64	0.60
Working Height (m)	3.50	3.50	3.50	3.50	3.50	3.50	3.50	3.50	3.50	3.50
Structural Action (1-way = 1, 2-way = 2)	1.00	1.00	1.00	1.00	1.00	1.00	1.00	1.00	1.00	1.00
Density (tonnes/m3)	2.5	2.5	2.5	2.5	2.5	2.5	2.5	2.5	2.5	2.5
Unconfined Compressive Strength (MPa)	50	50	50	50	50	50	50	50	50	50
Youngs Modulus (GPa)	7.5	7.5	7.5	7.5	7.5	7.5	7.5	7.5	7.5	7.5
Vertical/Horizontal Stress Ratio	1	1	1	1	1	1	1	1	1	1
Internal Angle of Friction (Degrees)	35	35	35	35	35	35	35	35	35	35
Joint Angle to Horizontal Plane (0 to 90)	90	90	90	90	90	90	90	90	90	90
Uniformly Distributed Beam Load (KN/m)	670.08	763.32	848.34	923.26	985.61	1032.02	997.78	772.88	500.59	180.91
virgin vertical stress (MPa)	0.59	0.69	0.78	0.88	0.98	1.08	1.00	0.60	0.21	-0.18
virgin horizontal stress (Mpa)	0.59	0.69	0.78	0.88	0.98	1.08	1.00	0.60	0.21	-0.18
Simply Supported Moment (KNm)	1.42E+06	1.43E+06	1.39E+06	1.30E+06	1.19E+06	1.05E+06	9.95E+05	7.70E+05	4.99E+05	1.80E+05
Abutment Shear (KN)	4.37E+04	4.67E+04	4.85E+04	4.91E+04	4.84E+04	4.65E+04	4.46E+04	3.45E+04	2.24E+04	8.08E+03
Re-distributed insitu stress at Seam Level Only(MPa)	0.00	0.00	0.00	0.00	0.00	0.00	0.00	0.00	0.00	0.00
Top Re-distributed Stress (MPa)	-58.88	-43.20	-31.88	-23.47	-17.09	-12.20	-9.48	-5.88	-2.79	-0.10
Bottom Initial Stress (MPa)	59.76	44.22	33.05	24.79	18.56	13.81	11.24	7.79	4.85	2.30
Voussoir Stress Block/Beam Thickness Ratio	0.50	0.51	0.51	0.51	0.52	0.53	0.54	0.57	0.63	0.96
Out of Balance Moment (KNm)	-1.40E+06	-1.39E+06	-1.33E+06	-1.23E+06	-1.09E+06	-9.22E+05	-8.32E+05	-5.70E+05	-2.66E+05	-1.24E+03
Balanced Moment (KNm)	2.82E+06	2.82E+06	2.72E+06	2.53E+06	2.28E+06	1.97E+06	1.83E+06	1.34E+06	7.65E+05	1.82E+05
Balanced Thrust (KN)	3.54E+05	3.04E+05	2.57E+05	2.14E+05	1.75E+05	1.39E+05	1.19E+05	8.31E+04	4.74E+04	1.68E+04
Horizontal Stress (MPa) - Assumes yield zone stress re	117.29	85.88	63.19	46.32	33.54	23.75	18.32	11.22	5.33	1.17
Confining Stress for Strength Calculation (MPa)	0.75	0.88	1.00	1.13	1.25	1.38	1.50	1.63	1.75	1.88
Triaxial Strength (MPa)- Hoek Brown Criterion	52.77	53.23	53.69	54.15	54.61	55.07	55.54	56.00	56.46	56.92
Crushing Factor of Safety(UCS/sig.bot)	0.45	0.62	0.85	1.17	1.63	2.32	3.03	4.99	10.59	48.77
	collapsed	**collapsed**	**collapsed**	**yielding**	**stable**	**stable**	**stable**	**stable**	**stable**	**stable**
Horizontal Abutment Thrust (KN)	3.54E+05	3.04E+05	2.57E+05	2.14E+05	1.75E+05	1.39E+05	1.19E+05	8.31E+04	4.74E+04	1.68E+04
Principle Plane Angle to Horizontal(Degrees)	7.02	8.73	10.67	12.90	15.49	18.54	20.49	22.54	25.25	25.70
Principle Stress (MPa)	119.07	87.90	65.43	48.75	36.12	26.42	20.87	13.16	6.52	1.44
Max Shear Stress (MPa)	59.54	43.95	32.72	24.38	18.06	13.21	10.44	6.58	3.26	0.72
Max Shear Stress Plane Angle to Horizontal(Degrees)	52.02	53.73	55.67	57.90	60.49	63.54	65.49	67.54	70.25	70.70
Joint Shear Stress (MPa)	14.45	13.18	11.90	10.61	9.30	7.97	6.84	4.66	2.52	0.56
Joint Normal Stress (MPa)	176.83	129.83	95.91	70.70	51.60	36.95	28.75	17.80	8.59	1.89
Joint Shear Strength (MPa)	124.32	91.41	67.65	50.01	36.63	26.38	20.63	12.96	6.52	1.82
Joint Shear Factor of Safety (s/v)	8.60	6.93	5.68	4.71	3.94	3.31	3.02	2.78	2.59	3.24
	stable	**stable**	**stable**	**stable**	**stable**	**stable**	**stable**	**stable**	**stable**	**stable**
Buckling Strength (MPa)	13.26	20.68	31.33	46.72	69.33	103.55	131.16	169.81	244.32	639.64
Average Horizontal Normal Stress (MPa)	58.65	42.94	31.59	23.16	16.77	11.87	9.16	5.61	2.67	0.58
Buckling Factor of Safety (B/sig.av)	0.23	0.48	0.99	2.02	4.13	8.72	14.32	30.26	91.64	1096.08
	buckling	**buckling**	**buckling**	**stable**	**stable**	**stable**	**stable**	**stable**	**stable**	**stable**
Effective Modulus	1.13	1.13	1.13	3.28	7.50	7.50	7.50	7.50	7.50	7.50
maximum horizontal displacement at abutment (mm)	630.21	540.64	457.48	130.62	46.57	36.99	31.80	22.17	12.64	4.48
abutment rotation (radians)	0.104	0.076	0.056	0.014	0.004	0.003	0.002	0.001	0.001	0.000
mid-span sag (m)	**2.03**	**2.03**	**2.03**	**0.75**	**0.22**	**0.14**	**0.11**	**0.07**	**0.03**	**0.01**
mid-span sag (m)	**2.03**	**2.03**	**2.03**	**0.80**	**0.20**	**0.11**	**0.08**	**0.05**	**0.03**	**0.01**
Factor of Safety	0.23	0.48	0.85	1.17	1.63	2.32	3.02	2.78	2.59	3.24
Subsidence/Mining Height	**0.58**	**0.58**	**0.58**	**0.21**	**0.06**	**0.04**	**0.03**	**0.02**	**0.01**	**0.00**

VOUSSOIR BEAM MODEL INPUT for W = 178.6 m, H = 80 - 300 m

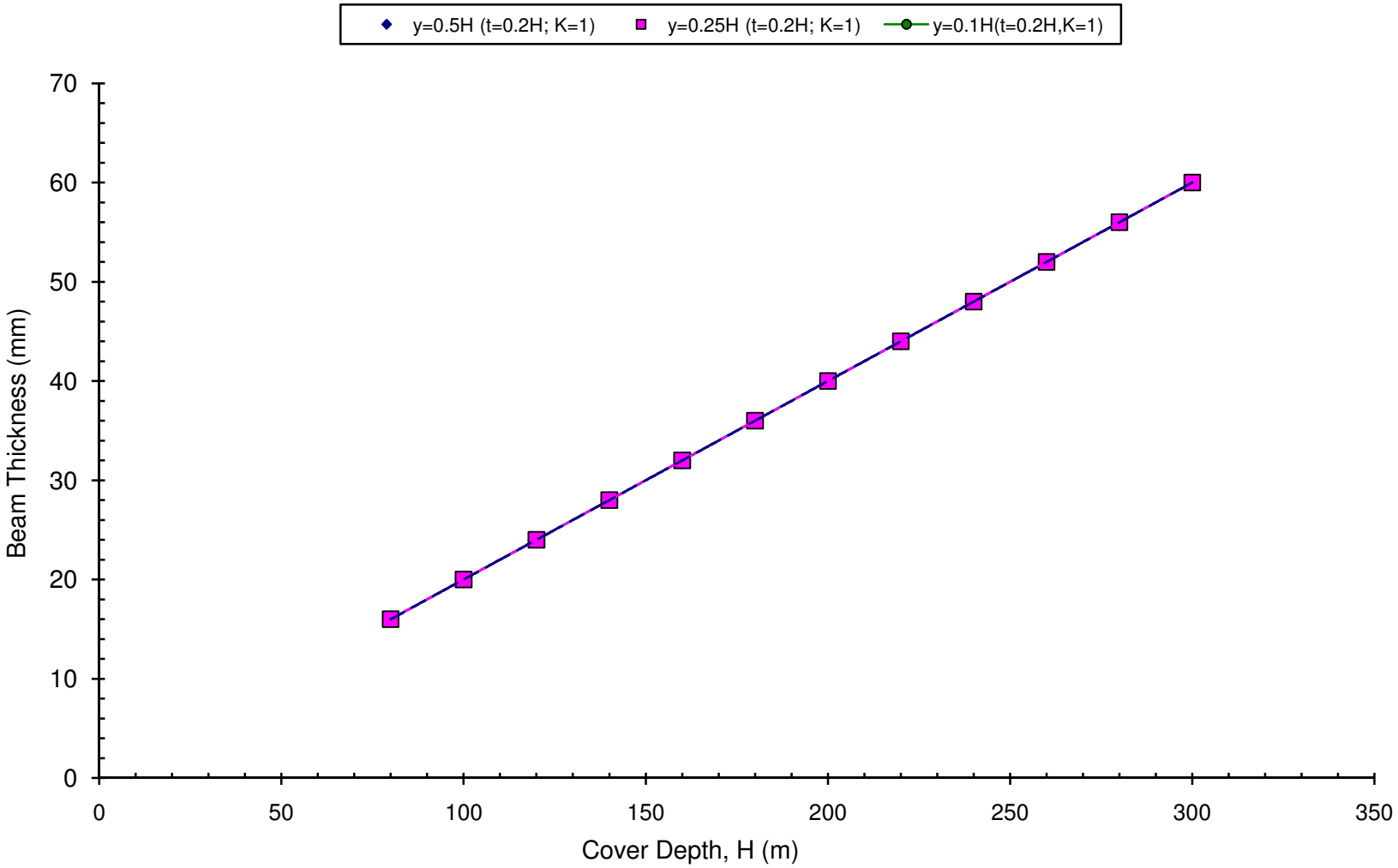

VOUSSOIR BEAM MODEL OUTCOMES FOR W = 178.6 m, H = 80 - 300 m,

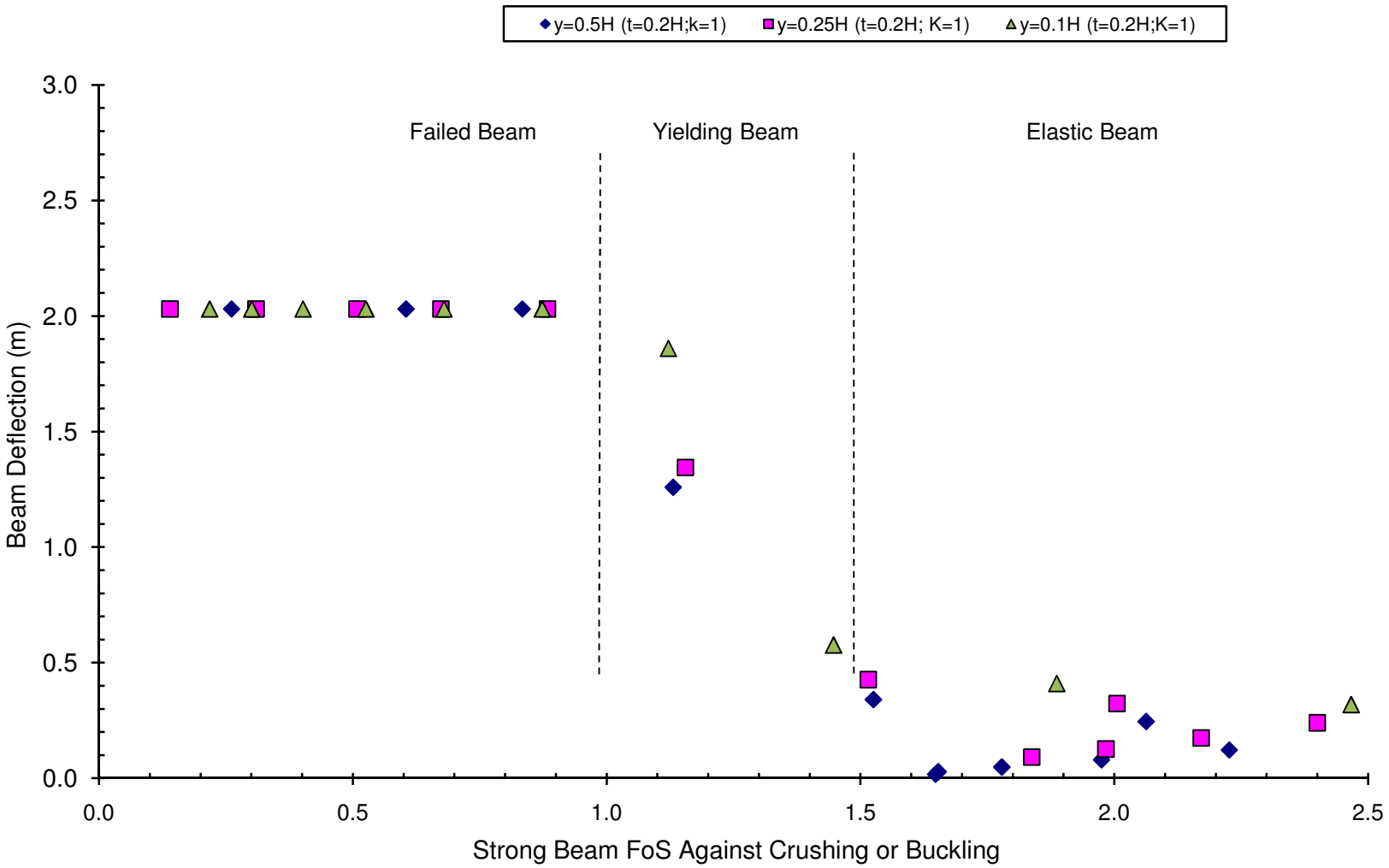

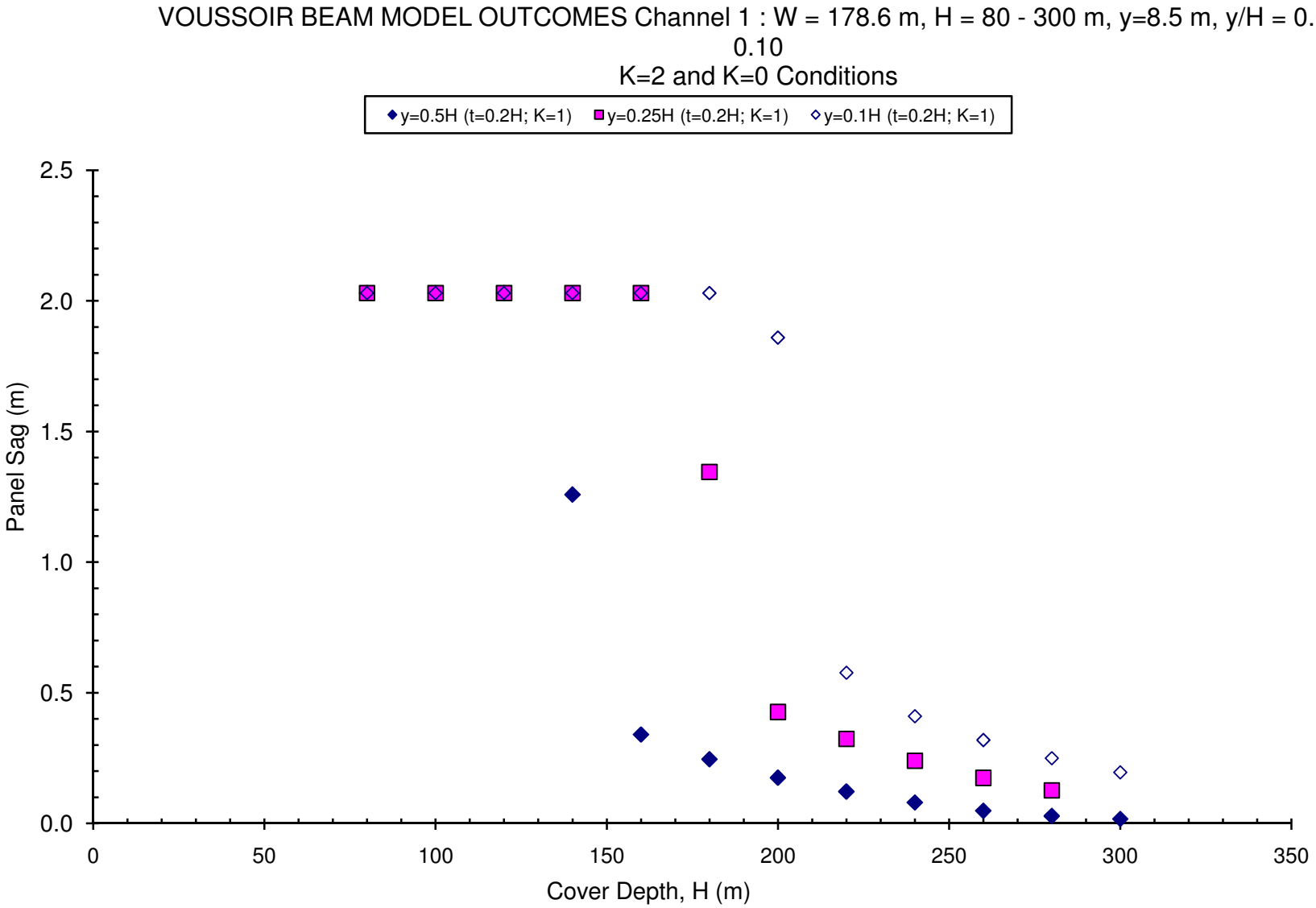
VOUSSOIR BEAM MODEL OUTCOMES Channel 1 : W = 178.6 m, H = 80 - 300 m, y=8.5 m, y/H = 0.02 - 0.10
K=2 and K=0 Conditions
y=0.5H (t=0.2H; K=1)
y=0.25H (t=0.2H; K=1)
y=0.1H (t=0.2H; K=1)
Panel Sag (m)
2.5
2.0
1.5
1.0
0.5
0.0
0
50
100
150
200
250
300
350
Cover Depth, H (m)

VOUSSOIR BEAM MODEL OUTCOMES for W = 178.6 m, H = 80 - 300 m

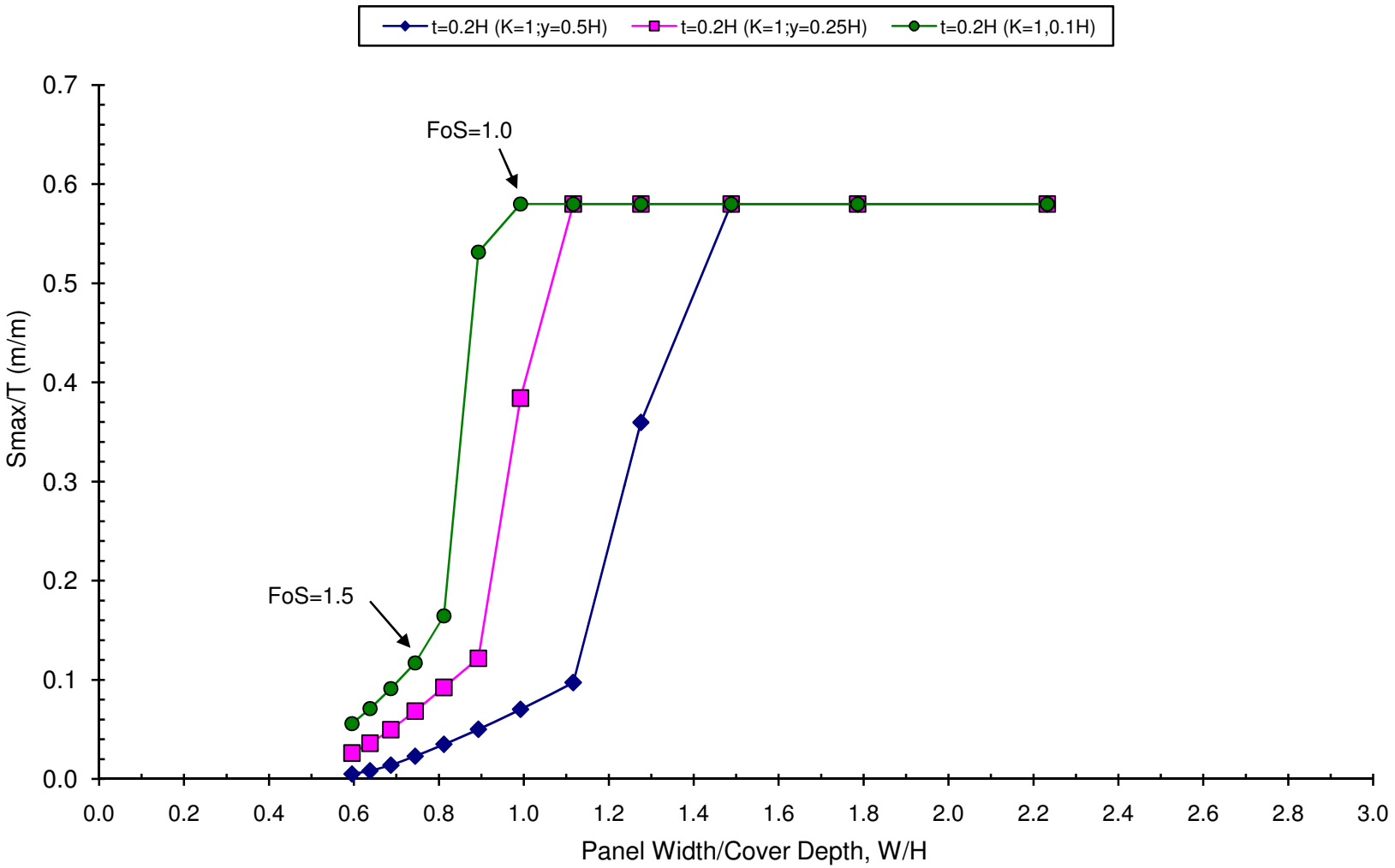

APPENDIX C - Analytical Model of Chain Pillar Subsidence Calculations and Extracts from LaModel® User Manual

UNSW Pillar Design Spreadsheet

West Wallsnd Colliery	LW Panel Pillars																			
INPUT DATA																				
Depth of Cover (m)	100	105	110	120	125	125	130	140	140	145	150	150	150	155	155	160	160	175	180	
Mining Height (m)	3.5	3.5	3.5	3.5	3.5	3.5	3.5	3.5	3.5	3.5	3.5	3.5	3.5	3.5	3.5	3.5	3.5	3.5	3.5	
Pillar Length - centres (m)	**105.5**	**105.5**	**105.5**	**105.5**	**105.5**	**105.5**	**105.5**	**105.5**	**105.5**	**105.5**	**105.5**	**105.5**	**105.5**	**105.5**	**105.5**	**105.5**	**105.5**	**105.5**	**105.5**	
Pillar Width - centres (m)	**35.5**	**35.5**	**35.5**	**35.5**	**35.5**	**35.5**	**35.5**	**35.5**	**35.5**	**35.5**	**35.5**	**35.5**	**35.5**	**35.5**	**35.5**	**35.5**	**35.5**	**35.5**	**35.5**	
Roadway Width for maximum pillar dimension	5.5	5.5	5.5	5.5	5.5	5.5	5.5	5.5	5.5	5.5	5.5	5.5	5.5	5.5	5.5	5.5	5.5	5.5	5.5	
Roadway Width for minimum pillar dimension	5.5	5.5	5.5	5.5	5.5	5.5	5.5	5.5	5.5	5.5	5.5	5.5	5.5	5.5	5.5	5.5	5.5	5.5	5.5	
Cut-Through Angle (degrees)	90	90	90	90	90	90	90	90	90	90	90	90	90	90	90	90	90	90	90	
Average Panel Span (m) {rib-rib width}	**178.6**	**178.6**	**178.6**	**178.6**	**178.6**	**178.6**	**178.6**	**178.6**	**178.6**	**178.6**	**178.6**	**178.6**	**178.6**	**178.6**	**178.6**	**178.6**	**178.6**	**178.6**	**178.6**	
SG (tonnes/m^3)	2.5	2.5	2.5	2.5	2.5	2.5	2.5	2.5	2.5	2.5	2.5	2.5	2.5	2.5	2.5	2.5	2.5	2.5	2.5	
Conversion (tonnes to N)	10000	10000	10000	10000	10000	10000	10000	10000	10000	10000	10000	10000	10000	10000	10000	10000	10000	10000	10000	
Abutment Angle (^{o})	21	21	21	21	21	21	21	21	21	21	21	21	21	21	21	21	21	21	21	
CALCULATIONS																				
Maximum Rib to Rib Pillar Length (w_2)	**100.0**	**100.0**	**100.0**	**100.0**	**100.0**	**100.0**	**100.0**	**100.0**	**100.0**	**100.0**	**100.0**	**100.0**	**100.0**	**100.0**	**100.0**	**100.0**	**100.0**	**100.0**	**100.0**	
Minimum Rib to Rib Pillar Width (w_1)	**30.0**	**30.0**	**30.0**	**30.0**	**30.0**	**30.0**	**30.0**	**30.0**	**30.0**	**30.0**	**30.0**	**30.0**	**30.0**	**30.0**	**30.0**	**30.0**	**30.0**	**30.0**	**30.0**	
w, Minimum Rib to Rib Pillar Width (ie $w_1 \sin\theta$)	**30.0**	**30.0**	**30.0**	**30.0**	**30.0**	**30.0**	**30.0**	**30.0**	**30.0**	**30.0**	**30.0**	**30.0**	**30.0**	**30.0**	**30.0**	**30.0**	**30.0**	**30.0**	**30.0**	
Minimum Pillar Width/Height Ratio	**8.6**	**8.6**	**8.6**	**8.6**	**8.6**	**8.6**	**8.6**	**8.6**	**8.6**	**8.6**	**8.6**	**8.6**	**8.6**	**8.6**	**8.6**	**8.6**	**8.6**	**8.6**	**8.6**	
Extraction Ratio (%)	**19.9%**	**19.9%**	**19.9%**	**19.9%**	**19.9%**	**19.9%**	**19.9%**	**19.9%**	**19.9%**	**19.9%**	**19.9%**	**19.9%**	**19.9%**	**19.9%**	**19.9%**	**19.9%**	**19.9%**	**19.9%**	**19.9%**	
Abutment Angle (Radians)	0.367	0.367	0.367	0.367	0.367	0.367	0.367	0.367	0.367	0.367	0.367	0.367	0.367	0.367	0.367	0.367	0.367	0.367	0.367	
Cut-Through Angle (Radians)	1.571	1.571	1.571	1.571	1.571	1.571	1.571	1.571	1.571	1.571	1.571	1.571	1.571	1.571	1.571	1.571	1.571	1.571	1.571	
Is the Panel Super-Critical?	Yes	Yes	Yes	Yes	Yes	Yes	Yes	Yes	Yes	Yes	Yes	Yes	Yes	Yes	Yes	Yes	Yes	Yes	Yes	
D (Peng & Chiang Loading Factor)	51.300	52.567	53.804	56.196	57.355	57.355	58.491	60.699	60.699	61.773	62.829	62.829	62.829	63.868	63.868	64.890	64.890	67.864	68.826	
R (Pillar 2nd Abutment Component)	0.97	0.97	0.96	0.95	0.94	0.94	0.94	0.93	0.93	0.92	0.92	0.92	0.92	0.91	0.91	0.91	0.91	0.89	0.89	
Dimensionless Pillar 'Rectangularity'	1.54	1.54	1.54	1.54	1.54	1.54	1.54	1.54	1.54	1.54	1.54	1.54	1.54	1.54	1.54	1.54	1.54	1.54	1.54	
Width/Height Ratio Exponent	1.00	1.00	1.00	1.00	1.00	1.00	1.00	1.00	1.00	1.00	1.00	1.00	1.00	1.00	1.00	1.00	1.00	1.00	1.00	
Effective Width Factor (Omega)	1.54	1.54	1.54	1.54	1.54	1.54	1.54	1.54	1.54	1.54	1.54	1.54	1.54	1.54	1.54	1.54	1.54	1.54	1.54	
Effective Width Interim	46.15	46.15	46.15	46.15	46.15	46.15	46.15	46.15	46.15	46.15	46.15	46.15	46.15	46.15	46.15	46.15	46.15	46.15	46.15	
Effective Pillar Width (m)	46.15	46.15	46.15	46.15	46.15	46.15	46.15	46.15	46.15	46.15	46.15	46.15	46.15	46.15	46.15	46.15	46.15	46.15	46.15	
Effective Pillar Loading Height (m)	100.00	105.00	110.00	120.00	125.00	125.00	130.00	140.00	140.00	145.00	150.00	150.00	150.00	155.00	155.00	160.00	160.00	175.00	180.00	
RESULTS																				
Tributary Area Loading (MPa)	**3.12**	**3.28**	**3.43**	**3.75**	**3.90**	**3.90**	**4.06**	**4.37**	**4.37**	**4.53**	**4.68**	**4.68**	**4.68**	**4.84**	**4.84**	**4.99**	**4.99**	**5.46**	**5.62**	
Pillar Strength (UNSW Squat Pillar 1999)	**25.91**	**25.91**	**25.91**	**25.91**	**25.91**	**25.91**	**25.91**	**25.91**	**25.91**	**25.91**	**25.91**	**25.91**	**25.91**	**25.91**	**25.91**	**25.91**	**25.91**	**25.91**	**25.91**	
Pillar Strength (UNSW w/h<5)	**N/A**	**N/A**	**N/A**	**N/A**	**N/A**	**N/A**	**N/A**	**N/A**	**N/A**	**N/A**	**N/A**	**N/A**	**N/A**	**N/A**	**N/A**	**N/A**	**N/A**	**N/A**	**N/A**	
Safety Factor under FTA Loading (Squat Pillar)	**8.30**	**7.91**	**7.55**	**6.92**	**6.64**	**6.64**	**6.39**	**5.93**	**5.93**	**5.73**	**5.53**	**5.53**	**5.53**	**5.36**	**5.36**	**5.19**	**5.19**	**4.74**	**4.61**	
Safety Factor under FTA Loading (w/h<5)	**N/A**	**N/A**	**N/A**	**N/A**	**N/A**	**N/A**	**N/A**	**N/A**	**N/A**	**N/A**	**N/A**	**N/A**	**N/A**	**N/A**	**N/A**	**N/A**	**N/A**	**N/A**	**N/A**	
No. SAs, n	2	2	2	2	2	2	2	2	2	2	2	2	2	2	2	2	2	2	2	
Single Abutment Loading (3D) - full	1.69	1.86	2.04	2.43	2.64	2.64	2.85	3.31	3.31	3.55	3.80	3.80	3.80	4.05	4.05	4.32	4.32	5.17	5.47	
Single Abutment Loading (3D) - pillar	**1.64**	**1.80**	**1.96**	**2.31**	**2.49**	**2.49**	**2.68**	**3.07**	**3.07**	**3.27**	**3.48**	**3.48**	**3.48**	**3.70**	**3.70**	**3.92**	**3.92**	**4.61**	**4.85**	
Single Abutment Loading (3D) - solid	0.05	0.06	0.08	0.12	0.15	0.15	0.17	0.24	0.24	0.27	0.31	0.31	0.31	0.36	0.36	0.40	0.40	0.56	0.62	
Cell Sensitivity (MPa)	0	0	0	0	0	0	0	0	0	0	0	0	0	0	0	0	0	0	0	
Total Pillar Loading with Single Abutment Loading	4.76	5.07	5.39	6.05	6.39	6.39	6.74	7.44	7.44	7.80	8.17	8.17	8.17	8.54	8.54	8.91	8.91	10.07	10.46	
Safety Factor (under Single Abutment Loading)	**5.44**	**5.11**	**4.80**	**4.28**	**4.05**	**4.05**	**3.85**	**3.48**	**3.48**	**3.32**	**3.17**	**3.17**	**3.17**	**3.04**	**3.04**	**2.91**	**2.91**	**2.57**	**2.48**	
Total Pillar Loading @ nA	6.50	7.00	7.52	8.60	9.17	9.17	9.76	10.98	10.98	11.62	12.27	12.27	12.27	12.95	12.95	13.63	13.63	15.80	16.55	
Safety Factor @ nA	**3.99**	**3.70**	**3.45**	**3.01**	**2.82**	**2.82**	**2.65**	**2.36**	**2.36**	**2.23**	**2.11**	**2.11**	**2.11**	**2.00**	**2.00**	**1.90**	**1.90**	**1.64**	**1.57**	
Total Pillar Loading under Double Abutment Loading	6.50	7.00	7.52	8.60	9.17	9.17	9.76	10.98	10.98	11.62	12.27	12.27	12.27	12.95	12.95	13.63	13.63	15.80	16.55	
Safety Factor (under Double Abutment Loading)	**3.99**	**3.70**	**3.45**	**3.01**	**2.82**	**2.82**	**2.65**	**2.36**	**2.36**	**2.23**	**2.11**	**2.11**	**2.11**	**2.00**	**2.00**	**1.90**	**1.90**	**1.64**	**1.57**	
Elastic Model Subsidence																				
Ecoal(GPa)	**2.00**	**2.00**	**2.00**	**2.00**	**2.00**	**2.00**	**2.00**	**2.00**	**2.00**	**2.00**	**2.00**	**2.00**	**2.00**	**2.00**	**2.00**	**2.00**	**2.00**	**2.00**	**2.00**	
Efloor(GPa)	**7.50**	**7.50**	**7.50**	**7.50**	**7.50**	**7.50**	**7.50**	**7.50**	**7.50**	**7.50**	**7.50**	**7.50**	**7.50**	**7.50**	**7.50**	**7.50**	**7.50**	**7.50**	**7.50**	
Eroof(GPa)	**3.00**	**3.00**	**3.00**	**3.00**	**3.00**	**3.00**	**3.00**	**3.00**	**3.00**	**3.00**	**3.00**	**3.00**	**3.00**	**3.00**	**3.00**	**3.00**	**3.00**	**3.00**	**3.00**	
Poissons Ratio floor/roof	**0.25**	**0.25**	**0.25**	**0.25**	**0.25**	**0.25**	**0.25**	**0.25**	**0.25**	**0.25**	**0.25**	**0.25**	**0.25**	**0.25**	**0.25**	**0.25**	**0.25**	**0.25**	**0.25**	
initial vertical stress (MPa)	**2.50**	**2.63**	**2.75**	**3.00**	**3.13**	**3.13**	**3.25**	**3.50**	**3.50**	**3.63**	**3.75**	**3.75**	**3.75**	**3.88**	**3.88**	**4.00**	**4.00**	**4.38**	**4.50**	
increase in vertical stress (MPa)	**4.00**	**4.37**	**4.77**	**5.60**	**6.05**	**6.05**	**6.51**	**7.48**	**7.48**	**8.00**	**8.52**	**8.52**	**8.52**	**9.07**	**9.07**	**9.63**	**9.63**	**11.42**	**12.05**	
Pillar Compression (m)	**0.007**	**0.007**	**0.008**	**0.009**	**0.010**	**0.010**	**0.011**	**0.012**	**0.012**	**0.013**	**0.014**	**0.014**	**0.014**	**0.015**	**0.015**	**0.016**	**0.016**	**0.019**	**0.020**	
Roof Compression (m)	**0.037**	**0.041**	**0.045**	**0.053**	**0.057**	**0.057**	**0.061**	**0.070**	**0.070**	**0.075**	**0.080**	**0.080**	**0.080**	**0.085**	**0.085**	**0.090**	**0.090**	**0.107**	**0.113**	
Floor Compression (m)	**0.015**	**0.016**	**0.018**	**0.021**	**0.023**	**0.023**	**0.024**	**0.028**	**0.028**	**0.030**	**0.032**	**0.032**	**0.032**	**0.034**	**0.034**	**0.036**	**0.036**	**0.043**	**0.045**	
Total Compression (m)	**0.059**	**0.065**	**0.070**	**0.083**	**0.089**	**0.089**	**0.096**	**0.111**	**0.111**	**0.118**	**0.126**	**0.126**	**0.126**	**0.134**	**0.134**	**0.142**	**0.142**	**0.169**	**0.178**	
2xCompression	**0.118**	**0.129**	**0.141**	**0.166**	**0.179**	**0.179**	**0.192**	**0.221**	**0.221**	**0.236**	**0.252**	**0.252**	**0.252**	**0.268**	**0.268**	**0.284**	**0.284**	**0.337**	**0.356**	
Floor Bearing Capacity																				
Weakest Floor Unit UCS (MPa)	30.0	30.0	30.0	30.0	30.0	30.0	30.0	30.0	30.0	30.0	30.0	30.0	30.0	30.0	30.0	30.0	30.0	30.0	30.0	
Weakest Unit Thickness (m)	0.3	0.3	0.3	0.3	0.3	0.3	0.3	0.3	0.3	0.3	0.3	0.3	0.3	0.3	0.3	0.3	0.3	0.3	0.3	
Floor Bearing Capacity (MPa)	602.1	602.1	602.1	602.1	602.1	602.1	602.1	602.1	602.1	602.1	602.1	602.1	602.1	602.1	602.1	602.1	602.1	602.1	602.1	
Pillar Stress (MPa)	3.1	3.3	5.4	6.1	6.4	6.4	6.7	7.4	7.4	7.8	8.2	8.2	8.2	8.5	8.5	8.9	8.9	10.1	10.5	
Floor Bearing Failure FoS	**192.9**	**183.7**	**111.6**	**99.5**	**94.2**	**94.2**	**89.4**	**80.9**	**80.9**	**77.2**	**73.7**	**73.7**	**73.7**	**70.5**	**70.5**	**67.6**	**67.6**	**59.8**	**57.5**	
Roof Bearing Capacity																				
Weakest Roof Unit UCS (MPa)	15.0	15.0	15.0	15.0	15.0	15.0	15.0	15.0	15.0	15.0	15.0	15.0	15.0	15.0	15.0	15.0	15.0	15.0	15.0	
Weakest Unit Thickness (m)	8.0	8.0	8.0	8.0	8.0	8.0	8.0	8.0	8.0	8.0	8.0	8.0	8.0	8.0	8.0	8.0	8.0	8.0	8.0	
Roof Bearing Capacity (MPa)	48.4	48.4	48.4	48.4	48.4	48.4	48.4	48.4	48.4	48.4	48.4	48.4	48.4	48.4	48.4	48.4	48.4	48.4	48.4	
Pillar Stress (MPa)	3.1	3.3	5.4	6.1	6.4	6.4	6.7	7.4	7.4	7.8	8.2	8.2	8.2	8.5	8.5	8.9	8.9	10.1	10.5	
Roof Bearing Failure FoS	**15.5**	**14.8**	**9.0**	**8.0**	**7.6**	**7.6**	**7.2**	**6.5**	**6.5**	**6.2**	**5.9**	**5.9**	**5.9**	**5.7**	**5.7**	**5.4**	**5.4**	**4.8**	**4.6**	

UNSW Pillar Design Spreadsheet

West Wallsnd Colliery	LW Panel Pillars																						
INPUT DATA																							
Depth of Cover (m)	55	70	70	85	90	100	100	100	110	120	120	130	130	130	135	140	140	140	140	140	145	145
Mining Height (m)	3.5	3.5	3.5	3.5	3.5	3.5	3.5	3.5	3.5	3.5	3.5	3.5	3.5	3.5	3.5	3.5	3.5	3.5	3.5	3.5	3.5	3.5
Pillar Length - centres (m)	**105.5**	**105.5**	**105.5**	**105.5**	**105.5**	**105.5**	**105.5**	**105.5**	**105.5**	**105.5**	**105.5**	**105.5**	**105.5**	**105.5**	**105.5**	**105.5**	**105.5**	**105.5**	**105.5**	**105.5**	**105.5**	**105.5**
Pillar Width - centres (m)	**40.5**	**40.5**	**40.5**	**40.5**	**40.5**	**40.5**	**40.5**	**40.5**	**40.5**	**40.5**	**40.5**	**40.5**	**40.5**	**40.5**	**40.5**	**40.5**	**40.5**	**40.5**	**40.5**	**40.5**	**40.5**	**40.5**
Roadway Width for maximum pillar dimension	5.5	5.5	5.5	5.5	5.5	5.5	5.5	5.5	5.5	5.5	5.5	5.5	5.5	5.5	5.5	5.5	5.5	5.5	5.5	5.5	5.5	5.5
Roadway Width for minimum pillar dimension	5.5	5.5	5.5	5.5	5.5	5.5	5.5	5.5	5.5	5.5	5.5	5.5	5.5	5.5	5.5	5.5	5.5	5.5	5.5	5.5	5.5	5.5
Cut-Through Angle (degrees)	90	90	90	90	90	90	90	90	90	90	90	90	90	90	90	90	90	90	90	90	90	90
Average Panel Span (m) {rib-rib width}	**310**	**310**	**310**	**310**	**310**	**310**	**310**	**310**	**310**	**310**	**310**	**310**	**310**	**310**	**310**	**310**	**310**	**310**	**310**	**310**	**310**	**310**
SG (tonnes/m^3)	2.5	2.5	2.5	2.5	2.5	2.5	2.5	2.5	2.5	2.5	2.5	2.5	2.5	2.5	2.5	2.5	2.5	2.5	2.5	2.5	2.5	2.5
Conversion (tonnes to N)	10000	10000	10000	10000	10000	10000	10000	10000	10000	10000	10000	10000	10000	10000	10000	10000	10000	10000	10000	10000	10000	10000
Abutment Angle (°)	21	21	21	21	21	21	21	21	21	21	21	21	21	21	21	21	21	21	21	21	21	21
CALCULATIONS																							
Maximum Rib to Rib Pillar Length (w_2)	**100.0**	**100.0**	**100.0**	**100.0**	**100.0**	**100.0**	**100.0**	**100.0**	**100.0**	**100.0**	**100.0**	**100.0**	**100.0**	**100.0**	**100.0**	**100.0**	**100.0**	**100.0**	**100.0**	**100.0**	**100.0**	**100.0**
Minimum Rib to Rib Pillar Width (w_1)	**35.0**	**35.0**	**35.0**	**35.0**	**35.0**	**35.0**	**35.0**	**35.0**	**35.0**	**35.0**	**35.0**	**35.0**	**35.0**	**35.0**	**35.0**	**35.0**	**35.0**	**35.0**	**35.0**	**35.0**	**35.0**	**35.0**
w, Minimum Rib to Rib Pillar Width (ie $w_1 \sin\theta$)	**35.0**	**35.0**	**35.0**	**35.0**	**35.0**	**35.0**	**35.0**	**35.0**	**35.0**	**35.0**	**35.0**	**35.0**	**35.0**	**35.0**	**35.0**	**35.0**	**35.0**	**35.0**	**35.0**	**35.0**	**35.0**	**35.0**
Minimum Pillar Width/Height Ratio	**10.0**	**10.0**	**10.0**	**10.0**	**10.0**	**10.0**	**10.0**	**10.0**	**10.0**	**10.0**	**10.0**	**10.0**	**10.0**	**10.0**	**10.0**	**10.0**	**10.0**	**10.0**	**10.0**	**10.0**	**10.0**	**10.0**
Extraction Ratio (%)	**18.1%**	**18.1%**	**18.1%**	**18.1%**	**18.1%**	**18.1%**	**18.1%**	**18.1%**	**18.1%**	**18.1%**	**18.1%**	**18.1%**	**18.1%**	**18.1%**	**18.1%**	**18.1%**	**18.1%**	**18.1%**	**18.1%**	**18.1%**	**18.1%**	**18.1%**
Abutment Angle (Radians)	0.367	0.367	0.367	0.367	0.367	0.367	0.367	0.367	0.367	0.367	0.367	0.367	0.367	0.367	0.367	0.367	0.367	0.367	0.367	0.367	0.367	0.367
Cut-Through Angle (Radians)	1.571	1.571	1.571	1.571	1.571	1.571	1.571	1.571	1.571	1.571	1.571	1.571	1.571	1.571	1.571	1.571	1.571	1.571	1.571	1.571	1.571	1.571
Is the Panel Super-Critical?	Yes	Yes	Yes	Yes	Yes	Yes	Yes	Yes	Yes	Yes	Yes	Yes	Yes	Yes	Yes	Yes	Yes	Yes	Yes	Yes	Yes	Yes
D (Peng & Chiang Loading Factor)	38.045	42.921	42.921	47.296	48.667	51.300	51.300	51.300	53.804	56.196	56.196	58.491	58.491	58.491	59.605	60.699	60.699	60.699	60.699	60.699	61.773	61.773
R (Pillar 2nd Abutment Component)	1.00	1.00	1.00	1.00	1.00	0.99	0.99	0.99	0.98	0.98	0.98	0.97	0.97	0.97	0.97	0.96	0.96	0.96	0.96	0.96	0.96	0.96
Dimensionless Pillar 'Rectangularity'	1.48	1.48	1.48	1.48	1.48	1.48	1.48	1.48	1.48	1.48	1.48	1.48	1.48	1.48	1.48	1.48	1.48	1.48	1.48	1.48	1.48	1.48
Width/Height Ratio Exponent	1.00	1.00	1.00	1.00	1.00	1.00	1.00	1.00	1.00	1.00	1.00	1.00	1.00	1.00	1.00	1.00	1.00	1.00	1.00	1.00	1.00	1.00
Effective Width Factor (Omega)	1.48	1.48	1.48	1.48	1.48	1.48	1.48	1.48	1.48	1.48	1.48	1.48	1.48	1.48	1.48	1.48	1.48	1.48	1.48	1.48	1.48	1.48
Effective Width Interim	51.85	51.85	51.85	51.85	51.85	51.85	51.85	51.85	51.85	51.85	51.85	51.85	51.85	51.85	51.85	51.85	51.85	51.85	51.85	51.85	51.85	51.85
Effective Pillar Width (m)	51.85	51.85	51.85	51.85	51.85	51.85	51.85	51.85	51.85	51.85	51.85	51.85	51.85	51.85	51.85	51.85	51.85	51.85	51.85	51.85	51.85	51.85
Effective Pillar Loading Height (m)	55.00	70.00	70.00	85.00	90.00	100.00	100.00	100.00	110.00	120.00	120.00	130.00	130.00	130.00	135.00	140.00	140.00	140.00	140.00	140.00	145.00	145.00
RESULTS																							
Tributary Area Loading (MPa)	**1.68**	**2.14**	**2.14**	**2.59**	**2.75**	**3.05**	**3.05**	**3.05**	**3.36**	**3.66**	**3.66**	**3.97**	**3.97**	**3.97**	**4.12**	**4.27**	**4.27**	**4.27**	**4.27**	**4.27**	**4.43**	**4.43**
Pillar Strength (UNSW Squat Pillar 1999)	**31.63**	**31.63**	**31.63**	**31.63**	**31.63**	**31.63**	**31.63**	**31.63**	**31.63**	**31.63**	**31.63**	**31.63**	**31.63**	**31.63**	**31.63**	**31.63**	**31.63**	**31.63**	**31.63**	**31.63**	**31.63**	**31.63**
Pillar Strength (UNSW w/h<5)	**N/A**	**N/A**	**N/A**	**N/A**	**N/A**	**N/A**	**N/A**	**N/A**	**N/A**	**N/A**	**N/A**	**N/A**	**N/A**	**N/A**	**N/A**	**N/A**	**N/A**	**N/A**	**N/A**	**N/A**	**N/A**	**N/A**
Safety Factor under FTA Loading (Squat Pillar)	**18.84**	**14.80**	**14.80**	**12.19**	**11.51**	**10.36**	**10.36**	**10.36**	**9.42**	**8.64**	**8.64**	**7.97**	**7.97**	**7.97**	**7.68**	**7.40**	**7.40**	**7.40**	**7.40**	**7.40**	**7.15**	**7.15**
Safety Factor under FTA Loading (w/h<5)	**N/A**	**N/A**	**N/A**	**N/A**	**N/A**	**N/A**	**N/A**	**N/A**	**N/A**	**N/A**	**N/A**	**N/A**	**N/A**	**N/A**	**N/A**	**N/A**	**N/A**	**N/A**	**N/A**	**N/A**	**N/A**	**N/A**
No. SAs, n	2	2	2	2	2	2	2	2	2	2	2	2	2	2	2	2	2	2	2	2	2	2
Single Abutment Loading (3D) - full	0.44	0.71	0.71	1.04	1.17	1.45	1.45	1.45	1.75	2.08	2.08	2.44	2.44	2.44	2.64	2.83	2.83	2.83	2.83	2.83	3.04	3.04
Single Abutment Loading (3D) - pillar	**0.44**	**0.71**	**0.71**	**1.04**	**1.17**	**1.43**	**1.43**	**1.43**	**1.72**	**2.04**	**2.04**	**2.37**	**2.37**	**2.37**	**2.55**	**2.73**	**2.73**	**2.73**	**2.73**	**2.73**	**2.92**	**2.92**
Single Abutment Loading (3D) - solid	0.00	0.00	0.00	0.00	0.01	0.01	0.01	0.01	0.03	0.05	0.05	0.07	0.07	0.07	0.09	0.10	0.10	0.10	0.10	0.10	0.12	0.12
Cell Sensitivity (MPa)	0	0	0	0	0	0	0	0	0	0	0	0	0	0	0	0	0	0	0	0	0	0
Total Pillar Loading with Single Abutment Loading	2.12	2.84	2.84	3.64	3.91	4.48	4.48	4.48	5.08	5.70	5.70	6.34	6.34	6.34	6.67	7.00	7.00	7.00	7.00	7.00	7.34	7.34
Safety Factor (under Single Abutment Loading)	**14.94**	**11.12**	**11.12**	**8.70**	**8.08**	**7.05**	**7.05**	**7.05**	**6.22**	**5.55**	**5.55**	**4.99**	**4.99**	**4.99**	**4.74**	**4.52**	**4.52**	**4.52**	**4.52**	**4.52**	**4.31**	**4.31**
Total Pillar Loading @ nA	2.55	3.55	3.55	4.68	5.09	5.94	5.94	5.94	6.86	7.83	7.83	8.86	8.86	8.86	9.39	9.94	9.94	9.94	9.94	9.94	10.51	10.51
Safety Factor @ nA	**12.38**	**8.90**	**8.90**	**6.75**	**6.21**	**5.32**	**5.32**	**5.32**	**4.61**	**4.04**	**4.04**	**3.57**	**3.57**	**3.57**	**3.37**	**3.18**	**3.18**	**3.18**	**3.18**	**3.18**	**3.01**	**3.01**
Total Pillar Loading under Double Abutment Loading	2.55	3.55	3.55	4.68	5.09	5.94	5.94	5.94	6.86	7.83	7.83	8.86	8.86	8.86	9.39	9.94	9.94	9.94	9.94	9.94	10.51	10.51
Safety Factor (under Double Abutment Loading)	**12.38**	**8.90**	**8.90**	**6.75**	**6.21**	**5.32**	**5.32**	**5.32**	**4.61**	**4.04**	**4.04**	**3.57**	**3.57**	**3.57**	**3.37**	**3.18**	**3.18**	**3.18**	**3.18**	**3.18**	**3.01**	**3.01**
Elastic Model Subsidence																							
Ecoal(GPa)	**2.00**	**2.00**	**2.00**	**2.00**	**2.00**	**2.00**	**2.00**	**2.00**	**2.00**	**2.00**	**2.00**	**2.00**	**2.00**	**2.00**	**2.00**	**2.00**	**2.00**	**2.00**	**2.00**	**2.00**	**2.00**	**2.00**
Efloor(GPa)	**7.40**	**7.40**	**7.40**	**7.40**	**7.40**	**7.40**	**7.40**	**7.40**	**7.40**	**7.40**	**7.40**	**7.40**	**7.40**	**7.40**	**7.40**	**7.40**	**7.40**	**7.40**	**7.40**	**7.40**	**7.40**	**7.40**
Eroof(GPa)	**3.00**	**3.00**	**3.00**	**3.00**	**3.00**	**3.00**	**3.00**	**3.00**	**3.00**	**3.00**	**3.00**	**3.00**	**3.00**	**3.00**	**3.00**	**3.00**	**3.00**	**3.00**	**3.00**	**3.00**	**3.00**	**3.00**
Poissons Ratio floor/roof	**0.25**	**0.25**	**0.25**	**0.25**	**0.25**	**0.25**	**0.25**	**0.25**	**0.25**	**0.25**	**0.25**	**0.25**	**0.25**	**0.25**	**0.25**	**0.25**	**0.25**	**0.25**	**0.25**	**0.25**	**0.25**	**0.25**
initial vertical stress (MPa)	**1.38**	**1.75**	**1.75**	**2.13**	**2.25**	**2.50**	**2.50**	**2.50**	**2.75**	**3.00**	**3.00**	**3.25**	**3.25**	**3.25**	**3.38**	**3.50**	**3.50**	**3.50**	**3.50**	**3.50**	**3.63**	**3.63**
increase in vertical stress (MPa)	**1.18**	**1.80**	**1.80**	**2.56**	**2.84**	**3.44**	**3.44**	**3.44**	**4.11**	**4.83**	**4.83**	**5.61**	**5.61**	**5.61**	**6.02**	**6.44**	**6.44**	**6.44**	**6.44**	**6.44**	**6.88**	**6.88**
Pillar Compression (m)	**0.002**	**0.003**	**0.003**	**0.004**	**0.005**	**0.006**	**0.006**	**0.006**	**0.007**	**0.008**	**0.008**	**0.009**	**0.009**	**0.009**	**0.010**	**0.011**	**0.011**	**0.011**	**0.011**	**0.011**	**0.011**	**0.011**
Roof Compression (m)	**0.013**	**0.020**	**0.020**	**0.028**	**0.031**	**0.038**	**0.038**	**0.038**	**0.045**	**0.053**	**0.053**	**0.061**	**0.061**	**0.061**	**0.066**	**0.070**	**0.070**	**0.070**	**0.070**	**0.070**	**0.075**	**0.075**
Floor Compression (m)	**0.005**	**0.008**	**0.008**	**0.011**	**0.013**	**0.015**	**0.015**	**0.015**	**0.018**	**0.021**	**0.021**	**0.025**	**0.025**	**0.025**	**0.027**	**0.029**	**0.029**	**0.029**	**0.029**	**0.029**	**0.031**	**0.031**
Total Compression (m)	**0.020**	**0.031**	**0.031**	**0.044**	**0.048**	**0.059**	**0.059**	**0.059**	**0.070**	**0.082**	**0.082**	**0.095**	**0.095**	**0.095**	**0.102**	**0.110**	**0.110**	**0.110**	**0.110**	**0.110**	**0.117**	**0.117**
2xCompression	**0.040**	**0.061**	**0.061**	**0.087**	**0.097**	**0.117**	**0.117**	**0.117**	**0.140**	**0.164**	**0.164**	**0.191**	**0.191**	**0.191**	**0.205**	**0.219**	**0.219**	**0.219**	**0.219**	**0.219**	**0.234**	**0.234**
Floor Bearing Capacity																							
Weakest Floor Unit UCS (MPa)	30.0	30.0	30.0	30.0	30.0	30.0	30.0	30.0	30.0	30.0	30.0	30.0	30.0	30.0	30.0	30.0	30.0	30.0				
Weakest Unit Thickness (m)	0.3	0.3	0.3	0.3	0.3	0.3	0.3	0.3	0.3	0.3	0.3	0.3	0.3	0.3	0.3	0.3	0.3	0.3	0.3	0.3	0.3	0.3
Floor Bearing Capacity (MPa)	689.6	689.6	689.6	689.6	689.6	689.6	689.6	689.6	689.6	689.6	689.6	689.6	689.6	689.6	689.6	689.6	689.6	689.6	0.0	0.0	0.0	0.0
Pillar Stress (MPa)	1.7	2.1	2.8	3.6	3.9	4.5	4.5	4.5	5.1	5.7	5.7	6.3	6.3	6.3	6.7	7.0	7.0	7.0	7.0	7.0	7.3	7.3
Floor Bearing Failure FoS	**410.8**	**322.8**	**242.4**	**189.7**	**176.2**	**153.8**	**153.8**	**153.8**	**135.7**	**121.0**	**121.0**	**108.8**	**108.8**	**108.8**	**103.4**	**98.5**	**98.5**	**98.5**	**98.5**	**0.0**	**0.0**	**0.0**
Roof Bearing Capacity																							
Weakest Roof Unit UCS (MPa)	15.0	15.0	15.0	15.0	15.0	15.0	15.0	15.0	15.0	15.0	15.0	15.0	15.0	15.0	15.0	15.0	15.0	15.0				
Weakest Unit Thickness (m)	8.0	8.0	8.0	8.0	8.0	8.0	8.0	8.0	8.0	8.0	8.0	8.0	8.0	8.0	8.0	8.0	8.0	8.0	8.0	8.0	8.0	8.0
Roof Bearing Capacity (MPa)	50.0	50.0	50.0	50.0	50.0	50.0	50.0	50.0	50.0	50.0	50.0	50.0	50.0	50.0	50.0	50.0	50.0	50.0	0.0	0.0	0.0	0.0
Pillar Stress (MPa)	1.7	2.1	2.8	3.6	3.9	4.5	4.5	4.5	5.1	5.7	5.7	6.3	6.3	6.3	6.7	7.0	7.0	7.0	7.0	7.0	7.3	7.3
Roof Bearing Failure FoS	**29.8**	**23.4**	**17.6**	**13.8**	**12.8**	**11.2**	**11.2**	**11.2**	**9.8**	**8.8**	**8.8**	**7.9**	**7.9**	**7.9**	**7.5**	**7.1**	**7.1**	**7.1**	**7.1**	**0.0**	**0.0**	**0.0**

UNSW Pillar Design Spreadsheet

West Wallsnd Colliery															
INPUT DATA															
Depth of Cover (m)	145	150	160	160	175	190	190	195	200	220	230	250	255	270	285
Mining Height (m)	3.5	3.5	3.5	3.5	3.5	3.5	3.5	3.5	3.5	3.5	3.5	3.5	3.5	3.5	3.5
Pillar Length - centres (m)	**105.5**	**105.5**	**105.5**	**105.5**	**105.5**	**105.5**	**105.5**	**105.5**	**105.5**	**105.5**	**105.5**	**105.5**	**105.5**	**105.5**	**105.5**
Pillar Width - centres (m)	**40.5**	**40.5**	**40.5**	**40.5**	**40.5**	**40.5**	**40.5**	**40.5**	**40.5**	**40.5**	**40.5**	**40.5**	**40.5**	**40.5**	**40.5**
Roadway Width for maximum pillar dimension	5.5	5.5	5.5	5.5	5.5	5.5	5.5	5.5	5.5	5.5	5.5	5.5	5.5	5.5	5.5
Roadway Width for minimum pillar dimension	5.5	5.5	5.5	5.5	5.5	5.5	5.5	5.5	5.5	5.5	5.5	5.5	5.5	5.5	5.5
Cut-Through Angle (degrees)	90	90	90	90	90	90	90	90	90	90	90	90	90	90	90
Average Panel Span (m) {rib-rib width}	**310**	**310**	**310**	**310**	**310**	**310**	**310**	**310**	**310**	**310**	**310**	**310**	**310**	**310**	**310**
SG (tonnes/m^3)	2.5	2.5	2.5	2.5	2.5	2.5	2.5	2.5	2.5	2.5	2.5	2.5	2.5	2.5	2.5
Conversion (tonnes to N)	10000	10000	10000	10000	10000	10000	10000	10000	10000	10000	10000	10000	10000	10000	10000
Abutment Angle (°)	21	21	21	21	21	21	21	21	21	21	21	21	21	21	21
CALCULATIONS															
Maximum Rib to Rib Pillar Length (w_2)	**100.0**	**100.0**	**100.0**	**100.0**	**100.0**	**100.0**	**100.0**	**100.0**	**100.0**	**100.0**	**100.0**	**100.0**	**100.0**	**100.0**	**100.0**
Minimum Rib to Rib Pillar Width (w_1)	**35.0**	**35.0**	**35.0**	**35.0**	**35.0**	**35.0**	**35.0**	**35.0**	**35.0**	**35.0**	**35.0**	**35.0**	**35.0**	**35.0**	**35.0**
w, Minimum Rib to Rib Pillar Width (ie $w_1 \sin\theta$)	**35.0**	**35.0**	**35.0**	**35.0**	**35.0**	**35.0**	**35.0**	**35.0**	**35.0**	**35.0**	**35.0**	**35.0**	**35.0**	**35.0**	**35.0**
Minimum Pillar Width/Height Ratio	**10.0**	**10.0**	**10.0**	**10.0**	**10.0**	**10.0**	**10.0**	**10.0**	**10.0**	**10.0**	**10.0**	**10.0**	**10.0**	**10.0**	**10.0**
Extraction Ratio (%)	**18.1%**	**18.1%**	**18.1%**	**18.1%**	**18.1%**	**18.1%**	**18.1%**	**18.1%**	**18.1%**	**18.1%**	**18.1%**	**18.1%**	**18.1%**	**18.1%**	**18.1%**
Abutment Angle (Radians)	0.367	0.367	0.367	0.367	0.367	0.367	0.367	0.367	0.367	0.367	0.367	0.367	0.367	0.367	0.367
Cut-Through Angle (Radians)	1.571	1.571	1.571	1.571	1.571	1.571	1.571	1.571	1.571	1.571	1.571	1.571	1.571	1.571	1.571
Is the Panel Super-Critical?	Yes	Yes	Yes	Yes	Yes	Yes	Yes	Yes	Yes	Yes	Yes	Yes	Yes	Yes	Yes
D (Peng & Chiang Loading Factor)	61.773	62.829	64.890	64.890	67.864	70.712	70.712	71.637	72.549	76.090	77.800	81.112	81.920	84.295	86.604
R (Pillar 2nd Abutment Component)	0.96	0.96	0.95	0.95	0.93	0.92	0.92	0.92	0.91	0.90	0.89	0.87	0.87	0.86	0.85
Dimensionless Pillar 'Rectangularity'	1.48	1.48	1.48	1.48	1.48	1.48	1.48	1.48	1.48	1.48	1.48	1.48	1.48	1.48	1.48
Width/Height Ratio Exponent	1.00	1.00	1.00	1.00	1.00	1.00	1.00	1.00	1.00	1.00	1.00	1.00	1.00	1.00	1.00
Effective Width Factor (Omega)	1.48	1.48	1.48	1.48	1.48	1.48	1.48	1.48	1.48	1.48	1.48	1.48	1.48	1.48	1.48
Effective Width Interim	51.85	51.85	51.85	51.85	51.85	51.85	51.85	51.85	51.85	51.85	51.85	51.85	51.85	51.85	51.85
Effective Pillar Width (m)	51.85	51.85	51.85	51.85	51.85	51.85	51.85	51.85	51.85	51.85	51.85	51.85	51.85	51.85	51.85
Effective Pillar Loading Height (m)	145.00	150.00	160.00	160.00	175.00	190.00	190.00	195.00	200.00	220.00	230.00	250.00	255.00	270.00	285.00
RESULTS															
Tributary Area Loading (MPa)	**4.43**	**4.58**	**4.88**	**4.88**	**5.34**	**5.80**	**5.80**	**5.95**	**6.10**	**6.71**	**7.02**	**7.63**	**7.78**	**8.24**	**8.70**
Pillar Strength (UNSW Squat Pillar 1999)	**31.63**	**31.63**	**31.63**	**31.63**	**31.63**	**31.63**	**31.63**	**31.63**	**31.63**	**31.63**	**31.63**	**31.63**	**31.63**	**31.63**	**31.63**
Pillar Strength (UNSW w/h<5)	**N/A**	**N/A**	**N/A**	**N/A**	**N/A**	**N/A**	**N/A**	**N/A**	**N/A**	**N/A**	**N/A**	**N/A**	**N/A**	**N/A**	**N/A**
Safety Factor under FTA Loading (Squat Pillar)	**7.15**	**6.91**	**6.48**	**6.48**	**5.92**	**5.45**	**5.45**	**5.31**	**5.18**	**4.71**	**4.51**	**4.15**	**4.06**	**3.84**	**3.64**
Safety Factor under FTA Loading (w/h<5)	**N/A**	**N/A**	**N/A**	**N/A**	**N/A**	**N/A**	**N/A**	**N/A**	**N/A**	**N/A**	**N/A**	**N/A**	**N/A**	**N/A**	**N/A**
No. SAs, n	2	2	2	2	2	2	2	2	2	2	2	2	2	2	2
Single Abutment Loading (3D) - full	3.04	3.25	3.70	3.70	4.43	5.22	5.22	5.50	5.79	7.00	7.65	9.04	9.40	10.54	11.75
Single Abutment Loading (3D) - pillar	**2.92**	**3.11**	**3.51**	**3.51**	**4.14**	**4.81**	**4.81**	**5.05**	**5.29**	**6.28**	**6.81**	**7.90**	**8.19**	**9.07**	**9.98**
Single Abutment Loading (3D) - solid	0.12	0.15	0.20	0.20	0.29	0.41	0.41	0.45	0.50	0.72	0.84	1.13	1.22	1.48	1.77
Cell Sensitivity (MPa)	0	0	0	0	0	0	0	0	0	0	0	0	0	0	0
Total Pillar Loading with Single Abutment Loading	7.34	7.69	8.39	8.39	9.48	10.61	10.61	11.00	11.39	13.00	13.83	15.53	15.97	17.31	18.67
Safety Factor (under Single Abutment Loading)	**4.31**	**4.11**	**3.77**	**3.77**	**3.34**	**2.98**	**2.98**	**2.88**	**2.78**	**2.43**	**2.29**	**2.04**	**1.98**	**1.83**	**1.69**
Total Pillar Loading @ nA	10.51	11.09	12.29	12.29	14.20	16.24	16.24	16.95	17.67	20.71	22.32	25.71	26.59	29.33	32.19
Safety Factor @ nA	**3.01**	**2.85**	**2.57**	**2.57**	**2.23**	**1.95**	**1.95**	**1.87**	**1.79**	**1.53**	**1.42**	**1.23**	**1.19**	**1.08**	**0.98**
Total Pillar Loading under Double Abutment Loading	10.51	11.09	12.29	12.29	14.20	16.24	16.24	16.95	17.67	20.71	22.32	25.71	26.59	29.33	32.19
Safety Factor (under Double Abutment Loading)	**3.01**	**2.85**	**2.57**	**2.57**	**2.23**	**1.95**	**1.95**	**1.87**	**1.79**	**1.53**	**1.42**	**1.23**	**1.19**	**1.08**	**0.98**
Elastic Model Subsidence															
Ecoal(GPa)	**2.00**	**2.00**	**2.00**	**2.00**	**2.00**	**2.00**	**2.00**	**2.00**	**2.00**	**2.00**	**2.00**	**2.00**	**2.00**	**2.00**	**2.00**
Efloor(GPa)	**7.40**	**7.40**	**7.40**	**7.40**	**7.40**	**7.40**	**7.40**	**7.40**	**7.40**	**7.40**	**7.40**	**7.40**	**7.40**	**7.40**	**7.40**
Eroof(GPa)	**3.00**	**3.00**	**3.00**	**3.00**	**3.00**	**3.00**	**3.00**	**3.00**	**3.00**	**3.00**	**3.00**	**3.00**	**3.00**	**3.00**	**3.00**
Poissons Ratio floor/roof	**0.25**	**0.25**	**0.25**	**0.25**	**0.25**	**0.25**	**0.25**	**0.25**	**0.25**	**0.25**	**0.25**	**0.25**	**0.25**	**0.25**	**0.25**
initial vertical stress (MPa)	**3.63**	**3.75**	**4.00**	**4.00**	**4.38**	**4.75**	**4.75**	**4.88**	**5.00**	**5.50**	**5.75**	**6.25**	**6.38**	**6.75**	**7.13**
increase in vertical stress (MPa)	**6.88**	**7.34**	**8.29**	**8.29**	**9.82**	**11.49**	**11.49**	**12.08**	**12.67**	**15.21**	**16.57**	**19.46**	**20.22**	**22.58**	**25.07**
Pillar Compression (m)	**0.011**	**0.012**	**0.014**	**0.014**	**0.016**	**0.019**	**0.019**	**0.020**	**0.021**	**0.025**	**0.027**	**0.032**	**0.033**	**0.037**	**0.041**
Roof Compression (m)	**0.075**	**0.080**	**0.091**	**0.091**	**0.107**	**0.126**	**0.126**	**0.132**	**0.139**	**0.166**	**0.181**	**0.213**	**0.221**	**0.247**	**0.274**
Floor Compression (m)	**0.031**	**0.033**	**0.037**	**0.037**	**0.044**	**0.051**	**0.051**	**0.054**	**0.056**	**0.067**	**0.073**	**0.086**	**0.090**	**0.100**	**0.111**
Total Compression (m)	**0.117**	**0.125**	**0.141**	**0.141**	**0.167**	**0.195**	**0.195**	**0.205**	**0.216**	**0.259**	**0.282**	**0.331**	**0.344**	**0.384**	**0.426**
2xCompression	**0.234**	**0.250**	**0.282**	**0.282**	**0.334**	**0.391**	**0.391**	**0.411**	**0.431**	**0.518**	**0.564**	**0.662**	**0.688**	**0.768**	**0.853**
Floor Bearing Capacity															
Weakest Floor Unit UCS (MPa)															
Weakest Unit Thickness (m)	0.3	0.3	0.3	0.3	0.3	0.3	0.3	0.3	0.3	0.3	0.3	0.3	0.3	0.3	0.3
Floor Bearing Capacity (MPa)	0.0	0.0	0.0	0.0	0.0	0.0	0.0	0.0	0.0	0.0	0.0	0.0	0.0	0.0	0.0
Pillar Stress (MPa)	7.3	7.7	8.4	8.4	9.5	10.6	10.6	11.0	11.4	13.0	13.8	15.5	16.0	17.3	18.7
Floor Bearing Failure FoS	**0.0**	**0.0**	**0.0**	**0.0**	**0.0**	**0.0**	**0.0**	**0.0**	**0.0**	**0.0**	**0.0**	**0.0**	**0.0**	**0.0**	**0.0**
Roof Bearing Capacity															
Weakest Roof Unit UCS (MPa)															
Weakest Unit Thickness (m)	8.0	8.0	8.0	8.0	8.0	8.0	8.0	8.0	8.0	8.0	8.0	8.0	8.0	8.0	8.0
Roof Bearing Capacity (MPa)	0.0	0.0	0.0	0.0	0.0	0.0	0.0	0.0	0.0	0.0	0.0	0.0	0.0	0.0	0.0
Pillar Stress (MPa)	7.3	7.7	8.4	8.4	9.5	10.6	10.6	11.0	11.4	13.0	13.8	15.5	16.0	17.3	18.7
Roof Bearing Failure FoS	**0.0**	**0.0**	**0.0**	**0.0**	**0.0**	**0.0**	**0.0**	**0.0**	**0.0**	**0.0**	**0.0**	**0.0**	**0.0**	**0.0**	**0.0**

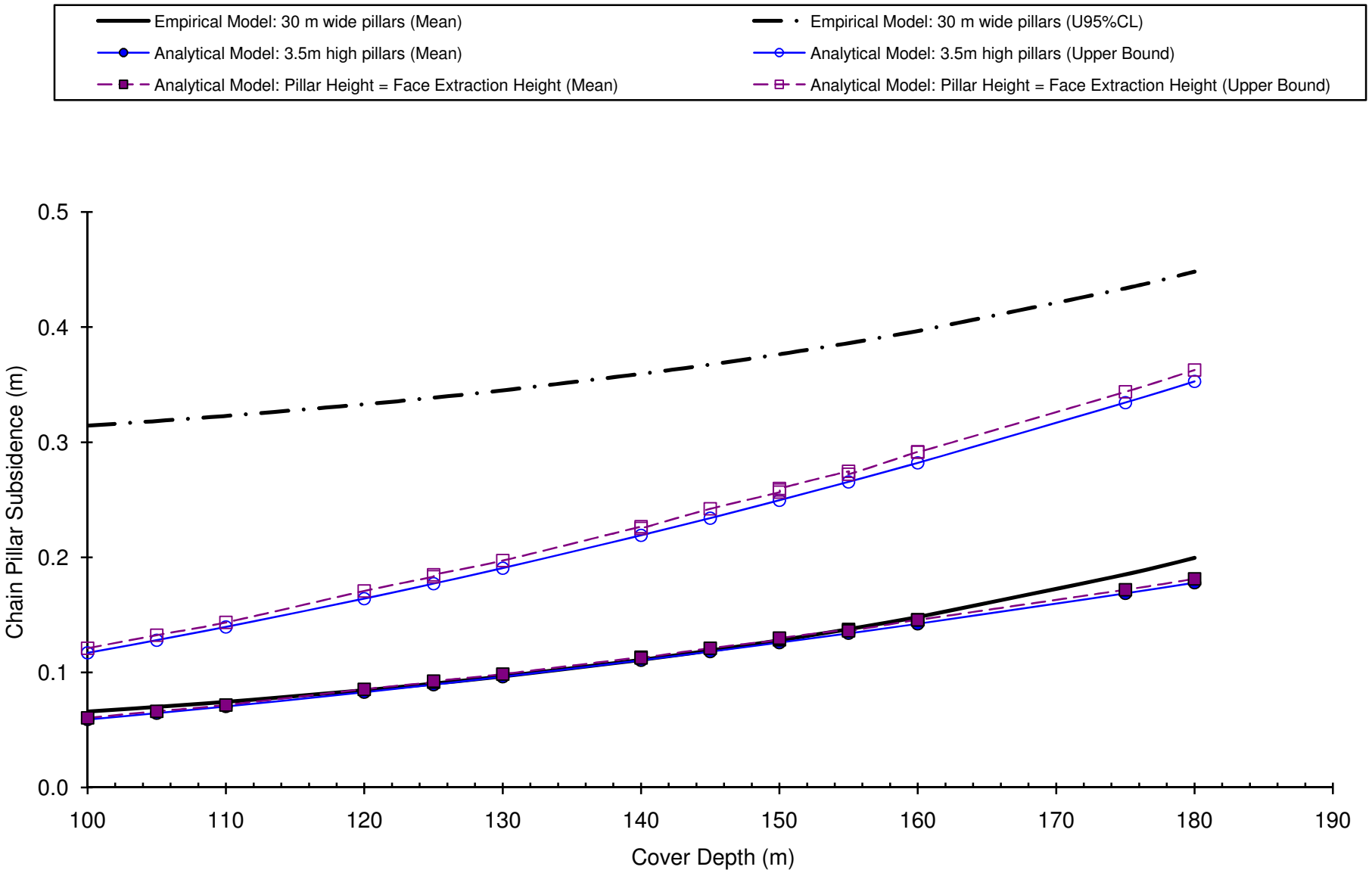
Empirical Model: 30 m wide pillars (Mean)
Empirical Model: 30 m wide pillars (U95%CL)
Analytical Model: 3.5m high pillars (Mean)
Analytical Model: 3.5m high pillars (Upper Bound)
Analytical Model: Pillar Height = Face Extraction Height (Mean)
Analytical Model: Pillar Height = Face Extraction Height (Upper Bound)
Chain Pillar Subsidence (m)
0.0
0.1
0.2
0.3
0.4
0.5
100
110
120
130
140
150
160
170
180
190
Cover Depth (m)

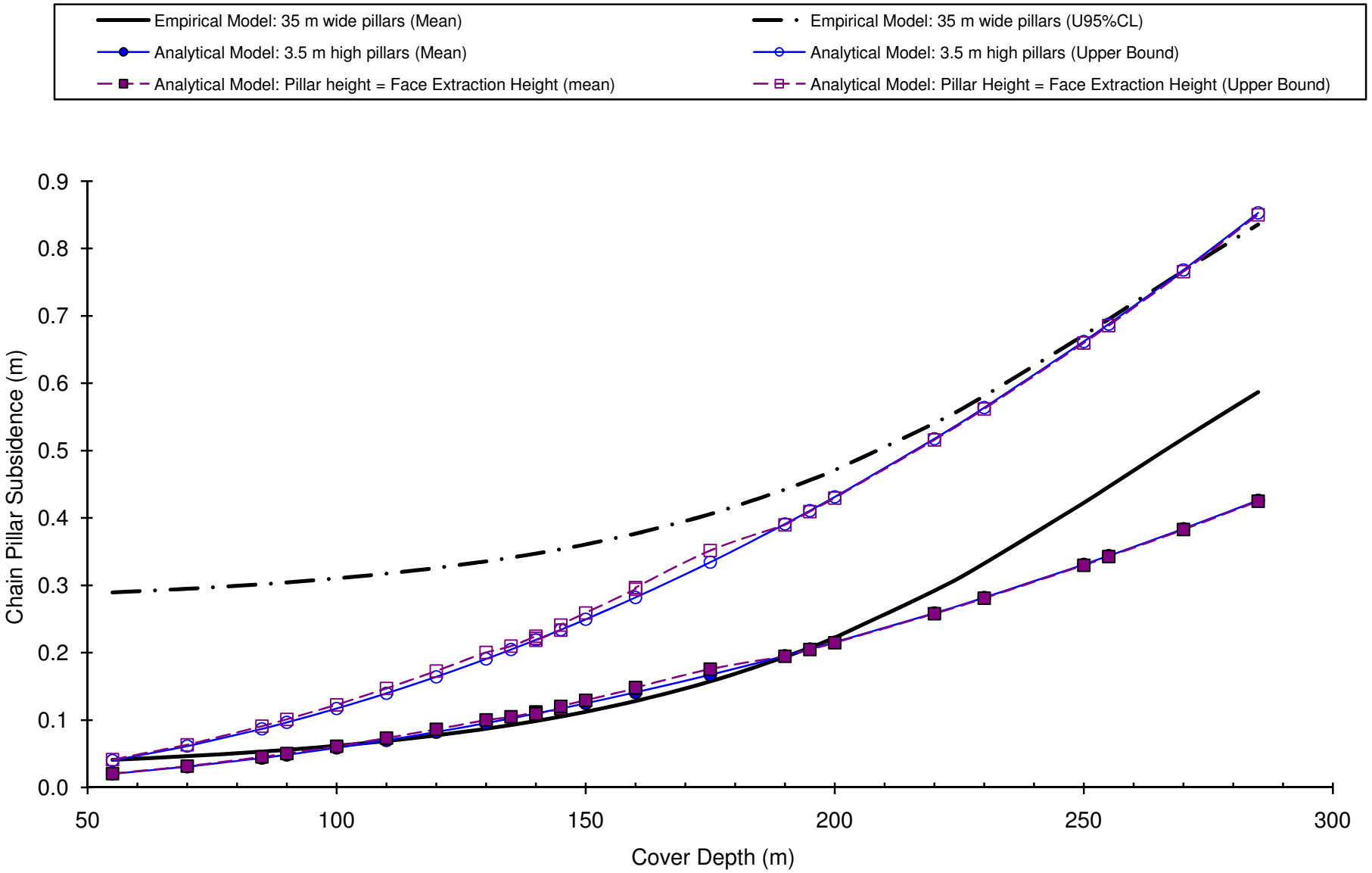
Empirical Model: 35 m wide pillars (Mean)
Empirical Model: 35 m wide pillars (U95%CL)
Analytical Model: 3.5 m high pillars (Mean)
Analytical Model: 3.5 m high pillars (Upper Bound)
Analytical Model: Pillar height = Face Extraction Height (mean)
Analytical Model: Pillar Height = Face Extraction Height (Upper Bound)
Chain Pillar Subsidence (m)
0.0
0.1
0.2
0.3
0.4
0.5
0.6
0.7
0.8
0.9
50
100
150
200
250
300
Cover Depth (m)

Coal mine subsidence prediction using a boundary-element program

K.A. Heasley and T.M. Barton

Abstract

This paper presents several case studies in which a mechanics-based boundary-element program is used to back-calculate the surface subsidence associated with various panels at several northern Appalachian coal mines. The program used in this case study is called LAMODEL, which incorporates a frictionless, laminated overburden into a general-purpose displacement-discontinuity code primarily designed for calculating the stresses and displacements in coal mines or other thin-seam or vein-type deposits. In this paper, the program is used to calculate both the underground convergence and the resulting surface subsidence at five longwall panels and a room-and-pillar section. The fitted subsidence from the model is compared with the field measurements and analyzed. The results from this work show that the LAMODEL program is not as accurate as available empirical subsidence-predictive methods; the expected correlation between the geology and the optimum input parameters is not evident. However, for a mechanics-based program, LAMODEL does provide moderately accurate subsidence calculations, and it is one of a few programs that can even attempt to practically calculate both underground stress and convergence and the resulting surface subsidence.

Introduction

Historically, the surface subsidence above underground coal mines has been predicted using profile or influence functions that use little or no mechanics to calculate the ground movement (Kratzch, 1983; Adamek et al., 1987; Heasley, 1988). Without a mechanistic input, establishing the exact seam convergence and function parameters to use in these empirical methods has typically required extensive and expensive field measurements to calibrate the function parameters to a specific mining area. A practical subsidence-predictive method based on mechanics has the appealing capability of allowing the determination of site-specific parameters from fundamental properties of the overburden with minimal field calibration work.

Recently, a laminated overburden model derived from plate mechanics was used to predict surface subsidence with fairly good results (Salamon, 1989a, 1989b, 1991; Yang, 1992). The model has shown the capability of fitting a generic, empirically derived subsidence curve for northern Appalachia (Heasley and Salamon, 1996). The combination of both of these capabilities in a single mathematical model gives it the potential to accurately calculate both underground stresses and displacement and the associated surface subsidence with the same mechanical basis. This laminated overburden model has now been coded into a full-featured displacement-discontinuity program, LAMODEL, for analyzing coal mine stresses and displacements, as well as surface subsidence (Heasley, 1998). In this program, the various properties of the seam and gob materials are mechanically combined with the laminated overburden properties to realistically calculate seam stresses and convergence. This calculated seam convergence can then be projected to surface subsidence using the laminated overburden mechanics.

This paper relates the application of the laminated overburden in LAMODEL to subsidence prediction at several longwall panels and a room-and-pillar section in northern Appalachia and provides an initial evaluation of the program's accuracy and utility for subsidence prediction.

The LAMODEL program

LAMODEL is a PC-based program for calculating the stresses and displacements in coal mines or other thin-seam or vein-type deposits. It is primarily designed to be utilized by mining engineers for investigating and optimizing pillar sizes and layouts in relation to overburden, abutment and multiple-seam stresses (Heasley, 1998). The program uses a displacement-discontinuity variation of the boundary-element method for determining and solving the elastic equations of equilibrium around the mine openings. LAMODEL simulates the overburden as a stack of homogeneous isotropic layers with frictionless interfaces and with each layer having the identical elastic modulus, Poisson's Ratio and thickness. This "homogeneous stratification" formulation does not require (or allow) specific material properties for each individual layer. Yet it still provides a realistic suppleness to the overburden that is not possible with the classic, homogeneous isotropic elastic overburden.

The two primary factors that influence the shape and magnitude of the subsidence (particularly in LAMODEL) are the gob compaction stiffness and the overburden flexural stiffness. Therefore, the primary parameters that are adjusted in LAMODEL for fitting the measured subsidence are the final gob modulus (E_f), which is used to control the gob stiffness, and the lamination thickness (t), which is used to control the overburden stiffness. In the process of analyzing the potential of LAMODEL for surface subsidence calcula-

K.A. Heasley, member SME, and **T.M. Barton** are mining engineers with the National Institute for Occupational Safety and Health, Pittsburgh Research Laboratory, Pittsburgh, PA. Preprint number 99-181, presented at the SME Annual Meeting, March 9-11, 1998, Orlando, FL. Revised manuscript accepted for publication November 1999. Discussion of this peer-reviewed and approved paper is invited and must be submitted to SME prior to Sept. 30, 2000.

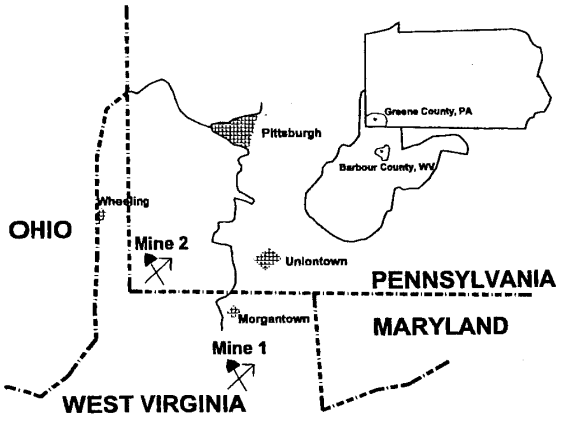

Figure 1 — Location map of the case study mines.

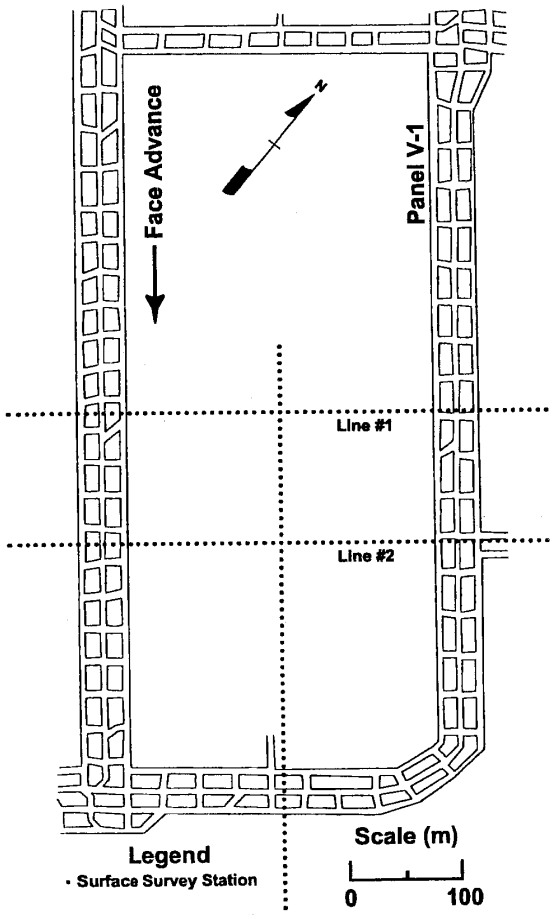

Figure 2 — Map of the V-1 panel.

tion presented in this paper, the measured subsidence is used to "calibrate" the model. This calibration process consists of an interactive trial-and-error process where the critical model parameters (in this case the lamination thickness and the final gob modulus) are initially estimated. The program is run to calculate the surface subsidence, the calculated subsidence is compared to the measured subsidence, the model parameters are adjusted to improve the fit and, then, the program is run again. This cycle continues until the calculated subsidence fits the measured subsidence as close as desired. The resulting values of the critical model parameters are considered to be "calibrated" to the given site conditions.

Table 1 — Panel dimensions used in the calibration models.

Panel	Length, m	Width, m	Seam thickness, m	Depth, m
V-1	640	285	1.8	120
D-3	1,250	180	1.8	230
D-5	1,050	168	1.8	230
C-3	256	168	1.7	180
E-1	1,430	194	1.8	277
E-2	1,730	194	1.8	247

Mine 1

The location of the first subsidence-prediction case study in this paper is a longwall mine in Barbour County in the northwest corner of West Virginia (see Fig. 1). This mine started production in 1975 with continuous miners in room-and-pillar sections. In 1982, the first longwall was installed and, by the time of the final subsidence monitoring in this study (1985), the mine had successfully completed five longwall panels (Jeran and Barton, 1985; Heasley, 1988). The mine operates in the Lower Kittanning seam that averages 1.8 m (5.9 ft) in thickness and has an overburden between 120 and 420 m (390 and 1,380 ft) across the property. The immediate roof of the seam consists of a thinly laminated sandy-shale overlain with a main roof of interbedded sandstones, shales and limestones. The mine area is also noted for high horizontal in situ stresses.

The V-1 panel. The first panel at which the subsidence was investigated using LAMODEL is called the V-1 panel. It is actually the fifth longwall panel to be extracted at the mine (see Fig. 2 and Table 1.). The panel advanced from the northwest towards the southeast, and, as shown in Fig. 2, there were two transverse lines and one longitudinal line of subsidence monitoring stations over the later half of the panel. For this initial subsidence-fitting exercise, the entire panel was discretized into LAMODEL. The overburden was set at a constant 120 m (390 ft), the elastic modulus of the rock mass was set at 20 GPa, the modulus of the coal was set at 2 GPa and the coal thickness was set at a constant 1.8 m (5.9 ft).

For this first calibration process on the V-1 panel, it was found that a wide range of lamination thicknesses and final gob moduli combinations could be fit equally well to the measured subsidence. A distributed sample of these parameter combinations is listed in Table 2 and shown in Fig. 3. The range of parameters shown in Table 2 covers the complete spectrum of reasonable behavior for this panel. For the thinnest laminations (1.5 m), the peak gob load is essentially equal to the overburden load (see Table 2). Therefore, at this lamination thickness, the gob is supporting the total overburden load at the middle of the panel and the flexural stiffness of the laminations is not effectively supporting any overburden load. On the other end of the spectrum, for the thickest lamination (7.5 m), the peak gob load is only about one-sixth of the overburden load, and the flexural stiffness of the

Table 2 — Calibrated LAMODEL parameters.

Lamination thickness, m	Final gob modulus, MPa	Peak gob stress, MPa	Average gob stress, MPa	Coal strength, percent of Bieniawski strength
Panel V-1				
1.5	124	3.0	2.0	100
4.5	100	2.5	1.6	100
7.5	1.38	0.5	0.4	100
Panel D-3				
1.5	383	5.7	4.5	100
4.5	372	5.4	3.6	100
7.5	324	4.3	2.3	100
Panel D-5				
1.5	383	5.7	4.5	60
4.5	372	5.4	3.6	60
7.5	324	4.3	2.3	60
Panel C-3				
3.0	340	4.2	–	100
4.5	293	3.3	–	100
6.0	212	1.8	–	100
Panel E-1				
3.0	203	6.7	–	100
6.0	179	5.1	–	100
9.0	141	3.2	–	100
Panel E-2				
3.0	170	5.9	–	55
6.0	149	4.2	–	75
9.0	84	1.7	–	95

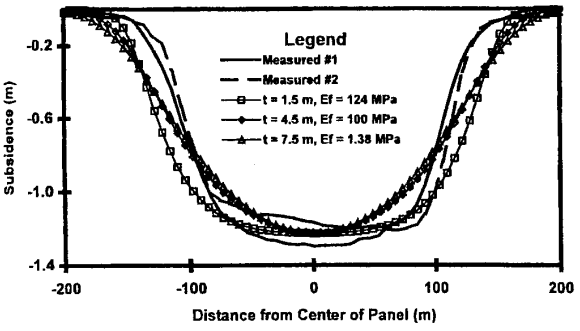

Figure 3 — The measured and fitted subsidence for the V-1 Panel.

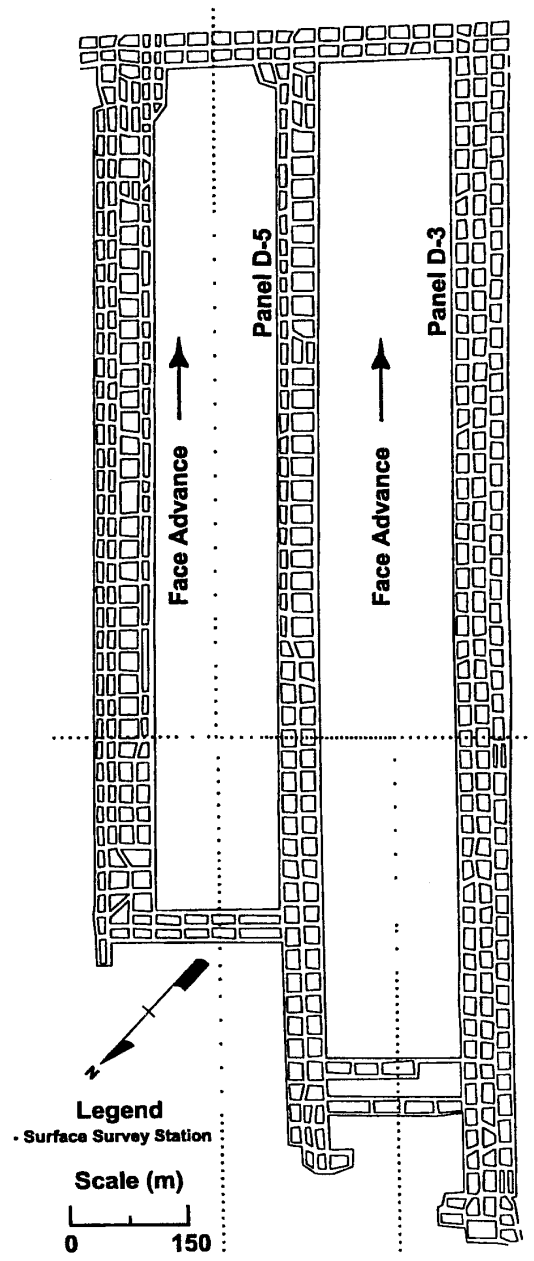

Figure 4 — Map of the D-3 and D-5 panels.

laminations is supporting the other five-sixths of the overburden load. Thus, for fitting LAMODEL to a given maximum subsidence, the thinnest, most flexible laminations require the stiffest gob, while the thickest, stiffest laminations mandate a softer gob.

The D-3 and D-5 panels. The next two panels at which the subsidence was investigated using LAMODEL are known as the D-3 and D-5 panels, and they are the first and second panels to be extracted at Mine 1 (see Fig. 4 and Table 1). Both of these panels advanced from the northwest towards the southeast, and each panel had its own longitudinal line of subsidence monitoring stations and a shared transverse line that extends over both the panels and the intervening gate road (see Fig. 4). Because these panels are considerably narrower (≤180 m) and deeper (≥230 m) than the V-1 panel, the surface subsidence is expected to be subcritical.

For the subsidence calculation at these two panels, a single LAMODEL grid was created that covered the initial half of both panels. The elastic modulus of the overburden and coal were set to the same values as used for the V-1 panel. However, the input coal strength was varied to fit the subsidence over the intervening gate roads. Essentially, both the convergence in the gate road and the associated overlying

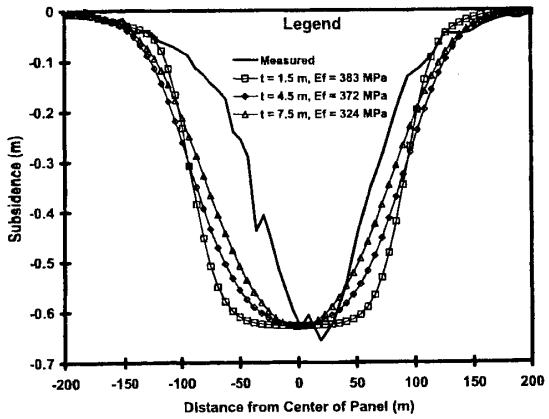

Figure 5 — The measured and fitted subsidence for the D-3 Panel.

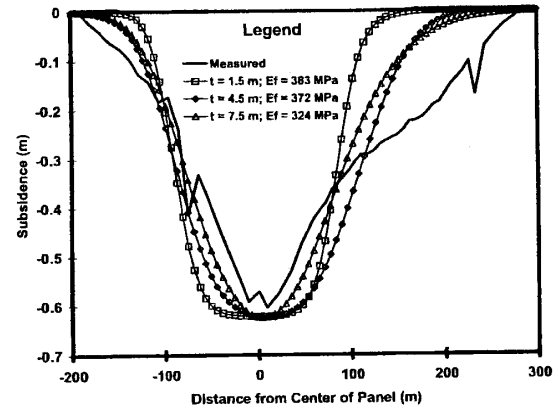

Figure 6 — The measured and fitted subsidence for the D-5 Panel.

subsidence were increased by decreasing the gate road coal strength. Typically, the coal strength is initially set at 100% of the strength determined by the Bieniawski pillar formula (Heasley, 1998). When more subsidence is needed over the gate roads for better calibration, the coal strength is lowered to some percentage of the recommended Bieniawski pillar strength (see Table 2). The calibrated subsidence for the D-3 and D-5 panels is shown in Figs. 5 and 6, respectively.

The C-3 panel. The next panel where the measured subsidence was calibrated using LAMODEL is called the C-3 panel, which is a room-and-pillar retreat section at Mine 1 (see Fig. 7 and Table 1). The chain pillars in the section were typically driven 13-m (43-ft) wide by 22-m (72-ft) long, with 5-m- (16-ft-) wide rooms and crosscuts. The overall retreat line moved from the southwest towards the northeast, with pillars being extracted systematically row by row, west to east using the split-and-fender cut sequence on a single pair of pillars at one time. On the surface above this section, the subsidence was monitored with two longitudinal survey lines and one doglegged transverse survey line of subsidence monitoring stations (see Fig. 7). For the subsidence calibration of this panel, the elastic modulus of the overburden and coal were set to the same values as previous LAMODEL runs at this mine. The calibrated subsidence for this panel is shown in Fig. 8 and the associated LAMODEL parameters are given in Table 2.

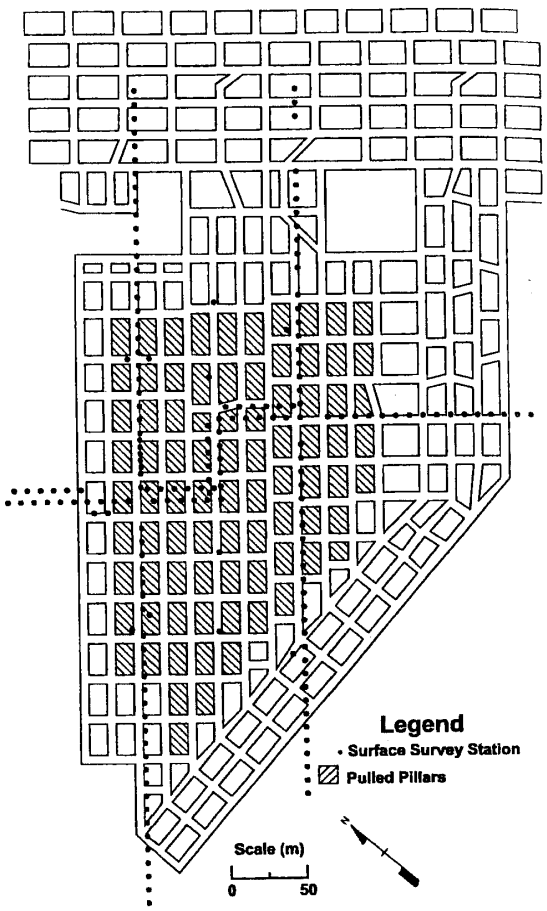

Figure 7 — Map of the C-3 panel.

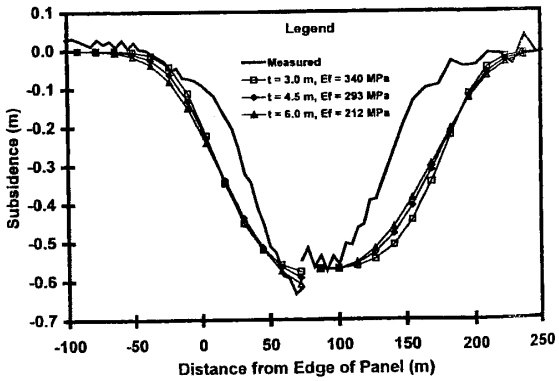

Figure 8 — The measured and fitted subsidence for the C-3 Panel.

Mine 2

The second case study mine in this paper is a longwall mine in Greene County in the southwest corner of Pennsylvania (see Fig. 1). The mine operates in the Pittsburgh seam, which averages 1.8-m (6-ft) in thickness and which has an overburden between 230 and 300 m (750 and 1,000 ft) across the property. In the study area, the immediate roof of the

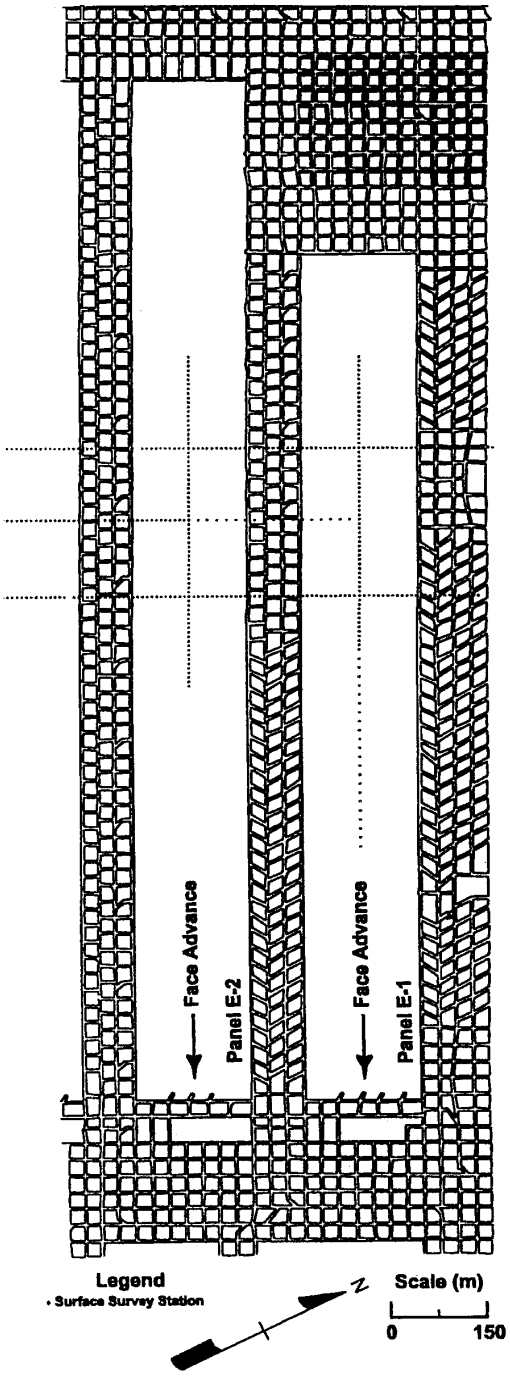

Figure 9 — Map of the E-1 and E-2 panels.

seam consists of limestone overlain with a main roof of interbedded shales, sandstones, limestones and coal (Moebs and Barton, 1985).

The E-1 and E-2 panels. The two panels at Mine 2, where LAMODEL was used to investigate the subsidence, are known as the E-1 and E-2 panels. These are the first and

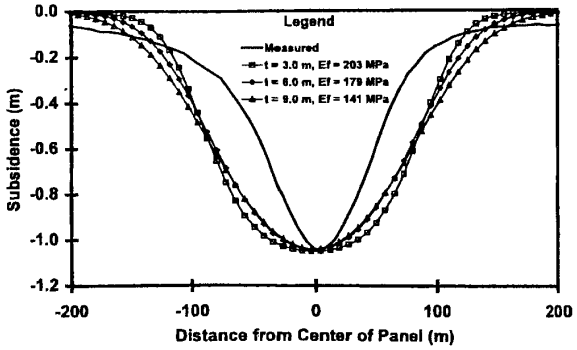

Figure 10 — The measured and fitted subsidence for the E-1 Panel.

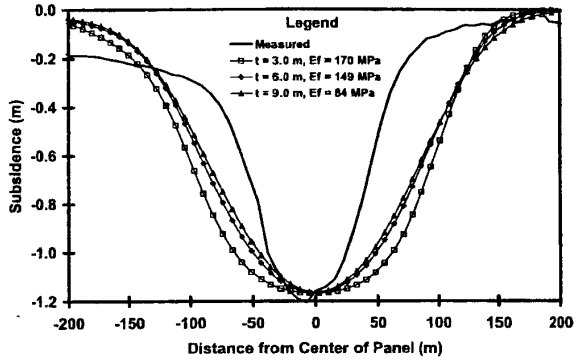

Figure 11 — The measured and fitted subsidence for the E-2 Panel.

second panels to be extracted at the mine (see Fig. 9 and Table 1). Both of these panels advanced from the northwest towards the southeast, and each panel had its own longitudinal line of subsidence-monitoring stations and shared three transverse lines that extended over both the panels and the intervening gate road (see Fig. 9). Because these two panels share a gate road similar to panels D-3 and D-5, they also allow/require the subsidence over the gate road to be adjusted by varying the coal strength (see Table 2).

For the subsidence calculation at these two panels, a single LAMODEL grid covered the initial half of both panels centering on the transverse profile line closest to the start of the panels. In the model, as in all the models in this paper, the elastic modulus of the rock mass was set at 20 GPa and the modulus of the coal was set at 2 GPa. The calibrated subsidence for these panels is shown in Figs. 10 and 11, and the associated calibrated parameters are given in Table 2.

Discussion

In this paper, surface subsidence from five northern Appalachian longwall panels and a room-and-pillar section was calculated in the process of evaluating the utility of using the LAMODEL program for subsidence calculation. This number of case studies provides a fairly substantial basis for understanding the subsidence predictive capabilities of the program, and the evaluation process has highlighted a number of characteristics and peculiarities of subsidence prediction with LAMODEL. First, it appears that the LAMODEL subsidence calculation is not as accurate as available empirical subsidence predictive methods. The program systemati-

cally produced subsidence troughs that were wider than observed. Also, the initial hope that one set of regional input parameters would be determined that would provide reasonable subsidence prediction throughout the given area was not achieved. The expected correlation between the geology and the optimum input parameters was not evident in this work. However, for a mechanics-based program, LAMODEL does provide moderately accurate subsidence calculations. Also, the laminated model demonstrated a considerable amount of flexibility for subsidence fitting through varying only two mechanical parameters, the lamination thickness and the gob modulus. LAMODEL is one of a few programs that can even attempt to calculate both underground stress and convergence and the resulting surface subsidence.

References

Adamek, V., Jeran, P.W., and Trevits, M.A., 1987, "Prediction of Surface Deformations over Longwall Panels in the Northern Appalachian Coalfield," US Bureau of Mines, RI 9142, 19 pp.

Heasley, K.A., 1998, "Numerical Modeling of Coal Mines with a Laminated Displacement-Discontinuity Code," Ph.D. Thesis, Colorado School of Mines, Golden, CO, May, 187 pp.

Heasley, K.A., and Salamon, M.D.G., 1996. "A new laminated displacement-discontinuity program: fundamental behavior," *Proceedings of the Fifteenth International Conference on Ground Control in Mining*, Colorado School of Mines, Golden, CO, August 13-15, pp. 111-125.

Heasley, K.A., 1988, "Computer Modeling of Subsidence and Subsidence-Control Methods," M.S. Thesis, The Pennsylvania State University, State College, PA, August, 203 pp.

Jeran, P.W., and Barton, T.M., 1985, "Comparison of the subsidence over two different longwall panels," *Proceedings: Mine Subsidence Control*, September 19, US Bureau of Mines, IC 9042, pp. 25-33.

Kratzch, H., 1983, *Mining Subsidence Engineering*, Springer-Verlag, Berlin.

Moebs, N.N., and Barton, T.M., 1985, "Short-term effects of longwall mining on shallow water sources," *Proceedings: Mine Subsidence Control*, September 19, US Bureau of Mines, IC 9042, pp. 13-24.

Salamon, M.D.G., 1991, "Displacements and stresses induced by longwall mining in coal," *Proceedings of the 7th Congress of the International Society for Rock Mechanics*, A.A. Balkema, Rotterdam, pp. 1199-1202.

Salamon, M.D.G., 1989a, "Subsidence prediction using a laminated linear model," *Proceedings of the 30th U.S. Symposium of Rock Mechanics*, A.A. Balkema, Rotterdam, pp. 503-510.

Salamon, M.D.G., 1989b, "Some applications of the frictionless laminated model," *Proceedings of the 30th U.S. Symposium of Rock Mechanics*, A.A. Balkema, Rotterdam, pp. 891-898.

Yang, G., 1992, "Numerical Approach to the Prediction of Subsidence due to Longwall Coal Mining using a Laminated Model," Ph.D. Thesis, Colorado School of Mines, Golden, CO, 218 pp.

LAMODEL MATERIALS

The LAMODEL program uses six different stress-strain models for the in-seam material behavior, exactly as used in the MULSIM program (Zipf, 1992a, 1992b). These material models include: linear elastic, strain-softening, elastic-plastic, bi-linear hardening, strain-hardening and linear elastic gob (see Figure B.1). These various models provide the flexibility of simulating a wide range of material responses, from the strain-softening coal in yield pillars to the strain-hardening longwall gob. Functionally, each material model is represented by a particular shape of stress-strain curves (see Figure B.1). The input parameters for a given material model essentially specify the exact shape of the stress-strain curves to LAMODEL. The specified material curve is then used in the program to enforce the boundary conditions for any element of that material. Because the program does not keep a record of past material behavior, the element response of each of these materials is forced to fall on the defined stress-strain curve regardless of loading history. In an unloading situation with the non-linear materials, this particular behavior may not be very realistic.

In the following paragraphs, this appendix briefly explains the behavior and input parameters for each of the material models. Most of this material is derived from Zipf's (1992a, 1992b) practitioner and programmer manuals for MULSIM/NL.

B.1 Linear Elastic

The linear elastic model is the simplest material behavior (see Figure B.1A). For this model, the stress is linearly related to the strain by the elastic modulus (E); therefore, the modulus is the only necessary input. Within LAMODEL, the stiffness (K) for this material is determined by dividing the elastic modulus by the seam thickness (t):

$$K = \frac{E}{t} \tag{1}$$

B.2 Strain-Softening

The idealized stress-strain curve for the strain-softening material approximates the behavior of coal specimens in the lab. In practice, it also approximates the yielding behavior of narrow pillars or the yielding edges of larger pillars. The exact stress-strain curve for the strain-softening model is specified by defining the point of peak stress (s_p) and peak strain (e_p), and the point of residual stress (s_r) and residual strain (e_r) as shown in Figure B.1B. In this model, the residual

strain must be greater than the peak strain, and the residual stress is assumed to remain constant for strain levels higher than the residual strain.

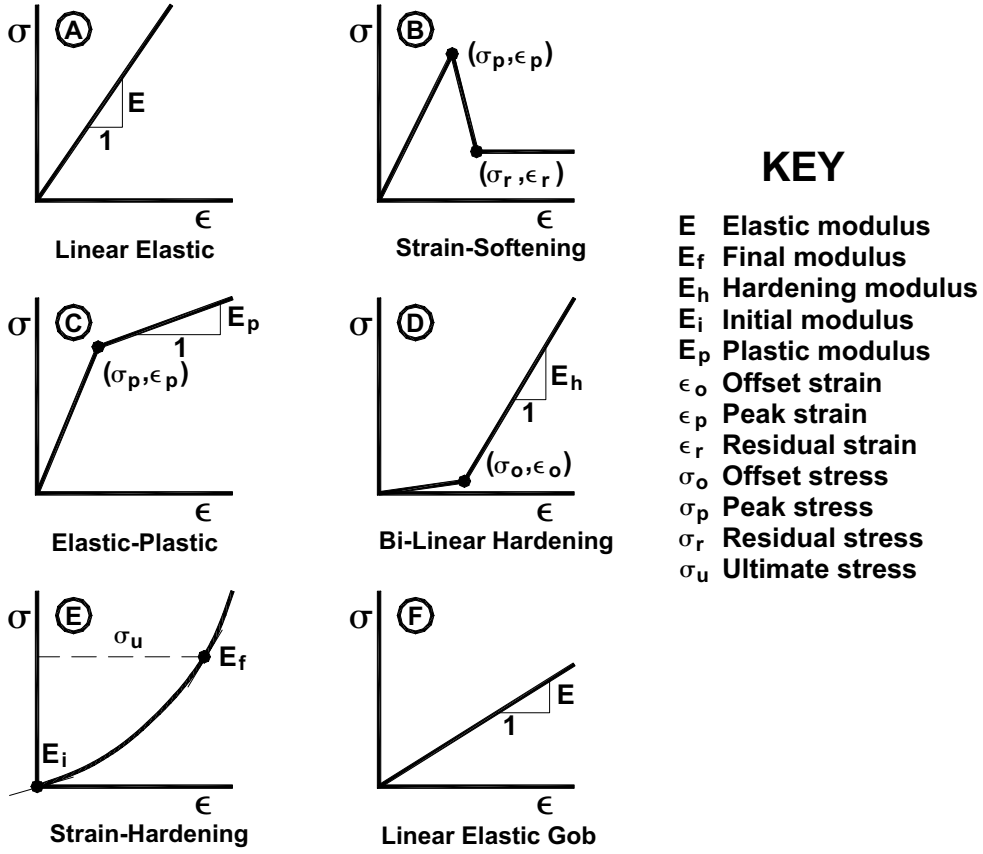

Figure B.1. Stress-Strain Curves for the material models in LaModel and Mulsim.

B.3 Elastic-Plastic

The idealized stress-strain curve for the elastic-plastic material approximates the "pseudo-ductile" behavior (Barron, 1992) of wide pillars or the confined core of medium pillars. The exact stress-strain curve for the elastic-plastic model is specified by defining the point of peak stress (s_p) and peak strain (e_p), and the plastic modulus (E_p) of the material after failure, as shown in Figure B.1C.

B.4 Bi-linear Hardening

This material model is intended to approximate the strain-hardening behavior of gob or backfill material. As seen in Figure B.1D, the idealized stress-strain curve allows some deformation, or offset, to occur before the material begins to acquire load. This offset is intended to simulate the roof convergence before the gob begins to compact and support the overburden.

The parameters required to specify the exact strain-hardening stress-strain curve are the coordinates of the offset point, specifically the offset stress (s_o) and the offset strain (e_o), and the hardening modulus (E_h). This gob material model also requires a gob height factor (n). The gob height factor accounts for the difference in height between the gob and the seam, and its value should be equal to the ratio of gob thickness to seam thickness. In LAMODEL, the nominal stiffness of the gob material is divided by the gob height factor in order to reduced the effective stiffness of the gob and accurately account for the difference in thickness between the gob and the seam.

B.5 Strain-Hardening

The strain-hardening material model uses an exponential stress-strain curve (see Figure B.1E), and like the bi-linear hardening model, this material is intended to approximate the strain-hardening behavior of gob or backfill. The fundamental basis of this gob model is the assumption that the tangent elastic modulus of the material increases linearly with stress. This linear increase in tangent modulus with stress has been documented by Pappas and Mark (1993a, 1993b) for various simulated gob materials. The mathematical derivation of this material model is provided by Zipf (1992a, 1992b), where he found that the material stress (s) is related to the material strain (e) by the following equation:

$$\sigma = \left[\frac{E_i \ \sigma_u}{E_f - E_i}\right]\left[e^{\left(\frac{E_f - E_i}{n \ \sigma_u}\right)\varepsilon} - 1\right]$$

where E_i is the initial tangent modulus at zero stress, E_f is the final tangent modulus at the ultimate stress (s_u) and n is the gob height factor. In this equation, the factor:

$$\left(\frac{E_f - E_i}{n \ \sigma_u}\right)$$

essentially controls the degree of non-linearity of the stress-strain curve. For specifying the material in LAMODEL, the required parameters are the initial tangent modulus (E_i), the final tangent modulus (E_f), the ultimate stress (s_u), and the gob height factor (n).

B.6 Linear Elastic Gob

This material model is a linear elastic stress-strain curve for simulating gob material. The only difference between this material and the linear elastic material for the coal is the capability of inputting a gob height factor (n). With the gob height factor, the stiffness of the linear elastic gob is calculated as:

$$K = \frac{E}{n\ t}$$

Thus, the gob height factor effectively reduces the gob stiffness to account for the greater effective thickness of the gob in relation to the seam thickness. For specifying the exact stress-strain curve of the linear elastic material in LAMODEL, only the elastic modulus (E) and the gob height factor (n) are required.

APPENDIX D - Analytical Steep Slope and Cliff Stability Calculations

Translational Slide Potential Analysis Spreadsheet

Design Case: Calibration

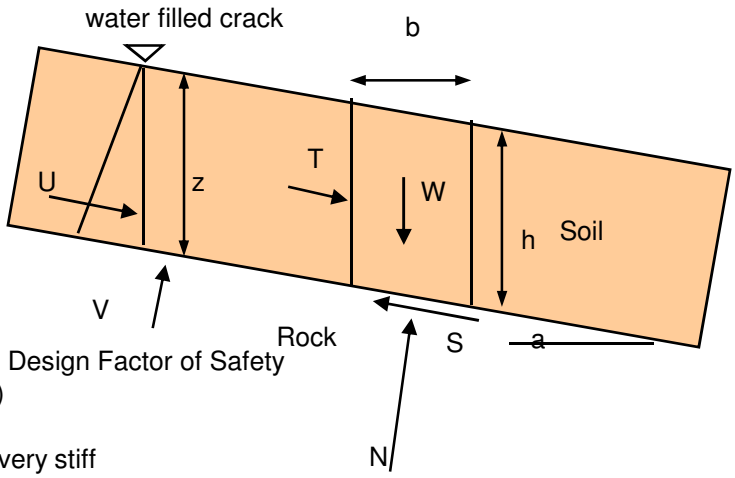

Input:

Slope Geometry:

h	0.5	m
b	1	m
a	30	degrees
z/h	1	
Fmin	1.25	Minimum Design Factor of Safety (see Key)

Soil Properties:

Type:	Sandy Clay (SC/CI), stiff-very stiff	
dry density	2	t/m3
mc(field)	0.1	Ww/Ws
mc(sat)	0.2	Ww/Ws

Drained Slope Strength Parameters

c'	5	kPa
phi'	28	degrees
field density	2.2	t/m3
sat density	2.4	t/m4

Key:

FoS Range	Slope Failure P
>2	Very Low
1.5 - 2	Low
1.25 - 1.5	Medium
1-1.25	High
<1	Very High

Stability Analysis Results:

Dry Slope Conditions:

W	10.78	KN/b	Weight of Soil Block
T	5.39	KN/b	Load
S	10.74	KN/b	Strength
FoS	1.99		Factor of Safety
Verdict:	OK		

Wet Slope (saturated):

W	11.76	KN/b	Weight of Soil Block
V	5.658	KN	Horizontal Water Force
T	5.88	KN/b	Load
S	8.18	KN/b	Strength
FoS	1.39		Factor of Safety
Verdict:	OK		

Wet Slope with Water Filled Crack:

W	11.76	KN/b	Weight of Soil Block
U	1.225	KN	Horizontal Water Force
V	5.658	KN/b	Uplift Water Force acting on sliding plane
T	6.94	KN/b	Load
S	8.18	KN/b	Strength
FoS	1.18		Factor of Safety
Verdict:	OK		

Translational

Design Case: Soil Cover Stability Analysis
Calibrated Material Strengths and Varying Soil Cover

Input:

Slope Geomet

h	0.2	0.5	1	1.5	2	2.5	3
b	1	1	1	1	1	1	1
a	35	35	35	35	35	35	35
z/h	1	1	1	1	1	1	1
Fmin	1.25	1.25	1.25	1.25	1.25	1.25	1.25

Soil Properties

Type:	Clayey Sand (SC), stiff-very stiff						
dry density	2	2	2	2	2	2	2
mc(field)	0.1	0.1	0.1	0.1	0.1	0.1	0.1
mc(sat)	0.2	0.2	0.2	0.2	0.2	0.2	0.2
Drained Slope							
c'	5	5	5	5	5	5	5
phi'	28	28	28	28	28	28	28
field density	2.2	2.2	2.2	2.2	2.2	2.2	2.2
sat density	2.4	2.4	2.4	2.4	2.4	2.4	2.4

Stability Analy

Dry Slope Cond

W	4.31	10.78	21.56	32.34	43.12	53.90	64.68
T	2.47	6.18	12.37	18.55	24.73	30.92	37.10
S	7.98	10.80	15.49	20.19	24.88	29.58	34.28
FoS	3.23	1.75	1.25	1.09	1.01	0.96	0.92
Verdict:	OK	OK	OK	Not OK	Not OK	Not OK	Not OK

Wet Slope (sat

W	4.70	11.76	23.52	35.28	47.04	58.80	70.56
V	2.393	5.982	11.964	17.945	23.927	29.909	35.891
T	2.70	6.75	13.49	20.24	26.98	33.73	40.47
S	6.88	8.05	9.99	11.93	13.87	15.81	17.75
FoS	2.55	1.19	0.74	0.59	0.51	0.47	0.44
Verdict:	OK	OK	Not OK	Not OK	Not OK	Not OK	Not OK

Wet Slope with

W	4.70	11.76	23.52	35.28	47.04	58.80	70.56
U	0.196	1.225	4.9	11.025	19.6	30.625	44.1
V	2.393	5.982	11.964	17.945	23.927	29.909	35.891
T	2.86	7.75	17.50	29.27	43.04	58.81	76.60
S	6.88	8.05	9.99	11.93	13.87	15.81	17.75
FoS	2.41	1.04	0.57	0.41	0.32	0.27	0.23
Verdict:	OK	OK	Not OK	Not OK	Not OK	Not OK	Not OK

Translational S

Design Case: **Mining impact - Western Slopes**
Calibrated Material Strengths

Input:

		Tilt						
	mm/m	0	2	5	10	15	20	30
Slope Geomet	degrees	0.00	0.11	0.29	0.57	0.86	1.15	1.72
h		0.5	0.5	0.5	0.5	0.5	0.5	0.5
b		1	1	1	1	1	1	1
a		25.00	25.11	25.29	25.57	25.86	26.15	26.72
z/h		1	1	1	1	1	1	1
Fmin		1.25	1.25	1.25	1.25	1.25	1.25	1.25

Soil Properties

Type:	Clayey Sand (SC), stiff-very stiff							
dry density	2	2	2	2	2	2	2	
mc(field)	0.1	0.1	0.1	0.1	0.1	0.1	0.1	
mc(sat)	0.2	0.2	0.2	0.2	0.2	0.2	0.2	
Drained Slope								
c'	5	5	5	5	5	5	5	
phi'	28	28	28	28	28	28	28	
field density	2.2	2.2	2.2	2.2	2.2	2.2	2.2	
sat density	2.4	2.4	2.4	2.4	2.4	2.4	2.4	

Stability Analy

Dry Slope Cond							
W	10.78	10.78	10.78	10.78	10.78	10.78	10.78
T	4.56	4.58	4.60	4.65	4.70	4.75	4.85
S	10.71	10.71	10.71	10.71	10.71	10.72	10.72
FoS	2.35	2.34	2.33	2.30	2.28	2.26	2.21
Verdict:	OK	OK	OK	OK	OK	OK	OK
Wet Slope (sat							
W	11.76	11.76	11.76	11.76	11.76	11.76	11.76
V	5.407	5.412	5.419	5.432	5.445	5.459	5.486
T	4.97	4.99	5.02	5.08	5.13	5.18	5.29
S	8.31	8.31	8.30	8.30	8.29	8.28	8.27
FoS	1.67	1.66	1.65	1.63	1.62	1.60	1.56
Verdict:	OK	OK	OK	OK	OK	OK	OK
Wet Slope with							
W	11.76	11.76	11.76	11.76	11.76	11.76	11.76
U	1.225	1.225	1.225	1.225	1.225	1.225	1.225
V	5.407	5.412	5.419	5.432	5.445	5.459	5.486
T	6.08	6.10	6.13	6.18	6.23	6.28	6.38
S	8.31	8.31	8.30	8.30	8.29	8.28	8.27
FoS	1.37	1.36	1.35	1.34	1.33	1.32	1.30
Verdict:	OK	OK	OK	OK	OK	OK	OK

Translational S

Design Case: **Mining Impact - Northern and Southern Slopes**
Calibrated Material Strengths

Input:

		Tilt						
	mm/m	0	2	5	10	15	20	30
Slope Geomet	degrees	0.00	0.11	0.29	0.57	0.86	1.15	1.72
h		0.5	0.5	0.5	0.5	0.5	0.5	0.5
b		1	1	1	1	1	1	1
a		20.00	20.11	20.29	20.57	20.86	21.15	21.72
z/h		1	1	1	1	1	1	1
Fmin		1.25	1.25	1.25	1.25	1.25	1.25	1.25
Soil Properties								
Type:		Clayey Sand (SC), stiff-very stiff						
dry density		2	2	2	2	2	2	2
mc(field)		0.1	0.1	0.1	0.1	0.1	0.1	0.1
mc(sat)		0.2	0.2	0.2	0.2	0.2	0.2	0.2
Drained Slope								
c'		5	5	5	5	5	5	5
phi'		28	28	28	28	28	28	28
field density		2.2	2.2	2.2	2.2	2.2	2.2	2.2
sat density		2.4	2.4	2.4	2.4	2.4	2.4	2.4

Stability Analy

Dry Slope Cond								
W		10.78	10.78	10.78	10.78	10.78	10.78	10.78
T		3.69	3.71	3.74	3.79	3.84	3.89	3.99
S		10.71	10.71	10.71	10.71	10.71	10.71	10.71
FoS		2.90	2.89	2.86	2.83	2.79	2.75	2.68
Verdict:		OK	OK	OK	OK	OK	OK	OK
Wet Slope (sat								
W		11.76	11.76	11.76	11.76	11.76	11.76	11.76
V		5.214	5.218	5.224	5.234	5.244	5.254	5.274
T		4.02	4.04	4.08	4.13	4.19	4.24	4.35
S		8.42	8.42	8.42	8.41	8.41	8.40	8.39
FoS		2.09	2.08	2.06	2.04	2.01	1.98	1.93
Verdict:		OK	OK	OK	OK	OK	OK	OK
Wet Slope with								
W		11.76	11.76	11.76	11.76	11.76	11.76	11.76
U		1.225	1.225	1.225	1.225	1.225	1.225	1.225
V		5.214	5.218	5.224	5.234	5.244	5.254	5.274
T		5.17	5.19	5.23	5.28	5.33	5.38	5.49
S		8.42	8.42	8.42	8.41	8.41	8.40	8.39
FoS		1.63	1.62	1.61	1.59	1.58	1.56	1.53
Verdict:		OK	OK	OK	OK	OK	OK	OK

Translational Cliff Slide on Bedding Parting

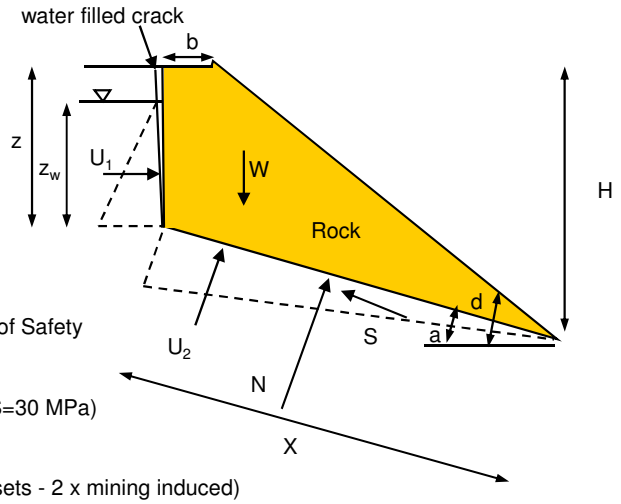

Design Case: Dry and Wet Conditions

Input:

Slope Geometry:

H	15	m
a	3	degrees
d	75	degrees
z_w/z	0	
Fmin	1.25	Minimum Factor of Safety
Earthquake acc'n	0	(see Key)

Rock Strength Properties:

Type:	Sandstone/Conglomerate (UCS=30 MPa)	
dry density	2.5	t/m3
UCS	30	MPa
GSI	50	Good/Fair (4 jnt sets - 2 x mining induced)
D	1	Damage Factor
mi	13	
mb	0.4	
s	0.0	
a	0.5	
UCS'	2.4	MPa
UTS'	0.0	MPa
phi(rock fabric)	35	degrees
c(rock fabric)	616	kPa

Key:

FoS Range	Slope Failure Potential	
>2	Very Low	
1.5 - 2	Low:	Average strengths
1.25 - 1.5	Medium:	Lower bound strengths
1-1.25	High:	Earthquake
<1	Very High	

Discontinuity Properties:

Contact Lithology	sandstone on shale	
Surface:	smooth/planar	
inc	0	roughness angle
cj	0	kPa
phij (basic)	15	degrees
phij+inc	15	degrees

Roughness	Angle (degrees)
slickensided	0
smooth	2
rough	6
steps	10
very rough	14

Stability Analysis Results:

zmin	13.22	Maximum crack depth (m)
bmin	29.90	Maximum Crack distance from crest (m)
Xmin	33.96	m
bmax	282.20	m
Option (1 or 2)	**1**	1=Optimum conditions; 2 = b set by User
b	1.00	
z	14.74	m
X	5.03	m

Bedding Slip:

W	10987.49	KN/b	Weight of Soil Block
U1	0.00	KN	Water Force (lateral)
U2	0.00	KN	Water Force (uplift)
T	575.04	KN/b	Load
S	2940.05	KN/b	Strength
FoS	5.11		Factor of Safety
Verdict:	OK		

Rockmass Failure:

phicrit	62.5	degrees	
z	4.24	m	
b	1.58	m	
X	12.13	m	
W	581.73	KN/b	Weight of Soil Block
U1	0.00	KN	Water Force (lateral)
U2	0.00	KN	Water Force (uplift)
T	516.00	KN/b	Load
S	7658.50	KN/b	Strength
FoS	14.84		Factor of Safety
Verdict:	OK		

Translational Cliff

Pre and Post-Mining - Dry Conditions

Design Case: Residual Shear Strengths Assumed

Input:	Tilt (mm/m)						
	0	5	10	15	20	25	30
Slope Geometry:	0.0	0.3	0.6	0.9	1.1	1.4	1.7
H	15	15	15	15	15	15	15
a	3.0	3.3	3.6	3.9	4.1	4.4	4.7
d	75.0	75.3	75.6	75.9	76.1	76.4	76.7
z_w/z	0	0	0	0	0	0	0
Fmin	1.25	1.25	1.25	1.25	1.25	1.25	1.25
Earthquake acc'n	0	0	0	0	0	0	0
Rock Strength Prc							
Type:	Sandstone/Conglomerate (UCS=30 MPa)						
dry density	2.5	2.5	2.5	2.5	2.5	2.5	2.5
UCS	30	30	30	30	30	30	30
GSI	50	50	50	50	50	50	50
D	1	1	1	1	1	1	1
mi	13	13	13	13	13	13	13
mb	0.4	0.4	0.4	0.4	0.4	0.4	0.4
s	0.0	0.0	0.0	0.0	0.0	0.0	0.0
a	0.5	0.5	0.5	0.5	0.5	0.5	0.5
UCS'	2.4	2.4	2.4	2.4	2.4	2.4	2.4
UTS'	0.0	0.0	0.0	0.0	0.0	0.0	0.0
phi(rock fabric)	35	35	35	35	35	35	35
c(rock fabric)	616	616	616	616	616	616	616
Discontinuity Prop							
Contact Lithology	sandstone on shale						
Surface:	smooth/planar						
inc	0	0	0	0	0	0	0
cj	0	0	0	0	0	0	0
phij (basic)	15	15	15	15	15	15	15
phij+inc	15	15	15	15	15	15	15
Stability Analysis							
zmin	13.22	13.16	13.10	13.04	12.99	12.95	12.91
bmin	29.90	28.14	26.59	25.21	23.97	22.85	21.83
Xmin	33.96	32.13	30.51	29.05	27.74	26.55	25.45
bmax	282.20	257.28	236.37	218.57	203.24	189.91	178.19
Option (1 or 2)	**1**	**1**	**1**	**1**	**1**	**1**	**1**
b	5.00	5.00	5.00	5.00	5.00	5.00	5.00
z	14.53	14.49	14.45	14.41	14.37	14.33	14.30
X	9.03	8.95	8.88	8.80	8.72	8.65	8.57
Bedding Slip:							
W	10987.49	10340.74	9771.12	9264.11	8808.78	8396.67	8021.14
U1	0.00	0.00	0.00	0.00	0.00	0.00	0.00
U2	0.00	0.00	0.00	0.00	0.00	0.00	0.00
T	575.04	592.82	608.93	623.55	636.82	648.87	659.80
S	2940.05	2766.24	2613.07	2476.68	2354.13	2243.15	2141.97
FoS	5.11	4.67	4.29	3.97	3.70	3.46	3.25
Verdict:	OK	OK	OK	OK	OK	OK	OK
Rockmass Failure							
phicrit	62.5	62.5	62.5	62.5	62.5	62.5	62.5
z	4.24	4.35	4.46	4.56	4.68	4.79	4.90
b	1.58	1.61	1.63	1.65	1.68	1.70	1.72
X	12.13	12.01	11.89	11.76	11.64	11.51	11.39
W	581.73	590.56	599.17	607.53	615.65	623.52	631.14
U1	0.00	0.00	0.00	0.00	0.00	0.00	0.00
U2	0.00	0.00	0.00	0.00	0.00	0.00	0.00
T	516.00	523.84	531.47	538.89	546.09	553.07	559.82
S	7658.50	7586.37	7513.61	7440.19	7366.08	7291.27	7215.74
FoS	14.84	14.48	14.14	13.81	13.49	13.18	12.89
Verdict:	OK	OK	OK	OK	OK	OK	OK

Translational Cliff

	Pre and Post-Mining - Wet Conditions						
Design Case:	Initial beddin dip of 3o + waterfilled crack						
Input:	Tilt (mm/m)						
	0	5	10	15	20	25	30
Slope Geometry:	0.0	0.3	0.6	0.9	1.1	1.4	1.7
H	15	15	15	15	15	15	15
a	3.0	3.3	3.6	3.9	4.1	4.4	4.7
d	75.0	75.3	75.6	75.9	76.1	76.4	76.7
z_w/z	1	1	1	1	1	1	1
Fmin	1.25	1.25	1.25	1.25	1.25	1.25	1.25
Earthquake acc'n	0	0	0	0	0	0	0
Rock Strength Prc							
Type:	Sandstone/Conglomerate (UCS=30 MPa)						
dry density	2.5	2.5	2.5	2.5	2.5	2.5	2.5
UCS	30	30	30	30	30	30	30
GSI	50	50	50	50	50	50	50
D	1	1	1	1	1	1	1
mi	13	13	13	13	13	13	13
mb	0.4	0.4	0.4	0.4	0.4	0.4	0.4
s	0.0	0.0	0.0	0.0	0.0	0.0	0.0
a	0.5	0.5	0.5	0.5	0.5	0.5	0.5
UCS'	2.4	2.4	2.4	2.4	2.4	2.4	2.4
UTS'	0.0	0.0	0.0	0.0	0.0	0.0	0.0
phi(rock fabric)	35	35	35	35	35	35	35
c(rock fabric)	616	616	616	616	616	616	616
Discontinuity Prop							
Contact Lithology	sandstone on shale						
Surface:	smooth/planar						
inc	0	0	0	0	0	0	0
cj	0	0	0	0	0	0	0
phij (basic)	15	15	15	15	15	15	15
phij+inc	15	15	15	15	15	15	15
Stability Analysis							
zmin	13.22	13.16	13.10	13.04	12.99	12.95	12.91
bmin	29.90	28.14	26.59	25.21	23.97	22.85	21.83
Xmin	33.96	32.13	30.51	29.05	27.74	26.55	25.45
bmax	282.20	257.28	236.37	218.57	203.24	189.91	178.19
Option (1 or 2)	**1**	**1**	**1**	**1**	**1**	**1**	**1**
b	5.00	5.00	5.00	5.00	5.00	5.00	5.00
z	14.53	14.49	14.45	14.41	14.37	14.33	14.30
X	9.03	8.95	8.88	8.80	8.72	8.65	8.57
Bedding Slip:							
W	10987.5	10340.7	9771.1	9264.1	8808.8	8396.7	8021.1
U1	856.69	848.36	840.74	833.78	827.39	821.55	816.20
U2	2200.51	2071.56	1958.03	1857.03	1766.38	1684.37	1609.68
T	1430.55	1439.78	1448.04	1455.43	1462.05	1467.97	1473.24
S	2338.41	2198.13	2074.38	1964.05	1864.80	1774.82	1692.67
FoS	1.63	1.53	1.43	1.35	1.28	1.21	1.15
Verdict:	OK	OK	OK	OK	OK	Not OK	Not OK
Rockmass Failure							
phicrit	62.5	62.5	62.5	62.5	62.5	62.5	62.5
z	4.24	4.35	4.46	4.56	4.68	4.79	4.90
b	1.58	1.61	1.63	1.65	1.68	1.70	1.72
X	12.13	12.01	11.89	11.76	11.64	11.51	11.39
W	581.73	590.56	599.17	607.53	615.65	623.52	631.14
U1	88.02	92.57	97.26	102.11	107.11	112.28	117.61
U2	251.97	255.79	259.52	263.14	266.66	270.07	273.37
T	556.64	566.58	576.38	586.03	595.55	604.91	614.13
S	7427.40	7349.77	7271.48	7192.51	7112.84	7032.43	6951.28
FoS	13.34	12.97	12.62	12.27	11.94	11.63	11.32
Verdict:	OK	OK	OK	OK	OK	OK	OK

APPENDIX E - Cliff Line Impact Assessment Details (ACARP, 2002)

10. The Assessment of Mining Impacts on Clifflines

This section presents methods that can be used for the assessment of mining impacts on clifflines and for predicting the likelihood of rockfalls.

10.1. Introduction

The method described in the final report on Stage 1 of this research project, for assessing the impacts of mining on clifflines, involved classifying the cliffs under four separate categories, namely:

1. Overall size and noticeable characteristics of the cliff.
2. Aesthetic quality and degree of public exposure.
3. Natural instability of the cliff formation.
4. Extent of the mining-induced ground movements.

The method covered a wide range of alternatives, but was essentially based on cliffs in the Southern Coalfield with heights up to 100 metres. All other cliffs above this height were included in a single group for the purposes of assessing the impacts.

An alternative, but similar, method of assessment was described by Radloff and Mills, Ref. 7.7, 2001, which classified the cliffs under four separate assessment categories, namely:

1. Physical characteristics.
2. Geological and mining characteristics.
3. Association with environmental features.
4. Human use aesthetics.

The method described by the authors included ratings for cliffs greater than 150 metres in height, which made the method more applicable to the Western Coalfield, where some very high cliffs exist. Since the two methods had many features in common, it was decided to integrate them, and, in that way, arrive at a single method that could have more universal application.

10.2. Development of the Method of Assessment

There was a certain amount of overlap between the first three categories and the method has, therefore, been amended and simplified, by the removal of Category 1, to avoid duplication of factors like cliff height, face length, face angle etc., which appeared in both Category 1 and Category 3. Other factors in Category 1, under the heading notable characteristics, were related to the appearance, and hence the aesthetic qualities, of the cliffs and these factors have been transferred to Category 2. The remainder of the factors, which could affect cliff stability, have been transferred to Category 3.

At the same time, the categories have been extended to include a wider range of values for each of the factors, extending the range of application of the method to include some of the higher cliffs that exist in the Western Coalfield.

The method therefore now employs only three classification categories and these are shown in Tables 10.1 to 10.3 below. Table 10.1 covers various factors that affect the extent of the mining-induced ground movements. Table 10.2 covers various factors that affect the aesthetic quality and degree of public exposure of the clifflines. Table 10.3 covers various factors that affect the natural instability of the cliff formation.

Table 10.1. Extent of the Mining-Induced Ground Movements

Score for each factor	0	1	2	4	6	Weighting
Mining induced vertical subsidence at the cliff	< 50 mm	< 100 mm	100 to 200 mm	200 to 500 mm	> 500 mm	**5**
Mining induced horizontal movement at the cliff	< 50 mm	50 to 100 mm	100 to 200 mm	200 to 300 mm	> 300 mm	**5**
Mining induced tilt at the cliff	< 1 mm/m	< 4 mm/m	< 7 mm/m	< 10 mm/m	> 10 mm/m	**5**
Mining induced strain at the cliff	< 1 mm/m	< 2 mm/m	< 5 mm/m	< 10 mm/m	> 10 mm/m	**5**
Depth of cover at the base of the cliff	> 400 m	300 to 400 m	200 to 300 m	100 to 200 m	< 100 m	**10**

Table 10.2. Aesthetic Quality and Degree of Public Exposure

Score for each factor	0	1	2	4	6	Weighting
Overall aesthetics of cliff formation	common	pleasant	distinctive	superb	spectacular	**20**
Ease of public viewing	very hard to view	hard to `view	easy to view from gravel roads	easy to view from sealed roads	tourist location	**10**
Overall height of cliff	<50m	50m to 75m	75m to 100m	> 100m	> 150m	**10**
Cliff type	rounded rock face with large talus slope	rounded rock face with minimal talus	sheer rock face with large talus	sheer rock face with minimal talus	sheer rock face with no talus	**5**
Shape of cliff face	rounded rock face	sheer rock face	sheer rock face with pagodas	sheer rock face with slender spires	Large overhangs notches or recesses	**5**
Location of cliff relative to others	Single feature	1 or 2 features	3 to 5 features	Major cliff line	Part of escarpment	**5**
Presence of archaeological sites	not related	related to a possible habitation site/s	related to a known habitation site/s	related to a prominent archaeological site/s	prominent shelter site/s with significant art	**10**
Ease of public walking access to cliff base areas exposed to rock falls	limited access, walk > 10km, no public walkways	access by walking >3km, no public walkways	access by walking >500 m, no public walkways	access by walking <500m, no public walkways	access by walking <500m, public walkways	**2**
Ease of public walking access to potentially unstable cliff top areas	limited access, walk > 10km, no public walkways	access by walking >3km, no public walkways	access by walking >500 m, no public walkways	access by walking <500m, no public walkways	access by walking <500m, public walkways	**2**
Ease of public vehicular access to cliff base areas exposed to rock falls	road access greater than 500m	road access less than 500m	4WD road access under cliff	unsealed road access under cliff	sealed road access under cliff	**5**
Ease of public vehicular access to potentially unstable cliff top areas	road access greater than 500m	road access within 500m	4WD road access to clifftop	unsealed road access to clifftop	sealed road access to clifftop	**5**
Buildings/structures above cliff face	within 10 km	within 5 km	within 1 km	within 100m	within 20m	**2**
Buildings/structures below cliff face	within 10 km	within 5 km	within 1 km	within 100m	within 20m	**5**
Dwellings above cliff face	within 10 km	within 5 km	within 1 km	within 100m	within 20m	**10**
Dwellings below cliff face	within 10 km	within 5 km	within 1 km	within 100m	within 20m	**20**

Table 10.3 Natural Instability of the Cliff Formation

Score for each factor	0	1	2	4	6	Weighting
Overall height of talus, cliff face, and crest slope.	< 50m	50m to 75m	75m to 100m	> 100m	> 150m	**2**
Cliff face height	< 20m	20m to 50m	50m to 75m	75m to 100m	> 100m	**5**
Talus slope height	< 20m	20m to 50m	50m to 75m	75m	> 100m	**1**
Cliff face length, or width	< cliff height	> cliff height	> 2 x cliff height	> 5 x cliff height	> 10 x cliff height	**4**
Cliff face angle	< 70o	> 70o	> 80o	> 90o	> 100o	**4**
Talus slope angle of repose	< 15o 1 in 3.73	> 15o 1 in 3.73	> 30o 1 in 1.73	> 40o 1 in 1.2	> 45o 1 in 1	**1**
Vegetation cover on cliff areas	dense vegetation and trees on talus and cliff	dense vegetation on talus and sparse vegetation on cliff	dense vegetation and trees on talus, none on cliff	sparse vegetation and trees on talus, none on cliff	no vegetation or trees on talus or cliffs	**2**
Degree of undercutting or weathering	clean sheer rock face	sheer rock face with small overhangs up to 1m	face with honeycomb weathering and small overhangs up to 2m	delicate honeycomb face or large overhangs i.e. 2m to 4m	delicate honeycomb face or large overhangs > 4m	**5**
Extent of horizontal jointing on cliff face	clean rock face no joints	minimal jointing > 20m	moderately jointed 10m to 20m	heavily jointed < 10m	Severely jointed < 5m	**5**
Extent of vertical jointing on cliff face	no continuous joints	joints continuing over several strata layers	continuously jointed over full height of cliff	several continuous joint systems	continuous open joints or fissures	**3**
In situ horizontal stress at seam level	< 10 MPa	10 to 20 MPa	20 to 30 MPa	30 to 40 MPa	> 40 MPa	**5**
Type of rock strata – rock strength	UCS >100 MPa	UCS > 75 < 100 MPa	UCS > 50 < 75 MPa	UCS > 30 < 50 MPa	UCS < 30 MPa	**5**
Location of cliff in relation to watercourses and valleys	not related	related to small creeks and minor tributaries	related to bluffs lining small valleys	part of major cliff lines lining valleys with talus	part of major cliff lines in gorges or escarpments	**2**
Location of cliff in relation to geological anomalies	not related	related to small faults & dykes < 500 mm	related to continuous vertical jointing	related to major faults & dykes > 500 mm	related to major thrust faults > 500 mm	**2**
Degree of exposure to ongoing weathering agents	not exposed to winds or creeks or streams	partly sheltered from winds and creeks or streams	exposed to winds and to small creeks or streams	exposed to wind action and next to major river	exposed to strong wind action and next to major river	**2**
Presence of water flows at base of slope	no stream or creek	stream or creek with gradient of less than 1 in 100	stream or creek with gradient of more than 1 in 100	river or creek with gradient of more than 1 in 75	river or creek with gradient > 1 in 50	**3**
Presence of loose & unstable blocks on cliff	few unlikely to fall	few could possibly fall	many could possibly fall	few likely to fall	many likely to fall	**5**
Loose and unstable blocks on talus	few unlikely to fall	few could possibly fall	many could possibly fall	few likely to fall	many likely to fall	**2**
Presence of natural cracks in cliff crest	none	one	two or three	several	many	**5**
Orientation of natural cracks relative to cliff line	no cracks or 90o to 60o	60o to 40o	40o to 20o	10o to 20o	< 10o	**5**

10.3. Application of the Method of Assessment to each Category

These tables allow the impact to be assessed under each category, using a point scoring system in which each factor is given a score and a weighting. The scores for each factor are then multiplied by the weighting and the resultant numbers for each factor are added to give a total score for each category. The scores are then expressed as a proportion of the highest possible score for the category, which is obtained by adding all of the weightings and multiplying the total by 6, i.e. the highest possible score for each factor. The proportions are then used to determine the impact classifications under each category using Table 10.4.

Table 10.4. Impact Classifications

Proportion of maximum score	Ranking	Classification
0 - 0.1	1	insignificant
0.1 - 0.2	2	very low
0.2 - 0.3	3	low
0.3 - 0.4	4	moderate
0.4 - 0.5	5	high
0.5 - 0.6	6	very high
> 0.6	7	extremely high

The maximum score for Table 10.1 is 180. The maximum score for Table 10.2 is 696 and the maximum score for Table 10.3 is 408. If the score for a particular cliffline is an exact decimal proportion that puts it at the top of one classification or the bottom of the next classification, then, the higher classification should be used. Factors relating to the position of the cliffline relative to the longwall and the widths of panels and pillars are reflected in the levels of ground movement given in Table 10.1 and have not been included separately.

10.4. Preparation of an Overall Impact Assessment

The classifications under each category can be combined to give an overall impact assessment for each cliffline using Tables 10.5 to 10.11. These tables have been compiled based upon the observation that if the extent of mining is extremely high, then, no matter what the classifications are within the other categories, the overall impact can not be insignificant. Similarly even if the extent of mining is insignificant, the overall impact can be as high as moderate if the classifications under the other categories are either very high or extremely high.

Tables 10.5 to 10.11 represent each of the mining classifications from an extremely high mining impact to an insignificant mining impact. The overall impact can be determined by selecting the table for the appropriate level of mining impact and then using the x and y axes to represent the impact classifications for the other two characteristics. For example, assume the classifications are:

- Aesthetic quality and degree of public exposure very high
- Natural instability of the cliff formation high
- The extent of mining induced ground movement moderate

Then, the overall impact assessment can be obtained by selecting Table 10.8 for the moderate mining impact and by looking up the classification in the square where the very high column meets the high row. In this example, the overall impact would be extremely high.

It should be noted that the overall impact assessment is not a measure of the likelihood of rock falls. This is a function of the extent of the mining-induced ground movements and the natural instability of the cliffline, which is discussed further in Section 10.5, below.

Cliff Impact Assessment Tables for Different Levels of Mining Impact

Table 10.5 - Extremely High Mining impact

EH	EH	VH	H	M	L	VL	I
EH	EH	EH	EH	EH	EH	EH	M
VH	EH	EH	EH	EH	EH	EH	M
H	EH	EH	EH	EH	EH	VH	M
M	EH	EH	EH	EH	EH	H	L
L	EH	EH	EH	EH	H	M	L
VL	EH	EH	VH	H	M	L	VL
I	M	M	M	L	L	VL	VL

Table 10.6 - Very High Mining Impact

VH	EH	VH	H	M	L	VL	I
EH	EH	EH	EH	EH	EH	EH	M
VH	EH	EH	EH	EH	EH	VH	M
H	EH	EH	EH	EH	EH	H	L
M	EH	EH	EH	EH	VH	M	L
L	EH	EH	EH	VH	H	M	VL
VL	EH	VH	H	M	M	L	VL
I	M	M	L	L	VL	VL	VL

Table 10.7 - High Mining Impact

H	EH	VH	H	M	L	VL	I
EH	EH	EH	EH	EH	EH	VH	M
VH	EH	EH	EH	EH	EH	H	L
H	EH	EH	EH	EH	VH	H	L
M	EH	EH	EH	VH	H	M	L
L	EH	EH	VH	H	M	L	VL
VL	VH	H	H	M	L	L	VL
I	M	L	L	L	VL	VL	VL

Table 10.8 - Moderate Mining Impact

M	EH	VH	H	M	L	VL	I
EH	EH	EH	EH	EH	EH	H	L
VH	EH	EH	EH	EH	VH	M	L
H	EH	EH	EH	EH	H	M	L
M	EH	EH	EH	H	M	L	VL
L	EH	VH	H	M	L	L	VL
VL	H	M	M	L	L	VL	VL
I	L	L	L	VL	VL	VL	I

Table 10.9 - Low Mining Impact

L	EH	VH	H	M	L	VL	I
EH	EH	EH	EH	EH	H	M	L
VH	EH	EH	EH	VH	H	M	VL
H	EH	EH	VH	H	M	L	VL
M	EH	VH	H	M	M	L	VL
L	H	H	M	M	L	VL	VL
VL	M	M	L	L	VL	VL	VL
I	L	VL	VL	VL	VL	VL	I

Table 10.10 - Very Low Mining Impact

VL	EH	VH	H	M	L	VL	I
EH	EH	EH	VH	H	M	L	VL
VH	EH	VH	H	M	M	L	VL
H	VH	H	H	M	L	L	VL
M	H	M	M	L	L	VL	VL
L	M	M	L	L	VL	VL	VL
VL	L	L	L	VL	VL	VL	I
I	VL	VL	VL	VL	VL	I	I

Table 10.11 - Insignificant Mining Impact

I	EH	VH	H	M	L	VL	I
EH	M	M	M	L	L	VL	VL
VH	M	M	L	L	VL	VL	VL
H	M	L	L	L	VL	VL	VL
M	L	L	L	VL	VL	VL	I
L	L	VL	VL	VL	VL	VL	I
VL	VL	VL	VL	VL	VL	I	I
I	VL	VL	VL	I	I	I	I

The impact assessments are to a certain extent subjective, but the factors used in each category have been quantified, to reduce the subjectivity as far as possible. The method has been designed to provide an overall assessment of the impacts taking into account the extent of the mining-induced ground movements, the aesthetic quality and degree of public exposure of the clifflines and the natural instability of the clifflines.

It is therefore possible that the overall impact could be assessed as moderate, if the quality of the cliffline and the cliff instability were relatively low, even though the likelihood of significant rock falls was very high,. Alternatively, it is possible that the overall impact could be assessed as very high, if the cliffs had a high aesthetic value and a high instability rating, even though the likelihood of rock falls was very low,.

The method has been tested over a wide range of cases and appears to give reasonable results, but it has been designed in such a way that the scores and weightings in the assessment tables can be changed to fine-tune the method in the light of local experience. The levels of impact that are obtained using the method are not intended to be prescriptive in terms of what is, or is not, acceptable in every case and each case must be considered on its merits. What might be acceptable in one mining area might not be acceptable in another. In many cases the acceptability of the impact might rest on the likely extent of damage due to rock falls. In others, the issue of public safety might be the overriding factor.

10.5. The likelihood of Rock Falls

The likelihood of a particular cliff collapse or rock fall is impossible to predict since the stability of the cliff can not be fully determined from the appearance of the rock face. In many cases the apparently unstable rocks will remain standing, whilst the apparently stable rocks will fall. It is clear, however, that rock falls are more likely to occur as the extent of the mining impact increases, particularly where the natural instability of the cliffline is high. It is, therefore, possible to predict the likely extent of rock falls from a statistical perspective.

In the graph shown in Fig. 10.1, the percentages of the lengths of clifflines that experienced rock falls have been plotted against the natural cliff instability classification for a number of recorded cases. It should be noted that there was only one case where 100% of a cliffline experienced falls. All other cases were less than 33%. It can be seen that the percentage of clifflines that experienced rock falls increased as the mining impact increased and as the cliff instability increased. This graph can be used to predict the upper-bound % damage to clifflines based upon the scores from Tables 10.1 and 10.3. For example, if the proportion of mining-induced ground movement, assessed from Table 10.1, was 0.4 and the natural instability of the cliffline was low, then, up to 21% of the cliffline could experience rockfalls.

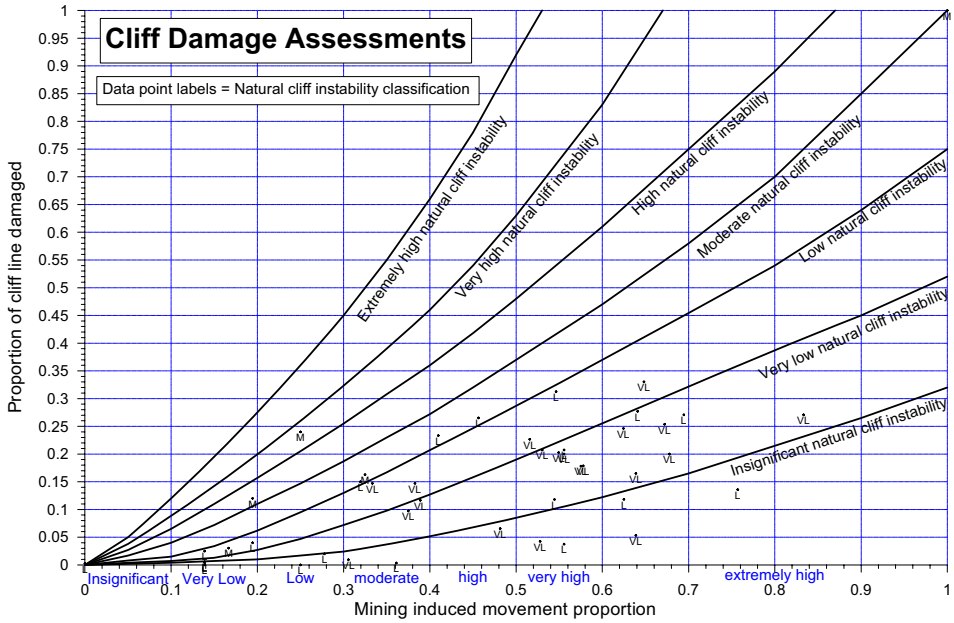

Fig. 10.1 Graph showing the likely incidence of rock falls for different levels of mining impact and different levels of cliffline instability.

It should be noted that the data used in developing the graph shown in Fig 10.1 were from the Southern and Western Coalfields and may not be representative of clifflines elsewhere. It should also be noted that the curves in this graph are upper-bound curves and in many cases the percentage of damage to clifflines could be significantly less than the maximum indicated by the graph. Similar graphs could advantageously be developed for specific mining areas where sufficient local data are available.

10.6. Testing of the method of assessment for subsidence impacts on clifflines

The method of assessment described above has been used to assess the subsidence impacts on a wide variety of clifflines including the following locations:

1. The Cataract and Nepean Gorges over Longwalls 15 to 17 at Tower Colliery.
2. The Bargo River Valley over Longwalls 14 to 19 at Tahmoor Colliery.
3. The Burragorang Valley over pillar extractions at Nattai North Colliery.
4. The clifflines of a tributary of Bullen Creek over Longwall 6 at Baal Bone Colliery.
5. The clifflines of the escarpment over Longwalls 1 to 7 at Angus Place Colliery.
6. The clifflines of the escarpment over Longwalls 8 to 11 at Angus Place Colliery.

The results of some of these analyses are shown in Table 10.12, below.

Photographs of typical cliffs at Tower Colliery, Tahmoor Colliery, Nattai North Colliery, Baal Bone Colliery and Angus Place Colliery are shown in Figs. 10.2 to 10.6, below.

Table 10.12 Some Examples of Cliff Assessment Results

	Tower Colliery Longwall 15	Tahmoor Colliery Longwall 17	Nattai North Pillar Extraction	Baal Bone Colliery Longwall 6	Angus Place Colliery Longwall 7	Angus Place Colliery Longwall 9
Aesthetic Quality	Very Low	Very Low	High	Very low	Low	Low
Natural Instability	Low	Low	Moderate	Very Low	Very Low	Low
Mining Impact	Very Low	Low	Extremely high	Extremely High	Moderate	Very High
Mining Impact Proportion	0.14	0.25	1.00	0.83	0.33	0.56
Overall Assessment	Very Low	Low	Extremely high	Low	Low	High
%Rock Falls	<2.5%	Nil	100%	27%	15%	21%

The cliffs at Baal Bone Colliery were rated as distinctive in terms of the overall aesthetics of the cliff formation, but had a very low total rating for the aesthetic quality and public exposure because of its remote location and relative inaccessibility. Similarly the cliffs at Angus Place Colliery were rated as pleasant in terms of the overall aesthetics of the cliff formation, but had a low total rating for the aesthetic quality and public exposure because of its remote location and relative inaccessibility.

In contrast, the cliffs at Nattai North Colliery were rated as spectacular in terms of the overall aesthetics of the cliff formation and had a high total rating for the aesthetic quality and public exposure because the cliffs can be easily viewed from a public road.

The cliffs at Tower Colliery and Tahmoor Colliery were generally rated as common or pleasant in terms of the overall aesthetics of the cliff formation, but had an insignificant to low total rating for the aesthetic quality and public exposure because the cliffs are not readily accessible to the public.

It can be seen that the greatest amount of damage occurred at the Nattai North Colliery even though the mining impact was also assessed to be extremely high at Baal Bone Colliery over Longwall 6. The reason for this is that the cliffs at Nattai North Colliery had a higher natural instability due to the massive scale of the cliffline, its exposure to ongoing weathering agents and the fact that the base of the cliff was directly undermined.

Fig. 10.2 Cliffs in the Cataract Gorge over Longwall 15 at Tower Colliery.

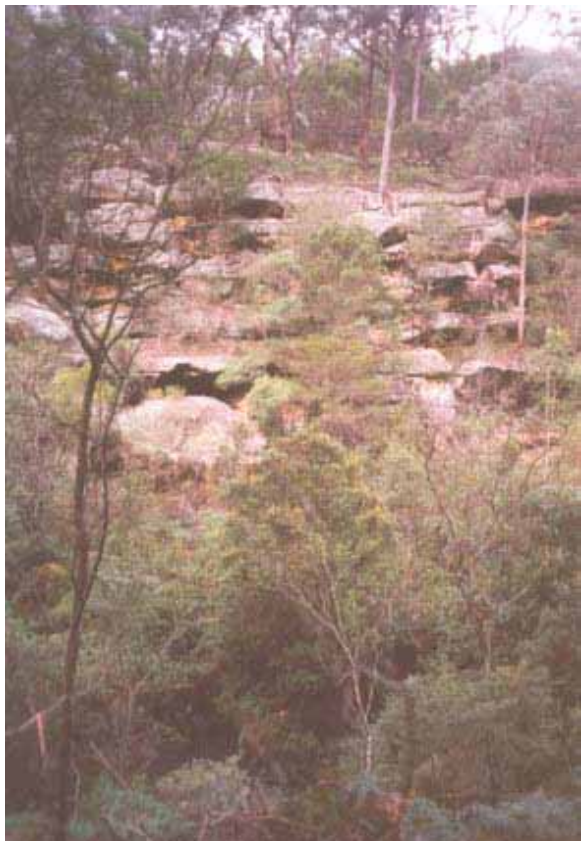

Fig. 10.3 Cliffs in the Bargo River Valley over Longwall 17 at Tahmoor colliery

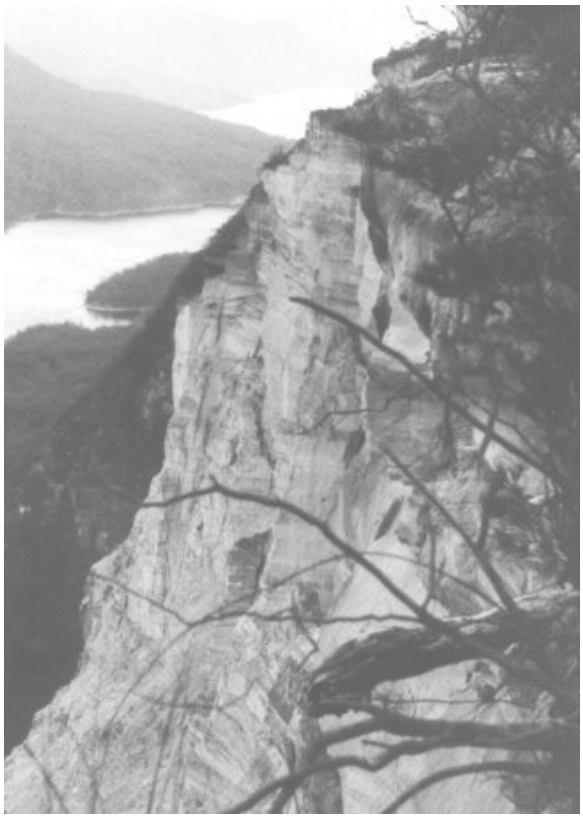

Fig. 10.4 Cliffs in the Burragorang Valley over Pillar Extractions at Nattai Colliery

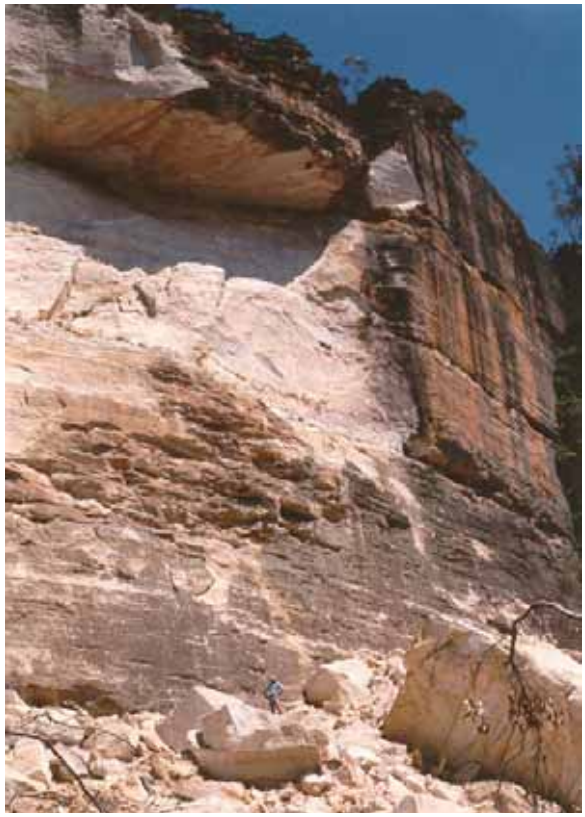

Fig. 10.5 Cliffs in a Tributary of Bullen Creek over Longwall 6 at Baal Bone colliery

Fig. 10.6 Cliffs over Longwall 2 at Angus Place Colliery

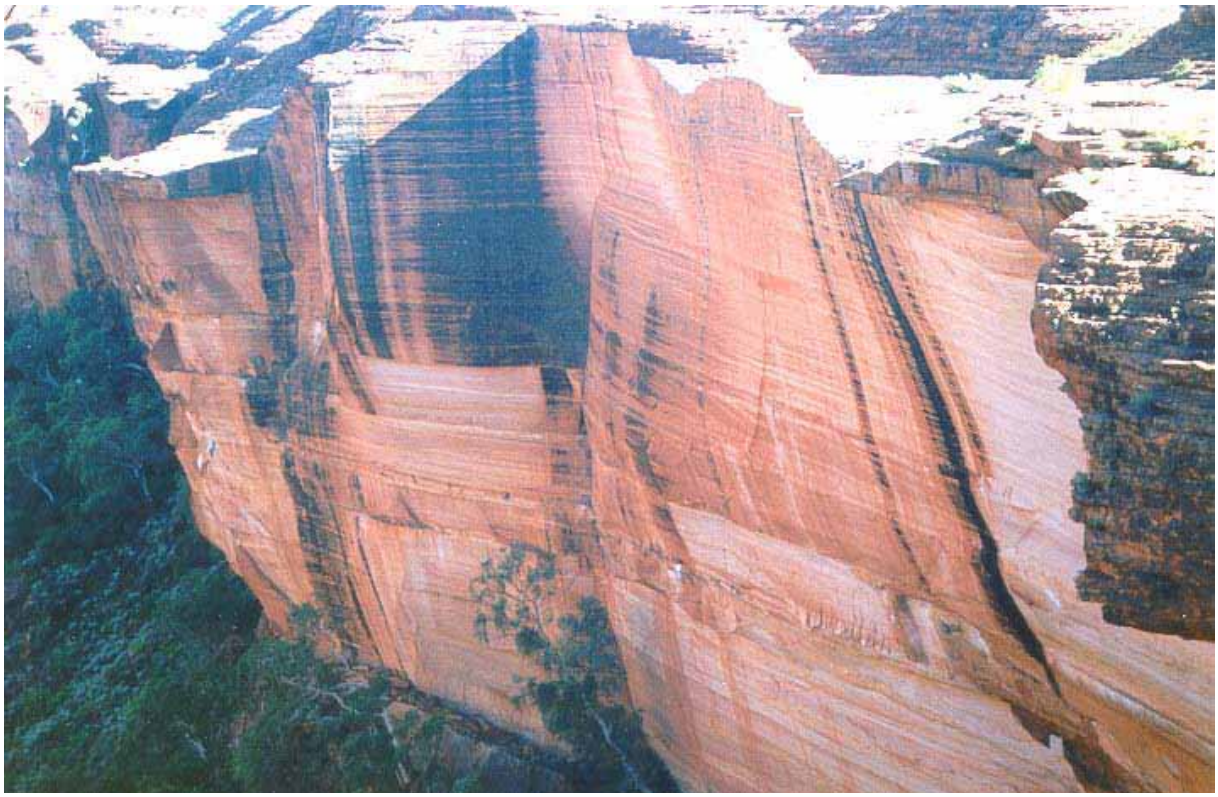

Fig. 10.7 Natural Rock Fall at Kings Canyon in Central Australia

The photographs in Figs. 10.1 and 10.4 to 10.6 show typical examples of rock falls that have occurred due to mining and indicate the immediate scarring of the landscape that occurs. Fig. 10.6, however, shows the natural regrowth that occurred on the talus slope within a period of ten years following the rock fall at Angus Place Colliery and it can be seen that nature quickly heals the scars.

For comparison, Fig. 10.7 shows a natural rock fall which occurred several years ago at Kings Canyon in Central Australia, as part of the normal process of erosion in the wall of the canyon. The canyon is a popular tourist attraction and its appeal to visitors has not been adversely affected by the fresh appearance of the rock face.

APPENDIX F – Aboriginal Heritage Site Impact Assessment Details

Job: West Wallsend Colliery - Potential Impacts on Aboriginal Artifact Sites																
Site#	Site Name	Site Name	LW	MGA Easting	MGA Northing	Z	RLo	RLi	Final Subs	Final Tilt	Final Strain	Dynamic Strain	Cracking Potential*	Gradient Increase	Runoff Velocity	Erosion Increase
							m	m	m	mm/m	mm/m	mm/m		%	Increase(%)	Potential*
1	38-4-0097 AS	AS(38-4-0097)	38	363232	6351735	0	49.022	49.021	0.00	0	0.0	0.0	VL	0.0	0	VL
2	38-4-0098 AS	AS(38-4-0098)	40	362716	6350950	0	52.866	52.706	-0.16	13	5.4	2.7	H	-0.3	-6	VL
3	Artefact Scatter1	AS1	41	361718	6354088	0	164.899	164.769	-0.13	6	1.6	0.8	M	0.6	7	L
4	Aubes Ridhe Rd AS1	AS1(AR Rd)	41	362248	6351710	0	137.940	137.425	-0.52	18	2.9	1.4	H	1.0	10	L
5	Brunkerville Trail AS1	AS1(BT)	50	361019	6351212	0	293.547	293.499	-0.05	2	0.3	0.2	VL	-0.1	-2	M
6	Artefact Scatter 2	AS2	41	361560	6354493	0	178.234	178.233	0.00	0	0.0	0.0	VL	0.0	0	VL
7	Artefact Scatter 3	AS3	41	361551	6354540	0	182.521	182.520	0.00	0	0.0	0.0	VL	0.0	0	VL
8	Artefact Scatter 4	AS4	47	361531	6352044	0	300.949	299.942	-1.01	9	0.0	0.0	VL	0.8	9	L
9	Artefact Scatter 5	AS5	43	361698	6352637	0	285.785	284.355	-1.43	4	-1.4	0.7	L	-0.4	-6	L
10	Artefact Scatter 6	AS6	na	360999	6350504	0	93.367	93.366	0.00	0	0.0	0.0	VL	0.0	0	VL
11	Artefact Scatter 7	AS7	48	361640	6351078	0	141.514	140.854	-0.66	22	2.9	1.5	H	1.9	14	M
12	Artefact Scatter8	AS8	47	361689	6351152	0	148.396	148.246	-0.15	6	3.0	1.5	H	0.6	8	L
13	*GGs/38-4-0461*	*GG(38-4-0461)*	*47*	*361433*	*6352372*	*0*	*217.198*	*216.656*	*-0.54*	*14*	*2.3*	*1.2*	*H*	*0.1*	*2*	*VL*
14	*GG38-4-0462*	*GG(38-4-0462)*	*48*	*361205*	*6352319*	*0*	*199.140*	*199.062*	*-0.08*	*4*	*1.1*	*0.6*	*M*	*-0.1*	*-3*	*VL*
15	*Aubes Ridge GG1*	*GG1(AR Rd)*	*40*	*362444*	*6351755*	*0*	*89.290*	*89.000*	*-0.29*	*15*	*4.7*	*2.4*	*H*	*0.9*	*10*	*L*
16	*Bangalow Creek GG1*	*GG1(BC)*	*43*	*361578*	*6352591*	*0*	*269.276*	*268.494*	*-0.78*	*2*	*2.1*	*1.1*	*H*	*-0.1*	*-4*	*VL*
17	*Cockle Crk GG1*	*GG1(CC)*	*42*	*362055*	*6352271*	*0*	*168.499*	*168.125*	*-0.37*	*11*	*2.4*	*1.2*	*H*	*-0.7*	*-8*	*L*
18	*Diega Creek GG1*	*GG1(DC)*	*48*	*361579*	*6350994*	*0*	*113.800*	*112.012*	*-1.79*	*15*	*-6.7*	*3.4*	*H*	*1.1*	*10*	*M*
19	*Bangalow Creek GG2*	*GG2(BC)*	*43*	*361557*	*6352650*	*0*	*276.987*	*276.168*	*-0.82*	*2*	*1.3*	*0.6*	*M*	*0.0*	*-1*	*VL*
20	*Diega Creek GG2*	*GG2(DC)*	*42*	*361996*	*6351675*	*0*	*106.881*	*106.854*	*-0.03*	*1*	*1.9*	*1.0*	*M*	*-0.1*	*-2*	*VL*
21	*Bangalow Creek GG3*	*GG3(BC)*	*43*	*361505*	*6352672*	*0*	*281.296*	*280.179*	*-1.12*	*8*	*-0.1*	*0.1*	*VL*	*-0.6*	*0*	*L*
22	*Diega Creek GG3*	*GG3(DC)*	*43*	*361875*	*6351630*	*0*	*112.202*	*110.639*	*-1.56*	*22*	*-5.8*	*2.9*	*H*	*1.6*	*13*	*M*
23	*Bangalow Creek GG4*	*GG4(BC)*	*43*	*361602*	*6352681*	*0*	*281.697*	*280.631*	*-1.07*	*9*	*0.5*	*0.2*	*VL*	*0.2*	*4*	*VL*
24	*Bangalow Creek GG5*	*GG5(BC)*	*43*	*361592*	*6352524*	*0*	*266.626*	*265.870*	*-0.76*	*1*	*1.6*	*0.8*	*M*	*-0.1*	*-3*	*VL*
25	*Bangalow Creek GG6*	*GG6(BC)*	*48*	*361328*	*6352318*	*0*	*201.916*	*200.963*	*-0.95*	*7*	*-2.3*	*1.1*	*M*	*0.0*	*1*	*VL*
26	*GGRange1*	*GGR1*	*43*	*361579*	*6352486*	*0*	*255.238*	*254.453*	*-0.79*	*6*	*2.4*	*1.2*	*M*	*0.4*	*-6*	*L*
27	**GGSD1**	**GGSD1**	**44**	**362778**	**6349783**	**0**	**70.107**	**70.106**	**0.00**	**0**	**0.0**	**0.0**	**VL**	**0.0**	**0**	**VL**
28	**GGSD1 /38-4-1007**	**GGSD1(38-4-1007)**	**44**	**362918**	**6349348**	**0**	**53.930**	**53.929**	**0.00**	**0**	**0.0**	**0.0**	**VL**	**0.0**	**0**	**VL**
29	**GGSD2**	**GGSD2**	**44,45**	**363099**	**6349675**	**0**	**44.264**	**44.199**	**-0.06**	**2**	**2.3**	**1.1**	**M#**	**0.0**	**2**	**VL**
30	*GNW1/38-4-0995*	*GNW1(38-4-0995)*	*48*	*361797*	*6351991*	*0*	*217.177*	*216.088*	*-1.09*	*8*	*-2.1*	*1.0*	*M*	*0.7*	*-8*	*L*
31	IF1	IF1	42	361789	6353240	0	225.824	224.625	-1.20	7	-2.5	1.3	M	-0.6	-8	L
32	IF10	IF10	43	361881	6351309	0	134.003	133.772	-0.23	12	3.4	1.7	H	0.7	8	L
33	IF11	IF11	43	361910	6351311	0	132.185	131.426	-0.76	23	1.6	0.8	M	2.3	15	M
34	IF2	IF2	42	361775	6352940	0	226.345	225.614	-0.73	10	1.0	0.5	L	0.9	9	L
35	IF3	IF3	38	363226	6352212	0	57.368	57.367	0.00	0	0.0	0.0	VL	0.0	0	VL
36	IF4	IF4	38	363217	6352210	0	56.846	56.845	0.00	0	0.0	0.0	VL	0.0	0	VL
37	IF5	IF5	48	361428	6351539	0	259.913	259.079	-0.83	10	-0.6	0.3	VL	-1.0	-10	L
38	IF7	IF7	50	361010	6350446	0	100.118	100.117	0.00	0	0.0	0.0	VL	0.0	0	VL
39	IF8	IF8	38	361698	6361135	0	0.000	0.000	0.00	0	0.0	0.0	VL	0.0	0	VL
40	IF8	IF8	48	361830	6351338	0	137.866	137.745	-0.12	7	3.2	1.6	H	-0.6	-8	L
41	IF9	IF9	48	361846	6351338	0	136.293	136.220	-0.07	2	2.7	1.3	H	0.0	0	VL
42	*Pigment in Creek?(near GG38-4-0461)*	*PIC?*	*47*	*361433*	*6352372*	*0*	*217.198*	*216.656*	*-0.54*	*14*	*2.3*	*1.2*	*M*	*0.1*	*2*	*VL*

Job: West Wallsend Colliery - Potential Impacts on Aboriginal Artifact Sites																	
Site#	**Site Name**	**Site Name**	**LW**	**MGA Easting**	**MGA Northing**	**Z**	**RLo**	**RLi**	**Final Subs**	**Final Tilt**	**Final Strain**	**Dynamic Strain**	**Cracking Potential***	**Gradient Increase**	**Runoff Velocity**	**Erosion Increase**
							m	**m**	**m**	**mm/m**	**mm/m**	**mm/m**		**%**	**Increase(%)**	**Potential***
43	**Stone Arch**	**SAH**	**49**	**361155**	**6351845**	**0**	**186.483**	**186.482**	**0.00**	**0**	**0.0**	0.0	**VL**	**0.0**	0	**VL**
44	**Stone Arrangment**	**SAT1**	**41**	**361593**	**6354191**	**0**	**175.943**	**175.942**	**0.00**	**0**	**0.0**	**0.0**	**VL**	**0.0**	**0**	**VL**
45	*Stone Arrangment2*	*SAT2*	*48*	*361446*	*6351548*	*0*	*262.071*	*261.062*	*-1.01*	*7*	*-1.4*	*0.7*	*L*	*-0.2*	*0*	*VL*
46	*Cockle Creek Shelter w Artefacts*	*SWA*	*42*	*361956*	*6352179*	*0*	*170.758*	*169.820*	*-0.94*	*17*	*0.0*	*0.0*	*L*	*0.9*	*-10*	*L*
47	**Stone Canns**	**STC**	**49**	**361059**	**6352193**	**0**	**203.207**	**203.206**	**0.00**	**0**	**0.0**	0.0	**VL**	**0.0**	0	**VL**
48	**Spring**	**SP**	**45,46**	**363447**	**6349257**	**0**	**35.361**	**35.360**	**0.00**	**0**	**0.0**	0.0	**VL**	**0.0**	**0**	**VL**
49	Scarred Tree 1	ST1	41	361667	6354093	0	163.094	163.088	-0.01	0	0.2	0.1	VL	0.0	0	VL
50	Scarred Tree 2	ST2	41	362166	6351667	0	117.420	116.647	-0.77	25	3.0	1.5	H	2.0	14	M
51	Scarred Tree 3	ST3	45	362921	6349684	0	67.526	67.191	-0.34	17	4.4	2.2	H	1.3	-12	M
52	Scarred Tree 4	ST4	43a	361156	6353938	0	347.610	347.609	0.00	0	0.0	0.0	VL	0.0	0	VL
53	Scarred Tree 5	ST5	43b	362007	6350676	0	72.438	72.400	-0.04	5	4.3	2.1	H	0.4	7	L
54	Scarred Tree 6	ST6	51	361384	6350405	0	89.137	89.136	0.00	0	0.0	0.0	VL	0.0	0	VL
55	Scarred Tree7	ST7	43a	361591	6352490	0	262.118	261.376	-0.74	2	2.3	1.1	H	0.1	3	VL
56	Scarred Tree8	ST8	na	360938	6352281	0	178.385	178.384	0.00	0	0.0	0.0	VL	0.0	0	VL
57	Scarred Tree9	ST9	49	361288	6352356	0	203.736	202.855	-0.88	5	-2.0	1.0	L	-0.3	-5	L
58	Scarred Tree10	ST10	49	361446	6351548	0	262.071	261.062	-1.01	7	-1.4	0.7	L	-0.2	0	VL
59	Western Domain 1 AHIMS registered	WD1	38	362866	6352734	0	42.991	42.981	-0.01	1	0.8	0.4	L	-0.1	-3	VL
60	Western Domain 2 AHIMS registered	WD2	38	362843	6352748	0	44.005	43.944	-0.06	6	2.8	1.4	H	-0.4	-7	L
61	Western Domain 3 AHIMS registered	WD3	38	362789	6352755	0	45.226	43.968	-1.26	41	1.4	0.7	M	2.5	-16	M
62	Western Domain 4 AHIMS registered	WD4	38	363042	6352680	0	41.116	41.115	0.00	0	0.0	0.0	VL	0.0	0	M
63	**Wet Soak (AHIMS Registered)**	**WD5**	**40**	**362040**	**6353879**	**0**	**120.552**	**120.551**	**0.00**	**0**	**0.0**	0.0	**VL**	**0.0**	**0**	**L**
64	Western Domain 6 AHIMS registered	WD6	39	362595	6352820	0	50.313	50.152	-0.16	14	6.9	3.4	H	-1.4	0	M
65	Western Domain 7 AHIMS registered	WD7	39	362525	6352833	0	53.101	50.801	-2.30	18	-7.7	3.9	H	-1.8	-13	M
66	Western Domain 8 AHIMS registered	WD8	40	362320	6352889	0	75.897	74.671	-1.23	39	-0.3	1.0	M	-3.8	-20	M
67	Western Domain 9 AHIMS registered	WD9	38	362809	6352743	0	45.137	44.513	-0.62	31	6.4	3.2	H	-1.4	-12	M

- Likelihood of cracking based on chain pillar cracking data for West Wallsend Longwalls 1 to 37

Italics - Sites that are likely to be susceptible to mine subsidence impacts

Bold - Key sites requiring impact control (i.e. no damage from subsidence cracking)

* -	Damage Potential Key and Indicative Probabilities of Occurrence
VL	Very Low (<1% Probability of Occurrence)
L	Low (1-10% PoO)
M	Moderate (10 - 25% PoO)
H	High (>25% PoO)

Cracking Damage Potential Category Criteria		Erosion/Sedimentation Damage Potential Category Criteria (Note: -ve slope changes indicate potential sedimentation increases)			
DP:	Predicted 'Smooth profile' Tensile Strain:	DP:	Predicted Surface Gradient Change:		Predicted Runoff Velocity Increase or Decrease (based on Manning Open Channel Flow Formula):
VL	<0.5 mm/m	VL	<0.3%		<1%
L	0.5 - 1 mm/m	L	0.3-1%		1-5%
M	1 - 2 mm/m	M	1-6%		5-25%
H	>2 mm/m	H	>6%		>25%

From: Steve2.dgs [steve2.dgs@westnet.com.au]
Sent: Tuesday, 14 July 2009 10:06 AM
To: Steve.dgs
Subject: FW: Revised Mine Plan for High Ranked Arch Sites
Attachments: Surface Sites for Mine Planning May 2009_2.zip; Crack Data.xls; Figure (XL 11 Subs Adjustment).pdf

-----Final Version of Original Message sent 29 May 2009 2:58 AM -----

From: Steve2.dgs [mailto:steve2.dgs@westnet.com.au]
Sent: 30 May 2009 5:00 PM
To: Mark Robinson
Cc: Paul Amidy
Subject: Revised Mine Plan for High Ranked Arch Sites

Mark,

1. Minimum chain pillar width for LW45/46 (GGSD 2)

As requested, I have assessed a range of minimum chain pillar widths that will reduce (but not eliminate) the potential for crack development at the GGSD2 Site between LW45/46 (now LWs 44/45) in the Southern Domain.

The assessment included a review of the measured crack data above the chain pillars between LWs 22 to 36 at West Wallsend colliery, and to statistically derive the minimum pillar width for a 'low' probability of cracking.

The centre of the 20 m diameter GGSD2 site is located in gently undulating terrain and is currently above the 30 m wide chain pillar between LW45 and 46. The site centre is presently 5.5 m from the rib-side of LW45 and 19.5 m from the rib-side of LW46. Out of 15 longwall blocks (LW22 to 36), twenty-two cracks (<= 0.1 m wide) have occurred (that we now about) above 12 out of 196 chain pillars formed (i.e. 6% of pillars), with 1 location experiencing cracking 12.1 m from the goaf, which was on one side of the pillar only (LW29). The LW30 ridge cracks were a function of steep topography and have been ignored.

It is considered however, that cracking will probably occur above the chain pillars where rock exposures exist, such that the probability of cracking should be based on the observed crack locations with respect to the nearest pillar/panel rib-side.

The cracking data has been collated on the attached spreadsheet (Crack Data.xls) and indicates the following probabilities of cracks occurring above a chain pillar at a given set-back distance from the nearest goaf edge rib:

Table 1 - Probability of Cracking Occurring at a Given Set-back Distance from the Goaf Edge above West Wallsend Chain Pillars

Set back distance from rib-side to nearest groove site edge (m)	% of Cracks Observed within range (poC)	Pillar Width Beneath GGSD2 Site	Probability of cracking at GGDS2 Site
0.0 - 0.5	32	**30**	High
0.5 - 5.5	18	40	Moderate
5.5 - 10.5	18	45	Moderate
10.5 - 15.5	18	50	Moderate
15.5 - 16.5	14	55	Moderate
>16.5	0	60	Low
Total	**100**		

* poC = % of cracks observed in range at given distance from nearest longwall panel ribside
Bold - Current position of GGDS2 above 35 m wide chain pillar between LWs 45/46.

Overall, it appears that the probability of the development of cracking is dependent on the distance from the nearest rib-side only (see spreadsheet charts). The predicted strains for all pillars was 2-3 mm/m, which is generally the magnitude where the onset of cracking would be expected. Increasing the pillar width by 10 to 15 m (i.e. w = 45 m and 55 m) does not appear to reduce the strain magnitudes significantly (see Figures 1 and 2 attached), however, the probability of a crack developing at the GGSD2 site is reduced by increasing the set-back distances.

Based on the above table, the probability of a crack (poC) occurring at the GGSD2 for the current mine layout (i.e. with a 30 m wide chain pillar) is 32% or a 'High' likelihood. By increasing the pillar width by 15 to 20 m, to give a pillar width 45 m to 55 m, the poC reduces from 18% to 14% or a 'Moderate' cracking' likelihood.

For a 'Low' probability of cracking, the chain pillar width would have to be increased to 60 m.

For 'Very Low' probability of cracking, the database is probably not large enough to be reliable. The default set-back distance for 'very unlikely' cracking potential is the angle of draw, or 0.5 times the cover depth. At the GGSD2 site, where the cover depth is 140 m, a set-back distance of 70 m would be required.

The proposed shift in LW45 to the west for each case is shown in the attached .dwg file. It is considered that the options represent ‘low’ probabilities of cracks developing at the GGDS2 site. It is understood that LW44 has been deleted due to the grinding groove site (K-2 site) above it. A 26.5^{o} design angle of Draw from the K1 and K2 sites has been adopted for a ‘very low’ probability of cracking (see Section 2 also)

2. Design Angle of Draw from the Western Domain Archaeology Sites

The design angle of draw for nil site damage is still set at 26.5^{o} due to sensitive nature of the sites (see previous e-mail for justification details). The steep topography is also a factor at some of the locations.

The current mine plan with the recommended LW set back distances from each of the arch. sites are shown in magenta. The new starting positions for the affected panels are shown in red.

Regards,

Steven Ditton
Principal Engineer

Ditton Geotechnical Services Pty Ltd
ACN 124 206 962

80 Roslyn Avenue
CHARLESTOWN NSW 2290

PO Box 5100
KAHIBAH NSW 2290

Tel: 02 4920 9798 Fax: 02 4920 9798
Mobile: 0413 094074 e-mail: steve.dgs@westnet.com.au

West Wallsend Colliery's Measured Tensile Crack Locations due to LWs 22 - 36

	H	d	l	w	LW#	W	recorded crack width (m)	d/H	w/H	W/H
Panels	150	-34.5	10	solid	36	178.6	0.1	-0.230	n/a	1.19
	210	-34	7.4	40	26	159		-0.162	0.19	0.76
	150	-32.8	35	solid	36	178.6	0.35	-0.219	n/a	1.19
	210	-31	7.7	40	26	159		-0.148	0.19	0.76
	205	-30	7.11	40	24/25	150		-0.146	0.20	0.73
	155	-29	30	solid	35	178.6	0.1	-0.187	n/a	1.15
	155	-29	30	solid	35	178.6	0.1	-0.187	n/a	1.15
	145	-28.7	10	35	33	175	0.1	-0.198	0.24	1.21
	200	-27.4	8.14	40	29	159		-0.137	0.20	0.80
	220	-27.4	5.1	34.5	32	172.5		-0.125	0.16	0.78
	200	-27.3	5	32.5	28	175	0.1	-0.137	0.16	0.88
	145	-21.8	10	35	33	175	0.1	-0.150	0.24	1.21
	210	-20.9	12.9	40	26	159		-0.100	0.19	0.76
	190	-20.4	24	35	29	159		-0.107	0.18	0.84
	205	-15.44	21	40	24/25	150		-0.075	0.20	0.73
	190	-15.2	24	35	29	159		-0.080	0.18	0.84
	145	-15.2	15.7	32.5	31	175	0.25	-0.105	0.22	1.21
	180	-14.7	6.5	solid	27	175	0.05	-0.082	n/a	0.97
	145	-14.2	10	35	33	175	0.3	-0.098	0.24	1.21
	195	-13.3	13.4	35	29	159		-0.068	0.18	0.82
	190	-11.2	24	35	29	159		-0.059	0.18	0.84
	195	-10.6	17.5	35	29	159		-0.054	0.18	0.82
	200	-10.3	8.14	40	26	159		-0.052	0.20	0.80
	195	-10.2	20	35	30	175		-0.052	0.18	0.90
	195	-7.4	22.1	35	29	159		-0.038	0.18	0.82
	180	-6.6	0.7	solid	33	175	0.3	-0.037	n/a	0.97
	200	-5.6	10	40	26	150		-0.028	0.20	0.75
	190	-5	24	35	29	159		-0.026	0.18	0.84
	195	-5	19.4	35	29	159		-0.026	0.18	0.82
	145	-4.21	5	32.5	28	175	0.1	-0.029	0.22	1.21
	145	-4.21	5	32.5	28	175	0.1	-0.029	0.22	1.21
	145	-2.9	5	32.5	28	175	0.1	-0.020	0.22	1.21
	210	-2.3	10	35	34	178.6	0.1	-0.011	0.17	0.85
	205	-1.5	5	35	33/34	175	0.04	-0.007	0.17	0.85
	215	-0.9	5	35	32/33	175	0.1	-0.004	0.16	0.81
	185	-0.5	34.4	35	29	159		-0.003	0.19	0.86
Chain	250	0	74	40	22	150		0.000	0.16	0.60
Pillars	250	0	32	40	22/23	150		0.000	0.16	0.60
	145	0	24	solid	28	175	0.1	0.000	n/a	1.21
	140	0	15.7	35	31/32	175	0.1	0.000	0.25	1.25
	135	0	17.2	solid	32	172.5		0.000	n/a	1.28
	135	0	17.2	solid	32	172.5		0.000	n/a	1.28
	145	0	17.3	35	33	175		0.000	0.24	1.21
	200	1.75	10	40	25	150		0.009	0.20	0.75
	195	2.05	20	35	30/29	175		0.011	0.18	0.90
	205	2.94	12.8	40	24/25	150		0.014	0.20	0.73
	205	3	12.8	40	24/25	150		0.015	0.20	0.73
	135	7.8	17.2	35	32	172.5		0.058	0.26	1.28
	145	7.8	17.2	35	32	172.5		0.054	0.24	1.19
	205	9.4	12.8	40	24/25	150		0.046	0.20	0.73
	205	10.5	12.8	40	24/25	150		0.051	0.20	0.73
	190	12.5	14.3	35	29	159		0.066	0.18	0.84
	205	13.25	12.8	40	24/25	150		0.065	0.20	0.73
	205	13.5	5	32.5	28/31	175	0.1	0.066	0.16	0.85
	215	13.9	29.5	40	22/23	150		0.065	0.19	0.70
	205	15.8	12.8	40	24/25	150		0.077	0.20	0.73
	220	16.3	42	40	24/25	150		0.074	0.18	0.68
	215	16.4	15.6	40	22	150		0.076	0.19	0.70
Panel Statistics										
Max	220	-0.50	35.0	40.0	36	178.6	0.35	-0.003	0.24	1.21
Min	145	-34.50	0.7	32.5	26	150.0	0.04	-0.230	0.16	0.73
Median	193	-14.45	10.0	35.0	29	173.8	0.10	-0.078	0.19	0.84
Pillar Statistics										
Max	250	16.40	74.0	40.0	33	175.0	0.10	0.077	0.26	1.28
Min	135	0.00	5.0	32.5	22	150.0	<0.1	0.000	0.16	0.60
Median	205	5.40	16.5	40.0	31	150.0	0.10	0.030	0.20	0.74

Bin	*Frequency*	*Cumulative %*
0	7	31.82%
2	1	36.36%
4	3	50.00%
6	0	50.00%
8	2	59.09%
10	1	63.64%
12	1	68.18%
14	4	86.36%
16	1	90.91%
16.5	2	100.00%
More	0	100.00%

d Data:

0
0
0
0
0
0
1.75
2.05
2.94
3
7.8
7.8
9.4
10.5
12.5
13.25
13.5
13.9
15.8
16.3
16.4

Statistics	
Mean	6.68
Standard Error	1.36
Median	5.40
Mode	0.00
Standard Deviati	6.38
Sample Variance	40.76
Kurtosis	-1.65
Skewness	0.29
Range	16.40
Minimum	0.00
Maximum	16.40
Sum	146.89
Count	22.00

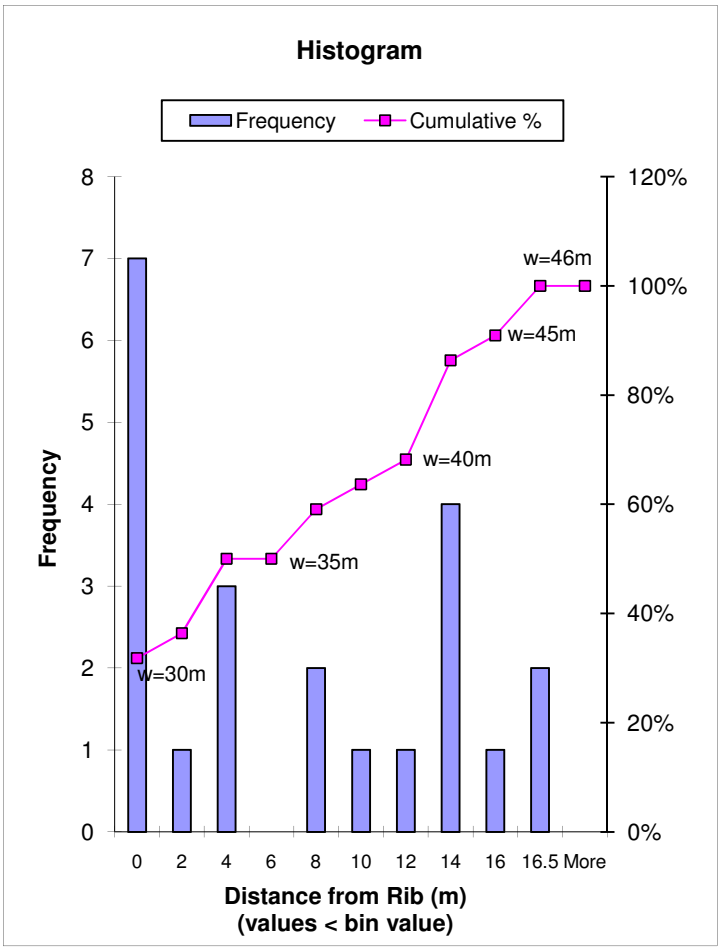

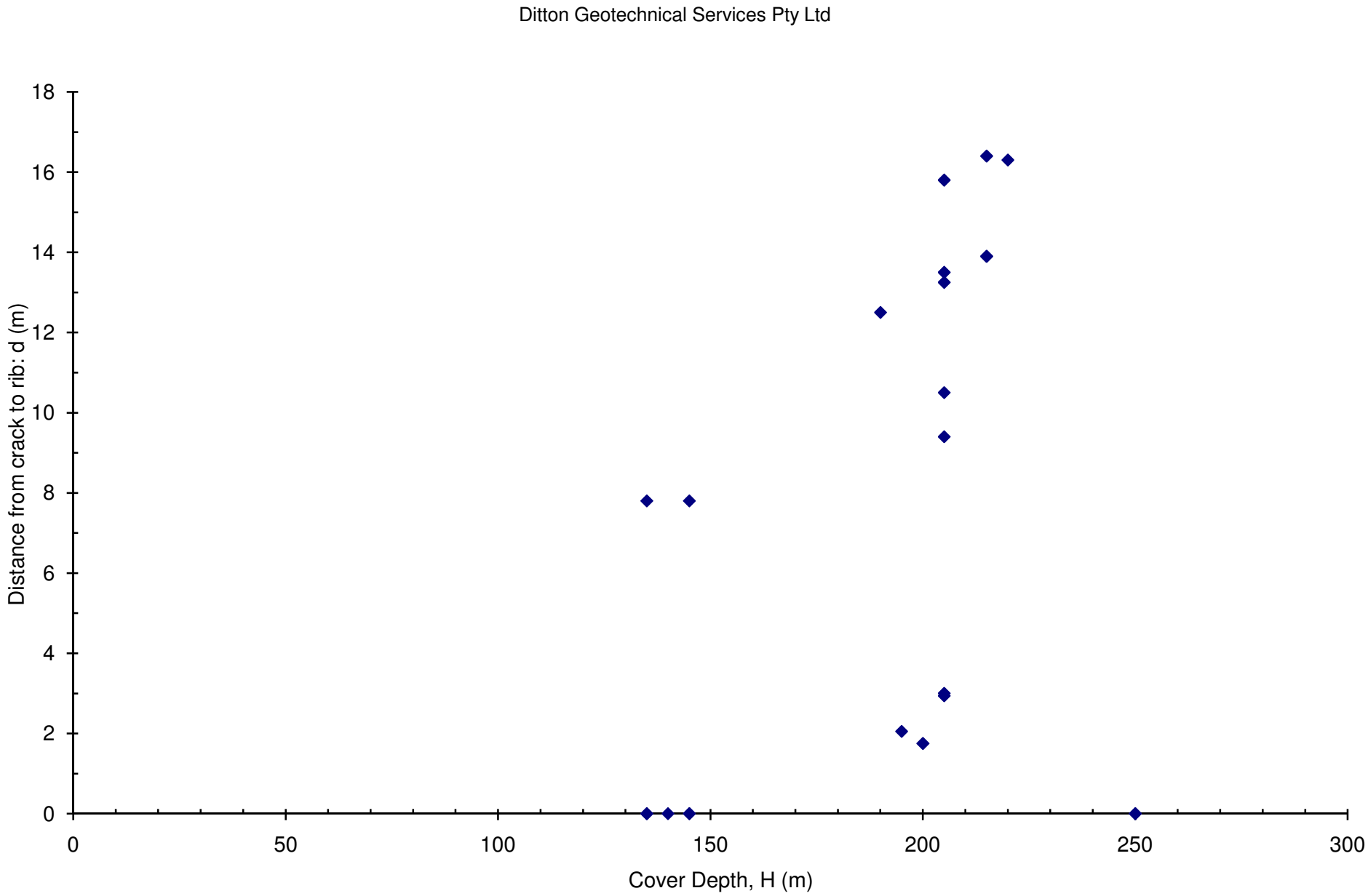
Ditton Geotechnical Services Pty Ltd
Distance from crack to rib: d (m)
Cover Depth, H (m)
0
2
4
6
8
10
12
14
16
18
0
50
100
150
200
250
300

Ditton Geotechnical Services Pty Ltd

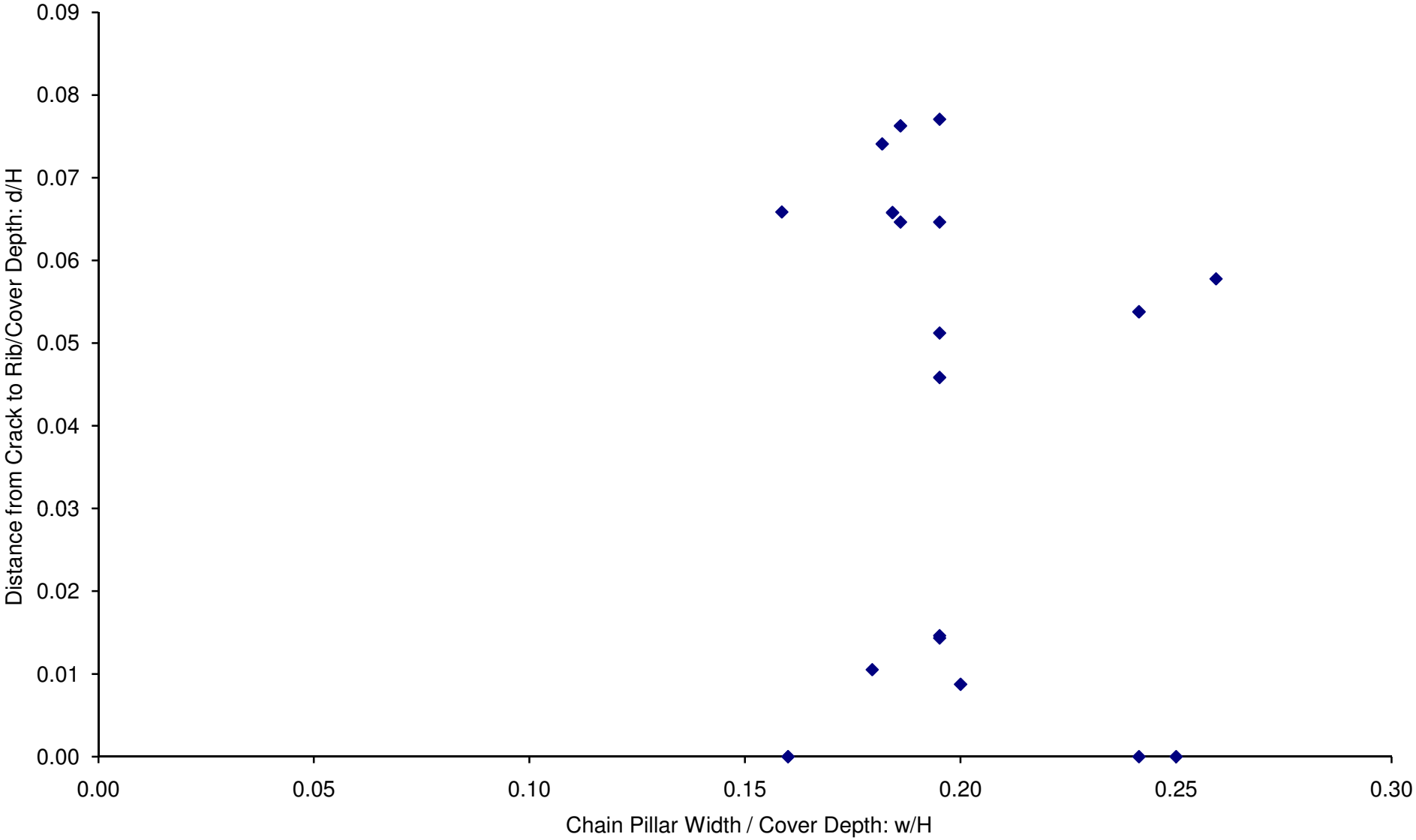

Ditton Geotechnical Services Pty Ltd

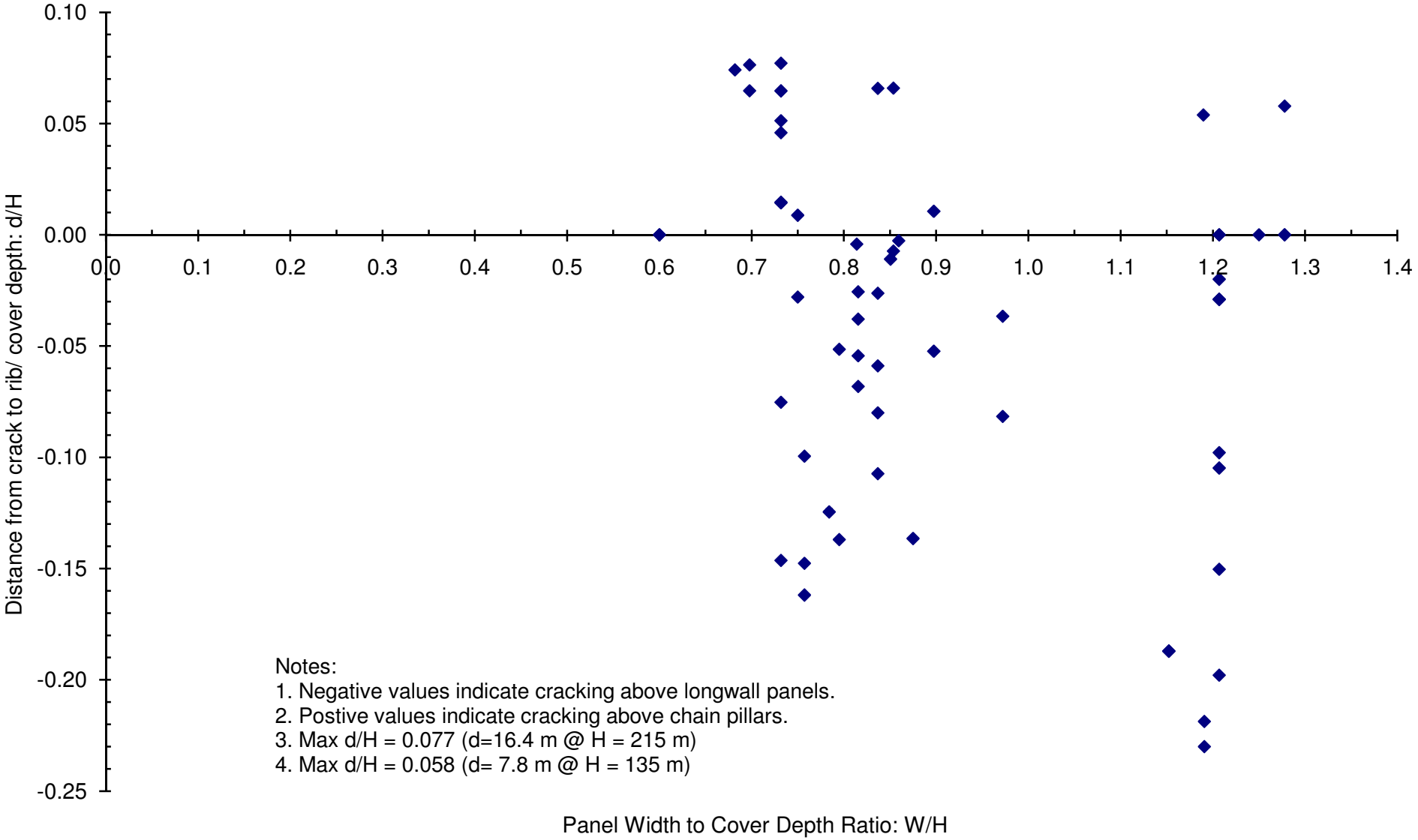

Notes:
1. Negative values indicate cracking above longwall panels.
2. Postive values indicate cracking above chain pillars.
3. Max d/H = 0.077 (d=16.4 m @ H = 215 m)
4. Max d/H = 0.058 (d= 7.8 m @ H = 135 m)

Ditton Geotechnical Services Pty Ltd

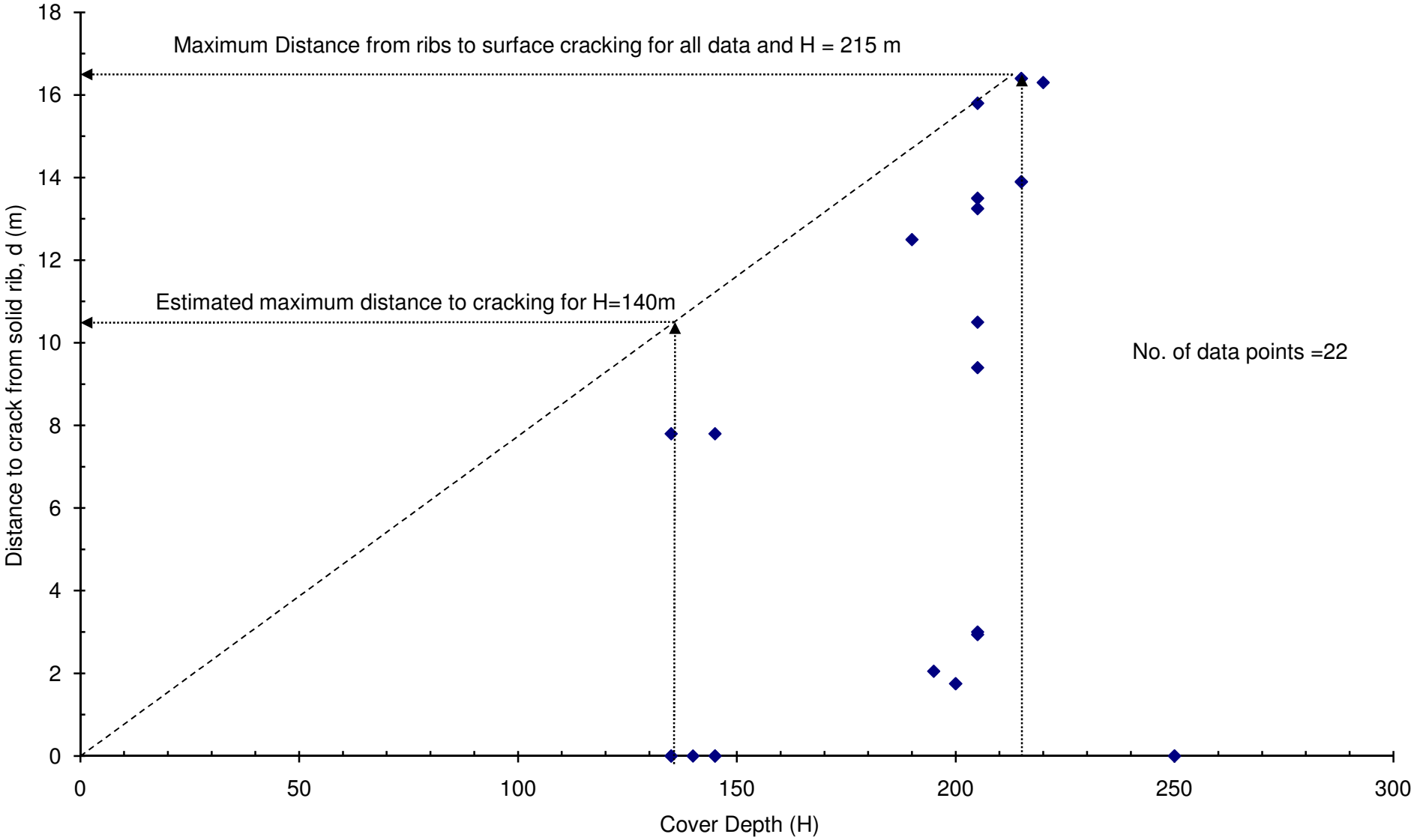

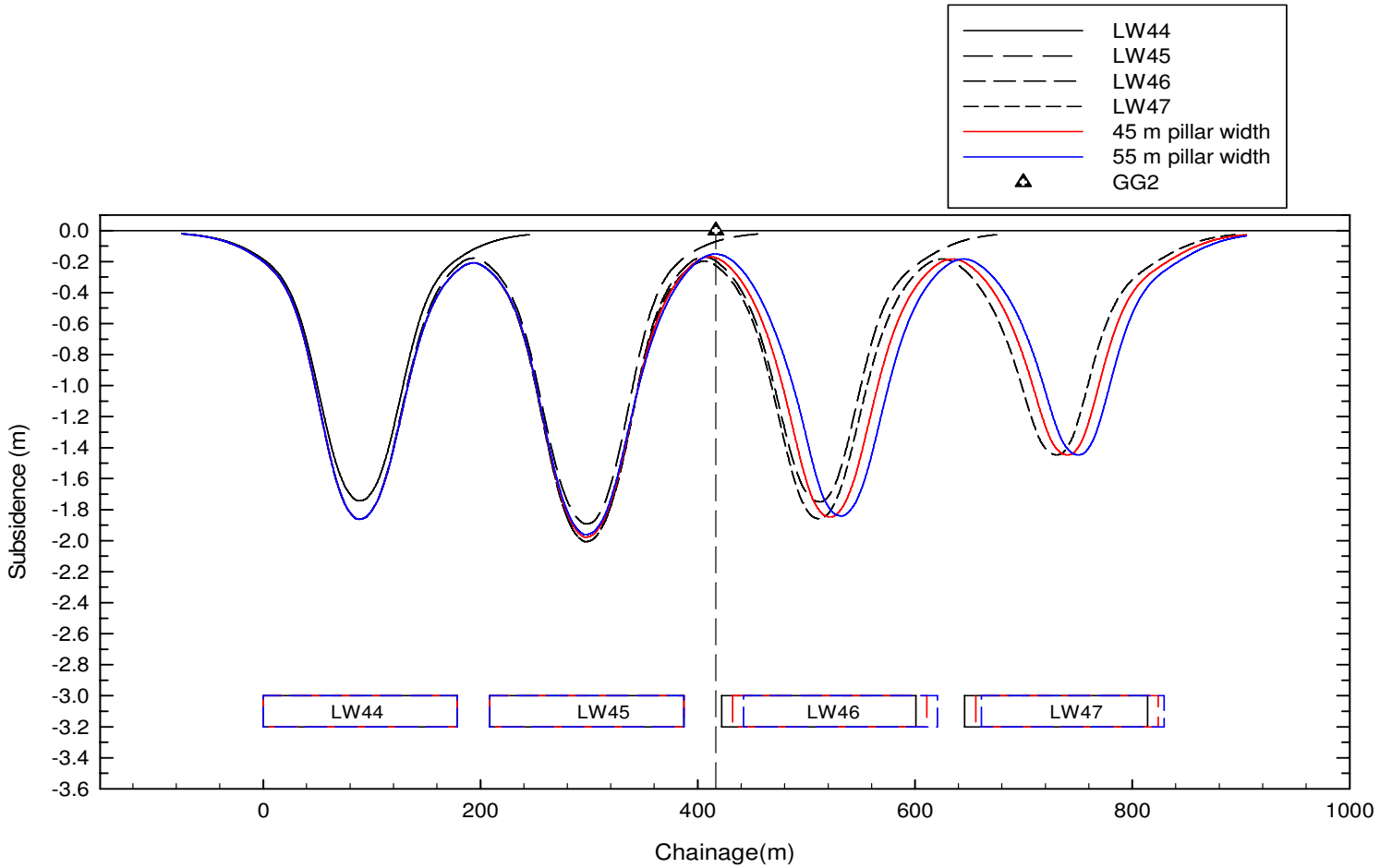

DgS	Engineer:	S.Ditton	Client:	West Wallsend Colliery WWD-012/1	
	Drawn:	S.Ditton			
	Date:	29.05.09	Title:	Predicted Subsidence Profiles for Proposed Pillar Width Increases between LWs 45 and 46 (based on ACARP, 2003)	
	Ditton Geotechnical Services Pty Ltd		Scale:	NTS	Figure No: F1

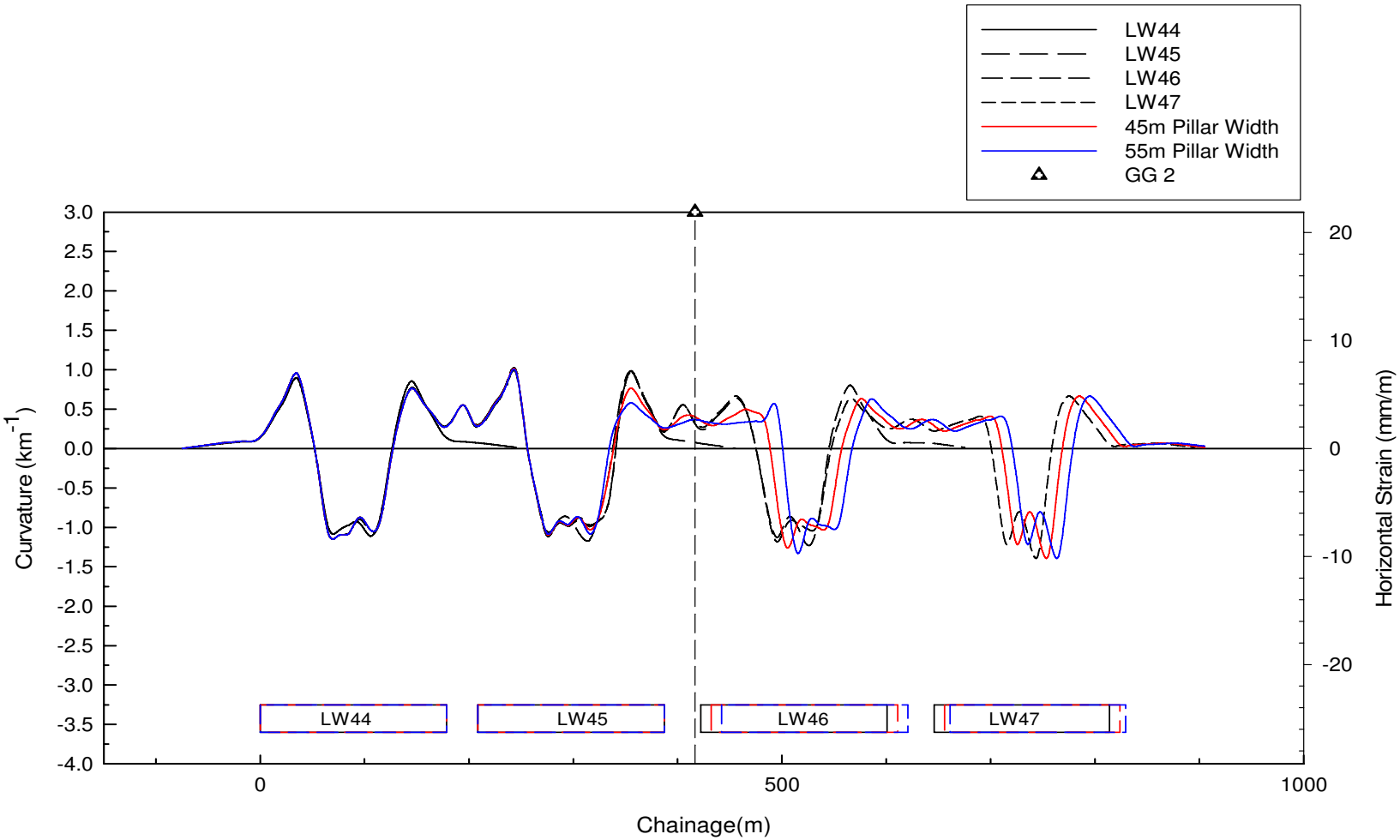

DgS	Engineer:	S.Ditton	Client:	West Wallsend Colliery WWD-012/1	
	Drawn:	S.Ditton			
	Date:	29.05.09	Title:	Predicted Strain Profiles for Proposed Pillar Width Increases between LWs 45 and 46 (based on ACARP, 2003)	
	Ditton Geotechnical Services Pty Ltd		Scale:	NTS	Figure No: F2